2013-05-22

The Study of Two Strategies for Decreasing Mutant Huntingtin: Degradation by Puromycin Sensitive AminoPeptidase and RNA Interference: A Dissertation

Joanna Chaurette
University of Massachusetts Medical School Worcester

THE STUDY OF TWO STRATEGIES FOR DECREASING MUTANT HUNTINGTIN: DEGRADATION BY PUROMYCIN SENSITIVE AMINOPEPTIDASE AND RNA INTERFERENCE

Dissertation Presented

By

Joanna Chaurette

Submitted to the Faculty of the

University of Massachusetts Graduate School of Biomedical Sciences, Worcester

in partial fulfillment of the requirements for the degree of

DOCTOR OF PHILOSOPHY

May 22, 2013

M.D./Ph.D. Program in Biomedical Sciences

THE STUDY OF TWO STRATEGIES FOR DECREASING MUTANT HUNTINGTIN: DEGRADATION BY PUROMYCIN SENSITIVE AMINOPEPTIDASE AND RNA INTERFERENCE

Dissertation Presented

By

Joanna Chaurette

The signatures of the Dissertation Defense Committee signify completion and approval as to style and content of the Dissertation

_____

Neil Aronin, M.D., Thesis Advisor

_____

Paul Dobner, Ph.D., Member of Committee

_____

Justin Fallon, Ph.D., Member of Committee

_____

Terence Flotte, M.D., Member of Committee

_____

Brian Lewis, Ph.D., Member of Committee

The signature of the Chair of the Committee signifies that the written dissertation meets the requirements of the Dissertation Committee

_____

David Weaver, Ph.D., Chair of Committee

The signature of the Dean of the Graduate School of Biomedical Sciences signifies that the student has met all graduation requirements of the school.

_____

Anthony Carruthers, Ph.D., Dean of the Graduate School of Biomedical Sciences

M.D./Ph.D. Program in Biomedical Sciences

May 22, 2013

Dedicated to my husband, Scott, and my son, Remy

ACKNOWLEDGMENTS

First and foremost I would like to thank my advisor, Neil Aronin, for his support and guidance. Dr. Aronin has been a model physician scientist in addition to being an amazing teacher and mentor. I was fortunate to have a phenomenal thesis research advisory committee who helped shape me as a scientist. Together, Brian Lewis, Terence Flotte, and David Weaver provided hours of thoughtful discussions and helped me look at my data in new ways. I would especially like to thank, David Weaver for extra help when I need it and for always having an open door. I am forever indebted to my lab family: Kathryn Chase, Lori Kennington, Edith Pfister, Wanzhao Liu, Sarah McGowan, and Erica Mondo for their technical expertise, support and for keeping me relatively sane through the entire process.

I would like to thank the directors and administrators of the MD/PhD program past and present: Elliot Androphy, Gyongi Szabo, Bill Schwartz, Sylvia Corvera, Anne Michelson , who have been instrumental in keeping track of me throughout my studies and providing support and advice throughout the transition from medical school to research and now back again to medical school. Peter Newburger served as one of my first mentors and made sure I managed the first transition to research with ease. I greatly value my conversations with Miguel Esteves, Chris Mueller, and Guangping Gao who provided me with more technical advice viral vectors than I could even imagine. I would like to thank Marian DiFiglia, Phil Zamore and Stephen Miller for conversations regarding experimental design.

A very special ‘thank you’ goes to my husband, Scott, for his patience and support throughout the good and bad times. My son, Remy, has been my inspiration the last three years. I would like to thank my parents, who from the beginning of my education, encouraged and nurtured my love of science and research.

ABSTRACT

Huntington's disease (HD) is a fatal neurodegenerative disease caused by a CAG repeat expansion in exon 1 of the huntingtin gene, resulting in an expanded polyglutamine (polyQ) repeat in the huntingtin protein. Patients receive symptomatic treatment for motor, emotional, and cognitive impairments; however, there is no treatment to slow the progression of the disease, with death occurring 15-20 years after diagnosis. Mutant huntingtin protein interferes with multiple cellular processes leading to cellular dysfunction and neuronal loss. Due to the complexity of mutant huntingtin toxicity, many approaches to treating each effect are being investigated. Unfortunately, addressing one cause of toxicity might not result in protection from other toxic insults, necessitating a combination of treatments for HD patients. Ideally, single therapy targeting the mutant mRNA or protein could prevent all downstream toxicities caused by mutant huntingtin. In this work, I used animal models to investigate a potential therapeutic target for decreasing mutant huntingtin protein, and I apply bioluminescent imaging to investigate RNA interference to silence mutant huntingtin target sites.

The enzyme puromycin sensitive aminopeptidase (PSA) has the unique property of degrading polyQ peptides and been implicated in the degradation of huntingtin. In this study, we looked for an effect of decreased PSA on the pathology and behavior in a mouse model of Huntington's disease. To achieve this, we crossed HD mice with mice with one functional PSA allele and one inactivated PSA allele. We found that PSA heterozygous HD mice develop a greater number of pathological inclusion bodies, representing an accumulation of mutant huntingtin in neurons. PSA heterozygous HD

mice also exhibit worsened performance on the raised-beam test, a test for balance and coordination indicating that the PSA heterozygosity impairs the function of neurons with mutant huntingtin. In order to test whether increasing PSA expression ameliorates the HD phenotype in mice we created an adeno-associated virus (AAV) expressing the human form of PSA (AAV-hPSA). Unexpectedly, testing of AAV-hPSA in non-HD mice resulted in widespread toxicity at high doses. These findings suggest that overexpression of PSA is toxic to neurons in the conditions tested.

In the second part of my dissertation work, I designed a model for following the silencing of huntingtin sequences in the brain. Firefly luciferase is a bioluminescent enzyme that is extensively used as a reporter molecule to follow biological processes *in vivo* using bioluminescent imaging (BLI). I created an AAV expressing the luciferase gene containing huntingtin sequences in the 3'-untranslated region (AAV-Luc-Htt). After co-injection of AAV-Luc-Htt with RNA-silencing molecules (RNAi) into the brain, we followed luciferase activity. Using this method, we tested cholesterol-conjugated siRNA, un-conjugated siRNA, and hairpin RNA targeting both luciferase and huntingtin sequences. Despite being able to detect silencing on isolated days, we were unable to detect sustained silencing, which had been reported in similar studies in tissues other than the brain. We observed an interesting finding that co-injection of cholesterol-conjugated siRNA with AAV-Luc-Htt increased luminescence, findings that were verified in cell culture to be independent of serotype, siRNA sequence, and cell type. That cc-siRNA affects the expression of AAV-Luc-Htt reveals an interesting interaction possibly resulting in increased delivery of AAV into cells or an increase in luciferase expression

within the cell. My work presents a method to follow gene silencing of huntingtin targets in the brain, which needs further optimization in order to detect sustained silencing.

Finally, in this dissertation I continue the study of bioluminescent imaging in the brain. We use mice that have been injected in the brain with AAV-Luciferase (AAV-Luc) to screen 34 luciferase substrate solutions to identify the greatest light-emitting substrate in the brain. We identify two substrates, CycLuc1 and iPr-amide as substrates with enhanced light-emitting properties compared with D-luciferin, the standard, commercially available substrate. CycLuc1 and iPr-amide were tested in transgenic mice expressing luciferase in dopaminergic neurons. These novel substrates produced luminescence unlike the standard substrate, D-luciferin which was undetectable. This demonstrates that CycLuc1 and iPr-amide improve the sensitivity of BLI in low expression models. We then used CycLuc1 to test silencing of luciferase in the brain using AAV-shRNA (AAV-shLuc). We were unable to detect silencing in treated mice, despite a 50% reduction of luciferase mRNA. The results from this experiment identify luciferase substrates that can be used to image transgenic mice expressing luciferase in dopaminergic neurons.

My work contributes new data on the study of PSA as a modifier of Huntington's disease in a knock-in mouse model of Huntington's disease. My work also makes contributions to the field of bioluminescent imaging by identifying and testing luciferase substrates in the brain to detect low level of luciferase expression.

TABLE OF CONTENTS

LIST OF TABLES

LIST OF FIGURES

CHAPTER I

INTRODUCTION

The goal of this dissertation is to investigate methods to modify levels of mutant huntingtin protein, the cause of Huntington's disease. Huntington's disease is an inherited neurodegenerative disease caused by a mutation in the huntingtin gene. The mutation is an expanded CAG repeat in exon 1 of the huntingtin gene that encodes a polyglutamine expansion in the huntingtin protein, conferring it with many toxic properties resulting in neuron dysfunction and cell death. There is currently no cure for Huntington's disease. The studies in the following chapters focus on how to decrease the amount of mutant huntingtin protein. For this dissertation, it is helpful to understand the molecular mechanisms of the disease, especially the process by which mutant huntingtin is handled by the cell. One essential question in the study of HD remains how mutant huntingtin is degraded. Mutant huntingtin accumulates in neurons, forming intracellular aggregates and inclusion bodies. Neurons eventually succumb to the toxic effects of mutant huntingtin and undergo cell death. Together, neuronal dysfunction and cell death result in declining mental and physical functioning and death in Huntington's disease patients.

I focus on two strategies that can be applied to treat Huntington's disease. The first study is of puromycin sensitive aminopeptidase (PSA), a potential modifier of the degradation of mutant huntingtin. Mutant huntingtin is misfolded and marked for degradation; however it accumulates resulting in cellular dysfunction. An increase in the degradation of mutant

huntingtin could clear the mutant protein and avoid the disruption of cellular processes. This mechanism would ideally prevent the onset and slow the progression of the disease.

A second approach is to slow or stop the production of mutant huntingtin protein. RNA interference (RNAi) is currently being studied as a method to reduce the amount of mutant huntingtin mRNA, resulting in lower levels of mutant huntingtin protein. A decrease of mutant huntingtin mRNA and protein would prevent downstream toxicity and cell death. A challenge of optimizing the design and delivery of RNAi has been the lack of an efficient way to evaluate, *in vivo*, the effectiveness of each sequence, structure, and delivery system. This work examines an *in vivo* system that can be used to screen silencing molecules in the brain. We present a luciferase reporter molecule containing human huntingtin sequences that can be used to test and compare RNAi approaches in the brain of mice. This method allows screening of silencing molecules and delivery systems in live animals. One benefit of this system is that silencing can be followed over time in the same mouse, preventing the need to collect mRNA and protein from multiple endpoints. RNAi molecules vary in terms of sequence, secondary structure, nucleotide and linkage modifications and delivery systems, making it imperative to methodically screen candidate molecules. A comparison of different RNAi strategies in the brain will provide an optimal design for RNAi therapy to treat Huntington's disease.

Chapter I provides an overview of Huntington's disease, including the molecular functions of normal huntingtin, the toxicities of mutant huntingtin, and a discussion of the current strategies for treating Huntington's disease. Chapter I also introduces published research which provides the rationale for my research.

A. Huntington's disease

1. What is Huntington's disease?

Huntington's disease (HD) is a neurodegenerative disease caused by an autosomal dominant mutation in the huntingtin gene [1]. The mutant allele contains an expansion of a CAG trinucleotide repeat in exon 1 encoding a poly glutamine (polyQ) repeat in the mutant huntingtin protein [2]. The expanded polyQ region of mutant huntingtin results in protein misfolding, aggregation, and confers upon it toxic properties, such as accumulation of mutant huntingtin, disruptions in mitochondrial function, and vesicle trafficking and recycling resulting in cellular dysfunction and ultimately, neuronal cell death [2]. Huntington's disease is a complex disease because of the multiple functions that huntingtin performs and the many toxicities that are caused by the mutant protein. Currently, there is no cure for HD.

Huntington's disease is inherited in an autosomal dominant manner. Typically, an affected parent carries one mutant allele so there is a 50% chance of passing on the disease. A normal huntingtin gene contains 6-36 CAG repeats. Persons with repeat numbers of 37 or above are considered to have Huntington's disease and will develop symptoms and signs as they age [2]. An inverse correlation exists between the numbers of repeats with the age of onset of the disease, the longer the number of repeats, the earlier the onset of symptoms. The trinucleotide repeat is unstable and prone to expansion, especially in spermatogenesis [3]. In homozygous patients, the onset of disease is dependent upon the length of the expansion rather than the presence of two mutant alleles The prevalence of HD in populations of Western European

descent is 4-10 cases per 100,000 [2]. 10% of HD patients are young people under the age of 20 years old, whose disease results from having 60 or more CAG repeats [2].

2. Clinical presentation and disease progression

In adult cases of HD, the earliest symptoms are changes in mood, including personality changes, depression, anxiety, irritability and obsessive compulsive disorder [4]. Apathy increases in severity with disease progression, and psychotic symptoms may develop concurrently with the onset of motor symptoms [4]. Sleep disturbances are common in Huntington's disease, including insomnia, daytime somnolence, and reduced total sleep time [5]. Motor symptoms typically begin with incoordination and chorea, a quick involuntary movement of the hands and feet. Motor symptoms progress to rigidity and dystonia, which refers to sustained muscle contractions causing twisting and stiff postures [6]. As the disease progresses, there is cognitive decline, difficulty talking, dysphagia, and weight loss. Fatality is often a result of falls, dysphagia, or aspiration [6]. Average age of onset is 40 years of age with death occurring within 15-20 years [7].

Juvenile HD is defined as onset of illness in children younger than 21 years of age and represents about 5% of all HD cases [8]. Juvenile cases are characterized by rigidity and akinesia, a reduction in movement. The most common presenting symptoms are cognitive decline and dysphagia, and as the disease progresses, symptoms include dystonia, seizures, chorea, rigidity and akinesia [9].

3. Nigrostriatal system and the function of the basal ganglia.

Huntington's disease is considered a neurodegenerative disease involving the cerebral cortex and basal ganglia.The basal ganglia are defined as a collection of nuclei consisting of the caudate nucleus, putamen, globus pallidus, subthalamic nucleus, and substantia nigra. It is best known for functioning in the initiation of movement, but recent insights have been made into the roles of the basal ganglia in learning-related plasticity, eye movements, as well as cognitive and emotional functions [10-13]. Disruptions of all of these functions likely contribute to the clinical presentation of HD. In post-mortem evaluation, 80% of HD brains showing atrophy of the frontal lobes and 95% showing atrophy of the caudate nucleus and putamen, collectively known as the striatum [14]. Here we focus on the basic organization of the basal ganglia and effect of striatal dysfunction as it contributes to the motor symptoms of HD. Information from the cortex projects to the striatum (caudate nucleus and putamen) activating medium spiny neurons (MSNs) [15]. There are two populations of MSNs: neurons expressing D1 dopamine receptors, substance P, and dynorphin, and neurons expressing D2 dopamine receptors and met-enkephalin [16, 17]. D1-expressing MSNs are part of the direct pathway to initiate movement, whereas D2-expressing MSNs are part of the indirect pathway that inhibits movement. To initiate movement, glutamatergic cortical input excites D1-expressing MSNs which project to the globus pallidus internal segment (GP_i). Neurons in the GP_i then project to the thalamus. The final connection is excitatory from the thalamus back to the cortex, completing the direct pathway [18] (Fig. 1-1 B). The indirect pathway begins with input from the cortex to D2-expressing MSNs (Fig. 1-1 A). These neurons project to the globus pallidus external segment (GP_e) inhibiting neurons that project to the subthalamic nucleus (STN) [18]. Neurons from the STN project to the substantia nigra pars reticulata (SN_r) which projects to the thalamus. The final connection is from the

thalamus to the cortex. Normally, the thalamus is inhibited by the GP_i/SN_r, resulting in no involuntary movements. Neurons of the cortex, STN, and thalamus release glutamate and are excitatory while neurons of the striatum, GP_e, GP_i, and SN_r release the inhibitory neurotransmitter, GABA. Neurons from the substantia nigra pars compacta (SN_c) project to MSNs in the striatum and release dopamine (DA). D1 and D2 receptors respond differently to DA: MSNs with D1 receptors are stimulated by DA and MSNs with D2 receptors are inhibited by DA.

To appreciate the function of the basal ganglia, it is useful to compare and contrast Huntington's disease with Parkinson's disease. These two diseases affect different cell populations within the basal ganglia, resulting in very different clinical pictures. In HD, early motor symptoms primarily consist of involuntary movements of the hand and feet, manifesting as chorea and incoordination [6]. The neurons most susceptible to the toxic effects of mutant huntingtin are the met-enkephalin-expressing D2 medium spiny neurons in the striatum that project to the GP_e [19, 20]. Loss of these cells results in disinhibition of the thalamus and a decrease in activity of the indirect pathway, resulting in involuntary movements such as chorea [21]. As HD progresses, D1 MSNs are also lost, decreasing activity of the direct pathway. In late stage HD, patients may display hypokinesia or hyperkinesia depending on the balance of direct versus indirect pathway activation [21].

Parkinson's disease (PD) is a neurodegenerative disease caused by a loss of dopaminergic cells from the substantia nigra pars compacta [22]. Whereas HD patients display increased involuntary movements, the clinical characteristics of PD include rigidity, akinesia, postural instability, a flexed posture, and a tremor at rest [23]. Two theories exist to describe the

pathophysiology of PD: the GP_i rate theory and the oscillator theory. The GP_i theory postulates that a loss of excitatory SN_c input of striatal D1 MSNs result in a decreased activity of the striatal input to the GP_i. This increases GP_i inhibitory effect on the thalamus and therefore also the motor cortex to impede the initiation of movement. This reduction in activity of the direct pathway and imbalance with the indirect pathway is opposite of the pattern seen in HD. The second theory of basal ganglia dysfunction in PD involves synchronized firing of neurons between the basal ganglia nuclei and cortex, so-called oscillations. Studies in PD patients with deep brain stimulation implants have revealed different oscillating patterns between the treated and untreated states [24, 25]. However, it remains unclear whether oscillations in the basal ganglia occur in the non-diseased state. The presence of pathologic changes in oscillations could also play a role in other movement disorders of the basal ganglia including HD. In fact, a difference in oscillations between normal and R6/1 mice (a mouse model of HD) have been described [26]. Regardless of the mechanism behind the basal ganglia dysfunction in movement disorders, it is clear that differential activity of D1 and D2 MSNs result in contrasting diseases. Decreased activity of D2 MSNs projecting to the GP_e results in the increased motor activity seen in HD, while decreased activity of D1 MSNs and increased activity of D2 neurons results in impeded motor initiation seen in PD.

4. The impact of Huntington's disease

HD patients face additional hardships coping with their disease. There is significant impact on their families and loved ones. As symptoms increase in severity, HD patients become unable to work or participate in activities they enjoy, resulting in a dramatic change in lifestyle.

Unable to drive, patients become increasingly dependent on caregivers for transport to frequent physician visits. The children of HD patients are faced with the decision of whether to undergo genetic testing to determine if they have inherited the incurable disease. Near the end of the disease, HD patients require full time care provided by nursing home facilities with an average cost for a semi-private room of $75,405 annually according to the 2013 Genworth Cost of Care Survey [27]. This value represents a fraction of the financial impact of HD when taking into account lost years of employment, the cost of medication, health care visits, and medical complications. The prevalence of HD is 4-10 per 100,000 people in the western world [7]. Many more are at risk for developing the disease. HD touches millions of people each year.

5. Current treatments

There is neither a cure for HD nor is there a way to slow its progression. The current treatments are based on symptom management. For chorea, there are benzodiazepines and dopamine depleting agents. Myoclonus, which is described as sudden involuntary muscle contractions, is treated with benzodiazepines and [7]. In Juvenile HD, patients receive levodopa for rigidity, muscle relaxants for spasticity, and antipsychotics for psychosis, irritability and chorea. To treat depression, anxiety, and obsessive compulsive behavior patients are often prescribed selective serotonin reuptake inhibitors (SSRIs), and for manic symptoms patients can take mood stabilizers and anticonvulsants [7]. Patients are often given hypnotics to improve sleep wake cycles. Clearly, the medication list can become quite long and with that organizational and financial challenges. Patients and their providers must seek balance between

benefit gain from a given medication and the side effect profile. Furthermore, none of these medications have the ability to alter the course of the disease.

A number of dietary supplements have demonstrated neuroprotective properties in cell culture or animal models. These include Coenzyme Q_{10}, nicotinamide, and creatine [28-32]. These supplements are thought to delay the onset and slow progression of the disease by increasing the ability for neurons to withstand toxic insults. Although these have shown benefit in the laboratory, their effectiveness in human patients has yet to be determined. Creatine is currently in clinical trials for Parkinson's disease and Huntington's disease [32].

B. The functions of huntingtin

1. Huntingtin is a conserved gene that is essential for development

Since the discovery of the huntingtin gene in 1993, much has been uncovered about its evolution and function [1]. The huntingtin gene is an ancient and highly conserved gene, tracing back to the amoeba and sea urchin [33]. The NH_2-terminal portion of the protein, containing the polyQ region, is the most recently evolved. In humans, huntingtin is expressed in all tissues with highest levels in the brain. The function of the polyQ repeat and the relationship between length and function is unclear. A wide variety of polyQ lengths are seen across different organisms. *Drosophila melanogaster* and *Ciona intestinalis*, both invertebrate organisms, do not have a glutamine repeat, whereas mice have a short repeat of 7Q [33].

One vital role of the huntingtin gene is in brain development. Mouse embryos null for huntingtin are nonviable, terminating at embryonic day 8.5 before the formation of the nervous system [34-36]. These embryos exhibit a shortened primitive streak and lack of head folds, indicating a failure of head development [37]. Several studies show that a minimum of 50% huntingtin protein expression is required for proper development. Mice expressing approximately one third the total amount of huntingtin are born with brain structure abnormalities and die shortly after birth [38]. Three independent groups created mice with "inactivated" huntingtin genes [34-36]. Two of the three groups found that mice with a single copy of huntingtin develop normally and were indistinguishable from their wild type (WT) littermates [34, 35]. Mice in the third study expressed one full length huntingtin and one truncated huntingtin protein and were found to exhibit behavioral and cognitive abnormalities [36]. The discrepancy in results could be related to the presence of a 20kDa truncated huntingtin protein in the latter study whereas the first two studies did not express truncated proteins. The implication from the first two studies is that in mice, having one functioning huntingtin allele is sufficient for normal anatomical development meaning that HD is caused not by a loss of function, but by the mutant allele's gain-of-function toxicity. Interestingly, this theory is supported by the third study which found that by leaving a 20kDA truncated huntingtin protein, the mice were found to possess behavioral abnormalities indicating a functional deficit.

Findings in human patients support this conclusion as patients with a single mutant huntingtin allele are born and develop normally compared with their siblings and peers until the onset of the disease as determined by the CAG repeat length. Furthermore, patients homozygous for mutant huntingtin (e.g. containing two mutant huntingtin alleles and completely lacking a normal huntingtin allele) are initially indistinguishable from patients heterozygous for the mutant

allele or those unaffected by the disease[39, 40]. This indicates that either huntingtin in humans is completely different from mouse and is not necessary for development or, more likely, that the mutant form of huntingtin retains its normal function in development. Caution should be used in describing development in HD patients as "normal" as there is preliminary evidence that presymptomatic children (ages 7-18) with a single HD gene containing a moderate expansion number (<60) may have slight changes in brain structure as measured by functional MRI [41]. In general, the accepted theory is that the CAG expansion confers upon huntingtin a deleterious gain-of-function mutation, but the effect of moderate or mild loss of function remains an important factor in the treatment of the disease.

2. Huntingtin has several protein binding domains

Huntingtin is a large protein of 348 kDa found predominantly in the cytoplasm [42]. It contains conserved domains that are important for interactions with other proteins, known as HEAT repeats (named for four of the proteins that it is found in: huntingtin, elongation factor 3 (EF3), protein phosphatase 2A (PP2A), and mammalian target of rapamycin 1 (mTOR1)) [43]. The polyQ region is also important for allowing huntingtin proteins to form homodimers via a polar zipper structure [44]. Not only does this enable huntingtin to bind to itself, but also allows it to bind other proteins with polyQ regions including transcription factors such as CREB-binding protein (CBP), TBP-associated factor 4 (TAF4), tumor protein 53 (TP53), and specificity protein 1 (Sp1) [43]. The polyQ stretch confers a degree of flexibility to the structure of huntingtin which has been shown to adopt multiple conformations by crystal structure [45].

The flexibility and presence of multiple protein binding domains presents the possibility that huntingtin is a mediator or scaffold that brings proteins closer together and facilitate interactions.

Although most huntingtin protein is found in the cytoplasm, there is evidence that huntingtin could play a role in the nucleus as well. The COOH-terminal portion of huntingtin contains a nuclear localization signal and a nuclear export signal, and the first 17 amino acids in the NH_2-terminal part of the protein, N17 region, bind to the nuclear pore protein, TPR (translocated promoter region) [2, 46]. These properties enable normal huntingtin to enter and exit the nucleus, potentially transporting bound molecules across the nuclear membrane. In contrast to normal huntingtin, after entering the nucleus, the mutant protein loses its ability to exit the nucleus causing an imbalance of import versus export of mutant huntingtin [46]. This results in its accumulation in the nuclear compartment [46]. In addition to binding TPR, the N17 region also binds to mitochondria and is co-localized with the Golgi and endoplasmic reticulum [47, 48].

3. Huntingtin is a neuroprotective protein

Huntingtin has several neuroprotective properties. Overexpression of normal huntingtin in cell culture increases survival following toxic insults, and in mouse models, huntingtin overexpression prevents apoptosis from excitotoxic chemicals [49, 50]. Inactivation of normal huntingtin in adult mice results in apoptotic cell death, an increase in severely abnormal behaviors characteristic of HD mice, and decreased lifespan [51]. Overexpression of normal huntingtin decreases the toxic effects of mutant huntingtin in cell culture [52]. One way in which

it might be neuroprotective is through the regulation and transport of brain derived neurotrophic factor (BDNF). BDNF is important for the survival of striatal neurons [53]. In cortical neurons, normal huntingtin facilitates the expression of BDNF [54]. In contrast, mutant huntingtin results in decreased BDNF transcription. There is reduced BDNF vesicle transport in medium spiny neurons (MSNs) (Fig. 1-2 J) [55]. In the striatum, huntingtin acts as a scaffold, binding vesicles containing BDNF to HAP1 (huntingtin associated protein 1), which interacts with dynactin to transport BDNF vesicles [55]. In neurons, huntingtin overexpression increases BDNF gene transcription by inhibiting the neuron restrictive silencing element (NRSE) and improves the transport of BDNF [56]. It is possible that a loss of normal huntingtin function could result in increased susceptibility to toxic events. Transgenic mice express the human huntingtin mutant gene with 128 CAG repeats (YAC128) expressed on a null background (no mouse huntingtin), have a more severe behavioral phenotype and shortened lifespan compared with YAC128 mice with normal mouse huntingtin [57]. In *Drosophila* expressing human huntingtin exon1 with 93 CAG repeats, removing the endogenous huntingtin gene accelerates neurodegeneration [58]. In summary, BDNF is critical for neuronal health and huntingtin plays direct roles in regulating its expression and transport.

In addition to roles in intracellular transport, huntingtin regulates synaptic activity through exocytosis and endocytosis at synaptic terminals. Endocytic recycling is important for cell health and membrane homeostasis. It is the process by which internalized receptors are returned to the cell surface for reuse. Huntingtin co-localized with Rab11, a protein that regulates vesicle formation, and decreases Rab11 activation, and mutant huntingtin binding to Rab11 results in endosomes with abnormal morphology and slowed recycling [59].

What is the role of the polyQ repeat? There is an inverse relationship between length of the polyQ in huntingtin and the amount of ATP in the cell, which reflects the energy status of the cell [60]. Mice with a deletion of the polyQ stretch develop normally with no gross abnormalities [61]. However, there are transient deficits on tests of learning and memory and a very subtle effect on motor skill on the accelerating rotarod test. Fibroblasts from these mice indicate an increased ATP energy status [61]. In addition, brain tissues from these mice have increased levels of microtubule-associated protein 1 light chain 3-II (MAP1 LC3-II also known as LC3-II), a marker for increased activation of the autophagy degradation pathway. Mice homozygous for the polyQ deletion live longer than WT mice [61]. This last finding suggests that the polyQ region in huntingtin plays a role in the regulation of a basal level of autophagy possibly through its interaction with autophagic vesicles [62].

C. Pathways of cell damage caused by mutant huntingtin

1. Mutant huntingtin mediates excitotoxic damage to neurons

In addition to the loss of neuroprotective BDNF, there is evidence for increased excitotoxicity caused by dysfunction at the corticostriatal synapse. Excitotoxicity is defined as excessive activation of glutamate and N-methyl-D-aspartate (NMDA) receptors leading to cell death. Injection of glutamate agonists into rat striatum results in the same pattern of cell loss as in HD [63]. Mouse models with full length human huntingtin have increased glutamate release and increased susceptibility to excitotoxicity [64]. There are electrophysiological findings that

indicate increased NMDAR sensitivity to NMDA and increased NMDA currents in striatal neurons of mutant huntingtin mice with 100Q [65, 66].

In addition to increased activation of glutamate receptors, in human HD post-mortem tissue, there is a reduced uptake of [^{3}H]glutamate compared with controls [67]. Glutamate uptake is mediated by the involvement of glial cells in regulating sensitivity to excitotoxicity revealing a non-cell autonomous contribution to HD pathogenesis. Expression of mutant huntingtin in astrocytes resulted in decreased expression of glutamate transporters and caused neuronal dysfunction, demonstrating the importance of glia in protection against excitotoxic damage to neurons [68].

2. Aberrant binding by mutant huntingtin results in transcriptional dysregulation

Mutant huntingtin disrupts the function of several transcription factors (Fig. 1-2 B, H). Specifically, mutant huntingtin binds transcriptional activators Sp1 and TATA binding associated factor 130 ($TAF_{II}130$) and the transcriptional coactivator CBP resulting in general transcriptional repression [43]. Affected genes include those for neurotransmitter receptors, synaptic transmission, cytoskeletal proteins, intracellular signaling and calcium homeostasis. Mutant huntingtin also binds the transcription machinery, which may globally reduce transcription [69]. By binding to CBP, mutant huntingtin decreases histone acetyltransferase (HAT) activities globally, causing a reduction in histone acetylation, a modification that opens chromatin structure allowing genes to be more easily accessed for transcription with the end result of decreasing transcription [70]. In addition to changing transcription and chromatin

structure, mutant huntingtin interacts with argonaute 2 (Ago2) resulting in fewer P-bodies compared with normal huntingtin [71]. Destabilization of P-bodies could increase the level of miRNAs in the cells and act to repress gene expression.

Aggregation of mutant huntingtin could reduce its ability to bind transcriptional activators and machinery proteins, and aggregate formation could thus protect cells from transcriptional dysregulation [72]. In cell culture, modification of mutant huntingtin exon 1 by small ubiquitin-like modifier (SUMO) decreases aggregation of mutant huntingtin and increases transcriptional repression, suggesting that sequestration of mutant huntingtin in aggregates can reverse its effect on transcription [73].

3. Mutant huntingtin and mitochondrial dysfunction

Mitochondrial dysfunction plays several roles in the toxicity of HD (Fig. 1-2 I). Mutant huntingtin impairs energy metabolism, increases the generation of free radicals, and disrupts calcium handling [74-76]. Mutant huntingtin binds to mitochondria, thereby impairing the transport of mitochondria in primary neuron cultures and altering the ultrastructure of the organelle [77]. Transport of mitochondria to cell processes is important in providing adenosine triphosphate (ATP) throughout the cell. Mitochondrial dysfunction can be seen in various imaging techniques in the brains of HD patients, specifically in the basal ganglia, cortex and thalamus [74]. Mitochondrial activity may be especially important for striatal cells. Mice with impaired mitochondrial function exhibit striatal degeneration and hyperkinetic movements [78, 79]. Mitochondrial impairment is not specific to neurons, although neurons might be more

susceptible to it. Altered mitochondrial calcium handling is seen in lymphoblasts from HD patients and skeletal muscle in a mouse model of HD [76].

4. Mutant huntingtin forms intracellular aggregates and inclusion bodies

In HD, huntingtin-containing aggregates are present in the medium spiny neurons of the striatum and neurons of all cortical layers [80]. There are two forms of aggregates distinguishable by light microscopy. One form is the neuronal intranuclear inclusion body, subsequently referred to as an inclusion body, which is spherical, ovoid, or elliptical in shape and found in the nucleus (Fig. 1-2 G). The majority of cells contain only one inclusion body per nucleus, but occasionally 2 or 3 can be found. The second form is cytoplasmic aggregates, which are spherical or oblong in shape, sometimes with extensions and within dystrophic neurites (Fig. 1-2 E, F) [80]. These two types of aggregates are found in different distribution in juvenile and adult HD. Inclusion bodies are found with greater frequency in juvenile HD than in adult HD and are distributed in the cortex [80]. Cytoplasmic aggregates are the prominent feature in adult HD, and these are also primarily distributed in the cortex.

Cleavage of huntingtin is an important process for the development of aggregates (Fig. 1-2 A). Both inclusion bodies and cytoplasmic aggregates contain NH_2-terminal fragments and do not stain with an antibody to an internal epitope used to detect larger fragments or full-length huntingtin [80]. Both normal and mutant huntingtin are cleaved by caspases and other unknown enzymes into multiple fragments [81]. Different fragments have different effects on the

formation of aggregates. For example, in cell culture, cleavage at arginine 167, creating a fragment known as cp-2, which decreases aggregation and increases toxicity [82].

There are opposing views on the role of mutant huntingtin aggregates regarding whether they are protective or toxic to neurons. For this discussion, we will consider aggregates and inclusion bodies to be equivalent as intracellular structures containing mutant huntingtin protein as well as other proteins. The first case holds that aggregates are protective against cellular damage by binding and removing toxic huntingtin monomers or oligomers from distribution in the cytosol. In HD post-mortem tissue, the neurons that are initially spared are those containing inclusion bodies and aggregates, and conversely, MSNs, the cells most susceptible to toxic effects of mutant huntingtin, do not show aggregates [83, 84]. One study followed the survival of cultured neurons expressing huntingtin exon1 fused with GFP and found a correlation between huntingtin inclusion formation and increased survival of neurons [85]. Additionally, it was found that sumoylation of huntingtin which decreases aggregation also increases cytotoxicity [86]. Alternatively, aggregates may contribute to cellular dysfunction by sequestering important cellular proteins out of the cytoplasm including transcription factors, motor proteins, proteasomal subunits and chaperone proteins [87-90]. Loss of these proteins and complexes could potentially deplete the neurons of their vital functions. Proteasome and transcriptional impairment occurs independent of aggregate formation [91-93]. Several studies found that silencing of molecular chaperones such as prefoldin or cytosolic chaperonin (CCT/TriC) result in increased aggregate formation and cell death [94-96].

Strict definitions for aggregates and inclusion bodies have yet to be adopted and it is possible that all aggregates are not equal [97]. The aggregate population in the striatum of R6/2

displayed more cytotoxicity than aggregates from the hippocampus and cerebellum [97]. The possibility of multiple conformations and contents of aggregates conferring differing toxicities could explain seemingly contradictory findings regarding the properties of huntingtin aggregates. As was previously discussed, huntingtin contains nuclear import and export signals and the polyQ expansion impairs its ability to export from the nucleus, and a potential distinction exists between nuclear and cytoplasmic aggregates/inclusions [46]. Whether aggregates are protective or detrimental or whether different aggregate conformations affect disease progression has yet to be determined. Once it is clear what role aggregates play, a potential therapy could be to alter aggregation and inclusion body formation.

5. Is the damage caused by mutant huntingtin permanent or reversible?

There is evidence supporting that the cellular damage inflicted by mutant huntingtin is reversible. In 2000, a conditional mouse model of HD was created with mutant huntingtin expression under tetracycline-regulated control [51]. After 18 weeks of transgene expression, a point at which neuropathology and motor dysfunction was evident, the mutant huntingtin transgene expression was repressed. After having the mutant transgene repressed for 16 weeks, the mice demonstrating less clasping behavior, there was reversal of reactive astrocyte gliosis, increased size of the striatum, and decreased nuclear huntingtin staining [51]. The observation that the HD phenotype and pathology are reversible in mice demonstrates that cell damage incurred from mutant huntingtin toxicity, if reversed prior to neuronal death, is not permanent.

D. The processing and degradation of mutant huntingtin

1. Post-translational modifications and cleavage alter toxicity of mutant huntingtin

There are many post-translational modifications that alter the toxicity and activity of huntingtin including palmitoylation, phosphorylation, ubiquitination, and sumoylation [7]. Palmitoylation of cysteine 214 in huntingtin aids its association with membranes for vesicle transport, and this modification is impaired by the polyQ expansion leading to decreased membrane binding [98]. Phosphorylation occurs at several different positions, mostly in the NH_2-terminal 17 amino acids and they are generally protective [99-101].

Rhes (Ras homolog enriched in the striatum) is a small G protein highly expressed in the striatum that functions in the sumoylation of huntingtin [102, 103]. Sumoylation of mutant huntingtin decreases aggregation and increases the concentration of soluble mutant huntingtin [86]. This modification and the down-stream effects result in an increase in toxicity and transcriptional dysregulation [73, 86].

Acetylation occurs on one site, lysine 444 of mutant huntingtin [104]. In *Caenorhabditis elegans*, increasing acetylation at this site targets mutant huntingtin to the autophagy-lysosomal system, while in experiments using mice injected with lentiviral expressed human huntingtin fragment with 72Q repeats, blocking acetylation resulted in accumulation of mutant huntingtin protein [104].

Caspases are proteases well-known for their apoptotic role in programmed cell death, however they are also implicated in non-cell death pathways such as synaptic plasticity and learning [105]. There are five predicted caspase cleavage sites in huntingtin, 3 sites cleaved by

caspases -2, -3, and -6, and two silent sites [81]. NH_2-terminal mutant huntingtin fragments have been linked to increased toxicity as they are preferentially found in affected neurons and increase susceptibility cells to death compared with full-length huntingtin [106, 107]. Preventing the cleavage of mutant huntingtin is a potential strategy for modifying disease progression. Completely blocking caspase cleavage was found to be protective in cells which could also have the effect of blocking cell death pathway [108]. Many studies have investigated the role of caspase cleavage using various mouse models and methods for inactivating either the caspase or the caspase cleavage site. R6/2 mice expressing dominant negative caspase-1 resulted in delayed onset of disease and extended survival [109]. In a YAC72 mice, dominant negative caspases -2, -6, and -7 were found to be protective while -3, -8, and -9 had no effect [110]. Another study inactivated the cleavage sites for caspase -3 and -6 in YAC 128 mice and came to consistent conclusion that blocking caspase 6 cleavage is protective, while caspase-3 had no effect [111]. However, a third study looked at 150Q huntingtin knock-in mice null for caspase-6 which did not exhibit protection from disease phenotype [112]. In summary, there is evidence for a role of caspases -1, -2, -6, and -7 in the progression of neuropathology especially caspases -2 and -6 which have known cleavage sites within the huntingtin gene.

Similar to caspases, increased levels of calpain are found in HD brains [113]. Calpain activation is caused by disturbances in Ca^{2+} homeostasis resulting from excitotoxicity or mitochondrial dysfunction. Calpains preferentially cleave mutant huntingtin over normal huntingtin and cleave in the same amino-terminal region as the caspase cleavage sites [81]. Aspartic endopeptidases are other enzymes that cleave huntingtin producing two different NH_2-terminal fragments, cp-A (cleaved between amino acids 101-124) and cp-B (cleaved between amino acids 146-214) [114].

2. The role of the ubiquitin-proteasome system in the degradation of mutant huntingtin

The first line of defense in degrading misfolded proteins is the ubiquitin-proteasome system (UPS) (Fig. 1-3 A). The proteasome functions in cells to degrade short lived proteins and damaged or misfolded proteins [115]. E3 ubiquitin ligases add ubiquitin molecules to lysine residues of the protein to target it for delivery to the proteasome. The proteasome is a multi-unit structure in the cytoplasm that unfolds and degrades proteins using a series of proteases and peptidases. When the peptides are released, they are further degraded by aminopeptidases into single amino acids. Not only is the UPS important for degrading damaged proteins, but it plays an important role in cell homeostasis [115]. The UPS may play a role in synapse function and plasticity and may also regulate cell signaling by degrading short lived proteins [116].

The expanded polyQ present in mutant huntingtin causes it to misfold and interact with E3 ubiquitin ligases, including Hrd1, E6-AP, E2-25K, Ube3a, and CHIP (C terminus of Hsp70-interacting protein) to ubiquitinate lysine residues 6, 9, and 15, thereby targeting it to the proteasome [73, 117-120]. Normal and mutant huntingtin can also be targeted to the proteasome and lysosome by phosphorylation by the inflammatory kinase, IKK, on serines 13 and 16 [99]. The proteasome can only degrade unfolded proteins, rendering it unable to degrade the fibrillar or aggregated forms of huntingtin. The proteasome is also inefficient at degrading polyQ tracts and *in vitro* studies show that the proteasome releases them intact [121]. This potentially results in expanded polyQ peptides that are free in the cytoplasm, able to contribute to aggregation and binding of other polyQ containing proteins. A single aminopeptidase, puromycin sensitive aminopeptidase (PSA) is the only identified aminopeptidase able to efficiently degrade polyQ

peptides [122]. Through its function of degrading polyQ peptides it could play a role in the degradation of both normal and mutant huntingtin and be a potential disease modifier. In fact, PSA overexpression reduces inclusion formation in cells transfected with mutant huntingtin[123]. Operating on the theory that inclusion bodies represent an accumulation of misfolded mutant proteins toxic to the cell, a reduction in inclusion number would represent decreased disease burden within the cell.

Not only does the proteasome fail to effectively degrade mutant huntingtin, but its function is impaired by the mutant protein (Fig. 1-2 D) [124]. It has been proposed that proteasomal dysfunction is caused by mutant huntingtin before the appearance of inclusion bodies. From this perspective, inclusion bodies may offer protection to the cell by removing the toxic fibrillar huntingtin products that interfere with proteasomal degradation.

In addition to impairment of proteasome function, mutant huntingtin aggregates sequester the proteasome *in vitro* [125]. There are two interpretations of this. One is that co-localization of proteasomal subunits with aggregates represents aberrant binding of proteasomal subunits which could alter their ability to function normally by altering their cell localization and distribution. Another interpretation is that the bound proteasomes are attempting to degrade aggregated protein. Primary neuronal cell cultures from a conditional mouse model of Huntington's disease have been used to study inclusion body formation and dissolution [126]. These cells develop inclusions within two days when the mutant allele is expressed and they disappear five days after the allele is suppressed [126]. In primary neuronal cell culture, this dissolution of aggregates is abolished with the administration of a proteasomal inhibitor, suggesting that the proteasome is functioning in some degree to degrade proteins from the aggregates [126].

3. The role of the autophagy-lysosome system in the degradation of mutant huntingtin

Autophagy is the process by which organelles and the majority of proteins from the cytosol are targeted for degradation (Fig. 1-3 B) [127]. A portion of cytosol is enclosed by a double membrane called an autophagosome [127]. This structure fuses with a lysosome for the degradation of the proteins by acidic hydrolases. Mice that lack Atg7, a gene essential for autophagy in neurons, develop ubiquitin-positive aggregates [128]. Thus, autophagy is vitally important for the prevention of inclusion bodies.

In HD patients, aggregates of mutant huntingtin bind and sequester mTOR (mammalian target of rapamycin), a negative regulator of autophagy [129]. Removal of mTOR activity in the cell increases general autophagy [130]. Mice with one huntingtin allele containing 200 CAG repeats have increased markers for autophagy early in the course of the disease [131]. Even though there may be increased activation of autophagic vacuoles, this does not necessarily mean that autophagosomes are able to complete the process of degradation. Mutant huntingtin has been shown to interact with autophagolysosome membrane resulting in a failure to enclose cytosolic components for degradation [132]. Regardless of the status of autophagy in Huntington's disease, its importance in degradation of mutant huntingtin is indisputable. In cell culture, blocking autophagy increases soluble huntingtin, aggregates, and toxicity [133]. Increasing autophagy decreases accumulation of mutant huntingtin in cell culture and decreases aggregates and improves behavior in mice [129, 134-136].

E. Mammalian models of Huntington's disease

1. Chemical models of Huntington's disease

The initial animal models of Huntington's disease were chemical models that involved injections of neurotoxins into the striatum. The result is a model of excitotoxic cell death. Kainic and quinolinic acids are glutamate agonists that result in striatal-specific neurodegeneration [2]. Injection of 3-nitropropionic acid and malonic acid are mitochondrial toxins, and mice injected with these agents have striatal neuron loss and replicate behavioral aspects of HD [137]. These models represent Huntington's disease because they affect the striatum more than other structures; however, they are not useful in the study the mechanism of mutant huntingtin toxicity. Chemical models of HD can be used to study modulators that may be neuroprotective.

2. Transgenic mouse models with a human huntingtin fragment.

Table 1-1 is a comparison of commonly used transgenic and knock-in mouse models of HD. The first transgenic mouse model of Huntington's disease was the R6/2 line. R6/2 mice contain a fragment of human huntingtin consisting of a single copy of exon 1 with 141-157 CAG repeats including the human huntingtin promoter, and it is expressed at 75% of the endogenous level of huntingtin mRNA [138]. The onset of HD symptoms is early and the progression rapid. In R6/2 mice, by five to six weeks of age there are abnormalities on the raised-beam test and rotarod test and decreases in brain size and volume [138]. Inclusions increase in size and number with the progression of the disease. There are decreases in D1 and D2 dopamine receptors in the striatum at 8 weeks, and by 12 weeks of age there is cell death of medium spiny neurons [138].

R6/2 mice die between 12-15 weeks of age [138]. The R6/2 mouse model exhibits a rapid progression of disease and is useful in screening potential therapeutics and modifiers of disease because the outcomes can be quickly measured. Development of disease is too rapid for a careful analysis of the progression of pathology and avenues of cellular dysfunction. Another drawback to this model for studying mechanism of huntingtin toxicity is that it expresses a fragment of huntingtin, and it is expressed in addition to the endogenous mouse huntingtin.

A second type of transgenic mouse expresses the first 171 amino acids of the huntingtin protein with 82Q or 18Q repeats, known as N171-82Q and N171-18Q [139]. It is driven by the mouse prion promoter that is only expressed in neurons with expression level that is less than endogenous huntingtin [139]. N171-18Q mice were indistinguishable from WT mice, however N171-82Q mice develop clasping and rotarod deficits at 15 weeks [139]. N171-82Q mice display nuclear inclusions in the cortex, hippocampus, amygdala and striatum, and decrease brain size (due to atrophy), and their lifespan is 10-24 weeks of age [139]. With a later onset compared with the R6/2 line, the benefit of N171-82Q mice is that the progression of HD can be studied, and similar to the R6/2 model demonstrates that the NH_2-terminal fragment of mutant huntingtin is sufficient to replicate many aspects of the disease. A limitation of this model is that, like R6/2 mice, the expression of mutant huntingtin fragment results in an increase in total huntingtin combined with endogenous mouse huntingtin.

3. Transgenic mouse models with full length human huntingtin

Several transgenic HD mouse lines have been made using yeast artificial chromosome (YAC) constructs containing a full length human huntingtin gene. The huntingtin transgene includes upstream and downstream sequences and all regulatory elements. Four strains of YAC mice were created with different CAG repeat lengths: 18, 46, 72, and 128 repeats [140]. The YAC18 construct represents the normal version of human huntingtin and were indistinguishable from WT mice. All four lines have increased total amount of huntingtin, with the transgene expressing approximately 33% -50% compared with endogenous huntingtin. YAC46 mice exhibit eletrophysiological abnormalities compared with YAC18 mice, but lack an increase in nuclear staining or other behavioral or pathological findings. YAC72 mice display hyperactivity at 7 months, and an increased number of nuclear staining cells [140]. YAC72 mice have microaggregates and a few macroaggregates, striatal-specific neuronal degeneration by 12 months of age, but lack the development of nuclear inclusion bodies [140]. YAC128 are the most commonly used YAC HD model. These mice display increased locomotor activity and rotarod deficits at 3 months, and then decreased activity at 12 months. In YAC128 mice, there is nuclear staining for mutant huntingtin throughout the striatum by 12 months of age, but no inclusions are apparent until 18 months of age [64]. YAC128 mice show age-dependent striatal neurodegeneration beginning at 9 months, however their lifespan is comparable to WT mice [64]. Benefits of this model are that human huntingtin expression is regulated by the human promoter, however a limitation of this model is that the total huntingtin level in these mice is increased. That YAC72 and YAC128 mice develop neurodegeneration prior to the development of inclusion bodies suggests that the inclusion bodies are not the cause of neuronal dysfunction and death in this model of HD. The observation that YAC46 mice do not develop the disease,

despite the electrophysiological differences from WT, could suggest that mice require a longer polyQ length to develop toxicity, or that development of HD is limited by their short lifespan.

A second full length human huntingtin transgenic approach uses a bacterial artificial chromosome (BAC). BACHD mice contain the whole human huntingtin gene, containing 97 mixed CAG and CAA repeats, encoding polyQ, and 20 kb flanking sequences at the 5′ and 3′ ends [141]. The BACHD transgene also has two lox P sites to excise exon 1 for conditional inactivation. The transgene is integrated five times into the genome, and is overexpressed, producing three times the endogenous amount of mRNA and about twice the endogenous protein. BACHD mice have progressive deficits on the rotarod and by 12 months a 32% decrease in striatal volume is present due to decreased cell volume, rather than from a change in neuron number [141]. Huntingtin aggregates can be found starting at 12 months of age, and unlike other mouse models of HD where the majority of aggregates and inclusions are found in the striatum, BACHD mice form aggregates primarily within the cortex [141]. This pattern of aggregate distribution is consistent with adult human HD where the aggregates are primarily cytoplasmic and located within cortical neurons. The importance of using transgenic mice expressing full-length human huntingtin is for studies of RNAi targeting the human gene.

4. Knock-in models of Huntington's disease

Knock-in mice have CAG repeats inserted into the endogenous mouse huntingtin gene (Hdh). These animals express endogenous levels of huntingtin unlike transgenic mouse models which contain additional copies of mutant huntingtin gene. Another benefit of this model over

transgenic models is that it eliminates the possibility of altering other genes by the insertion of DNA elsewhere in the mouse genome. Knock-in mice with 48Q repeats did not result in an HD phenotype, but repeat lengths of 90Q and 109Q resulted in inclusion and aggregate formation after 68 weeks without behavioral abnormalities [142, 143]. Mice with 140Q and 150Q show characteristics of HD and behavior and pathology with an earlier onset than the 90Q and 109Q mice, and these are commonly used as mouse models to study HD [144, 145].

One knock-in model with 150 CAG repeats exhibits a late onset and slowly progressing phenotype [146]. Homozygous 150Q mice display aggregates beginning at 9 months of age, and at 2 years of age display weight loss, decreased activity, rotarod deficits, and clasping [146]. Heterozygous mice were tested alongside the homozygous mice and displayed a more moderate phenotype [146].

Another widely used knock-in mouse model contains 140Q repeats and part of the human huntingtin first intron to replace the corresponding mouse sequences [145]. 140Q knock-in mice demonstrate early and progressive behavioral defects, with an increase in rearing behavior at 1 month and decrease in rearing behavior from 2 months onward [145]. Locomotor activity is also decreased and gait analysis reveals smaller stride length at one year [145]. Intranuclear inclusions are first noted in the striatum at four months and progressively grow in size and number [145]. 140Q mice display a slow progression of disease with moderate behavioral findings, notably an absence of tremor, clasping, or weight loss after one year [145]. One benefit of having a slow onset of disease is that 140Q mice can be used to study early disease pathogenesis and to test pre-symptomatic interventions [145, 147].

In mouse models, as in patients, disease onset is dependent on the length of the CAG repeat [148]. Unlike humans, mice tolerate much higher repeat number before manifesting behavioral and pathological findings. Knock-in mice with 50 CAG repeats, a length that would result in HD in patients, exhibit no detectable behavioral or pathological abnormalities [38]. While it is reassuring that in general, greater number of CAG repeats result in earlier disease onset in humans and murine models, the threshold for disease onset is dramatically different between mice and human. One possible explanation for this discrepancy is that there is insufficient time for the mutant gene products to accumulate within neurons of mice due to their short lifetime. It is also possible that differences in the sequences surrounding the repeat expansion, i.e. the first exon, modify the toxicity of the protein through conformation or stability. In knock-in mouse models, the Hdh140Q knock-in mice contain a portion of the human exon 1 and exhibit an earlier onset of both behavioral abnormalities and neuropathology than the Hdh150Q knock-in mice which has a completely murine exon 1 [145, 146]. The value in a slower progressing mouse model of HD is that it is believed to more closely represent the pathophysiology relevant to understanding the disease process.

5. Other animal models of HD

Rat models have several benefits over mouse models of disease. More behavioral and imaging tests are available for rats. One rat model of HD is a lentiviral delivered NH_2-terminal huntingtin fragment with 18, 44, 66, or 82 CAG repeats [149]. The expression of the huntingtin fragment is controlled by either the CMV (cytomegalovirus) or PGK (phosphoglycerate kinase) ubiquitous promoters [149]. Mice injected with vectors containing 44-82 repeats develop

aggregates and loss of DARPP-32 staining in a repeat length-dependent manner. Huntingtin expressed by the CMV promoter (a lower expressing promoter) results in fewer aggregates than with the PGK promoter. The second model is a transgenic rat that contains a 1.9kb fragment with 51Q repeats regulated by the rat huntingtin promoter [150]. At two months of age, these rats exhibit anxiety and cognitive decline compared with WT rats, and have motor deficits on the rotarod at 10 months, and striatal aggregates and inclusion bodies at 12 months of age [150]. The third rat model of HD contains a bacterial artificial chromosome (BAC) insertion of human huntingtin with 97 CAA/CAG repeats, the same BAC used to make the BAC97 mouse model [141, 151]. BAC97 rats have a single insertion site, with 2.5-4.5 higher expression of the mutant human huntingtin compared to endogenous rat huntingtin. By one month of age, BAC97 rats show deficits on the rotarod, have decreased anxiety and initial hypoactivity [151]. Beginning at 3 months aggregates are found in the cortex, amygdala and hippocampus, with few in the striatum, and aggregates are seen in the neuropil except for the outer layers of the cortex and striatum, where they are located in the nucleus [151].

Larger animals such as pigs, sheep, and non-human primates make good models for HD because the size and anatomy of their brains resemble that of humans. Several large animal models for HD are being characterized. A pig model was created that expressed NH_2-terminal huntingtin fragment (208 amino acids) with 105 glutamine repeats [152]. There was a very low rate of successful embryo transfer (<1-2%) and of four of five live births resulted in early death (1-2 days) with the longest survival greater than 4 months [152]. Unlike murine models, transgenic HD pigs contained apoptotic neurons with the greatest number within the striatum, which recapitulates one aspect human neuropathology and suggests that the pig model share similarities with human disease not found in smaller mammals [152]. A transgenic rhesus

monkey model for HD was created using human exon 1 fragment of huntingtin with 84Q repeats. These monkeys exhibit nuclear and neuropil aggregates, chorea, and dystonia, however these animals survived for less than one month of age [153]. A sheep model expressing full length human huntingtin with 73Q repeats show decreased staining for medium spiny neurons at 7 months of age [154]. While the large size, brain anatomy, and potential lifespan make these large-animal models attractive, their usefulness has been limited by unexpectedly poor viability of the animals.

F. Therapeutic approaches to treating Huntington's disease

1. Strategies to counteract excitotoxicity and increase neuroprotection

One therapeutic approach to treating HD is to reduce excitotoxicity that contributes to cell death. In R6/2 mice, Riluzole, a glutamate antagonist, resulted in an increase in body weight and an increase in survival compared with vehicle-treated R6/2 mice [155]. Riluzole did not show any beneficial effects in HD clinical trials [156]. Lamotrigine, a glutamate antagonist that reversibly inhibits vesicular monoamine transporter type 2 (VMAT2), also showed no positive results in clinical trials [157]. Tetrabenazine is a dopamine pathway inhibitor which is approved to control chorea and has promise in improving function in other areas as well [158]. In YAC128 HD mice, tetrabenazine decreased striatal cell death [159].

Neurons affected by HD have mitochondrial impairment leading to oxidative stress making these cells susceptible to excitotoxicity. Creatine is a potential therapeutic found to be neuroprotective in R6/2 and N171-82Q mouse models of HD possibly by maintaining energy

stability in neurons [30]. In HD patients, creatine prevented some weight loss and increased some scores on cognitive tests [160]. Coenzyme Q_{10} is a cofactor in the electron transport chain within the mitochondria and an antioxidant that has been shown to ameliorate the early behavioral effects of HD in a 140Q knock-in mouse model of HD although no effect was seen in the R6/2 mice [29, 161, 162]. Eicosapentaenoic acid (EPA) is an *n*-3 fatty acid with antioxidant and anti-inflammatory properties [163]. However, the clinical trials thus far have shown no benefit with either coenzyme Q_{10} or EPA [164-166].

Neuroprotection is another approach to help cells function despite the damaging effects of mutant huntingtin, and an approach to improve neuroprotection is to increase BDNF. One method of increasing BDNF is to give an infusion of the protein directly into the cerebrospinal fluid (CSF), by osmotic mini-pump. This was shown to increase the number of enkephalin-positive neurons in R6/1 transgenic mice (similar to R6/2 mice) [167]. Drawbacks for humans include that this delivery system would require permanent access to the CSF that would be prone to infection and inflammation, and the protein has a short half-life, therefore it would have to be given on a frequent or constant basis. A second method to increase BDNF is by viral gene delivery. Adenoviral delivery of BDNF to the striatum of R6/2 mice expressed by a glial-specific promoter, *gfa2*, delayed the behavioral impairment including clasping [168]. The drawbacks to viral delivery of BDNF gene depend on the virus utilized, but could include regulating gene expression, potential inflammation and integration into the genome disrupting expression of other genes. Other methods of increasing BDNF include implantations of mesenchymal stem cells that stably release BDNF and small molecules that can stimulate transcription of BDNF and BDNF receptors [28, 169-171]. BDNF mimetics and small molecule drugs, including SSRIs, memantine, and ampakines are being tested to increase BDNF [2].

2. Strategies to block proteolysis of huntingtin into toxic fragments

As described earlier, the NH_2-terminal huntingtin fragment has been linked to increased toxicity, and blocking caspase cleavage improves cell survival and disease progression in mouse models [106-110]. Minocycline, an antibiotic that inhibits caspase 1 and 3, was shown to improve disease phenotype in R6/2 mice, however the behavioral benefit could not be replicated by another research group [162, 172]. The discrepancies in results from these studies could be influenced by different behavioral procedures, mouse husbandry practices or chow formulation, however a phase II futility study of 114 HD patients found no benefit with minocycline [173].

3. Treatment by increasing gene transcription

Changes in gene transcription are one of the early events in Huntington's disease [174]. Decreased transcription leading to deficits in protein levels of important genes such as D1 and D2 dopamine receptors could contribute to neurodegeneration [175]. Histone deacetylase (HDAC) inhibitors block the de-acetylation of histones, leading to more histone acetylation opening chromatin for increased transcription. There have been mixed findings with HDAC inhibitors in mouse models, and a phase II clinical trial (PHEND-HD) has been completed testing sodium phenylbutyrate, a non-selective HDAC inhibitor, for safety and tolerability in HD patients [176-179]. While HDAC inhibitors alter transcription indirectly by binding an enzyme, another approach is to use compounds that interact with DNA directly. Anthracycline antibiotics bind DNA and were found to normalize nucleosome arrangement and correct chromatin changes

in HD mice in addition to increasing volume of the striatum, increasing survival in R6/2 mice, and increasing distance traveled in open field test (also R6/2 mice), however there are no clinical trials for anthracycline at this time [180].

4. Strategies to disrupt aggregates and increase clearance of mutant protein

Despite the debate over the relative harm or benefit of huntingtin aggregation, several aggregate blockers have been investigated. In animal models, Congo red, a chemical dye, decreased aggregation by blocking polyQ oligomerization. In one study, Congo red improved HD phenotype, but these results could not be replicated [181, 182]. Trehalose blocks inclusion formation to improve R6/2 mice disease phenotype, and Riluzole blocks aggregation in HD animal models [155, 183]. Increasing clearance of misfolded proteins is important for removing the toxic molecules from the cell, and there is evidence that both the ubiquitin-proteasome and autophagy-lysosomal pathways are impaired in HD [121, 124, 132]. In animal models of HD, increasing autophagy by treatment with the antibiotic rapamycin has shown great promise [127]. However this drug is not feasible in humans due to the major side effect of immunosuppression [184].

5. Strategies to reduce mutant huntingtin mRNA

Many possibilities exist to reduce huntingtin mRNA, such as interfering with transcription factor binding to the huntingtin promoter and the use of zinc-finger nucleases to

knock-out the huntingtin gene [185]. Here we focus on the post-transcriptional modulation of huntingtin mRNA levels, specifically gene silencing. There are two main approaches to gene silencing, RNA interference and the use of antisense oligonucleotides. The first approach is to administer double-stranded, short interfering RNA (siRNA) or short hairpin RNAs (shRNA) molecules that utilize the RNAi pathway. These small RNAs specifically target the huntingtin mRNA sequences in the cytoplasm as part of the RNA-induced silencing complex (RISC) [186]. The second method is to administer short DNA molecules known as antisense oligonucleotides (ASOs) to target and cleave mRNA in the nucleus and cytoplasm. The single-stranded ASOs bind to complementary sequences in the nucleus and cytoplasm then the complexes are degraded by the endogenous RNaseH enzyme to cleave target mRNA [187]. The drawbacks of using gene silencing include potential off-target effects and the challenge of delivering to the brain [188, 189].

siRNA has been tested in many animal models by intraparenchymal injection into affected regions of the brain or by intracerebroventriclular (ICV) infusion. In mice, intraparenchymal co-injection of adeno-associated virus (AAV) expressing mutant (100 CAG) exon 1 with cholesterol-conjugated siRNA (cc-siRNA) targeting huntingtin resulted in improved neuropathology and an improved behavior phenotype compared to mice injected with control cc-siRNA [190]. ASOs have been tested by intraparenchymal or ICV infusion as well. After ICV infusion, ASO spreads throughout many brain structures, but does not penetrate dense regions of white matter [191]. There is no immune activation and the effect of one treatment in mice can last up to 3 months [191]. However, like siRNAs, ASOs must be delivered repeatedly on a long term basis.

To avoid the need for repeated administration of silencing agent, several groups are working on using viral delivery of shRNAs to target huntingtin in mouse models. AAV is a non-replicating virus that does not integrate into the cell's genome. AAV-shRNAs have been tested in animal models of HD. shRNA reduced mutant huntingtin mRNA in the striatum of N171-82Q mice by 51-55% compared with control, resulting in improved gait and rotarod ability [192]. Another group used AAV to express shRNA in the striatum of the R6/2 mice, finding a reduction in mutant huntingtin mRNA (75%) and protein (60%), a decrease in size and number of intranuclear inclusions and normalization of gene expression in neurons [193]. The treatment had no effect on rotarod ability but delayed onset of clasping [193]. This approach would only require a single administration of the AAV-shRNA for long term expression of the silencing molecule. One challenge of this system is controlling the expression level.

A significant concern about gene silencing is the potential harm of silencing both alleles, as 50% reduction of huntingtin may cause behavioral abnormalities and complete absence of huntingtin leads to neuronal cell death [36, 194, 195]. Therefore, it is important to monitor the amount of silencing that is achieved. A benefit of these strategies is that they are sequence specific and can be targeted to single nucleotide polymorphisms (SNPs) that are different between the normal and mutant allele in each individual patient. There is a linkage between at least one SNP that makes it a target in approximately 50% of HD patients [196]. Approaches that focus on allele-specific silencing will decrease the probability of loss of normal huntingtin function as a consequence of treatment, while specifically targeting the disease-causing product.

G. Summary

This introduction provides an overview of the impact of the disease, the role of huntingtin in the brain, and the pathological features and mechanisms that are known about huntingtin protein. Huntingtin has many functions including an essential role in development. In adulthood, huntingtin is implicated in several areas of the cell. It has roles in vesicle recycling, regulation of transcription, maintaining the energy state of the cell, and has neuroprotective functions involving BDNF. When huntingtin is mutated with an expanded CAG repeat, not only does the protein partially lose its ability to function normally, it interacts with other proteins resulting in cellular dysfunction and death. A hallmark of the disease is the formation of aggregates and nuclear inclusion bodies. Whether these aggregates are protective or harmful has yet to be established. However, the formation of aggregates may indicate the accumulation of mutant protein and the cell's inability to rid itself of the toxic protein. This introduction summarizes the two pathways by which mutant huntingtin can be degraded: the ubiquitin-proteasome system and the autophagy-lysosome system. I introduced a protein called puromycin sensitive aminopeptidase, which is the subject of Chapter 2. This enzyme has been implicated in the activation of autophagy and the accumulation of inclusion bodies in cells expressing mutant huntingtin exon 1 fragment [123].

Lastly, in this introduction, I discussed the current and potential therapies aimed at preventing the onset of HD and/or slowing its progression. The majority of therapeutic strategies address only one downstream effect of mutant huntingtin such as change in gene transcription or neuroprotection. Decreasing mutant huntingtin is a single method to prevent all downstream toxicities. Approaches include targeting the mutant huntingtin protein or mRNA by increasing degradation, decreasing transcription or decreasing translation. A promising way to impede

translation is to degrade mutant huntingtin mRNA by RNAi. One challenge is in selecting the best structure, modifications and delivery systems for the silencing agent. In Chapter 3, I discuss the optimization of a system for screening silencing molecules in the brain using *in vivo* bioluminescent imaging.

Figure 1-1: Circuitry of the direct and indirect pathways of the basal ganglia. Schematic depicting the pathways through the basal ganglia: cortical input enters either the direct or indirect pathway by synapsing with medium spiny neurons in the striatum. A.) In the indirect pathway, dopamine receptor-containing medium spiny neurons (D2) project to the globus pallidus external segment (GPe), connecting to the subthalamic nucleus (STN). The subthalamic nucleus connects with the substantia nigra pars reticulate (SNr), which then synapses on the thalamus. B.) In the direct pathway, dopamine receptor-expressing medium spiny neurons (D1) project to the globus pallidus internal segment (GPi), which projects to the thalamus. Substantia nigra pars compacta (SNc) provides dopaminergic input to the striatum. Excitatory glutamate (GLUT) releasing connections are red. Inhibitory GABA releasing pathways are blue. The excitatory dopamine (DA) pathway is purple with "+", and the inhibitory dopamine connection is purple with "-".

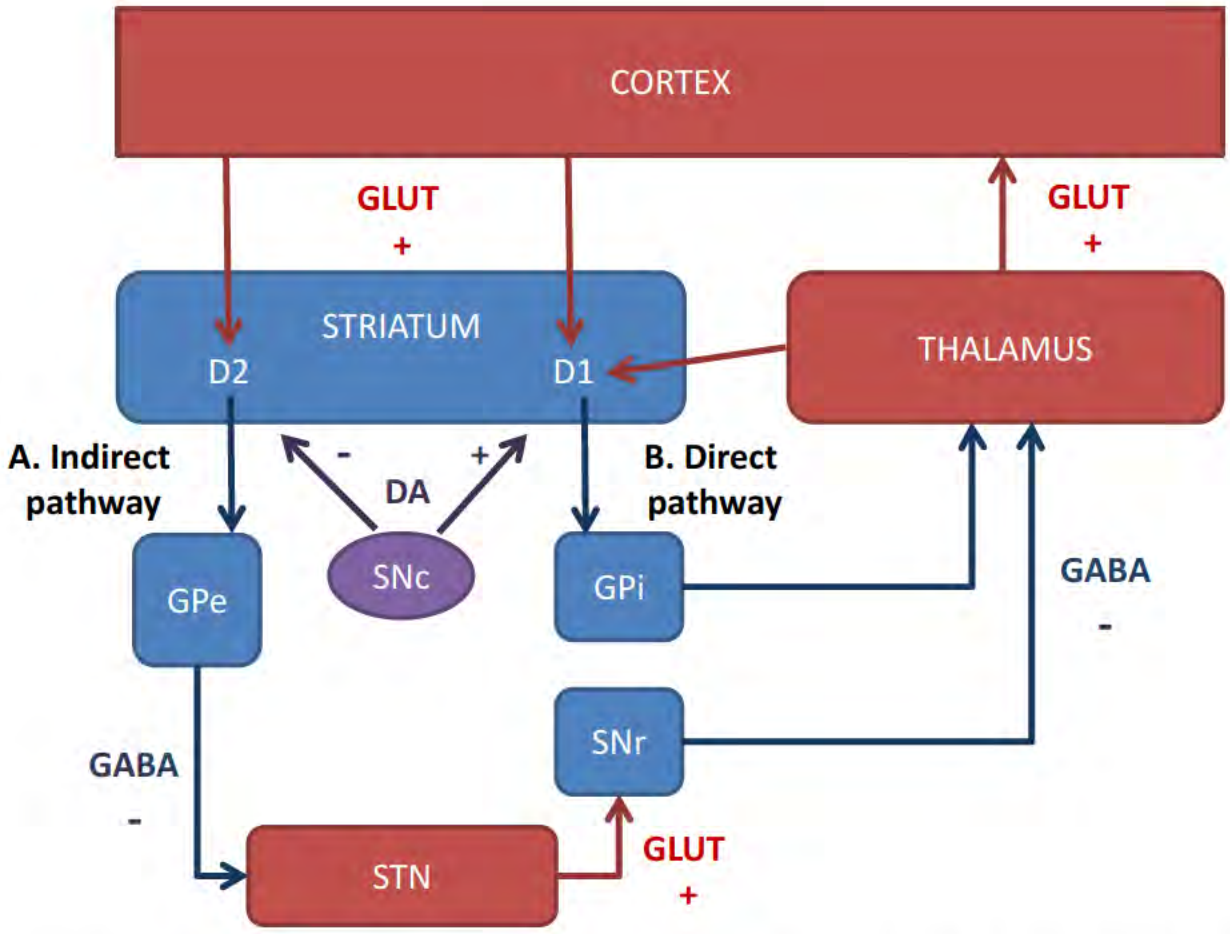

Figure 1-1: Circuitry of the direct and indirect pathways of the basal ganglia.

Figure 1-2: Mutant huntingtin negatively affects many cellular processes. A.) Cleavage of huntingtin generates NH_2-terminal fragments of mutant huntingtin that are more toxic than the intact protein. Abnormal protein interactions disrupt intracellular processes. B.) Mutant huntingtin binds dynactin and other polyQ containing proteins in addition to binding to itself forming oligomers and fibrillar intermediates. C.) NH_2-terminal fragments form soluble fibrils that interact and more severely impair huntingtin function. D.) Mutant huntingtin is targeted to the proteasome by ubiquitin modifications, but it cannot be degraded. E.) Dystrophic neurites are a pathological finding in neurons that contain full length and NH_2-terminal fragments. F.) Cytoplasmic aggregates are a pathological finding located in the cytoplasm of neurons. These also contain full length and NH_2-terminal fragments and are ubiquitinated. These aggregates are known to bind and sequester proteasomal subunits. G.) Neuronal intranuclear inclusion bodies are a pathological finding that consists of aggregated mutant huntingtin fragments in the nucleus. These inclusion bodies bind transcription factors and contribute to transcriptional dysregulation. H.) Transcriptional dysregulation is also caused by soluble mutant huntingtin that binds to transcription machinery and transcription activators to result in general transcriptional reduction. I.) Mitochondrial dysfunction is caused by mutant huntingtin binding to mitochondria to alter movement, structure and calcium handling. J.) Impaired vesicle trafficking and endosomal recycling results when mutant huntingtin binds Rab11 thereby altering endosome morphology and slowing endosome recycling.

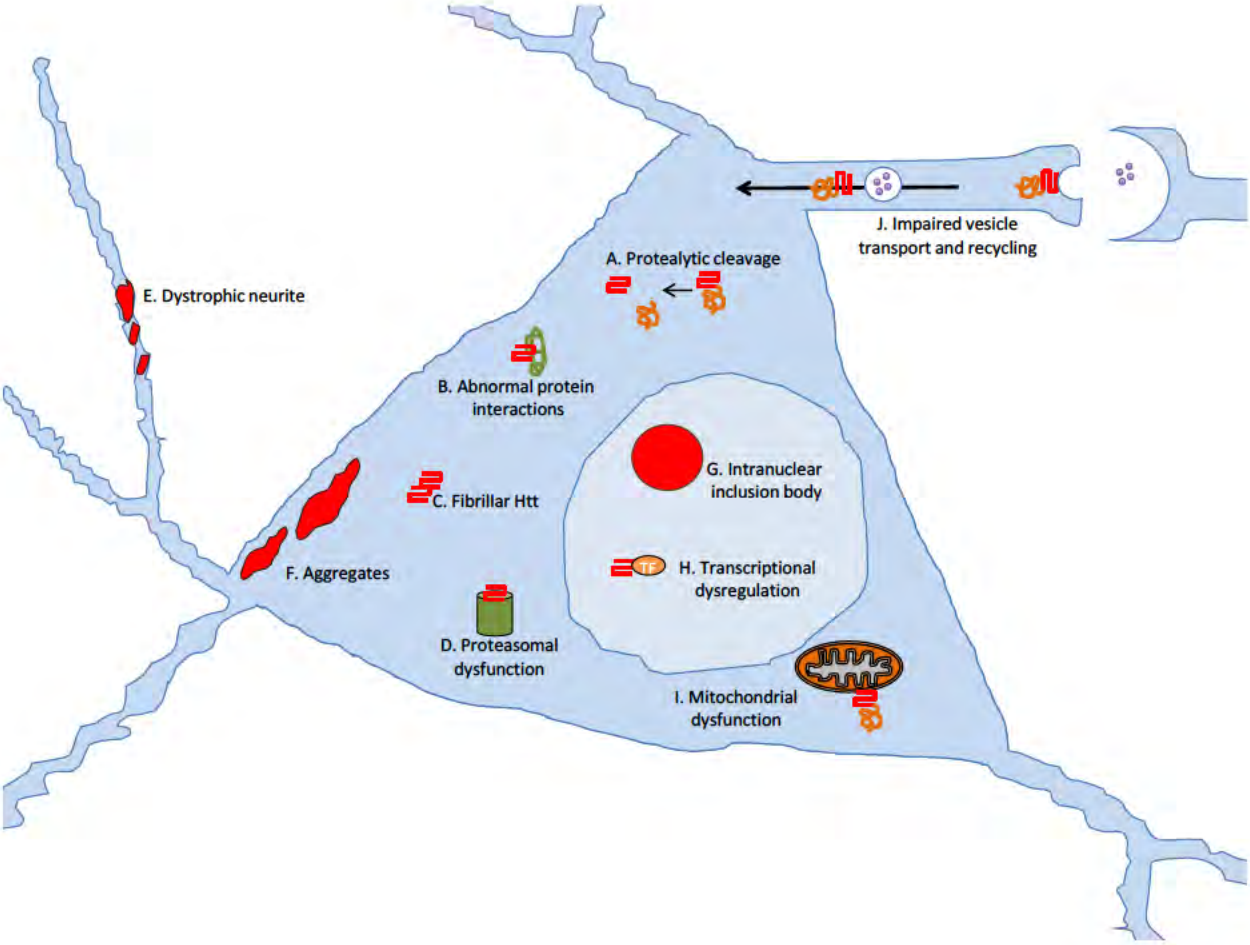

Figure 1-2: Mutant huntingtin negatively affects many cellular processes.

Figure 1-3: Diagram of huntingtin degradation pathways. A.) Ubiquitin-proteasome system: Proteins labeled with ubiquitin chains are targeted to the proteasome for degradation. Proteins are unfolded before they enter the proteasome. Multiple proteasomal endopeptidases cleave the proteins, and peptides released into the cytosol are further degraded by aminopeptidases. B.) Autophagy-lysosome system: A double membrane forms around proteins or organelles to be degraded, forming a structure called an autophagosome. The autophagosome fuses with the lysosome to create an autophagolysosome where the proteins are degraded by acidic lysosomal hydrolases.

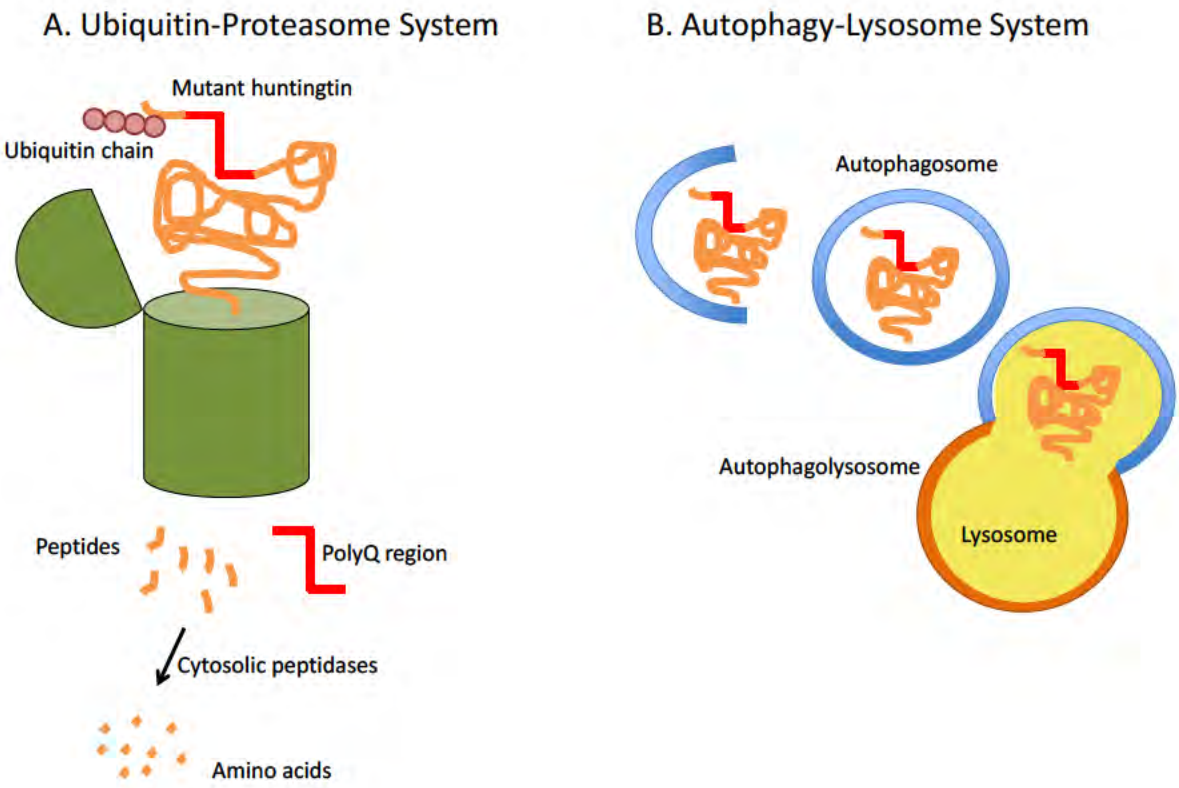

Figure 1-3: Diagram of huntingtin degradation pathways.

Table 1-1: Comparison of commonly used mouse models of Huntington's disease

Type of mouse model: Name, promoter, number of repeats	Relative expression of Huntingtin	Behavioral Phenotype	Neuropathology	Weight change	Life expectancy
Fragment: R6/2 , human htt, ~150 CAG repeats	Over expression: 75% of endogenous levels of mRNA	Rotarod deficit at 5 weeks, clapsing at 8 weeks	Nuclear inclusions and aggregates throughout the brain, reduced brain size (atrophy)	Progressive weight loss	12-15 weeks
Fragment: N171-82Q, mouse prion protein promoter, 82 CAG repeats	Over expression: less than endogenous levels of protein	Rotarod deficit at 15 weeks, clasping behavior at 15 weeks	Nuclear inclusions in cortex, hippocampus, amygdala and striatum, reduced brain size (atrophy)	Progressive weight loss	10-24 weeks
Full length human: YAC128, human htt promoter, 128 CAG repeats	Over expression: 50% endogenous huntingtin protein	Rotarod deficit by 24 weeks, clasping behavior	No nuclear inclusions, EM48 positive microaggregates in striatum, reduced cortex and striatum volume and cell number	Weight increase	Normal life span
Full length human: BACHD, human htt promoter, 97 CAG/CAA repeats	Over expression: 2X endogenous huntingtin protein	Rotarod deficit by 8 weeks	Neuropil aggregates, in cortex and striatum, decreased cortical and striatal volume	Weight increase	Normal life span
Knockin: HdhQ140, endogenous mouse promoter, fragment of human exon 1 with 140 CAG repeats	Endogenous levels	Hyperactivity, then hypoactivity, gait abnormalities	Nuclear inclusion bodies and aggregates in striatum, cortex, hippocampus and cerebellum at 4 months	No weight loss	Normal life span
Knockin: HdhQ150, endogenous mouse promoter and gene, 150 CAG repeats	Endogenous levels	Rotarod deficit at 100 weeks, hypoactivity and gait abnormalities, clasping	Nuclear inclusions in striatum at 9 months	Smaller size	Normal life span

Table 1-1: Comparison of commonly used mouse models of Huntington's disease

CHAPTER II

THE EFFECT OF REDUCED LEVELS OF PUROMYCIN SENSITIVE AMINOPEPTIDASE ON INCLUSION FORMATION AND BEHAVIOR IN A KNOCK-IN MOUSE MODEL OF HUNTINGTON'S DISEASE

This chapter provides evidence that a decrease in puromycin sensitive aminopeptidase (PSA) influences behavior and inclusion formation in Huntington's disease model mice. We also demonstrate the sensitivity of neurons to overexpression of PSA. I designed, carried out, and analyzed the majority of the experiments under the supervision of Neil Aronin. Ellen Sapp quantified the open field assay. Ken Rock provided the PSA knock-out mice. Miguel Esteves provided the AAV-hPSA-HA. A version of this chapter is currently being prepared as a manuscript for publication.

A. Abstract

Huntington's disease (HD) is an autosomal dominant neurodegenerative disorder caused by an expanded CAG repeat in the huntingtin gene encoding for a polyglutamine (polyQ) region in the protein [1, 2]. Mutant huntingtin accumulates in neurons, forming cytoplasmic aggregates and nuclear inclusion bodies. Both the ubiquitin-proteasome system and the autophagy-lysosomal system have contributing roles in degrading mutant huntingtin, but the primary mechanism of degrading mutant huntingtin remains unknown. Puromycin sensitive aminopeptidase (PSA), an enzyme previously implicated in MHC class I presentation and degradation of enkephalin, is highly expressed in the brain and has the unique ability to degrade polyQ peptides [197-199]. PSA expression reduces mutant huntingtin aggregates in several cell types and has a neuroprotective effect in mouse models of tau-induced neurodegeneration [123, 200].

The aim of this study was to investigate the role of PSA in the progression of Huntington's disease using a 140Q knock-in mouse model of HD [145]. Since PSA degrades polyQ regions and reduces inclusions in cells, we hypothesized that a decrease in PSA would worsen behavioral abnormalities and increase the number of inclusion bodies in neurons of knock-in mice. In this study we used $Psa^{+/-}$ $Hdh^{140Q/140Q}$ mice to test the effect of a PSA deficiency on HD phenotype. We found that reduced PSA resulted in impaired performance on the raised beam test and an increased number of intranuclear inclusion bodies. These findings demonstrate that a reduction in PSA expression worsens behavioral progression and alters inclusion formation in the HD mouse model. To test over-expression of PSA, we created an AAV vector expressing the human homolog of PSA (hPSA). Unexpectedly, over-expression of

hPSA in the brain of wild type mice resulted in dosage-dependent astrocyte activation and neuron death. The toxicity due to high expression levels of hPSA reveals the potency of the enzyme and the sensitivity of neurons to increased amount of PSA.

B. Introduction

Huntington's disease (HD) is an autosomal dominant neurodegenerative disorder caused by an expanded CAG nucleotide repeat within the mutant allele of the huntingtin gene [1]. This trinucleotide repeat is part of the coding region of the gene, resulting in a protein with an expanded polyglutamine (polyQ) region [2]. Mutant huntingtin accumulates in medium spiny neurons of the striatum forming insoluble cytoplasmic aggregates and nuclear inclusions resulting in cellular dysfunction and neuron loss [2, 80]. HD affects 4-10 in 100,000 people of European descent and is characterized by early motor and psychiatric symptoms followed by cognitive decline and death [2].

HD is one of nine neurological diseases caused by polyglutamine expansions, including dentatorubral-pollidoluysian atrophy (DRPLA), spinal and bulbal muscular atrophy (SBMA), several types of spinocerebellar ataxias (SCAs), all of which result in misfolding, accumulation, and aggregation of the polyQ containing protein [201]. Each disease affects a different subset of neurons [201]. In Huntington's disease, onset is inversely proportional to the length of the polyQ expansion [202]. This suggests that the length of the polyQ stretch confers toxicity, perhaps by a greater resistance to degradation by the cell. One approach to treating Huntington's disease is to decrease the amount of mutant protein in order to alleviate the cytotoxic burden of mutant huntingtin.

Huntingtin is degraded by both the ubiquitin-proteasome system (UPS) and the autophagy-lysosomal system [127]. Huntingtin is targeted to the proteasome by poly-ubiquitination on lysine residues [118]. Huntingtin is also phosphorylated on serines 13 and 16 by the IKK (inhibitor of kappa B kinase) that targets it for degradation by the proteasome and the lysosome [99]. Interestingly, the presence of an expanded polyQ region reduces the efficiency of phosphorylation, possibly contributing to the accumulation of mutant huntingtin [99]. In human HD tissue and HD transgenic mice, huntingtin-containing inclusion bodies and aggregates stain positive for ubiquitin [81].

In post-mortem brain tissue from HD patients, there is decreased proteasome activity suggesting that mutant huntingtin impairs its function [203]. The proteasome is only able to degrade soluble proteins prior to the formation of aggregates, therefore the role of the UPS would be most important early in the disease [124, 204-207]. In HD model neuronal cell culture, proteasome activators improve proteasome function and improve viability against toxic insult [208]. Treatment with proteasome inhibitors results in accumulation of mutant huntingtin protein and inclusion formation cell models and 140Q knock-in mouse model, although few mice were examined (n=2) [126, 209].

Autophagy is also a pathway for the degradation of huntingtin [62, 131, 210-212]. Mutant huntingtin aggregates sequester the mammalian target of rapamycin (mTOR), and the loss of mTOR activates autophagy [129]. Treatment with activators of autophagy reduces inclusion number and cell death in mutant huntingtin-expressing cells, decreases neurodegeneration in a fly model of HD, and improves behavior in a mouse model of HD [213, 214].

The mechanism by which the proteasome degrades polyQ repeats in mutant huntingtin is not known. In vitro experiments reveal that eukaryotic proteasomes digest polyglutamine polypeptides slowly, sometimes expelling polyglutamine stretches intact [121]. Similarly, the proteasome is unable to degrade NH_2-terminal mutant huntingtin, releasing incompletely digested fragments [125]. An insight into the degradation of polyQ repeats has been the identification of puromycin sensitive aminopeptidase (PSA), an enzyme with the ability to digest polyQ peptides [122]. In cell extracts, PSA has the ability to degrade polyQ stretches up to 30 amino acids in length [122]. Longer polyQ lengths were unable to be studied due to aggregation under the experimental conditions. Nevertheless, the authors concluded that PSA is the only enzyme identified with the ability to degrade polyQ peptides, a property that may be critical for degradation of the toxic NH_2-terminal fragments of mutant huntingtin [122].

PSA is a 99 kDa zinc metallopeptidase ubiquitously expressed enzyme with highest levels in skeletal muscle, heart, brain, kidney, liver and testes. In the brain, PSA is the most highly expressed aminopeptidase [199, 215]. PSA exists as membrane bound and soluble forms, implicated in enkephalin degradation, polyQ peptide degradation, and in processing peptides for MHC class I presentation [122, 197, 216, 217]. PSA also associates with the spindle apparatus in G2/M phase, suggesting that it could be involved in the cell cycle [218]. Reduction of PSA results in decreased migration, proliferation, and invasion of PC-3 cells, a prostate cancer cell line [219]. PSA knockout mice exhibit increased anxiety, decreased pain response, male reproductive abnormalities and female maternal behavior deficits [220-222].

Several studies show effects of PSA on the degradation and processing of proteins relevant to neurodegenerative diseases. Cu, Zn-superoxide dismutase-1 (SOD1) is a protein that is frequently misfolded in both familial and sporadic cases of amyotrophic lateral sclerosis

(ALS) [223]. In cell culture experiments, protein levels of SOD1 were inversely related to protein levels of PSA, and in a cell-free system SOD1 was shown to be a target of PSA proteolysis [223]. Tau is a protein that aggregates in both frontotemporal dementia (FTD) and Alzheimer's disease. Silencing PSA in cell culture results in accumulation of tau, however, the effects of PSA on tau are indirect as PSA was not shown to directly cleave tau [224, 225]. Another group found that PSA does degrade tau from extracts of brain from FTD and Alzheimer's patients' brains [226, 227]. PSA is up-regulated in the cerebellum of FTD model mice and FTD patients [226]. A *Drosophila* model of FTD with decreased PSA exhibit increased neurodegeneration and increased aggregation of tau [228]. An increase in PSA prevents neurodegeneration in FTD mice [226].

PSA expression has also been shown to affect the accumulation of mutant huntingtin. In transfected cell culture and muscle tissue expressing mutant huntingtin, reducing PSA resulted in a greater number of aggregates and cell death, while overexpressing PSA resulted in fewer aggregates and cell death [123]. The beneficial effects of PSA overexpression on huntingtin-expressing cells may be the result of an increase in autophagy, as chemically blocking autophagy negated the effects of PSA [123]. These findings in cell culture seem to suggest that the mechanism of huntingtin degradation by PSA is indirect, through the activation of autophagy rather than by increasing the rate of polyQ degradation. However, these experiments were performed in cell culture experiments with very high overexpression of PSA, which warrants caution in extrapolating this conclusion to the physiologic function of PSA in the brain.

The aim of this study is to investigate whether PSA level influences the phenotype in a knock-in mouse model of Huntington's disease. Previous studies have been limited to studying the interaction of a huntingtin fragment in cell culture and in the muscle tissue of PSA

heterozygous animals. Here, we use PSA heterozygous mice crossed with HD 140Q knock-in mice to investigate the effect of PSA reduction on disease-related phenotypes in a mouse model of Huntington's disease. The advantage to using a mouse model of HD is that mice can be tested for behavioral changes as well as pathological changes. To interpret the effect of PSA on HD, it is crucial to examine tissues and cells most affected by the disease.

Our study showed that at 12 months, the PSA heterozygous HD mice ($Psa^{+/-}Hdh^{140Q/140Q}$) had a worsening of balance and coordination on the raised beam test, and the number of nuclear inclusions was significantly increased. The results demonstrated that $Psa^{+/-}Hdh^{140Q/140Q}$ mice exhibit a more severe phenotype than $Psa^{+/+}Hdh^{140Q/140Q}$ mice. If a reduction in PSA worsens symptoms and increases inclusion number in a mouse model of HD, we wanted to explore whether an increase in PSA would delay the onset or reverse behavioral and pathologic outcomes. To test this, we created a gene therapy approach to deliver hPSA to the striatum. In testing the virus in wild type mice, we found that the virus caused toxicity in a dose dependent manner. The observed cell death and glial activation suggest that neurons are sensitive to over-expression of hPSA at the dose given.

C. Results

1. PSA knock-out animals do not breed well and are smaller than littermates.

The study of PSA knock-out animals ($PSA^{-/-}$) is a challenge for several reasons. In agreement with previous studies, we found that PSA knock-out mice do not breed well, producing very few litters [197]. For example, one would expect $Psa^{+/-}$ breeding pairs to produce $Psa^{+/+}$: $Psa^{+/-}$: $Psa^{-/-}$ at a 0.25:0.5:0.25 frequency. In our experience, the average litter size from a

representative sample of 15 litters was 4.73± 1.5 pups with a frequency of 0.42: 0.5: 0.083 (Table 2-2). A second reason discouraging the use of PSA knockout animals is that they are smaller compared with age and sex-matched heterozygous or wild type littermates [197]. PSA knock-out mice weigh about 65% as much as age-matched heterozygous littermates at one and six months of age (Fig. 2-1, unpaired t-test p=0.003 at 1 month, p=0.0247 at 6 months). Complete data on weight for each mouse is also shown in Table 2-1. This concurs with findings reported for a different line of PSA deficient mice, $Psa^{goku/goku}$, using the gene-trap method to disrupt PSA expression [222]. $Psa^{goku/goku}$ mice display body weight <70% of WT mice [222]. The difference in size precluded us from using $Psa^{-/-}$ mice in tests on the raised beam because their decreased size and weight could affect their performance in comparison with larger animals. The difference in size raises the possibility that developmental differences might exist which could affect the comparison between wild type and PSA knock-out HD animals. Since heterozygous animals breed normally, are born at expected frequency, and are equal in size to wild type littermates, we chose to use heterozygous mice to investigate the impact of a reduction in PSA in HD animals.

2. PSA mRNA and protein are expressed in a gene dosage-dependent manner.

In order to use $Psa^{+/-}$ animals to represent a reduction in PSA, we first assessed whether there is a gene dosage effect of the PSA gene. We looked at the relative mRNA and protein levels in $Psa^{-/-}$, $Psa^{+/-}$ and wild type striatum and cortex. Quantitative PCR (qPCR) from striatal tissue of PSA mice showed that heterozygous mice express about 50% the amount of PSA mRNA as wild type mice (Fig. 2-2 A, Tukey's pairwise comparison p=0.008). Western Blot

analysis of tissues from the cortex shows that heterozygous mice express about 50% as much protein as control mice (Fig. 2-2 B, Tukey's pairwise comparison p=0.0055). In the striatum, PSA protein levels in heterozygous mice were 60% of wild type levels, but this did not quite reach statistical significance. There was no detectable PSA mRNA or protein in the knock-out animals (Fig. 2-2 A, B, C, D). The significant reduction of PSA mRNA from the striatum and PSA protein from the cortex (and a non-significant reduction of protein in the striatum) in $Psa^{+/-}$ mice suggests that there is gene dosage effect; however there are few animals per group, resulting in low experimental power.

3. $Psa^{-/-}$ and $Psa^{+/-}$ mice do not display a locomotor defect on the raised beam test and do not form ubiquitin positive nuclear inclusion bodies.

In a previous study, some $Psa^{-/-}$ mice were observed to have a locomotor defect in their hind legs [197]. It was found that $Psa^{goku/goku}$ mice do not have abnormalities on the raised beam test, however in this study heterozygous mice were not tested [222]. The raised beam test evaluates the balance and coordination of a mouse as it crosses a narrow beam. To confirm the raised beam test finding in $Psa^{goku/goku}$ mice and to test Psa heterozygous mice, we tested $Psa^{-/-}$ and $Psa^{+/-}$ mice for behavioral defects on the raised beam test. We found no difference in either group compared with wild type mice at 6, 8 and 10 months of age (Fig. 2-3 A). $Psa^{goku/goku}$ mice have reduced activity in the open field test and reduced rearing compared with wild type mice [222]. In our observations regarding general activity, we found the opposite effect in our $Psa^{-/-}$ mice. $Psa^{-/-}$ mice exhibited an increase in home cage activity and an abnormal behavior of jumping off of the beam.

Inclusion bodies and visible aggregates of many mutant aggregating proteins can be detected by immunohistochemistry (IHC) with antibodies specific for ubiquitin. In sections from $Psa^{-/-}$ mice (9 and 22 months old), there was no staining for ubiquitin positive inclusion bodies or aggregates in the striatum (Fig. 2-3 B). There was cytoplasmic staining for ubiquitin but no more than in the wild type control. $Psa^{-/-}$ sections (from mice 9, 17, and 22 months old) were also stained for huntingtin aggregates to be certain that there is not impairment in degrading normal huntingtin. No staining for huntingtin inclusions was seen (Fig. 2-3 C). $Psa^{+/-}$ animals were also negative for huntingtin inclusion formation (assessed directly in subsequent experiments). The findings that $Psa^{-/-}$ and $Psa^{+/-}$ mice do not have a locomotor phenotype and $Psa^{-/-}$ mice do not have nuclear inclusions or cytoplasmic aggregates, allow us to use these measures as endpoints in our study of the effects of reduced PSA on HD mice.

4. PSA reduction does not accelerate the onset of locomotor deficits or reduce activity in $PSA^{+/-}$ $Hdh^{7Q/140Q}$.

A measure of progression of disease in the knock-in mice is the development of behavioral and locomotor abnormalities. Hypoactivity appears in heterozygous ($Hdh^{7Q/140Q}$) knock-in mice at around 4 months of age, and gait abnormalities appear at 1 year of age [145]. To test for an early effect of PSA heterozygosity on raised-beam behavior, we analyzed $Psa^{+/-}$ $Hdh^{7Q/140Q}$ and compared them with $Psa^{+/-}$ $Hdh^{7Q/7Q}$ and wild type mice ($Psa^{+/+}$ $Hdh^{7Q/7Q}$). We used the raised beam test to look for early interaction of PSA heterozygosity on heterozygous knock-in HD mice beginning at 3 months of age, continuing to 10 months of age (Fig 2-4 A). These mice were initially tested every week for the first month (no difference between the

groups, data not shown). Over time, mice in all groups became increasingly resistant to crossing the beam, therefore time points after 10 months were not tested. Because heterozygous knock-in HD mice with $Psa^{+/-}$ versus $Psa^{+/+}$ showed no difference on the raised beam test by 10 months of age, we conclude that there is no effect of the $Psa^{+/-}$ genotype on locomotor abilities of $Hdh^{7Q/140Q}$ mice at early time points.

We also tested these same mice in an open field test at 13 months of age. $Psa^{+/+}$ $Hdh^{7Q/140Q}$ mice showed reduced activity compared with all other groups, including $Psa^{+/-}$ mice, the latter of which showed no difference from wild type mice (Fig. 2-4 B). These results show that a PSA reduction unexpectedly improves activity in $Hdh^{7Q/140Q}$ mice (Tukey's multiple comparison p=0.00569). The increase in activity of $Psa^{+/-}$ $Hdh^{7Q/140}$ mice compared with $Psa^{+/+}$ $Hdh^{7Q/140Q}$ mice suggest that PSA heterozygosity might increase general activity in HD animals.

5. PSA deficiency in $Hdh^{7Q/140Q}$ mice does not affect the number of inclusion bodies

Inclusion body formation can be used to follow disease progression in knock-in mice. Inclusion bodies begin forming at four months of age and continue to increase in size and number as the mice age and the disease progresses [145]. At 1.5 years of age, there was no difference in the number of inclusion bodies in either the striatum or the cortex of $Psa^{+/-}$ $Hdh^{7Q/140Q}$ compared with $Psa^{+/+}Hdh^{7Q140Q}$ mice (Fig. 2-4 C). We did not test $Psa^{+/-}Hdh^{7Q/7Q}$ mice because in previous studies they did not exhibit huntingtin inclusion formation (Fig. 2-3).This demonstrates that the formation of inclusion bodies in $Hdh^{7Q/140Q}$ mice is not altered by a reduction in PSA.

6. PSA deficiency worsens locomotor deficits in 12 month old $Hdh^{140Q/140Q}$ mice

In our experience, $Hdh^{7Q/140Q}$ mice have a less severe phenotype than do $Hdh^{140Q/140Q}$ mice, so next we tested the effect of PSA reduction on homozygous knock-in mice ($Hdh^{140Q/140Q}$) to see if there was a change in a more severe disease model. In $Psa^{+/-}$ $Hdh^{140Q/140Q}$ mice, the relative decrease in the amount of PSA protein is similar to previous findings, although this difference is not statistically significant due to the large variation within each group (Fig. 2-5 A, B).

Previously, in the raised beam test, mice became resistant to crossing the raised beam, therefore, in order to preserve accuracy of the test we chose a single time point to test $Psa^{+/-}$ $Hdh^{140Q/140Q}$ mice for locomotor deficits. We chose to test these mice at one year of age, a time point where the animals are more advanced in their disease. $Psa^{+/-}Hdh^{140Q/140Q}$ mice took longer to cross the raised beam than $Psa^{+/+}Hdh^{140Q/140Q}$ mice (n.s.), and were significantly slower in beam crossing than wild type mice (Fig. 2-5 C). $Psa^{+/-}$ $HD^{140Q/140Q}$ mice had a significantly greater number of foot slips than the $Psa^{+/+}$ $HD^{140Q/140Q}$ mice and an increase compared with wild type mice. Findings that $Psa^{+/-}$ $HD^{140Q/140Q}$ mice performed worse on the raised beam test, in terms of footslips, than $Psa^{+/+}$ $HD^{140Q/140Q}$ mice suggest that PSA heterozygosity increases the progression or severity of the HD phenotype in the $Hdh^{140Q/140Q}$ mice at one year of age. This contradicts previous findings using $Hdh^{7Q/140Q}$ mice, possible due to an increased polyQ burden from twice the amount of mutant Hdh protein.

7. PSA reduction increases the number of nuclear inclusions in 12 month old $Hdh^{140Q/140Q}$ mice

We then looked at the formation of inclusion bodies in 12 month old $Psa^{+/-}Hdh^{140Q/140Q}$ mice. Since the number of inclusions correlates with the severity of the disease in knock-in HD mice, we predicted that a decrease in PSA will increase the number of inclusion bodies [145]. By stereological quantification, there was a significant increase in the number of intranuclear inclusion bodies in the $Psa^{+/-}Hdh^{140Q/140Q}$ mice (Fig. 2-6 A-C). No difference in the number of neurons was observed between the $Psa^{+/-}Hdh^{140Q/140Q}$ mice and the $Psa^{+/+}Hdh^{140Q/140Q}$ mice (Fig. 2-6 F). Interestingly, the $Psa^{+/-}Hdh^{140Q/140Q}$ mice had slightly smaller size of inclusions compared with $Psa^{+/+}Hdh^{140Q/140Q}$ mice; however this difference was not statistically significant (Fig. 2-6 D) (Unpaired t-test, $p=0.1981$).

Stereological quantification of cytoplasmic aggregates was also performed. These were differentiated from nuclear inclusion bodies as they are smaller and irregular in shape and are outside of the nucleus. The difference in the number of aggregates was not statistically significant, but the average number of cytoplasmic aggregates in the $Psa^{+/-}Hdh^{140Q/140Q}$ was less than the $Psa^{+/+}Hdh^{140Q/140Q}$ (Fig. 2-6 E) (Mann-Whitney U test, $p=0.1388$). The observations that the inclusion bodies are smaller and fewer aggregates are observed could point to a role of PSA in the distribution of mutant huntingtin between the nucleus and the cytoplasm.

8. PSA deficiency has no effect on soluble huntingtin and autophagy

To test whether the increased number of inclusion bodies represents a reduction in soluble huntingtin, we performed western blot analysis on cell extract from the striatum using

antibodies generated from amino acids 1-17 of human huntingtin (AB1 antibody [229]). We found no change in huntingtin levels among the groups (Fig. 2-7 A).

We tested whether a decrease of PSA in HD mice would result in a decrease in autophagy [123]. LC3-I is converted to LC3-II representing an increase in autophagy. We could not detect LC3-II, a marker of autophagy activation, and we did not find any change in the amount of LC3-I (Fig. 2-7 B).

9. AAV-hPSA-HA injection in wild type mice leads to hPSA expression in the brain.

To investigate the effect of an increase in PSA on behavior and pathology in HD mice, we created an AAV vector expressing human PSA (hPSA) tagged with the hemagglutinin (HA) epitope, for this study we will refer to it as AAV-hPSA-HA. Human PSA is 98% identical to mouse PSA at the amino acid level [199]. To test that the AAV-hPSA-HA virus expresses hPSA in the brain, we injected a series of doses, all 3µL in volume, into the striatum of wild type mice (Fig. 2-8 A). hPSA can be detected in brain extracts three weeks after intraparenchymal injection at concentrations as low as 1e10 GC (genome copies) using HA antibodies. These results demonstrate that AAV-hPSA-HA is expressed and can be detected using HA antibodies.

10. Overexpression of hPSA in wild type mice is toxic at high concentrations.

In AAV-hPSA-HA-injected wild type mice, we found extensive toxicity demonstrated both by the loss of neurons and by glial activation. In order to test whether PSA toxicity in mouse neurons is dose dependent, we injected 10-fold dilutions (1e12 GC, 1e11 GC, 1e10 GC, and 1e9 GC) of AAV-hPSA-HA, all 3µL in volume, into the striatum and looked for HA, GFAP, and DARPP-32 reactivity after three weeks. At 1e11 GC there was spread of hPSA-HA

throughout many sections of the striatum, but at ten-fold dilution (1e10 GC) the spread was limited to a few sections (Fig. 2-9 A). Doses of 1e10 and 1e9 GC resulted in very few HA positive cells (not shown). Staining for glial fibrillary acidic protein (GFAP) revealed a widespread activation of astrocytes in the 1e11 GC concentration and limited activation in the 1e10 GC and control injection sections (Fig. 2-9 B). In the 1e11GC concentration there was a complete loss of DARPP-32 staining for medium spiny neurons corresponding with the site of injection (Fig. 2-9 C). We confirmed that the cells expressing PSA are neurons by double immunofluorescence labeling of HA and DARPP-32 (Fig. 2-9 D). In summary, the extent of spread is greatest at the highest dose (1e11 GC) with the adverse effect of eliciting significant glial activation. At 1e10 GC concentration, the spread is limited, but there is minimal glial activation.

To test whether there were contaminants in the viral preparation which could account for the observed toxicity, we did a time course experiment to assess whether cell death and astrocyte activation corresponds with the expression of hPSA-HA. HA reactivity was detectable at one week after injection and preceded the activation of astrocytes and loss of DARPP-32 positive cells (Fig. 2-10). That HA reactivity is found before toxicity suggests that there are no contaminants in the virus preparation and that expression of hPSA-HA is toxic to cells at the measured level. To confirm that the virus was not contaminated, new preparations can be made parallel to a control virus to compare toxicities.

D. Discussion

We are the first to show that heterozygosity for the PSA gene affects the behavior and inclusion formation in a knock-in mouse model of Huntington's disease. On the raised beam test, the $Psa^{+/-}$ $Hdh^{140Q/140Q}$ mice had a greater number of foot slips compared with $Psa^{+/+}$ $Hdh^{140Q/140Q}$ mice (Fig. 2-5 C). Since there was worsened performance on the raised beam test, a test for balance and coordination, we conclude that there is functional impairment resulting from PSA heterozygosity.

We measured huntingtin protein from striatal cell lysates and did not detect a difference in the amount of full-length mutant huntingtin between the $Psa^{+/-}$ $Hdh^{140/140}$ and $Psa^{+/+}$ $Hdh^{140/140}$ groups (Fig. 2-7 A). Cell lysates for Western analysis were prepared by performing a low speed spin to remove mitochondria, lysosomes, and the nuclei. The fraction of mutant huntingtin measured consisted of the soluble, cytoplasmic, full-length mutant huntingtin (Fig. 2-11 A, B). This measurement did not include full-length huntingtin associated with aggregates and inclusion bodies, NH_2-terminal fragments or fibrillar forms of mutant huntingtin. Using stereological techniques, we show that decreased PSA results in a greater number of inclusions in neurons of the striatum (Fig. 2-6 C). This is consistent with previous findings in the muscle tissue of $Psa^{+/-}$ mice transfected with huntingtin exon 1 containing 74Q, in which the number of inclusions was increased [123]. The number and size of nuclear inclusions largely represent the insoluble NH_2-terminal fragment of mutant huntingtin. Our interpretation of these results is that PSA heterozygosity contributes to an accumulation of insoluble mutant huntingtin. In this interpretation there is no increase in full-length mutant huntingtin, but there is an increase of the

NH_2-terminal fragment of mutant huntingtin as measured by the number and size of cytoplasmic aggregates and intranuclear inclusion bodies. In addition to mHtt lost in insoluble fragments, it is preferentially membrane bound, and, hypothetically, could bind to any membrane after cell lysis [230]. There are several challenges in measuring the content of mutant huntingtin as it is distributed throughout multiple compartments, soluble and insoluble conformations, and preferentially membrane bound.

A caveat to our results in $Psa^{+/-}$ $Hdh^{140Q/140Q}$ mice is that we were unable to demonstrate that PSA protein was significantly reduced compared with PSA wild type animals in the striatum in two experiments, each with groups of 4 or less animals (Figs. 2-2, 2-5). Using groups of three mice we show that Psa mRNA is significantly reduced by 45% in striatum of $Psa^{+/-}$ mice. In the cortex, also n=3, PSA protein was reduced in $Psa^{+/-}$ mice by 55%. One reason for inconsistencies in showing a decrease in PSA protein may be that the sample size, and thus power of the experiment was too low to detect the differences. Examination of tissue from additional animals is needed to confirm that there is a difference in PSA expression level in $Psa^{+/-}$ mice.

Since the effect of Psa haploinsufficiency resulted in a greater number of inclusion bodies and an earlier deficit on the raised beam test, we sought to overexpress PSA in HD mice to determine if there was a therapeutic effect on inclusion formation and behavior. To overexpress PSA we created an AAV expressing human PSA tagged with the HA epitope. Upon testing this construct in wild type mice, we observed widespread cell loss and astrocyte activation three weeks after injection. Potential sources of toxicity include contaminants in the preparation of the virus, immunogenicity of the HA tag, expression of a foreign gene, and peptidase activity. The expression of hPSA-HA occurs before the astrocyte activation and cell death, suggesting that hPSA-HA expression is causing the toxicity rather than contaminants in the viral prep. There

were no problems reported in other viral preps performed at the same time in the same facility. The HA tag has previously been used to follow AAV-delivered protein expression in the mouse brain with no immunogenic result [231]. It is unlikely that hPSA would be identified as a foreign protein because it has a sequence consensus with the mouse PSA of 98% [199]. At lower doses of AAV-hPSA-HA, there is less glial activation while maintaining detectable HA reactivity three weeks after injection, suggestive of a dose response for toxicity. It was reported that high overexpression of PSA in *Drosophila* resulted in toxicity that was not found at lower expression levels of PSA [123]. Toxicity was not described in cell culture or in muscle cells overexpressing high levels of PSA [123]. Without details on the toxicity in Drosophila that was not published, there are several explanations, one being that neurons could be more sensitive to PSA or that all cells are sensitive to very high overexpression of PSA. There is a line of transgenic mice expressing human PSA at levels two to three fold higher than endogenous PSA without signs of developmental abnormality or glial activation [200]. As a transgenic model, these mice have had the opportunity to compensate for overexpression of PSA whereas mice injected with AAV-hPSA-HA are fully developed animals. This does not exclude the possibility that 2-3 fold overexpression of PSA is not toxic if suddenly expressed in adult neurons. It would be particularly informative to cross the transgenic PSA overexpressing mouse model with knock-in huntingtin mice in order to investigate the effect of low PSA overexpression on the progression of HD. A reduction in disease severity or a delay in onset in these mice would support our hypothesis that PSA is protective in HD. Our view is that suddenly increasing PSA expression in neurons to high levels is toxic in the adult mouse brain. We could test the effect of adult onset of PSA overexpression by creating a tetracycline-regulated expression system. In this way, the gene

can be turned on and off intermittently to avoid toxicity. It would be ideal to identify a small molecule enhancer that can increase expression or activity of the endogenous gene.

The mechanism of degradation of huntingtin is largely unknown. Understanding the degradation of huntingtin is important because it represents possible therapeutic interventions in the treatment of Huntington's disease. PSA is the only identified aminopeptidase able to degrade polyQ peptides efficiently making it a likely participant in the degradation of mutant huntingtin [121, 122]. PSA is a versatile aminopeptidase, able to cleave bonds between a wide range of amino acids at the NH_2-terminus of proteins, including huntingtin. This property is especially important for huntingtin as the first 17 amino acids of huntingtin, known as N17, is highly aggregate-prone; it binds to itself and to the polyQ region of other fragments, full mutant huntingtin, and normal huntingtin proteins to promote aggregate formation [232, 233]. It was found that deletion of the N17 decreased aggregation of mutant huntingtin [232]. It is possible that a reduction in PSA results in reduced degradation of the NH_2-terminal residues of huntingtin and a greater number of molecules subject to N17-mediated aggregation. This would increase the number of inclusions in $Psa^{+/-}$ HD mice. There might be more nuclear inclusions because huntingtin aggregates are trapped in the nucleus. This mechanism was proposed in diseases where tau protein accumulates and forms aggregates, (so-called tauopathies) including frontotemporal dementia (FTD) and Alzheimer's disease [227]. There are conflicting results of whether PSA acts directly on tau protein. One *in vitro* study using mass-spectroscopy to analyze cleavage products found that PSA purified by multiple methods does not result in tau degradation products [224]. Another in vitro study using NH_2-terminal tau antibodies found that purified hPSA cleaved tau *in vitro* [227]. These conflicting results point to two different

mechanisms: a mechanism of direct degradation of tau by PSA or indirect degradation of tau possibly by autophagy or the ubiquitin-proteasome system.

A second mechanism of PSA degradation of huntingtin is through the induction of autophagy. In cell culture models expressing an expanded huntingtin fragment, over-expressing PSA induces autophagy [123]. In our examination of markers of autophagy in the striatum, we could not detect the LC3-II band on western blot from HD mice, so we could not test the hypothesis that in $PSA^{+/-}$ mice autophagy would be decreased. In a transgenic mouse expressing human PSA resulting in a 2-3 fold increase in PSA activity and total PSA expression, there was no increase in autophagy [200]. More evidence for an indirect method of action is that PSA expression modifies other diseases that do not contain polyQ regions, such as mutant tau protein and mutant SOD1 [123, 200, 223] .

We assessed expression of PSA in the striatum of $Hdh^{140Q/140Q}$ mice and found no difference in expression compared with wild type mice, contradicting the finding in PC-12 cells that expression of HD exon 1-74Q induced expression of PSA [234]. The difference between the results in cell culture with that in mice and human disease is not unprecedented [234]. In neuroblastoma cells, SOD1 overexpression increased expression of PSA whereas in transgenic mutant SOD1 mice the expression of PSA in the brain was decreased [223]. The expression of PSA in frontotemporal dementia (FTD) patients was not altered except for in the cerebellum where it was increased significantly [228]. The cerebellum is a region of the brain unaffected by FTD (as in HD) and it is possible that increased PSA is protective in those tissues that are unaffected by the mutant protein.

One limitation is that our study does not uncover any clues to the mechanism by which PSA acts on mutant huntingtin. We were able to detect LC3-I, but not LC3-II by Western

analysis in all samples tested. LC3-I represents soluble protein, while LC3-II is conjugated with the phospholipid phosphatidylethanolamine and correlates with the number of autophagolysosomes [235]. LC3-I alone cannot be used to draw any conclusions about the upregulation of autophagy, therefore this data is not informative in terms of supporting or refuting a change in autophagy status among the mice examined. Supernatant fraction from brain lysate is expected to have an abundance of LC3-I, however LC3-II can be detectable at low levels even in wild type animals with increased LC3-II detected with polyQ expansion of huntingtin [61, 129, 236]. The next step to analyze autophagy in brain lysates would be to test the pellet fraction for enriched LC3-II protein. The protein extraction procedure in this study employed one high speed spin to isolate the supernatant fraction, and an alternative approach would be to use differential centrifugation, two slow speed spins, to first remove nuclei before separating cytoplasmic from membrane organelles [236]. It is possible that Western blot conditions must be adjusted to detect more subtle bands. In this experiment, the positive control would be the $Hdh^{140Q/140Q}$ group of mice, which should induce autophagy, while if Psa operates through augmentation of autophagy, we hypothesize that the Psa deficiency would reduce that increase [129].

Future experiments to extend the results found in this study would use viral delivery system to express hPSA at a lower level, by using a weaker promoter. The goal would be to test these constructs in an HD mouse model to look for an amelioration of the disease that could become gene therapy for HD patients. It is important to analyze the number of cells expressing AAV-hPSA and the spread of the virus throughout the brain. Alternatively, the HD knock-in mice could be bred with PSA overexpressing mice creating a mouse line that stably expresses both human PSA and mutant mouse huntingtin [200]. It is also important to show that PSA

degrades the NH_2-terminus using purified huntingtin and PSA in an *in vitro* assay to elucidate the mechanism of PSA degradation (direct degradation or indirect through autophagy). Mass spectrometry would be particularly useful in determining the fragments created by the degradation and to show NH_2-terminal degradation.

In this study, we find that $Psa^{+/-}$ $Hdh^{140Q/140Q}$ mice have a more severe locomotor phenotype and a greater number of intranuclear inclusions compared with HD mice. Assuming that there is a significant reduction in PSA protein, the behavioral and neuropathological findings support our hypothesis that a reduction in PSA would worsen HD in a knock-in mouse model. Our study is significant for using a knock-in model of HD which expresses full length huntingtin at endogenous levels rather than an overexpressed fragment of mutant huntingtin in cell culture or muscle tissue. HD knock-in mice recapitulate aspects of the human disease and can be used to examine changes in the context of the brain as well as changes in behavioral measurements. Based on our results with AAV-mediated overexpression of PSA, we conclude that neurons may be particularly sensitive to acute PSA overexpression in adulthood. This may limit the utility of AAV-based methods for overexpression and gene therapy using PSA.

E. Materials and Methods

1. Mouse lines and genotyping

FVB mice (female, 3-6 months old, FVB/NJ from Jackson Laboratory, Bar Harbor, ME) were injected with 3 µL volumes of AAV9-CMV-hPSA-HA with various doses (1e12 GC/mL, 1e11 GC/mL, 1e10 GC/mL or 1e12 GC/mL AAV9-CMV-Luc-Htt (control virus expressing firefly luciferase with huntingtin target sequences in the 3'-UTR).

PSA knock-out mice were obtained from Ken Rock (University of Massachusetts Medical School, Worcester, MA) [197]. DNA extracted from tail biopsies was used for genotyping by PCR. Primers for PSA were PSA.Ex5.L2 5'-GACAGGAAACCATATCCTGATGA-3', and PSA.Ex5.R2 5'-CTTTCCTTGCTCTGCTTTGC-3' and primers for the knock-out allele were LacZ.L2 5'-GACGTCTCGTTGCTGCATAA-3', and LacZ.L2 5'-CAGCAGCAGACCATTTTCAA-3'. Amplification products are 400bp for the knock-out allele and 180bp for the wild type allele. We use HotStarTaq Master Mix Kit (Qiagen). The program for PSA is 1) 95C for 15 min, 2) 95C for 30 sec, 3) 55C for 30 sec, 4) 72C for 90 sec 5) repeat steps 2-4 34 times, 6) 72C for 5 min.

Huntingtin knock-in mice were obtained from Scott Zeitlin (University of Virginia School of Medicine, Charlottesville, VA) [145].The primers for Hdh140Q are CAG140For 5'-CTGCACCGACCGTGAGTCC-3', CAG140Rev 5'-GAAGGCACTGGAGTCGTGAC-3'. These primers span a region of mouse huntingtin that is deleted in the knock-in allele. Knock-in allele is represented by a 156bp band and the wild type allele is represented by a 235bp band. The program for $Hdh^{140Q/140Q}$ is 1) 95C for 5 min, 2) 94C for 20 sec, 3) 67C for 30 sec, 4) 72C for 15 sec, 5) repeat steps 2-4 for 40 times, 6) 72C for 5 min. PCR products were separated by agarose gel electrophoresis and visualized by ethidium bromide staining and UV-transillumination. Mouse housing and procedures were approved by the University of Massachusetts Medical School animal protocol A-978-12.

2. Stereotactic injection

FVB mice (female, 3-6 months old, FVB/NJ from Jackson Laboratory, Bar Harbor, ME) were anesthetized with 250 mg/kg tribromoethanol (2.5 g 2, 2, 2, tribromoethanol dissolved in

5mL amylene hydrate into 200mL PBS). Anesthetized mice were placed on a heated pad in a stereotactic frame. Superglue (Loctite) was applied to the surface of the fur between the ears, avoiding eyes and exposed skin. After 10-20 seconds, the glue is gently pulled off to remove fur. The exposed skin is cleaned with betadine and an incision is made posterior to anterior. The skin is pulled aside and the needle is placed over the bregma. Unless otherwise stated, measurements for drilling the hole and placing the needle are: anterior 1mm, lateral 2mm and ventral 3mm from the bregma. Once the needle is lowered, it rests there for 2 minutes before infusion of 3µL at a rate of 125nl per minute (NanoFil syringe, World Precision Instruments). After infusion the mouse rests for 2 minutes before the needle is withdrawn. The incision is closed with clear, undyed suture (monocryl undyed monofilament) and the animals are allowed to recover on a heated pad at 37C.

3. Behavior

General materials and procedure for the raised beam test: Mice were placed on a platform with a bright light shining in the direction of travel. The there was another platform connected by a rod with a diameter of 1.5cm, 40cm above the table, and 63cm in length between the marks for quantification. At the opposite end of the beam was a dark box. Since mice prefer dark conditions, they were motivated to walk across the beam from the light to the dark box. The animals were housed 1-2 mice per cage and were identified by number so the experimenter was blinded to the genotype. The animals crossed the beam 3 times and were trained on the beam one week prior to testing. On the testing date, the time it took to cross the beam and the number of foot slips off of the beam were recorded for the third trial for each mouse. The handler was the

same for all testing days and blind to genotype. Frequency of testing varied by experiment as outlined below.

Raised beam test of $Psa^{-/-}$, $Psa^{+/-}$, and $Psa^{+/+}$ in Figure 2-3 A: Mice in each group were tested on different days and their data collected at 6, 8 and 10 months of age are shown.

Raised beam test of $Psa^{+/-}$ $Hdh^{7Q/140Q}$,$Psa^{+/-}$ $Hdh^{7Q/7Q}$, and controls in Figure 2-4 A: In our testing procedure, animals were tested for three trials at each of the following ages: 3, 4, 5, 6, 7, 8.5, 10 months of age.

Raised beam test of $PSA^{+/-}$ $Hdh^{140Q/140Q}$ and controls in Figure 2-5 C and D: mice were tested at 12 months of age.

Open field behavior: Mice were recorded for five minutes in a novel empty cage (16 cm x 27 cm). The motion of the mouse was traced on a video screen and scanned into image files. Distance traveled was quantified for each minute using imageJ software and converted into centimeters traveled. The values for the first minute were used for statistical analysis.

4. RNA extraction and real-time QPCR

$PSA^{+/-}$ mice: RNA isolation from striatum and cortex of PSA mice was performed using the MAXWELL16 automated nucleotide and protein extraction system (Promega). We followed manufacturer's protocol for tissue homogenization and lysate preparation, and reverse transcription was performed according to the protocol for Superscript III Reverse transcriptase

(Invitrogen). Sybr green RT-PCR kit (Qiagen) was used with the following program: 1) 95C for 15 minutes, 2) 95C for 15 sec, 3) 55C for 30 sec, 4) 68C for 30 sec, 5) repeat steps 2-4 40 times. Results were normalized to β-actin. Primers amplify a region from exon 23 that is present on both wild type and mutant (knock-out) alleles. Primer sequences are: PSA_forward: 5'-GCACCATCCAGCAGTGTTGTGAAA-3', PSA_reverse: 5'-AGCTGTTTGGTAGCTCCACCTCAT-3', Beta_actin_sense, 5'-CGAGGCCCAGAGCAAGAGAG-3', Beta_actin_antisense, 5'-CGGTTGGCCTTAGGGTTCAG-3'.

5. Western blot

The striatum was dissected and homogenized in NP-40 lysis buffer (Boston BioProducts Cat BP-119) with complete protease inhibitor. Samples were spun at 4C for 10 min at 16,000 x g. Supernatant aliquots were stored at -20C. 30ug of crude lysates were loaded onto gels (3-8% acetate for huntingtin and PSA, 12% Bis-Tris for LC-3). Dry transfer was performed using the iBlot system (7 minutes for huntingtin and PSA, 5 minutes for LC3). Primary antibodies and dilutions are: 1:500 Goat anti-Rat PSA (Chemicon ab3258), 1.0 µg/mL AB1 antibody (huntingtin) [229], 1:1000 rabbit anti-ubiquitin,1:10,000 mouse monoclonal anti-α-tubulin (Sigma), 1:1000 mouse monoclonal HA antibody (Covance, HA.11 clone 16B12), 2µg/mL LC3 (Novus Biologicals, NB100-2220). Secondary antibodies are: 1:5000 donkey HRP-conjugated anti-goat IgG (Promega V805A) and 1:100,000 rabbit anti-mouse IgG HRP-conjugated (Sigma A9044).

6. Immunohistochemistry

Mice were perfused transcardially with 20 mL of PBS followed by 15 mL of 4% paraformaldehyde in PBS. Brains were post-fixed at 4C in 4% PFA for 4 hours, then in 2% PFA overnight, and then stored in PBS. Coronal sections were cut on a vibratome at thickness of 40 microns and collected as serial sections. Sections were treated with 30% hydrogen peroxide solution diluted 1:10 in PBS. For blocking and antibody binding we followed the Rabbit IgG or M.O.M. peroxidase kit protocols (Vector Laboratories). Primary antibodies were incubated overnight at 4C. Antibodies were GFAP 1:1000 (rabbit polyclonal, Abcam ab7260), DARPP-32 1:1000 (rabbit monoclonal, Abcam ab40801), MW8 serum 1:10 (mouse monoclonal, Developmental Studies Hybridoma Bank from the University of Iowa), EM48 1:2000 (from Steven Hersch, Massachusetts General Hospital), HA monoclonal 1:1000 (Covance, HA.11 clone 16B12). Sections were developed for 2 minutes with 3, 3'-Diaminobenzidine (DAB) from Thermo Scientific, dehydrated and coverslipped.

7. Stereology

Sections were analyzed with a 60x oil immersion objective. Quantification began at the center of the mid-dorsal portion of the striatum just below the corpus callosum. The numbers of inclusions was counted using an Olympus BX51 microscope with a Nikon DS-Qi1MC camera. The nuclear inclusion bodies and cytoplasmic aggregates were counted for each field of view using the NIS-Elements RR 3.10 computer program while focusing up and down on the slide. Then the objective was moved to the adjacent field of view. Aggregates and inclusions from 35

fields of view were quantified and an average was taken for each mouse. There were no differences among sections or dependent on the distance from the corpus callosum, so the average number of inclusions per field of view was used for subsequent analysis.

8. Statistical analysis

SAS version 9.2 was used to calculate mixed method ANOVA. Other tests were done using IBM SPS statistics version 20 and GraphPad Prism version 6.00 for Windows.

Figure 2-4 A: Raised beam test of $Psa^{+/-}$ $Hdh^{7Q/140Q}$, $Psa^{+/-}$ $Hdh^{7Q/7Q}$, and controls. Mixed method ANOVA was used to analyze difference between the groups. This test was chosen because there are missing data for some of the time points.

Figure 2-5 C: Raised beam test of $Psa^{+/-}$ $Hdh^{140Q/140Q}$ and controls- latency to cross the beam. Natural log transformation was performed to achieve normal distribution and the transformed data passed the Leven's test for homogeneity of variances. A one-way ANOVA was used followed by Tukey's post-test for multiple comparison.

Figure 2-5 D: Raised beam test of $Psa^{+/-}$ $Hdh^{140Q/140Q}$ and controls- foot slips off of beam. These data are not normally distributed, and no transformation normalized the data. Therefore, the non-parametric Kruskall-Wallis test and Dunn's multiple comparisons test were used to analyze the differences between the three groups. Three outliers were included in the analysis.

Figure 2-4 B: Open field test. The distance traveled in the first minute after introduction to a novel cage was used for analysis. Distances were compared using one-way ANOVA with Tukey's multiple comparisons post-test.

Western blot: Data was tested for outliers using Grubb's test (http://www.graphpad.com/quickcalcs/Grubbs1.cfm) and significant outliers were removed. One-way ANOVA was used to test an effect of genotype and unpaired T-test was used for pairwise comparisons.

Measurements of inclusions and aggregates: Data sets were tested for normal distribution. Normally distributed data were analyzed by unpaired t-test. Data that were not normally distributed were analyzed by Mann-Whitney U test.

Figure 2-1: PSA homozygous knock-out mice are smaller in size than heterozygous mice. $Psa^{-/-}$ mice are smaller than $Psa^{+/-}$ mice at 1 and 6 months of age (unpaired t-test, 1 month $p=0.0030$ $n=3$ for $Psa^{+/-}$, $n=2$ for $Psa^{-/-}$; for 6 month $p=0.0247$ $n=4$ for $Psa^{+/-}$, $n=2$ for $Psa^{-/-}$). Mice are combined male and female as depicted individually in Table 2-1. *$p<0.05$, ** $p<0.01$. Data is presented as mean ± SD.

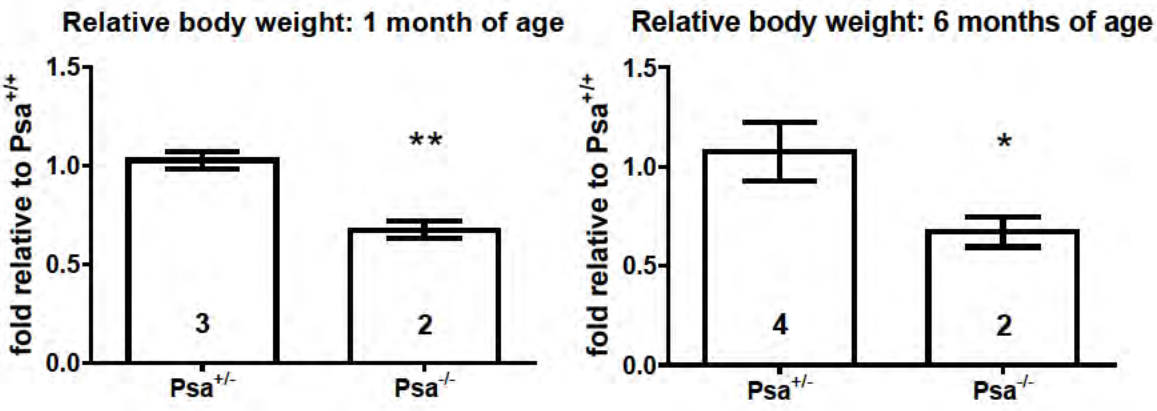

Figure 2-1: PSA homozygous knock-out mice are smaller in size than heterozygous mice.

Figure 2-2: PSA mRNA and protein are expressed in a gene dosage-dependent manner. A.) q PCR was done on striatal extracts of $Psa^{-/-}$, $Psa^{+/-}$, and $Psa^{+/+}$ mice. In the striatum, genotype of PSA mice affected PSA mRNA levels (One-way ANOVA p=0.0004). By pairwise comparison, mRNA levels for heterozygous mice is 49.8% of wild type mice (Tukey's pairwise comparison, mean difference between +/+ and +/- 0.6280 (95% CI 0.1632 to 1.093, p=0.00811), mean difference between +/+ and -/- 1.162 (95% CI 0.6253 to 1.699, p<0.001), n=5 for $Psa^{+/+}$ and $Psa^{+/-}$, n=3 for $Psa^{-/-}$). B.) Western blot of protein extracts from cortex of $PSA^{-/-}$, $PSA^{+/-}$, and $PSA^{+/+}$ mice were labeled with antibodies to mouse PSA and tubulin. Values for PSA protein are expressed relative to tubulin. In the cortex, the PSA genotype affected PSA protein levels (One-way ANOVA p=0.0005). By pairwise comparison, heterozygous mice have 47.5% PSA of wild type mice (Tukey's pairwise comparison mean difference between +/+ and. +/- 0.5007 (95% CI 0.1473 to 0.8540, p=0.00552), mean difference between +/- and -/- 0.4467 (95% CI 0.09334 to 0.8000, p= 0.01315), mean difference between +/+ and -/- 0.9473 (95% CI 0.594 to 1.301, p<0.001), n=3 per genotype). C) Western blot of protein extracts from striatum of $PSA^{-/-}$, $PSA^{+/-}$, and $PSA^{+/+}$ mice were probed with antibodies to mouse PSA and tubulin. Values for PSA protein are expressed relative to tubulin. In the striatum, PSA genotype affects PSA protein levels (One-way ANOVA p=0.0014). By pairwise comparison, protein extracts from striatum of heterozygous mice have 57.8% PSA as wild type (Tukey's pairwise comparison, mean difference between +/- and -/- 0.5840 (95% CI 0.1192 to 1.049, p=0.0137), mean difference between +/+ and -/- 1.047 (95% CI 0.5824 to 1.512, p<0.001), n=3 per genotype). D) Representative blot of striatal protein extracts for one mouse in each group done in triplicate. For all graphs * p<0.05, **p<0.01, ***p<0.001, data is presented as mean ± SD.

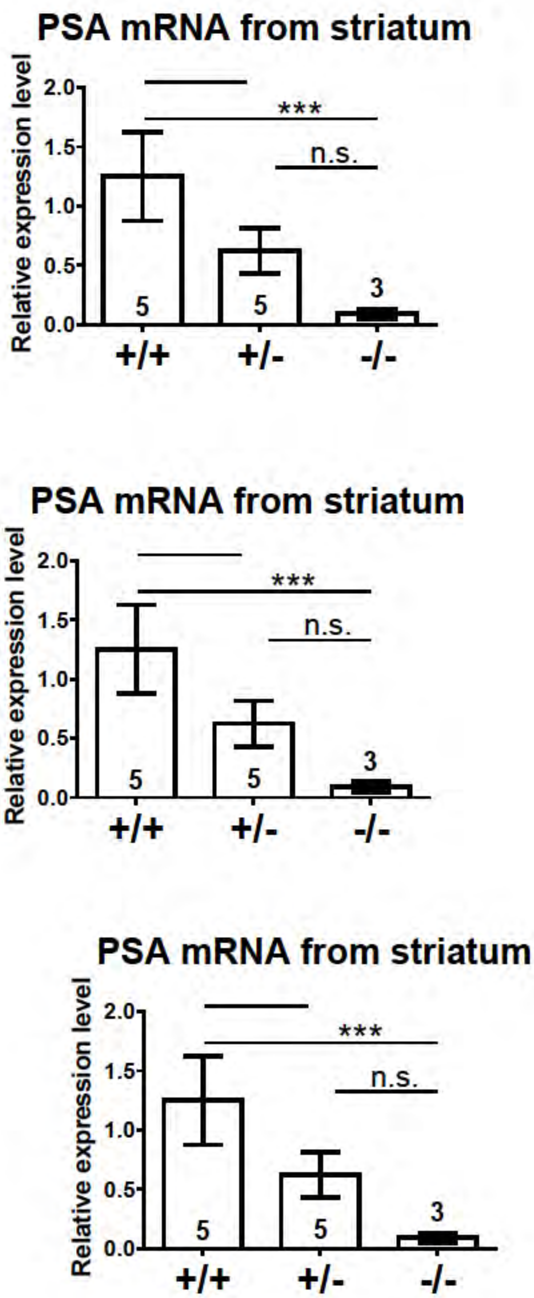

Figure 2-2: PSA mRNA and protein are expressed in a gene dosage-dependent manner.

Figure 2-3: There is no abnormal locomotor behavior or inclusion formation in PSA knock-out mice. $Psa^{-/-}$, $Psa^{+/-}$, and $Psa^{+/+}$ mice were tested on the raised beam for locomotor abnormality. A.) The left graph in panel A is a comparison of the time in seconds that it took the mice to cross the raised beam. The right graph shows the number of foot slips off the beam in the same groups of mice. There were no differences between the three groups at 6 months, 10 months and 14 months of age. For each graph two-way ANOVA was performed and found to be not significant ($p>0.05$). Data is presented as mean ± S.E.M., number of mice in each group is shown in the within the bars. B.) Fixed brains from a HD knock-in mouse ($Hdh^{7Q/140Q}$, 13 month old), PSA knock-out mice ($Psa^{-/-}$, 9 month old (n=1), 22 month old (n=1, not shown)), and wild type mice (9 month old (n=3), 22 month old (n=3, not shown) were labeled with an antibody that recognizes ubiquitin. Inclusion bodies can be seen in the HD knock-in mouse (arrows). There are no ubiquitin positive inclusion bodies in the $PSA^{-/-}$ mice or wild type mice examined. C.) Sections from HD knock-in mouse (13 months old), $PSA^{-/-}$ mice (17 months old; 9 and 22 month old not shown, n=1 for each age), and wild type mouse were labeled with EM48 for huntingtin aggregates (9 month n=3). There are no EM48 positive inclusions in the PSA knock-out mouse or the wild type mouse.

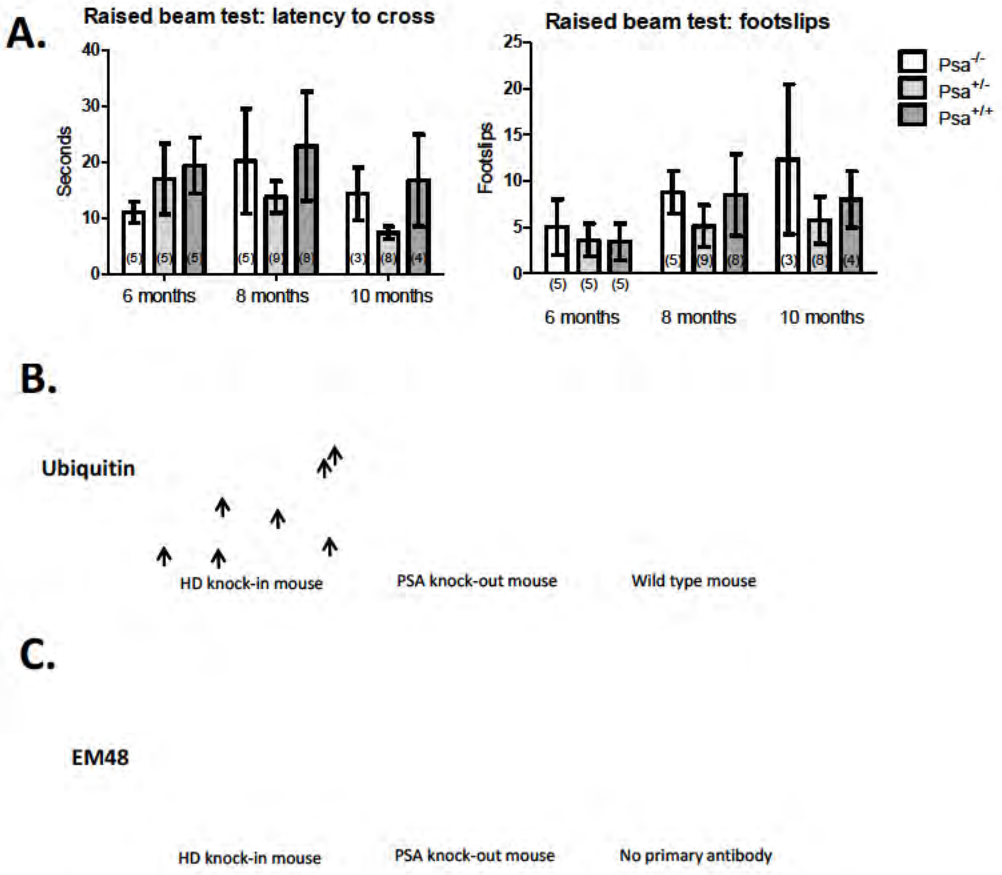

Figure 2-3: There is no abnormal locomotor behavior or inclusion formation in PSA knock-out mice.

Figure 2-4: Psa heterozygosity corrects huntingtin-related reduction in open field activity, however there are no differences observed on raised beam test or in the number of inclusion bodies. A.) Four groups of mice were tested on the raised beam test. $Psa^{+/+}$ $Hdh^{7Q/140Q}$ (n=7) have an increased latency to cross and in foot slips compared with $Psa^{+/+}$ $Hdh^{7Q/7Q}$ (n=14) (Mixed models ANOVA, p=0.0172 and p=0.0196, respectively. There were no differences among the other groups for latency to cross and footslips. $Psa^{+/-}Hdh^{7Q/7Q}$ n=9, for $Psa^{+/-}$ $Hdh^{7Q/140Q}$ n=4. Tukey's multiple comparison revealed no significant differences at any age). Data is presented as mean ± SEM. B.) At 13 months of age, the same groups of mice were tested for activity using the open field test. Each mouse was video recorded once for 5 minutes in the open field box and distances traveled in the first minute were used for comparison (see methods section). $Psa^{+/+}Hdh^{7Q/140Q}$ mice traveled less distance than the other groups, and $Psa^{+/-}Hdh^{7Q/140Q}$ genotype corrected this difference in distance traveled (One-way ANOVA between all groups, p=0.0010, Tukey's multiple comparison test, for $Psa^{+/-}Hdh^{7Q/140Q}$ vs. $Psa^{+/+}Hdh^{7Q/140Q}$ mean diff. 65.03cm (95% CI 18.98 to 111.1, p=0.0057), for $Psa^{+/-}Hdh^{7Q/7Q}$ vs. $Psa^{+/+}Hdh^{7Q/140Q}$ mean diff. 45.71cm (95% CI 8.68 to 82.73, p=0.0154), for $Psa^{+/+}Hdh^{7Q/140Q}$ vs. $Psa^{+/+}$ $Hdh^{7Q/7Q}$ mean diff. -51.22cm (95% CI -85.67 to -16.78, p=0.00361). Data is presented as mean ± S.D.). C.) We performed immunohistochemistry for mutant huntingtin aggregates in brain sections of $Psa^{+/-}$ $Hdh^{7Q/140Q}$ and $Psa^{+/+}$ $Hdh^{7Q/140Q}$ using EM48 antibody. There was no difference in the number of inclusion bodies in the striatum or in the cortex at 1.5 years of age (unpaired t-test, cortex p=0.1425, striatum p=0.6802, $Psa^{+/-}$ $Hdh^{7Q/140Q}$ n=3, $Psa^{+/+}$ $Hdh^{7Q/140Q}$ n=5). Data is presented as mean ± S.E.M. inclusions per field of view. For all graphs *p<0.05, **p<0.01.

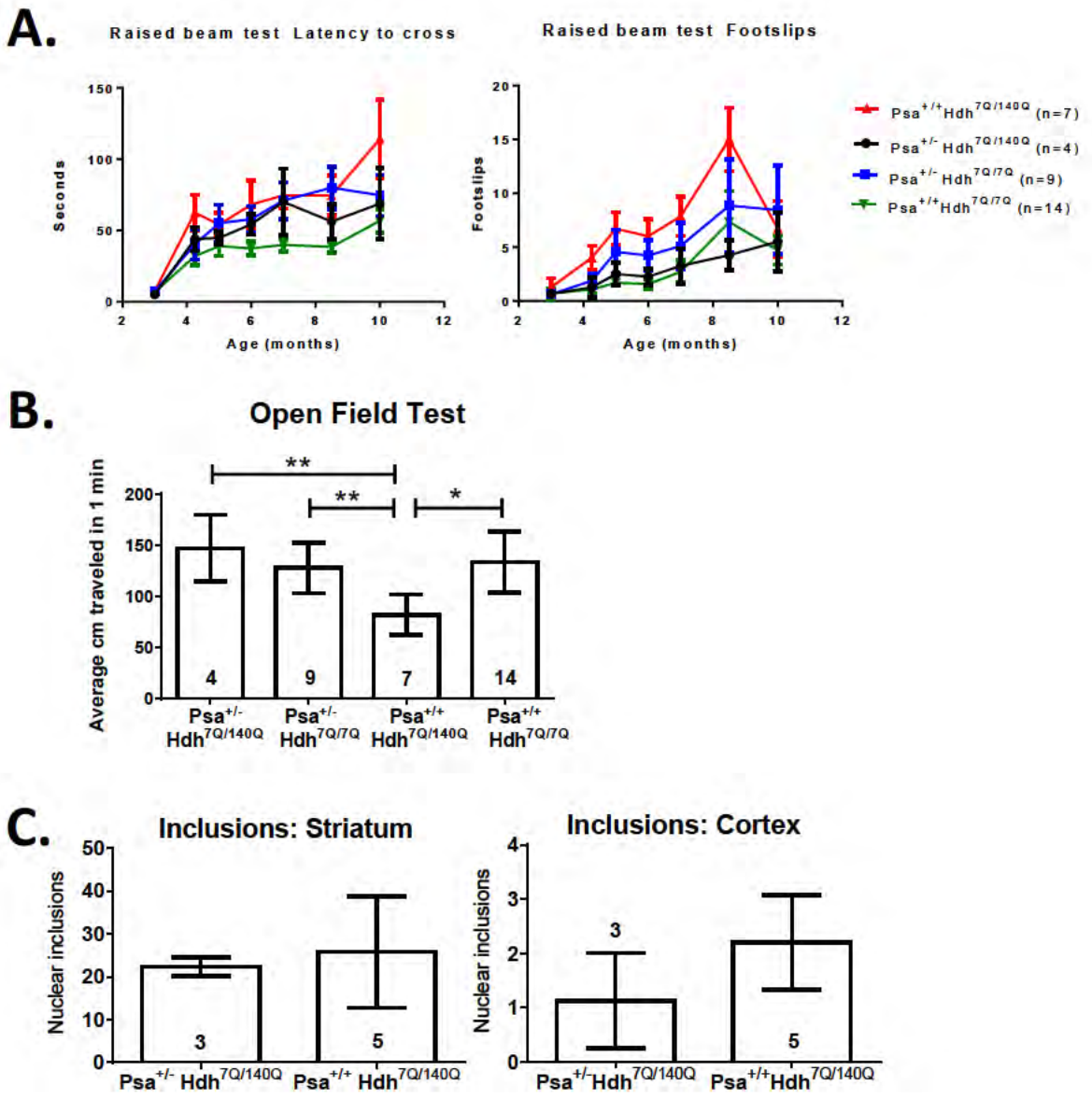

Figure 2-4: Psa heterozygosity corrects huntingtin-related reduction in open field activity, however there are no differences observed on raised beam test or in the number of inclusion bodies.

Figure 2-5: $Psa^{+/-}$ $Hdh^{140Q/140Q}$ mice exhibit deficits on the raised beam test. A.) $Psa^{+/-}$ $Hdh^{140Q/140Q}$ mice appear to express less PSA protein than $Psa^{+/+}$ $Hdh^{140Q/140Q}$, however the difference is not statistically significant due to large variation within the groups (t-test p=0.0654, n=4). B.) Representative blot of one sample from each group in triplicate. C.) $Psa^{+/-}$ and $Psa^{+/+}$ $Hdh^{140Q/140Q}$ mice were tested on the raised beam test at 1 year of age and compared with wild type ($Psa^{+/+}$ $Hdh^{7Q/7Q}$, n=11) mice. $Psa^{+/-}$ $Hdh^{140Q/140Q}$ mice (n=16) had a greater latency to cross the beam compared with wild type mice (Tukey's multiple comparisons, mean diff. 0.7886 (95%CI 0.1363 to 1.441, p=0.0177). There was no difference between the $Psa^{+/+}$ $HD^{140Q/140Q}$ mice (n=20) compared with the other groups. $Psa^{+/-}Hdh^{140Q/140Q}$ mice also had significantly greater foot slips off of the beam compared with the other two groups. (Tamhane's Post Hoc test $Psa^{+/-}$ $Hdh^{140Q/140Q}$ vs $Psa^{+/+}$ Hdh $^{140Q/140Q}$, mean diff. 7.76 (95% CI 1.3835 to 14.1415, p=0.017) $Psa^{+/-}$ $Hdh^{140Q/140Q}$ vs $Psa^{+/+}$ Hdh $^{7Q/7Q}$, mean diff. 9.426 (95% CI 3.2362 to 15.6161, p=0.00289). The majority of wild type mice had no foot slips at all. *$p<0.05$, **$p<0.01$ Data is presented as mean ± SD.

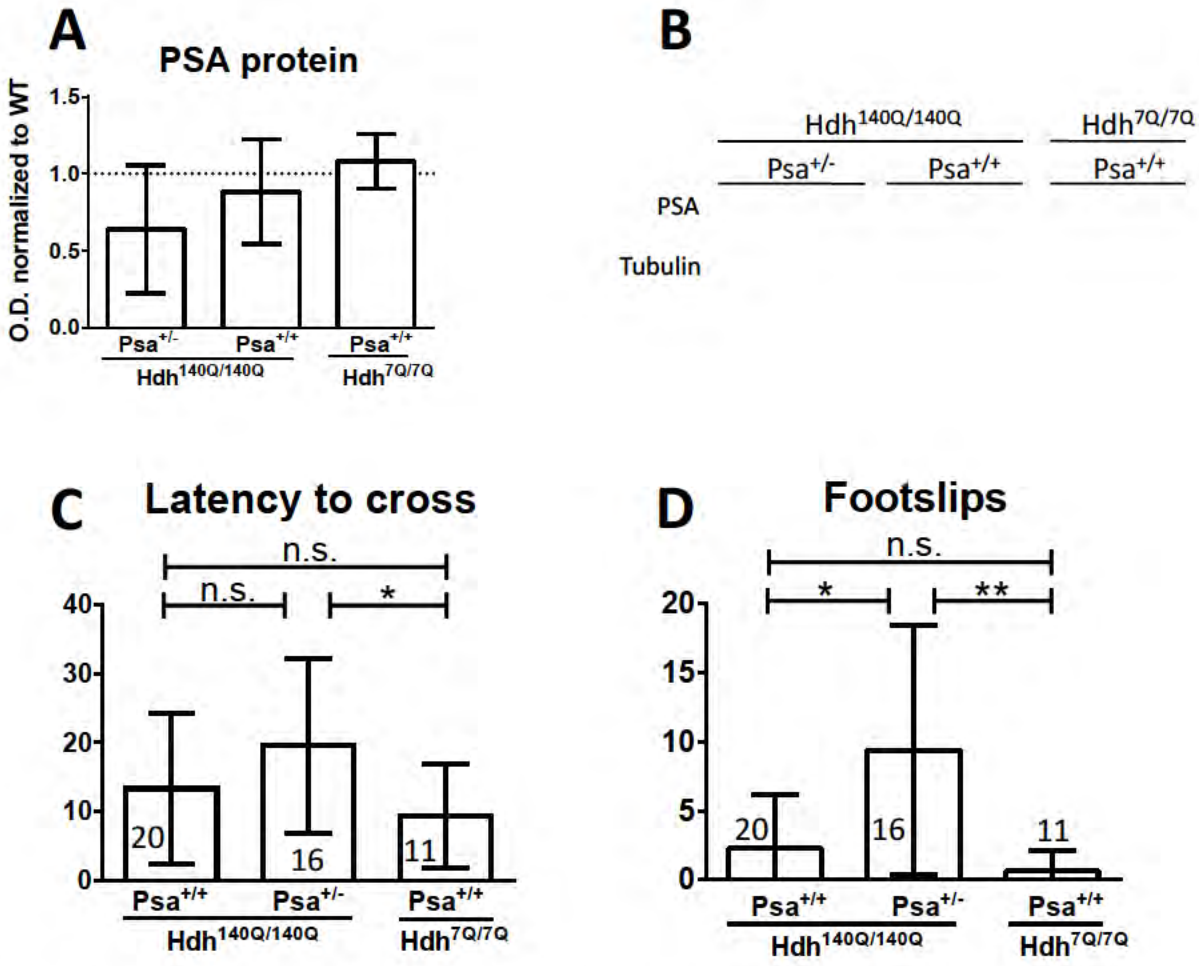

Figure 2-5: $Psa^{+/-}$ $Hdh^{140Q/140Q}$ mice exhibit deficits on the raised beam test.

Figure 2-6: There is increased inclusion body formation in $Psa^{+/-}$ $Hdh^{140Q/140Q}$ mice. A.) Fixed brains from 12 month old $Psa^{+/-}$ $Hdh^{140Q/140Q}$ and $Psa^{+/+}$ $Hdh^{140Q/140Q}$ mice were labeled with MW8, an antibody that labels mutant huntingtin inclusion bodies and aggregates. Nuclear inclusion bodies are circular and regular in size within a section. Inclusion bodies are indicated with arrows in the enlarged image. Cytoplasmic aggregates are smaller and irregularly shaped. Aggregates are indicated with arrowheads in the enlarged image. B.) Sections from $Hdh^{140Q/140Q}$ mice were labeled with MW8 (red) and DAPI (blue) stained to show co-localization of inclusion bodies with the nucleus. C.) Inclusion bodies were stereologically quantified throughout the striatum, and an average per field of view for each mouse was used for comparison. There are a greater number of inclusion bodies in the $Psa^{+/-}Hdh^{140Q/140Q}$ (n=9) compared with $Psa^{+/+}Hdh^{140Q/140Q}$ (n=8) (unpaired t-test, p=0.0154). D.) $Psa^{+/-}$ HD mice (n=9) have smaller inclusion bodies than $Psa^{+/+}$ HD mice (n=8) on average, although this difference was not statistically significant (unpaired t-test, p=0.1981). E.) $Psa^{+/-}$ $Hdh^{140Q/140Q}$ mice (n=9) have a greater number of cytoplasmic aggregates than $Psa^{+/+}$ $Hdh^{140Q/140Q}$ mice (n=8), although this difference is not statistically significant. (Mann-Whitney U-test, p=0.1388). F.) There was no difference in the number of neurons as quantified by Nissl staining (unpaired t-test, p=0.4605). *$p<0.05$ Data is presented as mean ± SD.

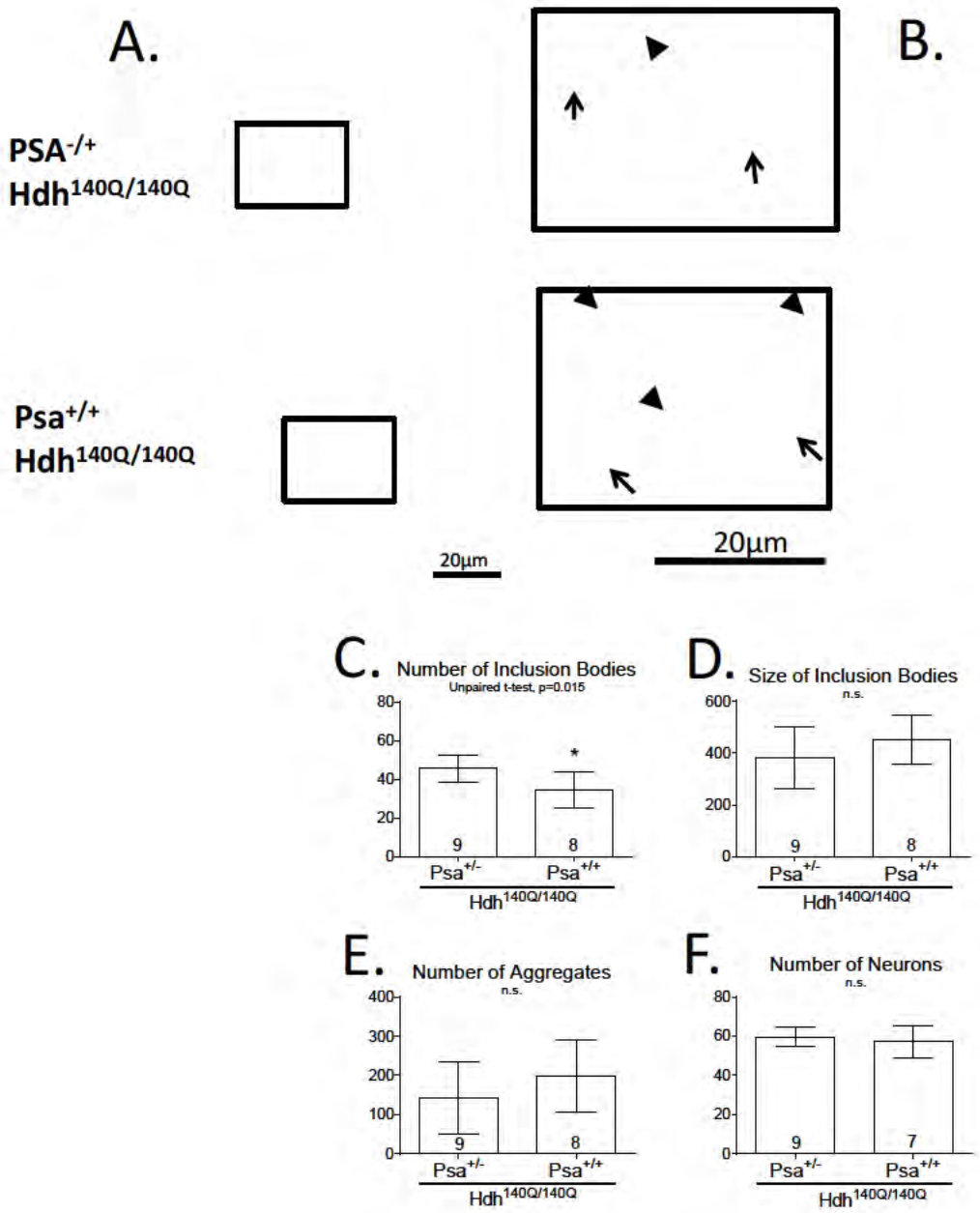

Figure 2-6: There is increased inclusion body formation in $Psa^{+/-}$ $Hdh^{140Q/140Q}$ mice.

Figure 2-7: $Psa^{+/-}$ $Hdh^{140Q/140Q}$ mice display no change in soluble huntingtin or LC3-I levels. A.) Western analysis was performed on protein extract from striatal tissue of 16 month old mice. There was no difference in soluble huntingtin levels between the groups (One-way ANOVA, p= 0.2095, n=5 for each group, each sample was done in triplicate). Representative western blot of triplicates of one mouse per genotype. B.) Antibodies recognizing LC3 were used to detect conversion of LC3-I to LC3-II. LC3-II could not be detected in our samples with our conditions. There was no difference in LC3-I levels among the groups (One-way ANOVA, p=0.9682, n=5 for each group, each sample was done in triplicate). Each lane was normalized to tubulin and then normalized to a wild type sample on the same blot. Data are represented as average fold-difference from wild type ± SD. Representative western blot of triplicates of one mouse per genotype.

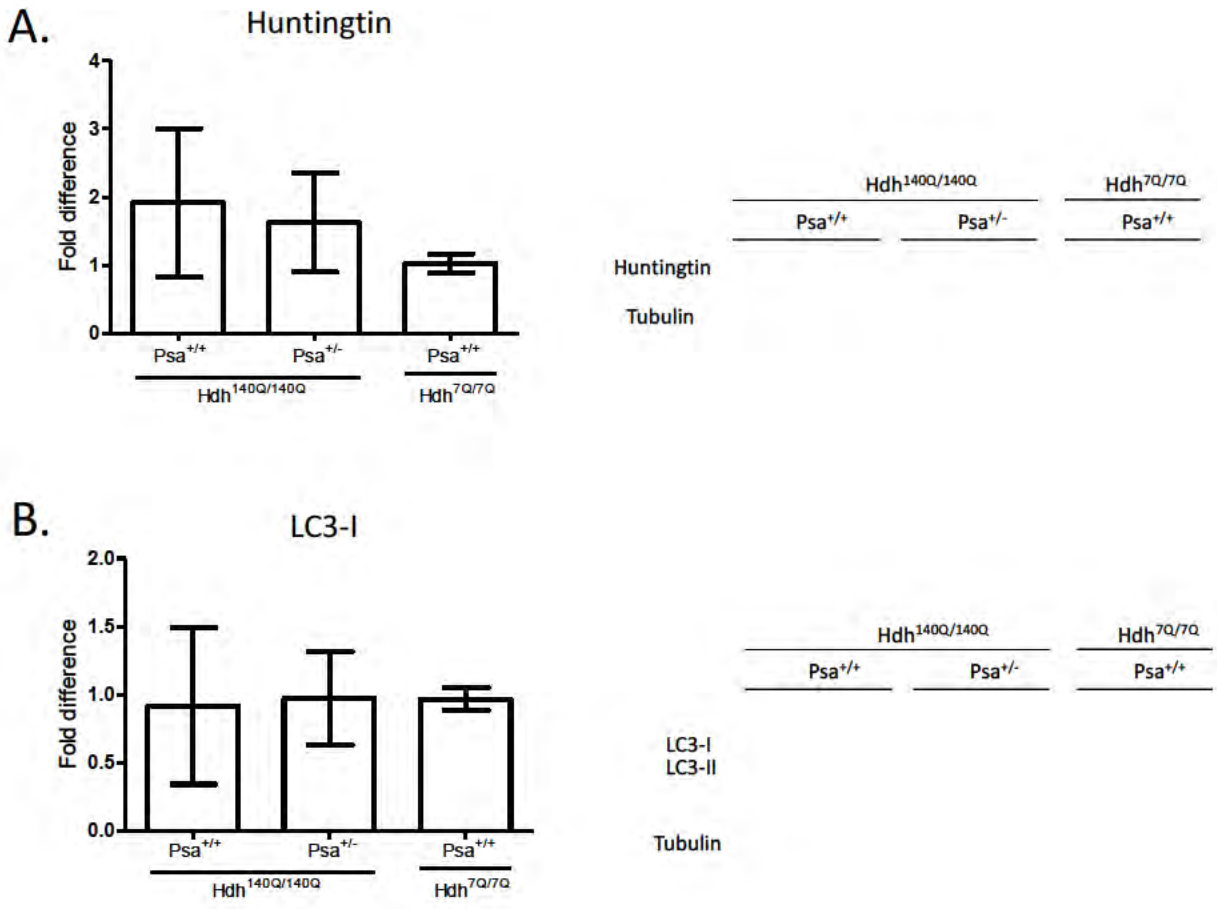

Figure 2-7: Psa$^{+/-}$ Hdh$^{140Q/140Q}$ mice display no change in soluble huntingtin or LC3-I levels.

Figure 2-8: Dosage-dependent hPSA expression from AAV-hPSA-HA injected striatal tissue. Western blot for hPSA-HA using antibodies that recognize HA epitope show a decrease in expression of hPSA protein across the dilutions of AAV-hPSA-HA injected striatal extracts. There is no detectable expression in 1e9 GC dose or control injection samples (n=3 for all groups, control injection is AAV-GFP, NI is no injection, all injections 3µL in volume, samples processed 3 weeks after injection. All samples were processed 3 weeks after injection). Data is presented as mean ± SD.

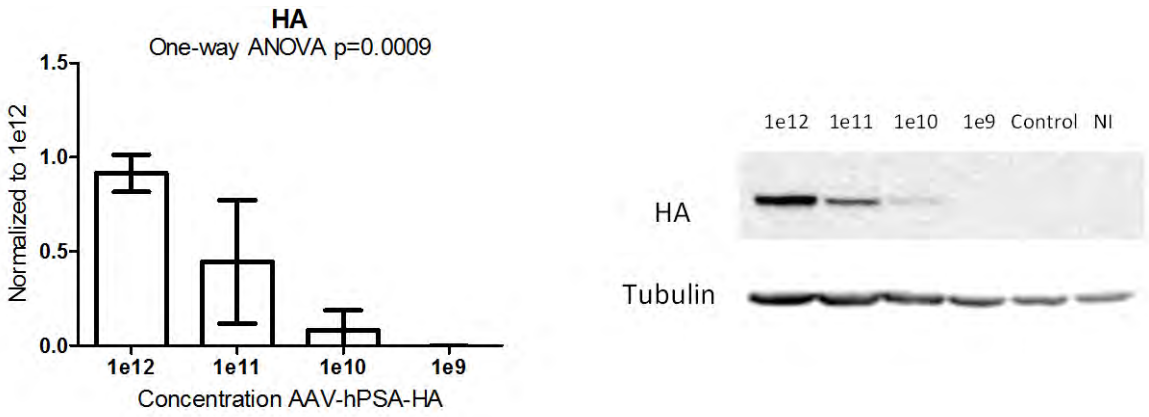

Figure 2-8: Dosage-dependent hPSA expression from AAV-hPSA-HA injected striatal tissue.

Figure 2-9: Dilution of AAV-hPSA-HA shows dosage-dependent toxicity. A.) Coronal sections were taken 3 weeks after injection of AAV-hPSA-HA and labeled with HA antibody. There is HA positive staining for the hPSA-HA transgene that can be seen at 1e11 GC and 1e10 GC doses. HA positive staining areas are delineated by the dashed line. B.) 1e11 GC dose of AAV-hPSA-HA shows widespread astrocyte activation (delineated by dashed line) at 4X and 60X oil immersion magnifications. Dose of 1e10 GC showed astrocyte activation only at the injection site. Control injection of 1e12 GC AAV-luciferase (control injection) elicited a small amount of GFAP activation around the injection site. The 60X magnification column shows representative images within astrocyte activation area. C.) There is decreased staining for DARPP-32 positive medium spiny neurons in the 1e11 GC dose of AAV-hPSA-HA. There does not appear to be a change in staining for the 1e10 GC dose compared with control injection. D.) HA double labeling with DARPP-32 shows co-localization of hPSA-HA with medium spiny neurons as well as cells that are negative for DARPP-32 staining. (n=3 for all doses, images are from representative samples).

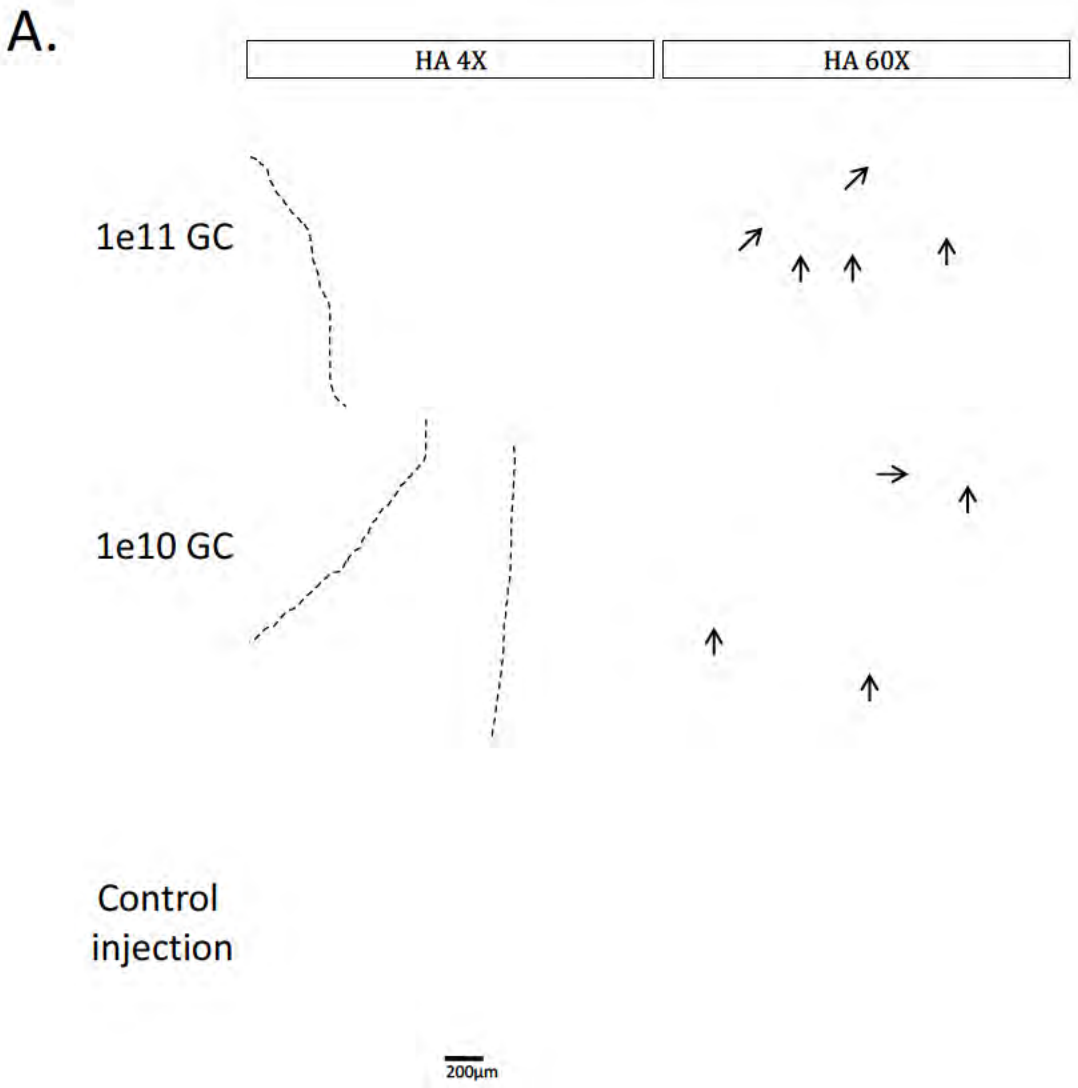

Figure 2-9: Dilution of AAV-hPSA-HA show dosage-dependent toxicity.

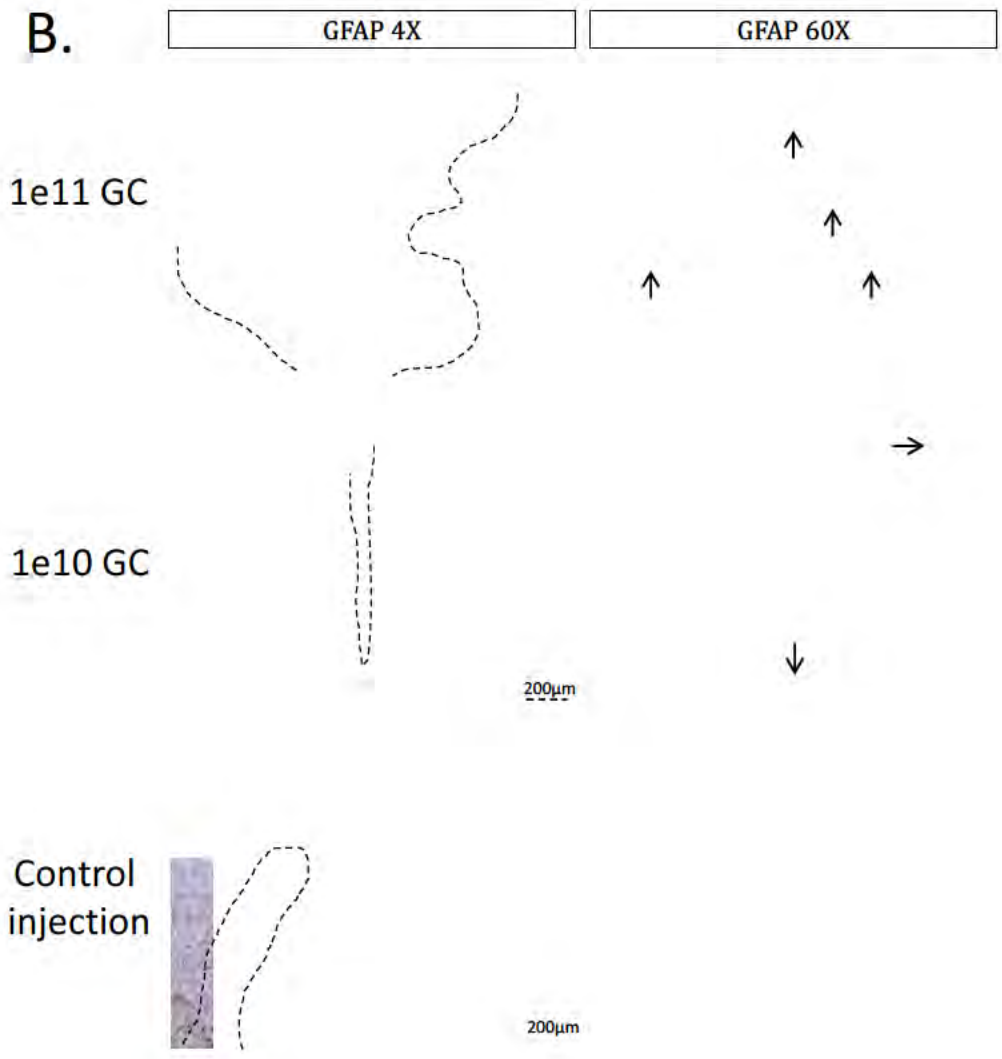
B.
GFAP 4X
GFAP 60X
1e11 GC
1e10 GC
200µm
Control injection
200µm

C.

DARPP-32 4X	DARPP-32 60X

1e11 GC

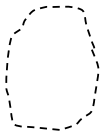

200µm

1e10 GC

200µm

Control injection

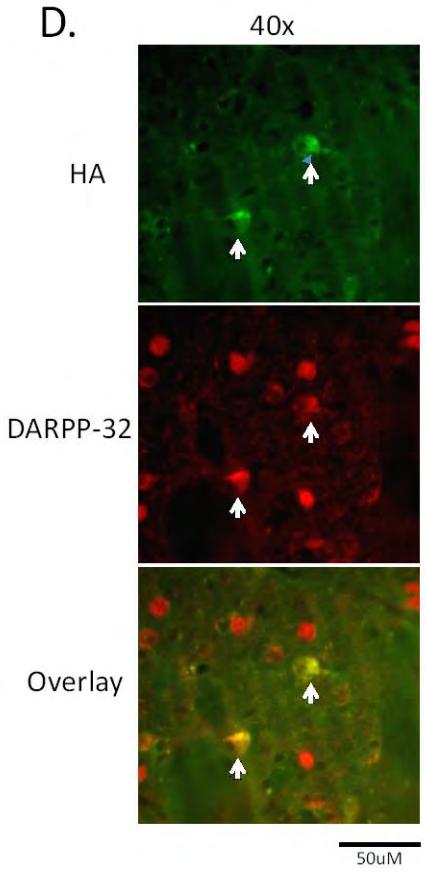
D.
40x
HA
DARPP-32
Overlay
50uM

Figure 2-10: AAV-hPSA-HA is toxic to cells. A time course experiment was performed examining brain sections 1, 2, and 3 weeks after injection of AAV-hPSA-HA (1e12 GC) into the striatum (n=3 for each group, representative images shown). The first row shows that HA staining is detectable at one week (compared with no injection in the last column), becomes darker at two weeks, and then disappears at week three. The second row shows that GFAP staining is intense and very concentrated at weeks 2 and 3. In the third row are images staining for DARPP-32 positive neurons. These images show a reduction of DARPP-32 staining by the second week, and then a loss of reactivity by the third week indicating a complete loss of DARPP-32 positive neurons.

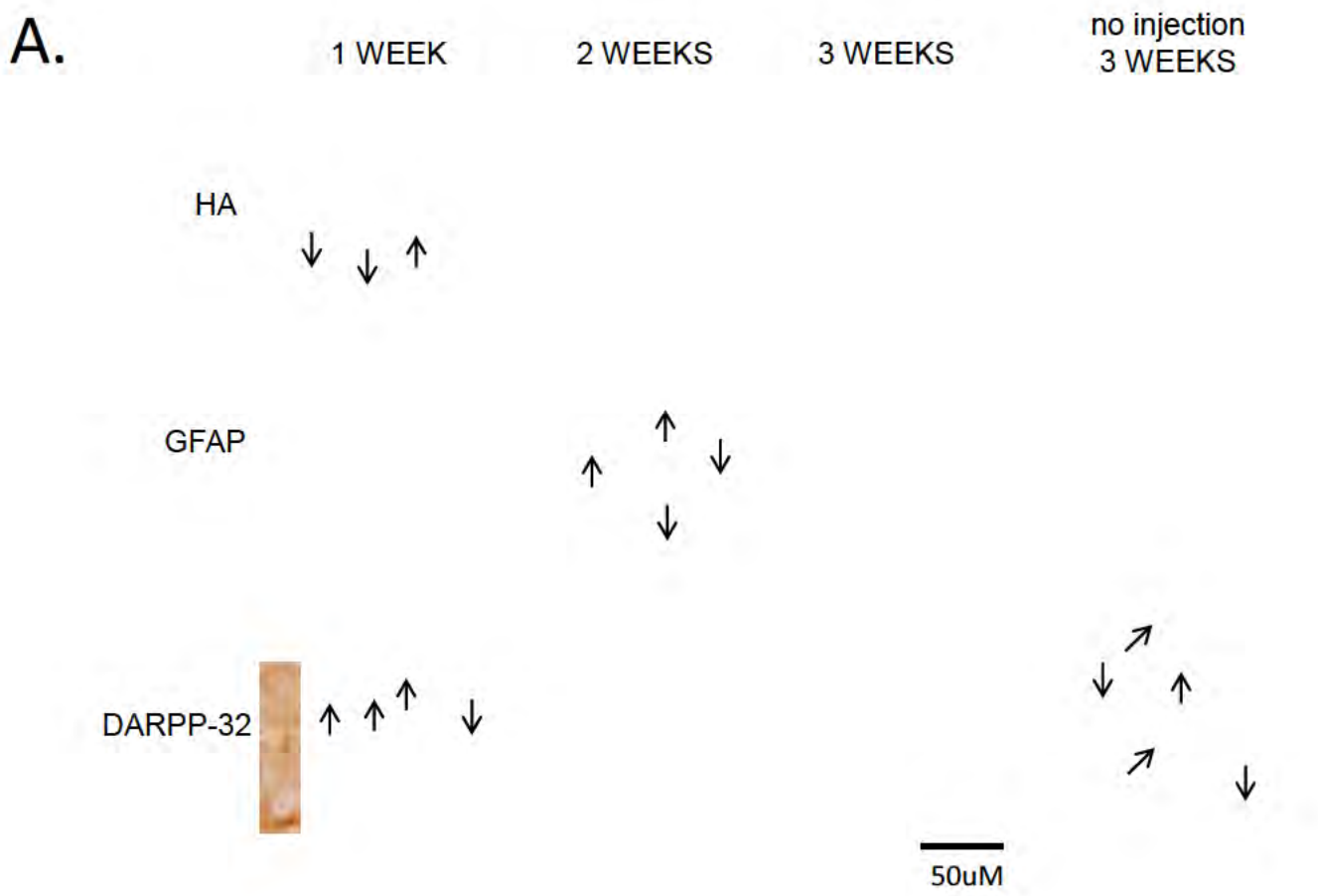

Figure 2-10: AAV-hPSA-HA is toxic to cells.

Figure 2-11: Mutant huntingtin protein is distributed among cytosolic and nuclear compartments in soluble and insoluble forms. A.) Full-length mutant huntingtin protein is found in its soluble state in the cytoplasm and nucleus and it is also found to be associated with cytoplasmic aggregates and intranuclear inclusion bodies. Full-length huntingtin can be cleaved into NH_2-terminal and COOH-terminal fragments. The NH_2-terminal mutant huntingtin fragments oligomerize into fibrillar huntingtin that accumulates and results in formation of cytoplasmic aggregates and intranuclear inclusion bodies. B.) Estimated distribution of full-length mutant huntingtin and NH_2-terminal mutant huntingtin fragments. The majority of full-length mutant huntingtin is localized in the cytosolic compartment. The majority of NH_2-terminal mutant huntingtin is estimated to be in an aggregated form, either as cytoplasmic aggregates or intranuclear inclusion bodies.

A.

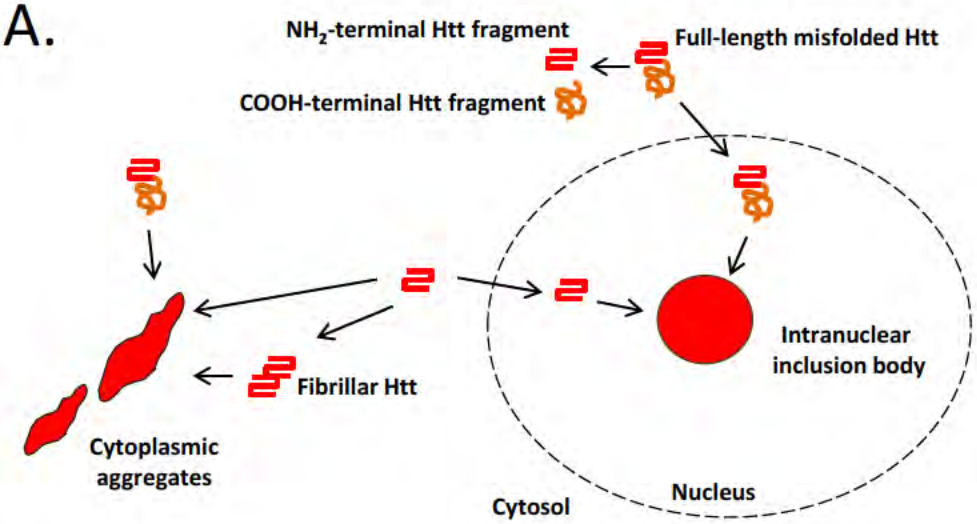

B.

[Full-length Htt]$_{total}$: soluble cytosolic Htt > soluble nuclear Htt > insoluble aggregates and inclusion bodies

[NH_2-terminal Htt fragment]$_{total}$: insoluble aggregates and inclusion bodies > fibrillar form > soluble form

Figure 2-11: Mutant huntingtin protein is distributed among cytosolic and nuclear compartments in soluble and insoluble forms.

Table 2-1: Weight of $Psa^{+/+}$, $Psa^{+/-}$, and $Psa^{-/-}$ mice at 1 and 6 months of age.

Age	Sex	Mouse ID	Parent ID	DOB	Psa Genotype	Weight (g)	Average bodyweight of +/- & +/+ (g)	-/- weight as percentage of +/- and +/+
1 month	Female	363	339x343	3/8/09	+/-	17.3	17.30	64.16
		364	339x343	3/8/09	+/+	17.3		
		365	339x343	3/8/09	-/-	11.1		
	Male	366	339x343	3/8/09	+/+	19.9	20.40	68.63
		367	339x343	3/8/09	+/-	21.4		
		368	339x343	3/8/09	+/-	19.9		
		369	339x343	3/8/09	-/-	14		
6 months	Female	326	114x174	9/8/08	+/+	24.6	25.35	61.93
		327	114x174	9/8/08	+/-	27.2		
		337	224x214	10/31/08	+/-	23.4		
		347	294X305	11/15/08	+/+	26.2		
		338	224x214	10/31/08	-/-	15.7		
	Male	339	224x214	10/31/08	+/-	34.7	30.03	65.59
		361	213X166	9/28/08	+/+	27.2		
		331	265x266	9/12/08	+/-	28.2		
		360	213X166	9/28/08	-/-	19.7		

Table 2-1: Weight of $Psa^{+/+}$, $Psa^{+/-}$, and $Psa^{-/-}$ mice at 1 and 6 months of age.

Table 2-2: Genotype frequency of offspring from $Psa^{+/-}$ breeding pairs. Data from three mating pairs of $Psa^{+/-}$ mice reveal a less than expected frequency of $Psa^{-/-}$ progeny and a more than expected frequency of $Psa^{+/+}$ progeny. According to Mendelian inheritance pattern, the expected frequency for $Psa^{+/-}$ crossed with $Psa^{+/-}$ is 25%, 50%, and 25% for genotypes WT, HET, and KO respectively. WT, $Psa^{+/+}$; HET, $Psa^{+/-}$; KO, $Psa^{-/-}$. Average litter size is 4.73 ±1.5 pups.

Parent ID	DOB	WT	HET	KO
85, 88	1/20/2008	4		
85, 88	2/15/2008		2	
85, 88	3/14/2008	2	1	3
85, 88	4/9/2008	2	2	
85, 88	5/1/2008	2	5	
F10a, F10b	4/13/2007		5	
F10a, F10b	5/22/2007		5	
F10a, F10b	8/10/2007	4	2	
F10a, F10b	9/10/2007	2	1	
F10a, F10b	10/17/2007	2		2
F10a, F10b	11/13/2007		5	
71, 91	1/27/2008	2	2	
71, 91	2/15/2008	2	2	
71, 91	3/15/2008	4	3	1
71, 91	5/28/2008	4	1	
Sum		30	36	6
% total		41.67	50.00	8.33

Table 2-2: Genotype frequency of offspring from Psa$^{+/-}$ breeding pairs.

CHAPTER III

THE OPTIMIZATION OF IN VIVO IMAGING FOR MEASURING GENE SILENCING OF HUNTINGTIN TARGET SEQUENCES

This chapter describes work I have performed optimizing an *in vivo* system for following RNA interference in the brain. This work was conducted under the guidance of Neil Aronin. Phil Zamore provided the initial concept. I planned and executed the majority of the experiments presented in this chapter. Edith Pfister designed and cloned the miRNA constructs. AAV constructs were packaged by Guangping Gao and Beverly Davidson.

A. Abstract

Huntington's disease (HD) is an autosomal dominant neurodegenerative disorder caused by a CAG trinucleotide repeat expansion in the huntingtin gene. Several types of RNAi constructs have been used to silence huntingtin in mice, including siRNA, shRNA, and miRNA. Screens to identify the best candidate sequences for silencing are done in cell culture which many not bear any resemblance to cells of the target tissue. No method exists to quickly screen RNAi molecules in the brain, preventing the identification and comparison of RNAi that could be optimal in the brain rather than in cell culture. The lack of techniques for *in vivo* screening impedes identification of the optimal RNAi designs for neurodegenerative diseases. We propose using an *in vivo* reporter system to rapidly compare miRNA and siRNA in the mouse brain.

For this study, two adeno-associated viruses (AAVs) expressing firefly luciferase with six huntingtin target sites in the 3'-untranslated region (UTR) were generated (AAV-Luc-Htt). These two vectors represent huntingtin alleles with single nucleotide polymorphisms (SNP) that differ between the two vectors. Measurement of *in vivo* luminescence allows for comparison of the silencing efficiencies of RNAi against these two vectors, indicating the degree of allele-specific silencing. Allele-specific silencing refers to the knockdown of a mutant allele by targeting a SNP that differs from the normal allele. Using allele-specific silencing, expression of the mutant allele can be reduced without affecting expression of the normal allele.

In this study, several methods of *in vivo* luciferase gene expression in the brain were tested. Bilateral co-injection of AAV-Luc-Htt was found to be the most sensitive method for detecting silencing of luciferase activity. Using the AAV-Luc-Htt system, silencing of luciferase activity in was shown with cholesterol conjugated siRNA, AAV-shRNA and AAV-miRNA.

These results are promising, but more work must be done to use the AAV-Luc-Htt co-injection method to assess allele-specific huntingtin silencing in the brain.

B. Introduction

Huntington's disease (HD) is an autosomal dominant neurodegenerative disease caused by a CAG trinucleotide repeat expansion in the huntingtin gene [1]. CAG repeats of less than 36 result in a normal phenotype whereas 37 or greater repeats results in Huntington's disease. HD patients suffer from psychiatric symptoms, motor symptoms, and cognitive decline before neurodegeneration of the cortex and basal ganglia results in death. There is no treatment to slow the progression of the disease, and current therapies only ameliorate symptoms [7].

In HD, the mutant huntingtin protein is misfolded, imparting it with toxic functions. Mutant huntingtin binds to other proteins resulting in transcriptional dysregulation, it impedes vesicle recycling and transport, and causes proteasomal dysfunction [2]. Mutant huntingtin mRNA can also be toxic, as it can form foci in the nucleus that co-localize with muscleblind, a protein implicated in trinucleotide repeat toxicity, and to induce RNA interference (RNAi) [237].

RNAi is a candidate strategy for treating Huntington's disease and other dominant neurodegenerative diseases. The benefit of this approach is that degradation of mRNA prevents the transcript from being translated, mitigating mRNA toxicity as well as all downstream toxic effects of the mutant protein. RNAi was discovered in 1998, as a pathway by which short RNA duplexes mediate degradation of complementary mRNA in *Caenorhabditis elegans* [238]. There are two pathways by which RNAi operates in differentiated cells: the short interfering RNA

(siRNA) pathway and the microRNA (miRNA) pathway [186]. In the siRNA pathway, short 19-21 nucleotide double strand RNAs in the cytoplasm are processed by the enzyme Dicer and loaded into the RNA-induced silencing complex (RISC), which binds and cleaves the complementary mRNA. In the miRNA pathway, miRNA is transcribed in the nucleus where it folds into a secondary structure that is cleaved by the enzyme Drosha into a short hairpin RNA (shRNA). The shRNA exits the nucleus and is processed by Dicer and loaded into RISC. Endogenous miRNAs generally contains mismatches to the target sequence that result in translational repression of the mRNA, however, miRNAs engineered to be fully complementary to their target result in RISC cleaving the mRNA target [239].

RNAi constructs are described as allele-specific when they preferentially degrade one allele. Allele-specific RNAi can be designed to target any sequence difference between two alleles such as single nucleotide polymorphisms (SNPs) or a microdeletion associated with the mutant allele [240-242]. Targeting the CAG repeat with a miRNA also shows allele-specific silencing, however the same results were not seen with siRNA [196, 243-245]. Reduced levels of huntingtin may have adverse effects, especially if the total knockdown of huntingtin is greater than 50% [49, 194, 195, 246]. One way to avoid excessive silencing of huntingtin is to use allele-specific silencing. In a study examining 109 HD patients and 116 non-HD controls for SNPs in the huntingtin gene, it was found that by targeting 5 sequences 75% of HD patients could be treated with allele-specific silencing [196]. The use of allele-specific silencing is the most specific way to treat HD, yet no one has shown SNP-directed silencing *in vivo* using RNAi.

RNAi is particularly well-suited for treating dominantly inherited genetic diseases such as Huntington's disease. Several groups tested siRNA in rodent models of HD. Cholesterol

conjugated siRNA (cc-siRNA) has been used to silence huntingtin in rodent models of Huntington's disease resulting in fewer inclusions and ameliorated behavioral abnormalities [247, 248]. Unconjugated siRNA against huntingtin was delivered by intraventricular injection into newborn R6/2 mice [249]. Viral delivery of shRNA and miRNA is also being extensively studied in mice resulting in improved behavior and decrease in size and number of nuclear inclusions [250-252]. Work is also being done in rhesus macaques using shRNA targeting huntingtin [253]. Of note, there is potential toxicity associated with using a shRNA structure thought to be due to high expression level leading to oversaturation of RNAi machinery [254, 255]. This toxicity is eliminated by using a miRNA-based design [255]. Each of these studies utilizes different sequences, structures, and promoters thereby preventing a direct comparison between them, and none of these studies used silencing strategies that are allele-specific.

In vivo bioluminescent imaging (BLI) is a method by which expression of luciferase is imaged using a light sensitive camera [256]. This method enables gene expression to be followed over time without sacrificing the animal. The BLI technique is fast, convenient, low cost, has the potential for medium throughput screening and can be performed longitudinally within each animal. BLI has been used for detecting tumor location and growth, gene therapy spread, clearance of pathogens, and the migration of adoptively transferred cells [256, 257]. BLI has also been used to follow the silencing of genes using siRNA and shRNA in the liver and in tumors [257-264]. Studies of RNAi targeting luciferase have been useful for describing the dynamics of siRNA silencing *in vivo* and have shown that luminescence correlates with mRNA and protein levels in treated tissues [258, 265]. BLI has also been used to study the brain including measuring brain tumor growth, gene transfer in rats, biodistribution of stem cells after strokes, and to monitor rhythmic gene expression in the olfactory bulbs of SCN lesioned rats [266-268].

Lentiviral injection of luciferase gene in mice shows that BLI can be detected in the striatum, olfactory bulb, substantia nigra and globus pallidus [265]. One study used luciferase to follow silencing in the brain by packaging luciferase plasmid DNA with siRNA in different lipid-mediated delivery strategies [269]. However, no group has compared the dynamics of silencing or systematic comparison of siRNA and miRNA sequences in the brain. Here, we present results from an initial investigation into the use of viral-delivered luciferase and bioluminescent imaging to follow gene silencing in the brain.

In this study we created two AAV expressing firefly luciferase reporter genes each with six huntingtin target sequences in the 3'-untranslated region (UTR). Using these reporters we can test the silencing of huntingtin-targeting RNAi with therapeutic potential. Silencing of luciferase activity was detected using cc-siRNA and AAV-shRNA targeting luciferase, and AAV-miRNA targeting human huntingtin. Allele-specific silencing was demonstrated by comparing the efficiency of an AAV-miRNA to silence a matching SNP target versus a mismatched target. We conclude that using AAV-Luc-Htt as a reporter molecule is a promising method for testing silencing, especially for studying allele-specific silencing of huntingtin target sites *in vivo*, however it needs further optimization to improve sensitivity to fully function as a way to detect gene-silencing dynamics in the brain.

C. Results

1. Adeno-associated virus delivery of luciferase with human huntingtin SNP sites can be detected in the mouse striatum.

In order to express luciferase in the brain, we generated two adeno-associated viruses (AAV) encoding luciferase mRNA, each with six huntingtin RNAi target sites in the 3'-UTR (AAV-Luc-Htt) (Fig. 3-1 B). We used a recombinant AAV2/9 vector, expressing serotype 2 inverted terminal repeats (ITRs) and serotype 9 capsid proteins with luciferase expression driven by the cytomegalovirus (CMV) promoter. Serotype 9 was chosen because it has shown good tissue distribution in the brain and specific tropism for neurons in mice [270]. A summary of viruses used in this chapter can be found in Table 3-2. Each virus represents an allele of the huntingtin gene with six SNP-containing target sequences (Fig. 3-1 B). Since each virus has matching target sites that differ only by one single nucleotide, the SNP site, we can potentially use these vectors to evaluate allele-specific silencing *in vivo*. The first four target sequences are from human huntingtin and the last two are found in mouse huntingtin.

Luminescence from AAV-Luc-Htt was detected *in vivo* following intracranial injections into the striatum. A trial of five 10-fold diluted doses identified 1e9GC as the lowest detectable dose by BLI, with 1e10GC producing a level significantly above background (Fig. 3-1 C). There appeared to be a large degree of variation within each dose, with standard deviation values up to 50% of the mean. To study the variability at a single dose, a group of 9 mice, injected with 5e9GC AAV-Luc-Htt, were imaged repeatedly for 28 days (Fig. 3-2 A). Luminescence was detected 24 hours after injection and reached stable baseline luminescence by day 10. A 95% confidence interval (CI) was calculated for each day and the lower interval was used to determine the percent silencing that would be necessary for detection among this group of mice. The percent silencing needed to detect silencing on any given day ranged from 26% to 46% with an average of 37% silencing minimum needed to detect silencing. To look at variation using values from a stably expressing baseline, we looked at three days, 15, 19, and 21, comparing the

variability in one week for each mouse (Fig. 3-2 B). From these three days, the 95% CI was calculated and individual mice would require silencing of 5-46%with an average of 28% silencing to achieve statistically significant decrease in luminescence. One experimental approach could be to test silencing for each mouse after establishing a stable baseline. A source of variation could be due to differences in luciferin absorption and distribution. Luciferin is the substrate that interacts with luciferase to produce luminescence. It is most commonly delivered at 150mg/kg by intraperitoneal (ip) injection 10 minutes before imaging, in concordance with the vast majority of published BLI studies and the manufacturer recommendations for imaging. As a large fraction of luciferin is absorbed into the gut after ip injection, variations may arise from the animal's diet prior to injection or by slight positioning differences of the needle within the ip space. If differences in luciferin distribution result in intramouse variation, then normalizing luminescence within the same animal would reduce variations.

We propose an experimental design using bilateral intracranial AAV-Luc-Htt injections in which one side of the brain acts as a control for the contralateral side (Fig. 3-3 A). In this method, AAV-Luc-Htt is co-injected with RNAi molecules into the striatum on one side of the brain and co-injected with control RNAi molecules on the contralateral side. We expect that groups without silencing will have a ratio of luminescence close to 1.0 and groups with successful targeting of luciferase will have an active RNAi/control RNAi ratio less than 1.0. To test this design we injected two groups of mice, either unilaterally or bilaterally, and followed luminescence for one week (Fig. 3-3 B). First, we analyzed the unilateral injection group to compare luminescence between the injected and un-injected side. Although the luminescence is statistically different between the AAV-Luc-Htt injected and un-injected hemispheres, there were no significant differences between the sides on any given day (Mixed methods ANOVA

$p<0.0001$, Tukey's multiple comparisons). These results confirm that although a difference was detected overall, the system is not sensitive enough to detect the equivalent of 100% silencing on any specific time point due to increased variation seen by analyzing flux. This lack of sensitivity could be a result of crossover of luminescence from the injected hemisphere, either from light scatter through the tissue or spread of the virus. It could also be due to the sensitivity of the assay resulting from a combination of factors including a low concentration of AAV-Luc-Htt and high baseline variation in luciferase expression. We then calculated the left- to right-side ratio of both groups. The ratio for the bilaterally injected group was approximately 1.0 as expected from identical injections without RNAi. The ratio of luminescence from the un-injected side was slightly higher than expected at 0.25 illustrating that there is a spread of light or virus to the contralateral side. If we consider the unilaterally injected group to represent complete silencing and the bilateral group to represent no silencing, there is a difference between the groups, significant at each time point (Mixed methods ANOVA $p<0.0001$, Tukey's multiple comparisons). The 95% CI was calculated from the average ratio for each day (mean ratio 1.164 95% CI 0.7595-1.569). From this confidence interval, we would need a 35% decrease in luminescence on any given day to detect silencing. By analyzing the same data as luminescent flux, the minimal detectable silencing would be 40%, which is higher than the variation calculated for the mice in Figure 3-2 which only required 37%.We conclude that normalizing luminescence within each mouse by calculating a left to right side ratio, results in a more sensitive assay, able to detect smaller differences in silencing than comparing left side to right side luminescence.

One caveat to the bilateral injection experimental design is the potential for crossover of luminescence from light-scattering or spread of virus through diffusion, or transport. AAV

serotype 9 have been shown to undergo retrograde transport after a single 1μL injection to the striatum, with viral mRNA detected in retrograde projection targets including the ventral tegmental area, thalamus, substantia nigra pars compacta, amygdala, and hippocampus, including the contralateral hippocampus [271]. Through diffusion from the injection site there can also be extensive spread of the AAV9 gene and gene product into midline structures including subventricular zone, septal nuclei [270, 271]. In addition to the spread of virus or viral products within the brain, one must also consider the light scattering effect of tissue. The D-Luciferin substrate emits short wavelength light, 560nm, resulting in high light scattering properties through all tissues, including the brain [272, 273]. The effects of viral diffusion, retrograde transport, and light scattering are important factors in the study design, which could limit the sensitivity of the assay.

2. RNAi constructs targeting firefly luciferase and human huntingtin SNP sites are functional in cell culture.

RNAi constructs were tested in cell culture for their ability to silence luciferase and huntingtin target sites. Structures and sequences are summarized in Table 3-1. We tested 6 different siRNA preparations, four experimental siRNA and two control siRNA (Fig. 3-4 A). Two of the siRNAs, cc-siLuc and cc-siCon, contain a cholesterol modification that improves siRNA transport into cells and enhances resistance to exo- and endonucleases [274]. Paradoxically, cholesterol conjugated siRNA (cc-siRNA) were noted to have much higher IC_{50} compared with un-conjugated siRNA, approximately 8 nmol compared with 0.13 nmol for firefly luciferase siRNA.

We also tested AAV-miRNA silencing constructs to verify silencing of the corresponding target site in cell culture. AAV-miR2307T and AAV-miR2273G were tested at three different concentrations and compared with cells not infected with virus (Fig. 3-4 B). At the highest dose tested (100,000 MOI), there was 37% silencing by AAV-miR2273 (Tukey's multiple comparison $p<0.0001$) and 56% silencing by AAV-miR2307 (Tukey's multiple comparison $p<0.0001$) compared with the lowest dose tested (10,000 MOI) that showed no silencing. All siRNA, cc-siRNA, and AAV-miRNA tested silenced expression of luciferase in cell culture.

3. Cholesterol-conjugated siRNA reduced luminescence 24 hours after injection

To test silencing of luciferase activity *in vivo*, we used cc-siRNA targeting luciferase mRNA (cc-siLuc). The left side of the brain was co-injected with AAV-Luc-Htt and cc-siLuc and the right side was injected with AAV-Luc-Htt and control cc-siRNA (cc-siCon). A second set of mice were bilaterally injected with AAV-Luc-Htt in phosphate buffered saline (PBS). The resulting luminescence was compared between left and right sides as flux (photons /second), and as the ratio between the left and right sides of each mouse (Fig. 3-5 A, B). There was no difference between the luminescent flux from cc-siLuc or cc-siCon injections, however when we compared the ratio between the left and right sides of each mouse there was a 52.6% decrease in luminescent ratio of the cc-siRNA treated mice compared with the PBS control mice 24 hours after injection (Repeated measures one-way ANOVA $p<0.0010$, Sidak's multiple comparisons test mean diff. 0.4847, 95% CI 0.4051 to 0.5644, $p<0.0001$) (Fig. 3-5 B). This experiment demonstrates an instance where by comparing luminescence, there was no detectable silencing,

however by normalizing the ratio within each mouse, silencing was detected 24 hours after injection.

4. Cholesterol-conjugated siRNA increased luminescence in brain and in cell culture.

An unexpected result was seen in the cc-siRNA injected group. We observed that co-injections of cc-siRNA and AAV-Luc-Htt resulted in greater luminescence than injections of virus with PBS and this enhancement persisted for at least 12 days after injection (Fig. 3-5 A). After 168 days, the difference in luminescence significantly decreased 10-fold in the cc-siRNA mice, however luminescence remained stable in the PBS injected mice. There remained a statistically significant 1.9fold difference when comparing the cc-siRNA and PBS injected groups (cc-siLuc vs PBS, Unpaired t-test p=0.0017; cc-siCon vs PBS, Unpaired t-test p=0.0007, Fig. 3-5 C). In order to compare cc-siRNA with PBS within the same mouse, we injected a group of mice on the right side with AAV-Luc-Htt and cc-siCon and the left side with AAV-Luc-Htt and PBS (Fig. 3-5 D). In a comparison between sides of the same mouse, there was a 2.35 fold increase in luminescence on days 5 and 12 after injection (2-way ANOVA, p=0.0015), but we found no difference after about six months (Fig. 3-5 D). These results suggest that cholesterol conjugation transiently increases luminescence when co-injected with AAV-Luc-Htt by an unknown mechanism.

To explore this effect, we tested the combination of cc-siRNA and AAV-Luc-Htt in cell culture. HeLa cells were incubated with AAV-Luc-Htt and either cc-siCon, non-conjugated siCon, or no siRNA (Fig. 3-6 A). We also tested cc-siCon and siCon without AAV-Luc-Htt to

show that the siRNA were not contaminated with AAV-Luc-Htt. We found that there is a 1.5-fold increase in luminescence with cc-siCon relative to no siRNA treated cells (Unpaired t-test, p=0.0091, p=0.0001 respectively) (Fig. 3-6 A). We did a series of dilutions of AAV-Luc-Htt with the same amount of cc-siCon and found 2.6-fold difference in luminescence in the 1e5 MOI incubated cells (2-way ANOVA, $p<0.0001$) (Fig. 3-6 B). There was no difference in cells incubated with AAV-Luc-Htt and cholesterol without siRNA (Fig. 3-6 C). To test whether the effect of cc-siRNA to increase BLI from AAV-Luc was serotype specific, we tested serotype 2 (AAV2-Luc) and found a similar 1.8 fold increase (Unpaired t-test p=0.0045) (Fig. 3-6 D). A different sequence of cc-siRNA targeting GFP (cc-siGFP) resulted in a 1.2 fold increase, and in a different cell type (Neuro2A cells) cc-siCon led to a 1.4 fold increase in luminescence (Unpaired t-test, p=0.0062 and p=0.0242 respectively) (Fig. 3-6 E, F). In summary, we found that the combination of cc-siRNA and AAV-Luc increased luminescence in cell culture independent of siRNA sequence, serotype of virus, or cell type.

5. siRNA targeting luciferase reduces luminescence *in vivo*.

To test siRNA that was not conjugated with cholesterol, we co-injected mice with siRNA and AAV-Luc-Htt then measured luminescence. We tested siRNA targeting luciferase target sequences (siLuc) as well as huntingtin SNP target sequences, 2307 and 2273 (si2307, si2273), and a control siRNA (siCon). Due to concerns that luciferase out-expressed siRNA, we used a very high dose, 14nmol. Unexpectedly, on day 1, siLuc injected mice showed an increase in luminescence on the siLuc injected side, which disappeared on day 2. We detected a significant difference in luminescent flux of the siLuc side overall (Fig. 3-7 A, Mixed method ANOVA

p=0.0064). The ratio of luminescence from siRNA injected side to PBS injected side was compared with the ratio at one year after injection as a reference time point. A significant difference was detected in the ratio of luminescence in the siLuc group on the third day after injection resulting in a 43% decrease in luminescence. The fact that both methods of analyzing data, luminescence and ratio, agree lend support to the conclusion of silencing by siLuc. However, a difference was also detected in the siCon injected group suggesting possible variation in the injection technique or solution preparation, making it difficult to draw firm conclusions from these experiments (Fig. 3-7 D). No differences were observed in groups injected with si2307 or si2273 (Fig. 3-7 B, C). The 2307 and 2273 target sites and RNAi sequences were chosen for this study because they feature a human SNP site that shows allele-discriminating properties in cell culture assays and have therapeutic potential [196]. Despite having a low IC_{50} values, neither si2307 nor si2273 demonstrated robust silencing in cell culture experiments, achieving a maximum of only 40-50% silencing (Figure 3-4 A). It is possible that this assay is not sensitive enough to detect silencing by si2307 and si2273.

6. AAV-Luc-Htt co-injection with AAV-shLuc results in reduction of luciferase activity.

We next tested the ability of AAV-delivered short hairpin RNA (shRNA) targeting luciferase to silence AAV-Luc-Htt. The AAV-shRNA targeting luciferase (AAV-shLuc) differs from AAV-Luc-Htt in that it is packaged in AAV serotype 8 and employs the U6 promoter for transcription (Table 3-2). U6 is a polymerase III promoter that is specifically used to express small RNAs, and AAV-Luc-Htt uses the polymerase II CMV promoter to express luciferase. The U6 promoter functions to transcribe small RNAs at a higher level than the CMV promoter (Edith

Pfister, unpublished data). The AAV-shLuc virus had been prepared for use in a different study (unpublished) and was chosen for this study because it was readily available and because serotypes 8and 9 share many characteristics. AAV8 and AA9 both are predominantly found in neurons, however AAV8 can also be found in oligodendrocytes and astrocytes whereas AAV9 is highly specific for neurons [270, 275]. In a comparison of AAV serotypes after intrastriatal injections, AAV8 spread into the striatum while AAV9 distributed along the corpus callosum, transducing slightly more neurons compared with AAV8 [270]. These differences are important to consider when interpreting results in experiments using mixture of AAV serotypes. In the current study, the left side was co-injected with AAV-Luc-Htt and AAV-shLuc while the right side was co-injected with AAV-Luc-Htt and PBS (Fig. 3-8). The side injected with AAV-shLuc was significantly decreased 23% compared with PBS control (Mixed model ANOVA, p=0.0002). This difference demonstrates that it is possible to detect luciferase silencing by co-injection of AAV-Luc-Htt and AAV-shRNA.

7. AAV-miRNA targeting SNP site 2273 does not silence luciferase activity *in vivo*.

We next wanted to test vectors targeting huntingtin SNP sites. For this experiment we created two viruses, one targeting the SNP site 2273 G and the other targeting SNP site 2273 A (AAV-miR2273G or –miR2273A, Table 3-2). These viruses have the same serotype as the AAV-Luc-Htt (serotype 9), however there are two differences. The AAV-miR2273 viruses contain the chicken β-actin promoter with CMV enhancer (CBA promoter) rather than a CMV promoter because it results in a 6.4-fold greater expression [276]. The silencing vectors were also designed to have a self-complementary AAV (scAAV) genome rather than the single stranded

AAV (ssAAV) genome of the AAV-Luc-Htt. Self-complementary genomes confer increased transduction into host cells, resulting in greater saturation within the expected distribution for AAV serotype [277]. It is our intention that the scAAV9 vectors would match or exceed the distribution of the ssAAV9 and have a greater degree of expression and probability of co-transducing neurons. On the left side of the brain we co-injected AAV-Luc-Htt with AAV-miR2273G) matching the target SNP, 2273. On the right side we co-injected AAV-Luc-Htt with AAV-miR2273A, which contains a mismatch to the SNP site. We used a 1:1 ratio between AAV-miR2273 and AAV-Luc-Htt viruses. We saw no significant difference in the luminescence between the sides of the brain (Fig. 3-9 A). In previous experiments, AAV-miR2273G was shown to silence the SNP site in cultured cells; however, a high MOI only resulted in modest silencing (Fig. 3-4 B). This lack of result *in vivo* may be due to it not being a very robust silencing structure.

To test an increased dose of AAV-miR2273, we co-injected mice with 9:1 ratio of AAV-miR2273 to AAV-Luc-Htt. One group received the matching vector, a second group received the mismatching vector, and a third group received a control vector (AAV-miRCon). The right side of all mice was injected with AAV-Luc-Htt and PBS. The matching vector did not differ in luminescence compared with PBS. Unexpectedly, there was an increase in luminescence in the injections with mismatching and control vectors (ANOVA $p=0.0496$, $p=0.0076$ respectively) (Fig. 3-9 B). No difference was found between the left to right ratio of luminescence between the groups (Fig. 3-9 C). The lack of silencing luciferase activity upon co-injection with AAV-miR2273 matching the target site shows that it is inefficient at silencing luciferase to a level that is detectable by this *in vivo* imaging method. As mentioned previously, the siRNA did not show robust silencing in cell culture experiments, even at high concentrations (Figure 3-4 A).

Similarly, silencing experiments in cell culture using AAV-miR2273 did not reach 50% reduction of luminescence even at high MOI (Figure 3-4 B). Silencing *in vivo* would likely be difficult and possibly out of the sensitivity of this study's design. The increased luminescence in the control injection suggests that could be internal error in creating the AAV injection solution in this experiment. One possible interpretation is that miR mismatch and miRCon co-injection increased luminescence while PBS had no effect and miR match displayed mild silencing. In summary, these results are inconclusive, and the system may not be sensitive enough to describe subtle silencing without a large number of animals or an improvement in the sensitivity.

8. AAV-miRNA targeting huntingtin SNP site 2307 resulted in silencing of luminescence in an allele-specific manner.

In order to test silencing of a different human huntingtin target site, we used a miRNA complementary to the target sequence containing SNP site 2307 (AAV-mir2307, Table 3-2). This virus was previously created for a different project and differs from AAV-Luc-Htt in that is was packaged using AAV serotype 1 and also uses the polymerase III promoter U6 rather than the polymerase II CMV promoter. As stated previously, different serotypes confer different properties in terms of tissue distribution and transduction capabilities. Serotype 1 is known to have tropism predominantly for neurons, but is also able to transduce microglia and astrocytes at a significantly higher rate than serotype 9 [275, 278]. In previous experiments this vector was shown to silence luciferase in cell culture (Fig. 3-4 B). We tested a 1:1 ratio of AAV-Luc-Htt and AAV-miR2307 compared with PBS. There was no significant difference between the luminescence on either side (Fig. 3-10 A). We increased the amount of AAV-miR2307 to five

times that of AAV-Luc-Htt and repeated the experiment. In a second group of mice, the same AAV-miR2307 was co-injected with the reporter virus that has the alternative, mismatching, SNP site. The right side of each mouse was injected with reporter virus and PBS (Fig. 3-10 B). Results show that mice with the matching reporter construct had a reduced amount of luminescence overall compared with the contralateral side injected with PBS (Mixed model ANOVA, $p=0.0051$). The second group with the mismatching reporter construct had no difference in luminescence between each side of the mouse. Surprisingly, although the luminescence differed significantly in the matching group, the ratio of left to right side did not differ significantly compared to the ratio of the mismatched group (Fig. 3-10 C). This discrepancy limits the conclusions that can be drawn from the results. Although we proposed the ratio calculation as a method to reduce variation from luciferin absorption, it is possible that it may introduce other sources of variation including spread of viruses to midline/contralateral structures which is compounded by the use of different serotypes. For this experiment, the decrease in luminescence with AAV-miR2307 co-injection suggests that this vector is functional against the human huntingtin target sequence containing the 2307 SNP site. Reduction in luminescence was not seen with the mismatching vector, suggesting that the matching vector may demonstrate allele-specific specificity. This experiment should be repeated using matching serotypes as well as comparing luminescence in unilateral injection groups to strengthen conclusions.

9. A re-injection approach is not sensitive enough for detection of decreases in luminescence.

In order to compare silencing to a stable baseline of luminescence, we established stable expression of AAV-Luc-Htt luminescence before re-injecting the same location with AAV-miR2307. Mice were injected with AAV-Luc-Htt and imaged after 7-14 days. Using a 5:1 ratio of AAV-miR2307 to AAV-Luc-Htt or the same volume of PBS, we injected the AAV-miR2307 at the same location and followed the luminescence over time. We found no decrease in luminescence in either group (Fig. 3-11 A, B). The PBS control injection led to a transient increase of luminescence compared to no injection, indicating that re-injection may disturb what should be a stable bioluminescence (Fig. 3-11 B). This experiment were repeated in three different cohorts (n=4 for each), and each time there was no detectable inhibition of luminescence by AAV-miR2307.

C. Discussion

In this study, we created two AAV-luciferase reporter vectors with huntingtin sequences in the 3'-UTR to follow gene silencing *in vivo*. These vectors present a method for testing gene silencing over time as mice can be measured repeatedly by bioluminescent imaging. This is a pilot study, meant to guide the optimization of the luciferase silencing system for application in a systematic comparison of RNAi in the brain. We co-administered the reporter virus with silencing molecules and viruses to study silencing dynamics in the brain.

We found that in animals with stable AAV-luciferase expression, luminescence varied greatly between animals and between the same animal on consecutive days. We hypothesize that this is due to the variable rate of luciferin absorption the intraperitoneal space. We tried several methods of delivering luciferin including tail vein injections and implanted pump delivery of luciferin. Tail vein injections deliver a reliable dose directly into the circulation, avoiding the absorption through gut, subcutaneous fat or intraperitoneal tissue, however the veins become damaged upon repeated access, making it impractical for daily injections. We considered using an intraperitoneal-implanted pump, such as an Alzet® osmotic pump, however the volume constraints require using dramatically less luciferin than the standard dose recommended by Xenogen for use with their *in vivo* imaging system. Less luciferin would result in correspondingly lower light output possibly affecting the sensitivity of the assay. However, this method has been used successfully in imaging the olfactory bulbs in rats [268]. An alternative is to implant a central port for each mouse. This would add another procedure reducing the system's convenience and speed. The bilateral injection method was our solution to correct for the daily variation. We present data both as absolute values of luminescence as well as a ratio of luminescence from the treated side versus control side. For experiments with siRNA, we compared luminescence to a time point representing stable AAV expression that is well past the duration of silencing observed for siRNA, approximately 25 days in non-dividing cells [260]. While providing an internal control, this method presents additional issues. We found that luminescence from one side of the brain crosses over to the other side as illustrated in Figure 3-2 C. This is likely a combination of light scattering through the tissue and spread of the virus to midline or contralateral structures of the brain. While correcting for one source of variation, the spread of luminescence across the midline presents its own limitation, reducing the sensitivity of

the assay. We also found discrepancies between results seen by analyzing luminescence but were not significant when comparing ratios, such as in experiments with AAV-miR2307 (Fig. 3-10 B, C). We found that in a single group of animals, if we calculate the ratio of the left to right side injection, the minimum silencing that can be detected is improved from 40% to 35%. This highlights the limitations of this method to robustly identify silencing of luciferase. Throughout this study presented both the luminescent data and results presented as a ratio in order to evaluate the system for such inconsistencies.

Injections with 0.9nmol cc-siRNA targeting firefly luciferase resulted in an initial 52% decrease in luminescence on day one that was not sustained over time. This difference was seen by the ratio method and not by the comparison of flux. The duration of silencing may be limited by the increasing level of expression from the AAV-Luc-Htt vector, which begins low and increases over several weeks until reaching a stable plateau. The amount of cc-siRNA remains fixed or begins to diminish as molecules not incorporated into RISC are degraded by the cell, leading to a fundamental imbalance between the amount of siRNA and luciferase transcript within the cell. While silencing was observed with cc-siRNA, it may need a higher dose to demonstrate a sustained decrease in luminescence. Several studies have used cc-siRNA to silence huntingtin in mice and rat models, one of which uses intravenous injection and another uses neonatal intraventricular injections [247-249]. In one study, 0.5nmol of huntingtin-targeting cc-siRNA was co-injected with AAV-Htt100Q. Treated mice developed smaller intranuclear inclusions, fewer neuropil aggregates, with greater survival of neurons, and improved behavioral phenotype. Huntingtin protein was reduced by 56-66% after 3 days [248]. In this study, we used a higher dose of cc-siRNA, nearly twice as much, and showed 52% silencing of luciferase

activity one day after injection, however we did not see a difference on the second or third days after injection.

For testing siRNA without cholesterol conjugation, we increased the dose to 14nmol to favor silencing of luciferase. At this dose, we detected a 43% decrease in luminescence three days after injection with siLuc. The difference in silencing dynamics compared with cc-siRNA may be due to the absence of a cholesterol moiety which may facilitate transmembrane transport of cc-siRNA. Several groups who have measured silencing of luciferase in the liver by siRNA observe silencing to peak 2-3 days after injection which would correspond with the timing observed in this experiment [258-260]. The single day of silencing likely represents the peak knockdown further highlighting the limited sensitivity of this assay. Testing of huntingtin specific siRNA did not result in silencing of luminescence. One factor may be that the huntingtin-specific siRNA was not as robust at silencing as the siLuc siRNA, as depicted in the dual luciferase assays shown in Figure 3-4. The maximal silencing achieved in cell culture, under highly efficient transfection conditions is a modest 40-50% reduction in luciferase activity. Even if we were able to achieve this maximal silencing efficiency *in vivo*, the BLI assay may currently have adequate sensitivity for detection. Another limitation is the single injection. There are many studies following single intravenous injections of naked siRNA to silence genes in the liver, which readily takes up siRNA into hepatocytes. Studies of unconjugated siRNA in the brain predominantly use convection delivery, repeated injection, or infusion into the lateral ventricles [279-282]. A continuous, high-dose, delivery methods may be necessary to achieve detectable silencing in the brain.

We proceeded to test the silencing properties of two AAV-miRNAs targeting huntingtin sequences as well as one AAV-shRNA targeting luciferase. AAV-shLuc and AAV-miR2307 decreased luminescence, globally, by 23% and 42% respectively. Interestingly, there was no difference in silencing when AAV-miR2307 was used with the mismatching construct, suggesting preferential silencing of the match target sequence. AAV-miR2273G did not result in any silencing. Differences in luminescence were not significant at any individual day for any of these vectors reflecting limitation in sensitivity of this assay. These vectors differed from each other in many different ways including promoter, serotype, and genome structure as summarized in Table 3-2. Due to these inconsistencies, the trends identified in these experiments cannot be used to directly compare silencing vectors. Nevertheless, there are several notable observations. The two viruses effective in silencing luciferase used the U6 promoter to express the silencing hairpin RNA. The U6 promoter is an RNA polymerase III promoter that expresses short RNA at a high level compared with polymerase II promoters such as CMV and CBA promoters (E. L. Pfister, unpublished data). Also, AAV-miR2307 was effective when used at a higher, 5:1 ratio, compared with an equal ratio of silencing virus to reporter virus. Based on these observations, future experiments should employ the U6 promoter and 2:1 (or greater) ratio of silencing virus to luciferase virus. An additional discrepancy between the silencing constructs includes the design of the hairpins, each of which differed in their stem and loop length, sequence, and complementarity. The nomenclature to identify the hairpin as short hairpin RNA (shRNA) or microRNA (miRNA) reflects the predicted method of RNA processing. These differences could impact the validity of processing, which could alter the silencing efficacy (E. L. Pfister, unpublished data). Future experiments should compare viral hairpin RNA constructs with identical promoters, serotype, and hairpin structure.

Several groups have used viral delivery of shRNAs to target huntingtin in mouse models. AAV-delivery of shRNA expressed under the U6 promoter in a different transgenic mouse model, N171-82Q HD mice, reduced levels of the human huntingtin transgene mRNA in the striatum by 51-55% two weeks after injection [192]. This resulted in improved gait and rotarod performance [192]. Another group used AAV and the U6 promoter to express shRNA in the striatum of a transgenic mouse model, finding a reduction in mutant huntingtin mRNA (75%) and protein (60%) 10 weeks after injection [193]. There was a decrease in size and number of intranuclear inclusions and normalization of gene expression in neurons. The treatment had no effect on rotarod ability but delayed onset of clasping [251]. A study was done to test RNAi as a post-symptomatic therapy for HD by injecting AAV-expressing shRNA under control of the U6 promoter into the striatum of mice with a mutant huntingtin transgene after the onset of symptoms. shRNA therapy decreased aggregates and restored dopamine releasing protein (DARP) expression, a gene that is down-regulated in affected striatum [252]. In another study, normal rhesus macaques were injected with AAV-U6-miRNA targeting huntingtin. They found a 45% reduction in huntingtin mRNA 6 weeks after injection [253]. Huntingtin silencing from AAV-shRNA was also shown using a rat model of HD. First, rats were injected with AAV-U6-shHtt, and after 2 weeks they were injected with AAV-NH_2-terminal Htt70Q. They found no toxicity from the shRNA expression and observed silencing of huntingtin two weeks after injection of AAV-Htt70Q [283]. These previous studies employ the U6 promoter, which is the same promoter used in the two vectors in this study that successfully decreased luminescence.

Bioluminescent imaging is a valuable tool for following reporter gene expression in vivo, primarily as it is noninvasive and allows for repeated measurements. BLI has been used in several studies of gene silencing. One group used liposomal siRNA directed at luciferase in mice

expressing ROSA26-SLS-luciferase in tissues expressing Cre-recominase from the ubiquitous probasin promoter [259]. Since the animals expressed luciferase ubiquitously, they measured luminescence in *ex vivo* tissues and saw knockdown only in the liver 4, 8 and 16 days after IV injection, with the greatest silencing on day 4 at 75% [259]. They did not find silencing in spleen, heart, lung, kidney, or adrenals and did not examine the brain [259]. Another group used siRNA targeting luciferase in lipid nanoparticles delivered by IV injection resulting in a maximum inhibition of bioluminescence in the liver 3 days after injection [258]. At the highest dose they saw nearly complete silencing for 2 weeks. Using high pressure tail vein injection (HPTV) of luciferase plasmid and siRNA polyplexes, silencing was observed for 3 weeks with silencing greatest on day 3 [260]. Using naked siRNA and luciferase plasmid in a HPTV injection there was 81% silencing of luciferase in liver after 3 days [284]. In this study we detected silencing on day 3 with siRNA and day 1 with cc-siRNA. These studies found silencing to be the greatest 3-4 days after treatment, which confirms what we saw with unconjugated siLuc where silencing was the greatest 3 days after injection. In this study, we chose to focus primarily on "naked" unconjugated siRNA which has limited ability to cross cell membranes, but with the advantage of a lower risk of toxicity in the brain. The drawback to using unconjugated siRNA is that due to a low efficiency of uptake into cells it requires high concentrations to be effective.

The use of different AAV serotypes limits the conclusions that can be made as each serotype have slightly different properties of spread and transduction into cells. All viruses used in this dissertation are recombinant adeno-associated viruses (rAAVs), meaning that they share the inverted terminal repeats (ITRs) of serotype 2, but express a different gene for the capsid protein. The capsid protein binds the virus to the cell surface receptors, thus defining the tropism for that virus. Recombinant AAV expressing capsid proteins from serotype 1, 8, or 9, are notated

as rAAV2/1, rAAV2/8, and rAAV2/9 or simply as AAV1, AAV8, and AAV9. Each serotype binds to one or more specific cell surface molecules: sialic acid for AAV1, heparin sulfate proteoglycan for AAV2, laminin receptor for AAV8, and galactose for AAV9 [285-288]. There are many published comparisons of tissue spread among serotypes, however no single study to date compares serotypes 1, 8 and 9 that were used in mouse injection experiments. Several studies report equal spread of AAV1, 5, 7 and 8 throughout the mouse and rat striatum [289-291]. One study found serotypes spread differently depending on their concentration, and that all serotypes spread equally well at high doses, however a low dose, AAV5 and 7 were superior to AAV8 [289]. AAV9 and rh10 have been shown to have a far greater spread than AAV7, 8, 9, and rh10 [270]. Although the total spread was impressive in the AAV9-injected animals, the variation among the three animals was very large, with the number of transduced cells ranging from 12 to 1,282 within the striatum [270]. In a second study, the same group showed single injection into the striatum of AAV9 filling the medial aspect of the striatum and diffusing to nearby structures, including septal nuclei [271]. To summarize the published findings, no groups has compared the spread from single injections of AAV1, 8, and 9, however serotypes 1 and 8 spread through the striatum equally well and there is a possibility that AAV9 shows superior spread to AAV8. The concentration of the virus may play a role, with lower concentrations limiting spread. The co-injection experiments in this chapter employ lower concentrations of the AAV9 reporter virus compared with the AAV1, 8, or 9 silencing virus. Taken together, although the reporter virus is packaged in the high potency and high spread serotype, the low concentration may limit its spread relative to the silencing constructs.

AAV can also spread by diffusion and anterograde/retrograde transport to distant anatomical locations in the brain. This has been shown in serotypes 1, 5, 8 and 9, possibly by a

serotype –independent mechanism [271, 291, 292]. Viral mRNA from injections of AAV9 into the striatum have been detected in the substantia nigra pars compacta, hippocampus, amygdala and thalamus [271]. There is the possibility that virus can cross to the contralateral side of the brain, in one study, a small degree of positive cells were found on the contralateral side, up to 15% in some sections [271].

A valuable addition to this study would be a comparison of viral spread and the degree of overlap of the reporter virus and silencing virus. A mismatch in distribution of the co-injected viruses could underrepresent the effectiveness of the silencing vectors. This can be evaluated by fluorescently labeling cells transduced by each virus and assessing the degree of co-labeling. A gene for a fluorescent protein marker, such as green fluorescent protein (GFP), can be included in the silencing virus, and thus cells expressing the silencing hairpin RNA would also express a fluorescent protein. Fluorescent proteins cannot be used in the luciferase reporter construct, as including two genes would exceed the DNA packaging limits of the AAV. However, immunofluorescent staining can be performed with fluorescently labeled antibodies against the luciferase protein, or by tagging the luciferase with an easily labeled tag, such as hemagglutinin. One could also use fluorescent in situ hybridization (FISH) to evaluate spread and co-localization of the luciferase mRNA with a fluorescent protein in the silencing virus. siRNA can also be labeled with fluorescent tags such as Cy5 or Cy3 and co-localized with fluorescently labeled luciferase mRNA or protein. In this way, one could assess the degree of co-transduction and determine whether the lack of silencing is due to inefficiency of RNAi or due to inefficient co-transduction of cells.

Other limitations of this study are that in many experiments there were fewer animals than were required to achieve reasonable experimental power. This was due to the unexpectedly high variation. For most experiments, there was only one independent experiment for each reported result, and aspects of each experiment differed in various ways, including viral components, doses, and injection sites.

In our experiments with cc-siRNA, we observed an unexpected result that co-injection of cc-siRNA with AAV-Luc-Htt initially increased luminescence ten-fold compared with PBS. After six months the increase was attenuated to a two-fold difference in luminescence in one experiment and the effect was eliminated in a second experiment (Fig. 3-5 A, C). A similar increase in luminescence was observed in cell culture co-transfections of cc-siRNA and AAV where the effect was independent of siRNA sequence, AAV serotype, or cell type. There are several possible explanations: cc-siRNA could alter AAV transduction efficiency, it could increase viral gene expression, or cc-siRNA could increase the delivery of AAV from the pipet tip, resulting in increased delivery of AAV.

An experiment to test whether the cc-siRNA improves the viral transduction into cells can be done by labeling the viral capsid with Cy5 fluorescent dye. By exposing cultured cells to Cy5-labeled virions with and without cc-siRNA, the degree of transfected viral particles can be quantified [293]. This experiment would reflect cellular transport of the capsid rather than the expression of a fluorescent or luminescent protein. Cy5 labeled virus can also be used *in vivo* to study the effect on cell tropism and anatomical spread. Comparing Cy5 labeled AAV with and without cc-siRNA could reveal differences in the number of cells, area of transduction, and cell-type specificity, through co-labeling with cell-type specific antibodies. In order to study if the

effect is related to enhanced transcription or translation, cells (or mice) stably expressing AAV-Luciferase could be transfected (or re-injected) with cc-siRNA. Increased luminescence would be observed with an increase in transcription or translation, and Western analysis and quantitative PCR could be used to detect relative increases in protein and mRNA, respectively. This is one way to discern whether the interaction is independent of AAV transduction into cells and whether there is enhancement of transcription or translation. Improvement in AAV transduction efficiency would present an advance to gene therapeutics and the effect of cc-siRNA warrants further study. While this thesis was being edited, these experiments were repeated by a different member of the lab using different reagents. Unfortunately, they were unable to replicate these results.

The present study demonstrates the possibilities and limitations in using AAV-Luc-Htt and BLI to follow gene silencing in the brain. There is a large variation within experimental groups which contributed to our inability to detect modest decrease in luminescence. If this model requires large numbers of mice in order to achieve statistical significance, then would not be a reasonable tool for screening applications. There is the potential that with stronger RNAi potency, new luciferase substrate with left-shifted spectrum that AAV-Luc-Htt can be used to compare sequences, hairpin structures, promoters, and delivery of RNAi and potentially validate allele-specific silencing of huntingtin sequences in the mouse brain.

E. Materials and Methods

1. Stereotactic injection

FVB mice (female, 3-6 months old, FVB/NJ from Jackson Laboratory, Bar Harbor, ME) were anesthetized with 250 mg/kg tribromoethanol (2.5 g 2, 2, 2, tribromoethanol dissolved in 5mL amylene hydrate into 200mL PBS). Anesthetized mice were placed on a heated pad in a stereotactic frame. Superglue (Loctite) was applied to the surface of the fur between the ears, avoiding eyes and exposed skin. After 10-20 seconds, the glue is gently pulled off to remove fur. The exposed skin is cleaned with betadine and an incision is made posterior to anterior. The skin is pulled aside and the needle is placed over the bregma. Unless otherwise stated, measurements for injection location are: anterior 1mm, lateral 3mm and ventral 2mm from the bregma. Once the needle is lowered, it rests there for 2 minutes before infusion begins by micropump syringe (NanoFil syringe, World Precision Instruments). Injections were performed at a rate of 125nl per minute, for values see below. After infusion the mouse rests for 2 minutes before the needle is withdrawn. The incision is closed with clear, undyed suture (monocryl undyed monofilament) and the animals are allowed to recover on a heated pad at 37C.

AAV dilution series (Figure 3-1 C): Mice were injected unilaterally with 1µl of AAV9-CMV-Luc-Htt (AAV-Luc-Htt) at each concentration: 1e13 GC/mL, 1e12 GC/mL, 1e11 GC/mL, 1e10 GC/mL, 1e9 GC/mL; n=3-5 mice per concentration.

Unilateral control injection (Figure 3-2 A, B): Mice were injected with 5e9GC AAV-Luc-Htt on the right side cortex (coordinates: at the bregma (anterior 0.0) lateral 2mm, ventral 2mm), volume of injection is 0.67µL, n=9 mice.

Injection of cholesterol conjugated siRNA (Figure 3-5): Mice were co-injected on the left side with 2e10GC AAV-Luc-Htt and 0.9nmol cc-siRNA targeting luciferase from *Photinus pyralis* (firefly luciferase, siLuc, Table 3-1). The same mice were co-injected on the right side with

2e10GC AAV-Luc-Htt and 0.9nmol control cc-siRNA targeting luciferase from *Renilla reniformis* (renilla luciferase, siCon, Table 3-1). A second group of mice were injected bilaterally with 2e10 GC AAV-Luc-Htt and PBS. A third group of mice were injected with 2e10 GC AAV-Luc-Htt and 0.9nmol cc-siCon on the right side and with 2e10GC AAV-Luc-Htt and PBS on the left side. The total volume of each injection was 4μL, n=5 per group.

Injection of siRNA (Figure 3-7): For each siRNA, groups of mice were co-injected on the left side of the brain with 5e9GC AAV-Luc-Htt and 14nmol siRNA. The right side was injected with 5e9GC AAV-Luc-Htt and of PBS. Total injection volume is 3.75μL, n=4-8 per group

Injection of AAV-shRNA targeting firefly luciferase (Figure 3-8): Mice were injected with 5e9GC AAV-Luc-Htt and 1.15x10GC AAV-shLuc (Table 3-1), at a 1:2 GC ratio of AAV-Luc-Htt and AAV-shLuc. On the right side, each mouse was injected with 5e9GC AAV-Luc-Htt and 1.65μL PBS. Total volume of injection was 1.9μL, n=9 mice per group.

Injection of AAV-shRNA targeting SNP site 2273 (Figure 3-9): For results shown in Figure 3-9 A, mice were injected into the cortex at measurements from the bregma: anterior: 0mm, lateral 3mm, ventral 1mm. The left side was injected with 5e9GC AAV-Luc-Htt and 5e9GC AAV-miR2273G (Table 3-1). The right side was injected with the same amount of AAV-Luc-Htt and 5e9GC AAV-miR2273A (Table 3-1). Total volume of injection was 0.6 μL at a ratio of 1:1 GC between the AAV-Luc-Htt and AAV-miRNA, n=8 mice per group. For results shown in Figure 3-9 B, C, groups of mice were injected on the left side with 5e9GC AAV-Luc-Htt and 4.5e10GC of either AAV-miR2273G, AAV-miR2273A, or AAV-miRCon (Table 3-1). Each mouse was injected on the right side with 5e9GC AAV-Luc-Htt and PBS. Total volume of each injection was 3.71μL at a ratio of 9:1 GC between AAV-Luc-Htt and AAV-miRNA, n=5 mice per group.

Injection of AAV-miRNA targeting SNP site 2307 (Figure 3-10): For results shown in Figure 3-10 A (n=5) the left side was injected with 5e9GC AAV-Luc-Htt, 5e9GC AAV-miR2307 (Table 3-1), and PBS. The right side was injected with the same amount of AAV-Luc-Htt and of PBS. Total volume of injection was1.5µL at a ratio of 1:1 between the AAV-Luc-Htt and AAV-miRNA. For results shown in Figure 3-10 B, C, one group of mice (n=11) was injected on the left side with 5e9GC AAV-Luc-Htt and 2.5e10GC AAV-miR2307 (Table 3-1). The right side was injected with the same amount of AAVLuc-Htt and PBS. A second group of mice (n=8) were injected on the left side with 5e9GC AAV-Luc-Htt with the 2307C SNP site and 2.5e10GC AAV-miR2307 and on the right with PBS. All injections were 1.9µL in volume at a ratio of 1:5 between the AAV-Luc-Htt and AAV-shRNA.

AAV-miR2307 re-injection (Figure 3-11 A, B): Mice were injected with 5e9GC AAV-Luc-Htt. After 7-12 days, mice were re-injected 2.5e10 GC AAV-miR2307. All injections were 1.9µL in volume, n= 4 mice per group.

2. Imaging mice

Mice were anesthetized with 5% isofluorane and placed into the Xenogen (now Caliper) *in vivo* imaging system (IVIS 100). 10 minutes prior to imaging, mice are injected with 150mg/kg D-luciferin into the intraperitoneal (ip) space (from a 30mg/mL stock solution dissolved in sterile water). Luminescent measurements were taken by 1 minute exposure. A region of interest is drawn over each injection site to quantify luminescence from the injected area. Data was collected as flux (photons / second).

3. Cell culture experiments

Testing of AAV-Luc-Htt and cc-siRNA: HeLa cells were grown to confluence in 24 well plates. Cells were incubated with dilutions of AAV-Luc-Htt with 0.9nmol of control cc-siRNA (targeting *Renilla* luciferase or GFP) per well. Doses of virus were 1000 MOI, 10,000 MOI, 100,000 MOI. AAV-Luc-Htt at 100,000 MOI was also incubated with 0.9nmol of cholesterol. Cells were lysed after 24 hours by adding 100uL passive lysis buffer (Promega Dual-Luciferase Reporter Assay System) and placed on a shaker for 20 minutes at room temperature. Cell lysates were measured for luminescence in a Glomax luminometer.

Dual luciferase assay: HeLa cells were grown to confluence in 24-well plates. Different concentrations of siRNA were made in serum-free media with either 0.025 μg/well pSiCheck with the target sequences or a combination of 0.025μg/well pAAV-Luc-Htt and 0.05μg/well pRLTK. The siRNA and vector mixture was combined with lipofectamineLTX (Invitrogen) and 400μL was placed into each well. Concentrations of siRNA were: 20 nmol, 10 nmol, 2 nmol, 1 nmol, 0.5 nmol, 0.2 nmol, 0.05 nmol, 0.02 nmol, 0.005 nmol, 0.002 nmol, and 0.0005 nmol. Doses for cc-siRNA were: 80 nmol, 60 nmol, 40 nmol, 20 nmol, 10 nmol, 6 nmol, 2 nmol, 1 nmol, 0.6 nmol, and 0.2 nmol. Each concentration was performed in triplicate. After 24 hours the cells were lysed with 100uL of passive lysis buffer and measured for luminescence using the Promega Dual Luciferase Reporter Assay System and Glomax luminometer. Data were graphed and the IC50 was calculated using Igor Pro software (WaveMetrics, Portland, OR).

Testing of AAV-miRNA silencing: HeLa cells were grown to confluence in 24 well plates. Each dilution of AAV-miRNA was made in serum-free media (OptiMEM) and 200uL containing the designated MOI of virus was added to each well of cells. The cells were incubated with virus overnight and checked for GFP activity. Then they were transfected with 0.025ug/well pSiCheck

vector (Promega) containing the target sequence using Lipofectamine LTX (Invitrogen). pSiCheck vectors express both Firefly and *Renilla* luciferases. The target sequence is inserted into the 3'-UTR of Firefly luciferase and silencing of firefly luciferase is normalized to the constant expression of *Renilla* luciferase. Cells were lysed after 24 hours and measured for Firefly and *Renilla* luciferase activity. All concentrations were performed in triplicate.

4. Cloning

Target sites were synthesized as ultramer oligos with 15nt of sequence flanking each SNP site. We created two ultramers with each SNP site. Ultramer C1 has one variation of each SNP nucleotide, and ultramer C2 has an alternate SNP nucleotide. The sequences are C1: 3'-CTAGAGCCTTTGGAAGTCTGCGCCCTTGTGCCCTGCCGAGAAGCTGCTGCTGCAGATCAACCCCGAGGAGATGGGGACAGTAATTCAACGCTAGAAGAGCCTGCTCCCTCATCCACTGTGTGCACTTCAGTCTCAGTGCCGAGCTCAGCGCCTTGGCTCTGCTGTCTGAGCAGCTATCTCGGCTAGACACAT-5' and C2: 3'-CTAGAGCCTTTGGAAGTCTGTGCCCTTGTGCCCTGCCGAGAAGCTGCTGCTACAGATCAACCCCGAGGAGATGGGGACAGTACTTCAACGCTAGAAGAGCCTGCTCCCTCATCTACTGTGTGCACTTCAGTCTCAGTGCCGAGCACAGCGCCTTGGCTCTGCTGTCTGAGCAGCTCTCTCGGCTAGACACAT-5'. SNP sites are underlined. Xba1 sites were added before and after each ultramer for insertion into the 3'-UTR of pGL3-control vector and we sequenced the resulting clones to check for correct insertion. The luciferase genes with ultramers were amplified with a SalI site, the PCR product was digested with EcoRI and SalI, and inserted into pAAV-CMV backbone.

Figure 3-1: Allele-specific gene silencing, AAV-Luc-Htt design and *in vivo* testing. (A) Allele-specific RNAi is designed to discriminate between single nucleotide polymorphisms (SNPs), preferentially cleaving the matching SNP site over the mismatching SNP site. In Huntington's disease, allele-specific RNAi is designed to target the SNP variation present on the CAG expanded allele. (B) We have created two luciferase reporter constructs containing huntingtin target sequences in the 3'-UTR. Each colored bar is a 30bp fragment of sequence surrounding the indicated SNP site. Each SNP is identified by a four digit code and the letter representing the SNP nucleotide. The first four sites are human huntingtin SNP sites and the last two sites are found in mouse huntingtin. C.) Mice were unilaterally injected with 10-fold dilutions of AAV-Luc-Htt and imaged after two weeks. The 1e10GC injected mice emit more light than all other groups (One-way ANOVA $p<0.0001$, Tukey's multiple comparison test, all groups n=5). BG, background. Data is presented as mean ± SEM, $^{**}p<0.01$, $^{***}p<0.001$.

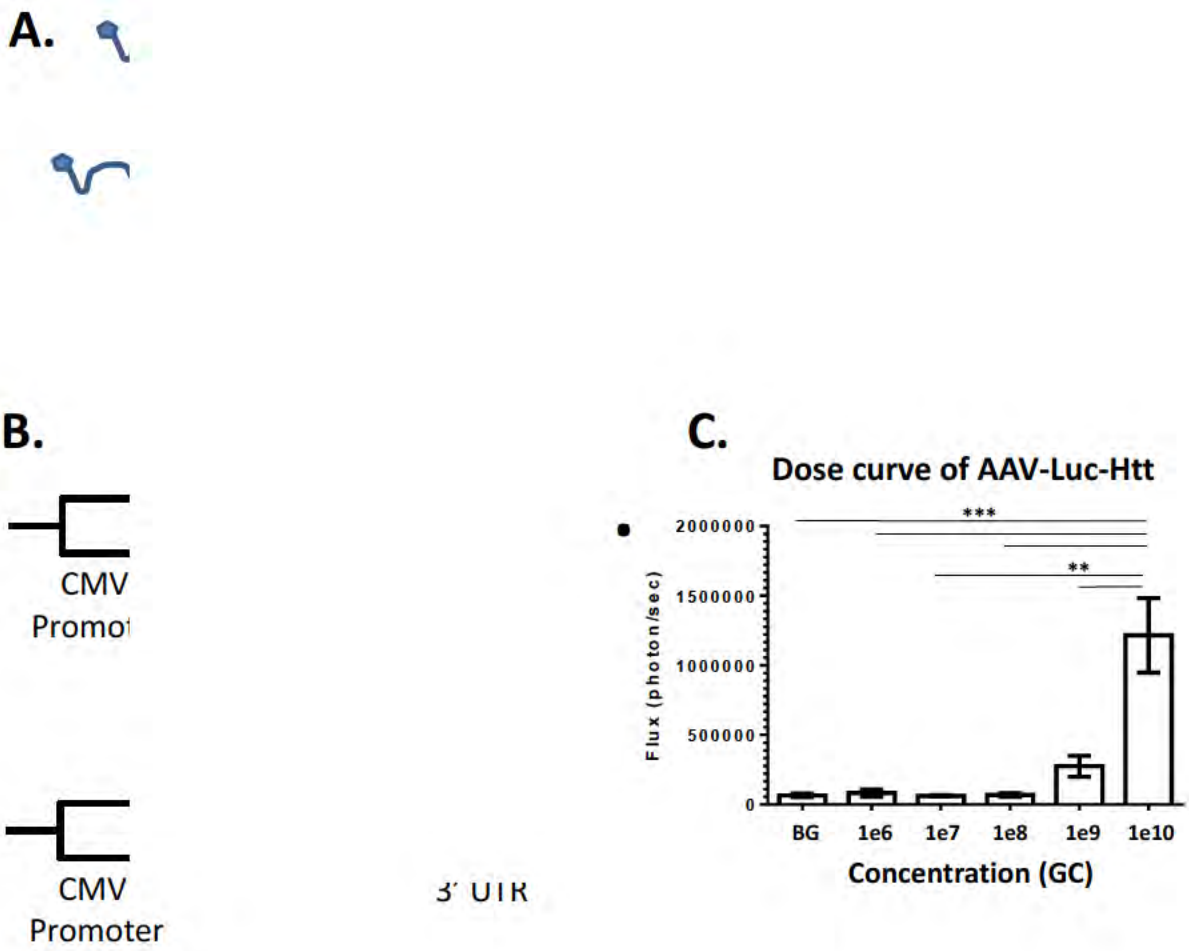

Figure 3-1: Allele-specific gene silencing, AAV-Luc-Htt design and *in vivo* testing.

Figure 3-2: Variation in luminescence of AAV-Luc-Htt injected mice. A.) Mice (n=9) were injected with 5e9GC AAV-Luc-Htt on the right side and imaged over 28 days. Stable baseline is achieved starting at day 10. B.) Three days within the stable baseline are selected for comparison (15, 19, and 21), and data points are plotted as luminescence (flux, photon/second) for each mouse. Each mouse displays different degree of variability, with standard deviations ranging from 5-40% of its total flux. All data is presented as mean ± SD.

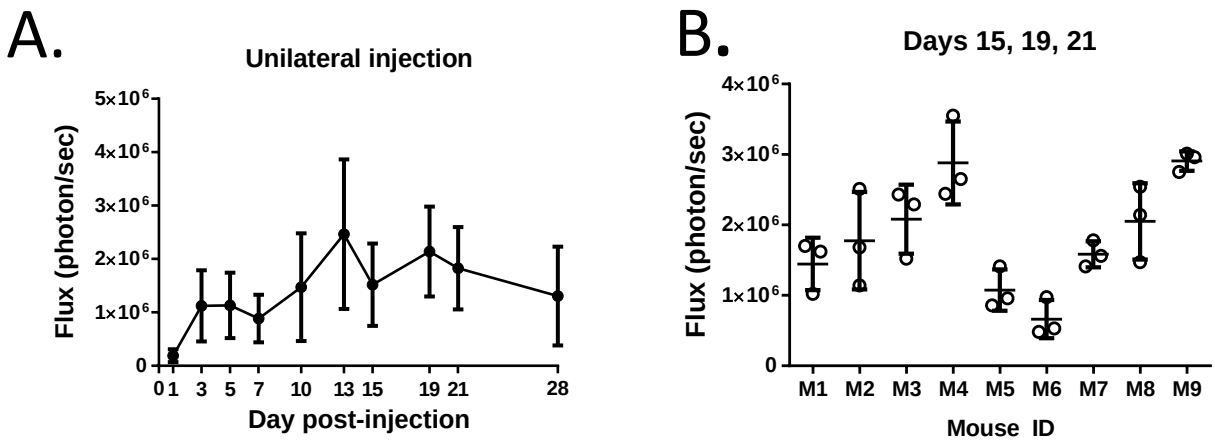

Figure 3-2: Variation in luminescence of AAV-Luc-Htt injected mice.

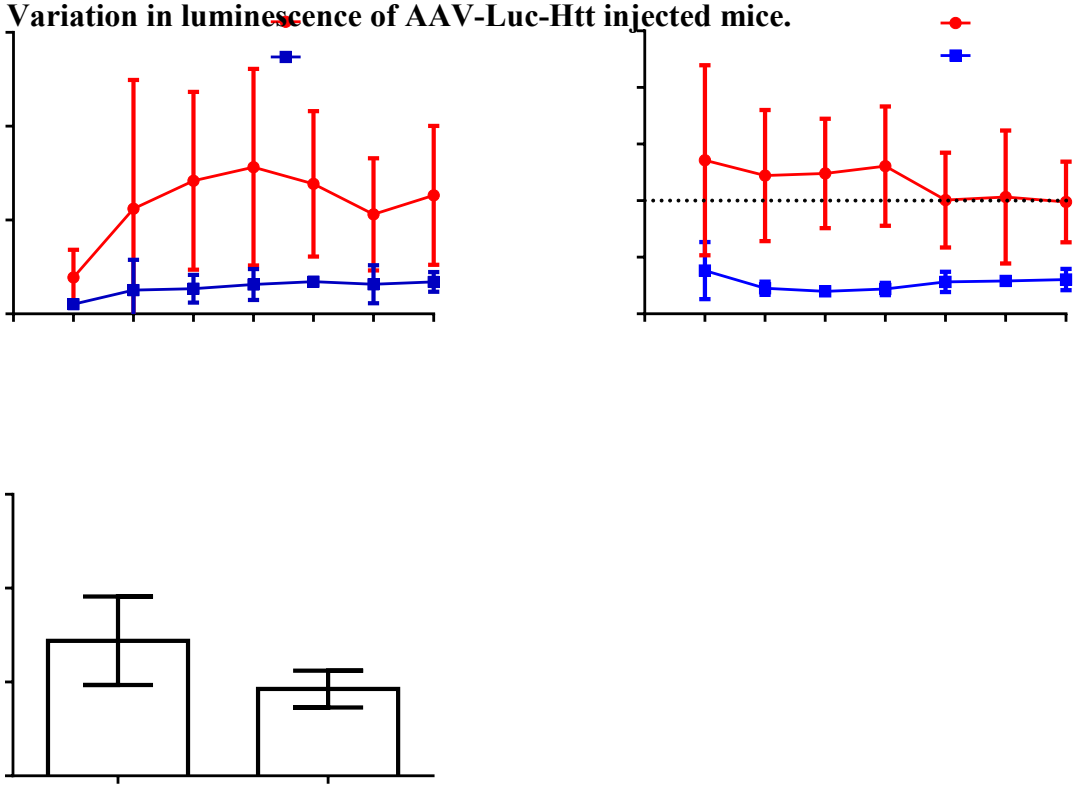

Figure 3-3: Experimental design for *in vivo* measurement of RNAi gene silencing. A.) Luciferase reporter constructs with the huntingtin target SNP sites are packaged in AAV capsid (AAV-Luc-Htt). AAV-Luc-Htt virus is co-injected into the left side of the brain with experimental RNAi molecules. The right side is co-injected with the reporter construct and either control RNAi molecules or PBS. Beginning 24 hours after injection, the mice are anesthetized, injected into the ip space with the luciferase substrate and imaged to measure luminescence. A region of interest, ROI, is drawn over each side of the brain, then quantified and analyzed both as luminescence (flux, photons/second) and as a ratio of experimental / control injected side. B.) Mice were injected with 5e9GC AAV-Luc-Htt in the right striatum (unilateral injection, n=5) or into each hemisphere (bilateral injection, n=7) and imaged for seven days. The ratio is calculated as the flux from the left hemisphere divided by the flux from the right hemisphere. The ratios from each day were compared at each time point (Mixed method ANOVA for ratio group, $p<0.0001$; for unilateral injection group, $p< 0.0001$, Tukey's multiple comparisons). Both groups showed a difference between the left and right sides, however only the ratio group showed differences between sides on each day. All data is presented as mean ± SD. *$p<0.05$, **$p<0.01$, ***$p<0.001$, ****$p<0.0001$.

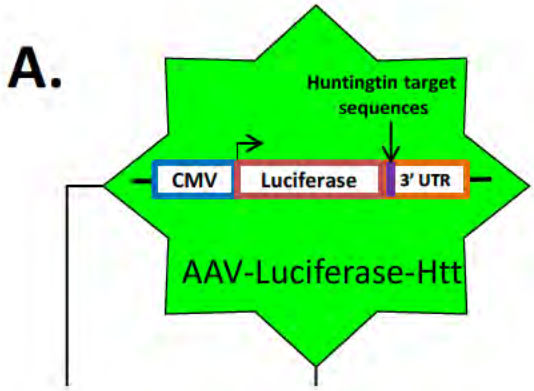

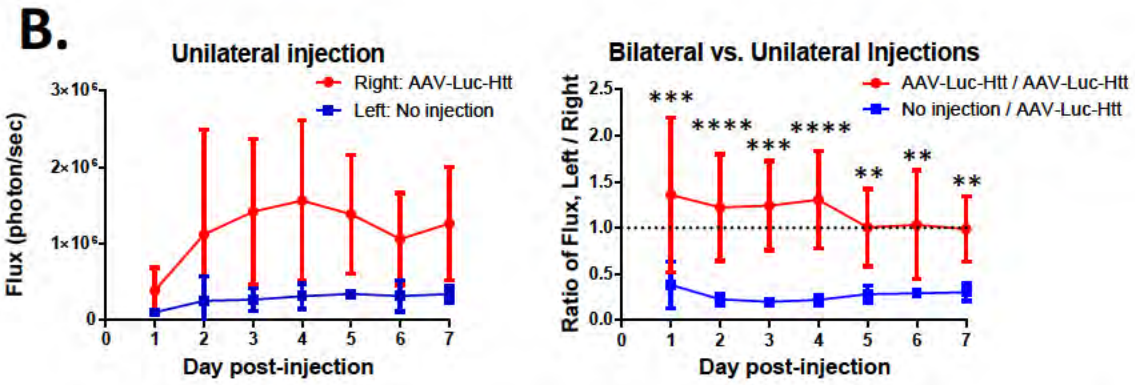

Figure 3-3: Experimental design for *in vivo* measurement of RNAi gene silencing.

Figure 3-4: RNAi constructs silence luciferase and huntingtin targets in cell culture. (A) siRNA and cc-siRNA molecules were tested against their target sequences in dual luciferase assays. siRNA are tested at 11 doses and cc-siRNA are tested at 10 doses, each dose is done in triplicate. Data is presented as luminescence of target normalized to control luciferase for each dose. IC_{50} values were calculated from the curve using Igor Pro wave-fitting software (WaveMetrics, Portland, OR). (B) Cells were infected with the AAV-miRNA and then transfected with the matching reporter construct to measure silencing of huntingtin target sites. Luminescence was normalized to cells transfected with reporter construct and no AAV. At 100,000 MOI of AAV-miR2273, there was a 32% silencing compared with 10,000 MOI/well (mean diff. 0.5854 (95% CI 0.5030 to 0.6679, $p<0.0001$)) for 30,000 MOI there was 10% silencing (mean diff. 0.2798 (95% CI 0.1400 to 0.4197, $p=0.0001$)). For AAV-miR2307 there was a 55% silencing compared with 10,000 MOI (mean diff. 0.3910 (95% CI 0.2511 to 0.5309, $p<0.0001$)) and for 30,000 MOI 12% silencing (mean diff. 0.4560 (95% CI 0.3736 to 0.5385, $p<0.0001$)). Data is presented as mean ± SD. *** $p<0.001$, ****$p<0.0001$

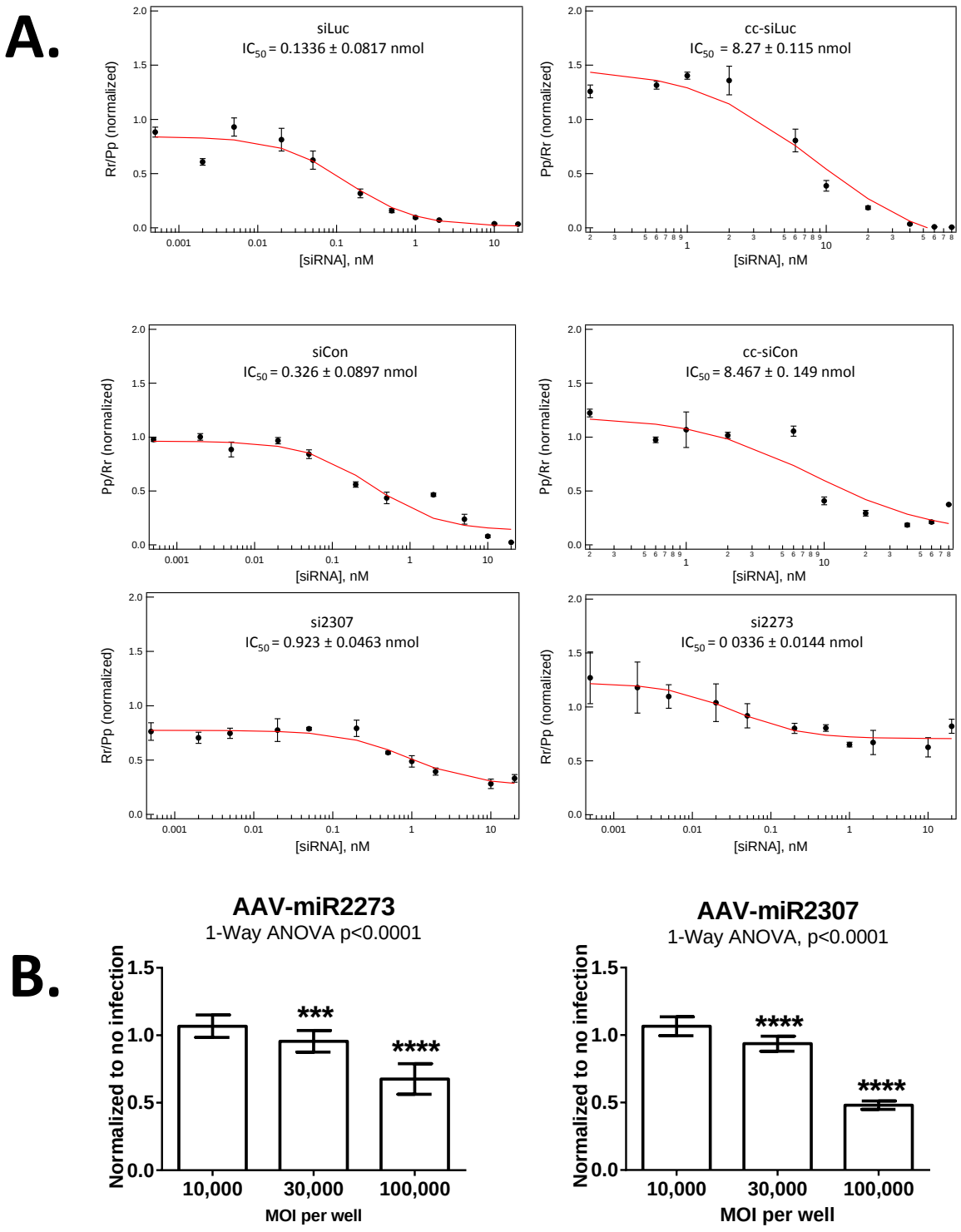

Figure 3-4: RNAi constructs silence luciferase and huntingtin targets in cell culture.

Figure 3-5: Cholesterol-conjugated siRNA silences luciferase activity in the brain 24 hours after injection. (A) To test silencing by cholesterol-conjugated siRNA, mice were co-injected with AAV-Luc-Htt and cc-siRNA. In one set of mice, the left side of the brain was co-injected with AAV-Luc-Htt and cc-siLuc, and the right side was co-injected with AAV-Luc-Htt and cc-siCon. There was no difference in the luminescence from either injection over time. In a second set of mice, both sides were injected with AAV-Luc-Htt and PBS alone. There was no difference in either of the injections over time. (B) For the same experiment, results were calculated using each mouse as its own control. The luminescence from the left was divided by luminescence on the right side. One day after injection, there was a difference between the ratio in the cc-siRNA treated group compared with the PBS treated group. There was a decrease of 52.6% (Sidak's multiple comparisons test, mean diff. 0.4847 (95% CI 0.4051 to 0.5644, $p<0.0001$, n=5 for both groups). There were no differences at the other time points. (C) To investigate the effect of cc-siRNA on long-term luciferase activity in the same mice, we compared luminescent flux at 168 days. Comparison of left side injections and right side injections show a 1.9- and 1.7-fold differences respectively (Unpaired t-test $p=0.0017$ and $p=0.0007$, respectively) (D) To compare the effect of cholesterol-conjugated siRNA on AAV-Luc-Htt, mice were co-injected on the left side with PBS and on the right side with cc-siCon. We found a significant increase in luminescence on the cc-siCon side at 5 and 12 days after injection (2-Way ANOVA $p=0.0015$, Tukey's multiple comparison test, n=5). After 6 months, there was no difference in luminescence between the sides of the brain. Data is presented as mean ± SEM. ***$p<0.001$, ****$p<0.0001$

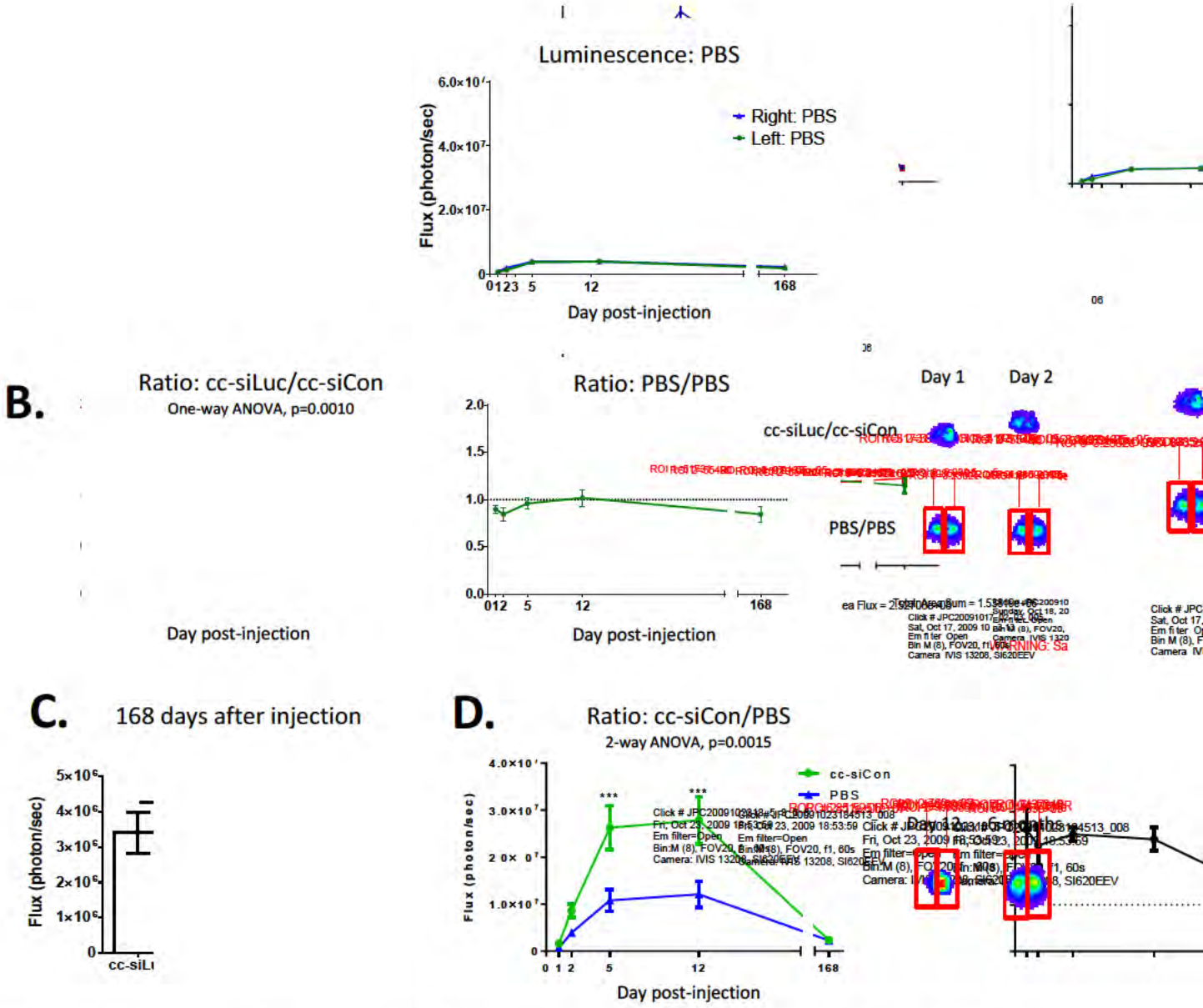

Figure 3-5: Cholesterol-conjugated siRNA silences luciferase activity in the brain 24 hours after injection.

Figure 3-6: Cholesterol-conjugated siRNA increases luminescence in AAV-Luc-Htt treated cells. (A) HeLa cells were incubated with 10,000 MOI AAV-Luc-Htt and either control cc-siRNA (cc-siCon), unconjugated control siRNA (siCon), no siRNA. Cells were also incubated with only cc-siCon or siCon to ensure no contamination with AAV-Luc-Htt. There was a significant increase in the luminescence with a mixture of AAV-Luc-Htt and cc-siCon compared with both no siRNA and siCon treated groups (T-test, $p=0.0091$ and $p=0.0001$ respectively). (B) Different concentrations of AAV-Luc-Htt were combined with cc-siCon or no siRNA. Overall, there was an increase in luminescence in the cells treated with cc-siRNA (2-way ANOVA $p<0.001$). At 100,000 MOI there was a 2.62-fold increase in luminescence in cc-siRNA treated cells (Bonferroni posttest, mean diff. 11570 (95% CI 9531 to 13600, $p<0.0001$)). (C) 100,000 MOI AAV-Luc-Htt was tested with cholesterol and there was no difference from the untreated group. (D) AAV2-Luciferase was incubated with either cc-siCon or no siRNA. There was a 1.81-fold increase in luminescence in the cc-siRNA treated cells (T-test $p=0.0045$). (E) Cells were incubated with 1000 MOI AAV-Luc-Htt and cc-siRNA targeting GFP (cc-siGFP). There was a 1.22-fold increase in luciferase in the cc-siGFP group (T-test, $p=0.0062$). (F) Neuro2A cells were incubated with 1,000 MOI AAV-Luc-Htt and cc-siGFP and there was a 1.45-fold increase in luminescence in the cc-siGFP treated group (T-test, $p=0.0242$). Data is presented as mean ± SD. *$p<0.05$, **$p<0.01$, ***$p<0.001$

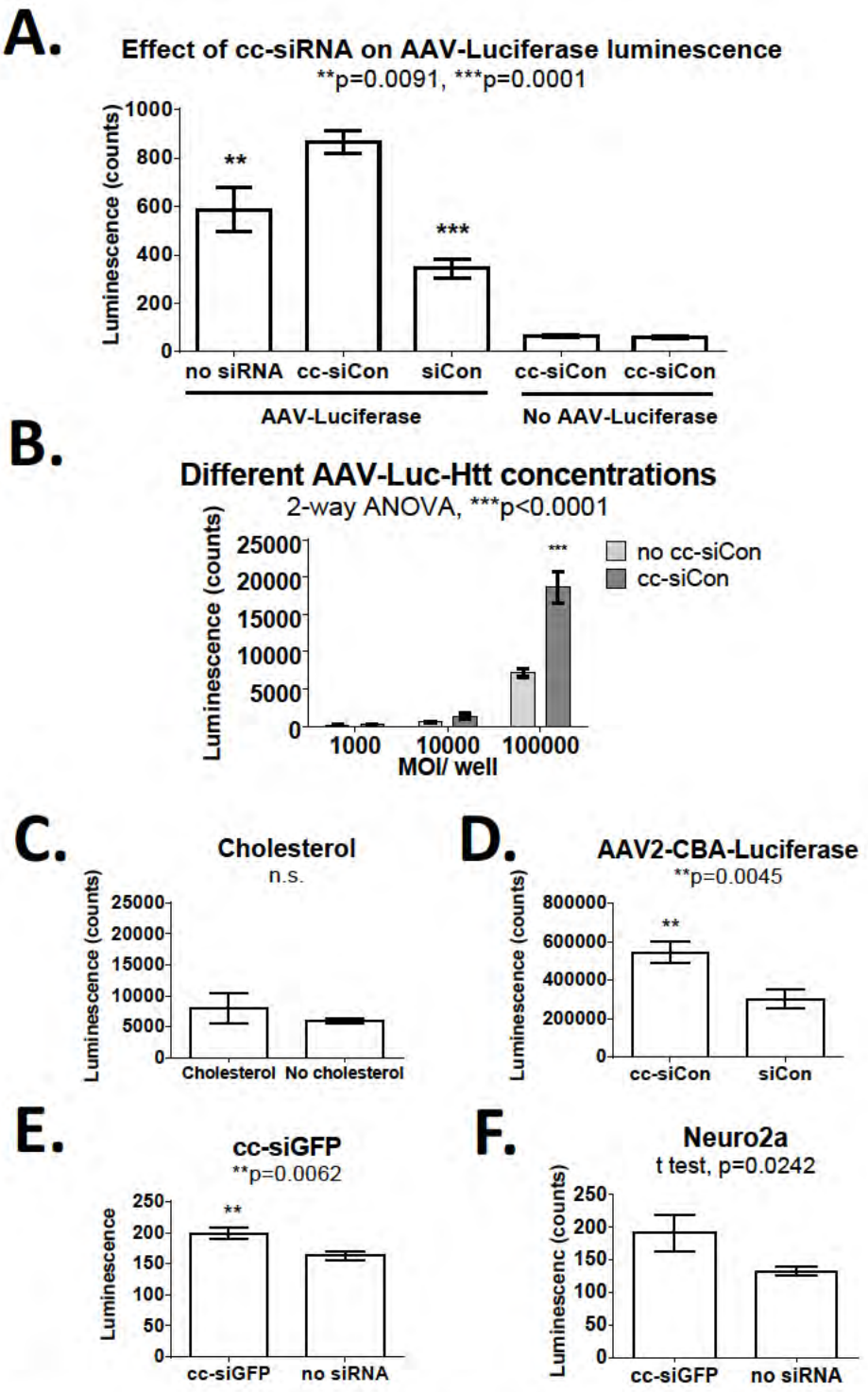

Figure 3-6: Cholesterol-conjugated siRNA increases luminescence in AAV-Luc-Htt treated cells.

Figure 3-7: siRNA silences luciferase activity in the brain. A-D.) Mice were injected on the left side with 14nmol siRNA and AAV9-Luc-Htt and on the right side with PBS and AAV9-Luc-Htt. (A) Co-injection with 14nmol siLuc resulted in an overall decrease in luminescence over time compared with the injections of PBS (n=8, 2-way mixed methods ANOVA p=0.0064). The ratio of left side to right side luminescence shows a 43% silencing of luciferase activity day 3 after injection compared with ratio one year after injection (One-way ANOVA p=0.0008, Dunnett's multiple comparisons test, mean diff 0.5174 (95% CI 0.05767 to 0.9771, p=0.027). B, C.) Groups of mice were co-injected with 14nmol siRNA targeting SNP site 2307 (n=5), and 2273 (n=6). There were no differences in luminescence between sides or any difference in the left to right ratio compared with one year later. D.) Mice were co-injected with AAV-Luc-Htt with control siRNA on the left side and PBS on the right side. There was a decrease in the luminescence on the siCon side overall (2-way mixed methods ANOVA, p=0.0369, n=4). However, there was no difference in the ratio of left to right side luminescence compared with one year. Data is presented as mean ± SEM. *$p<0.05$

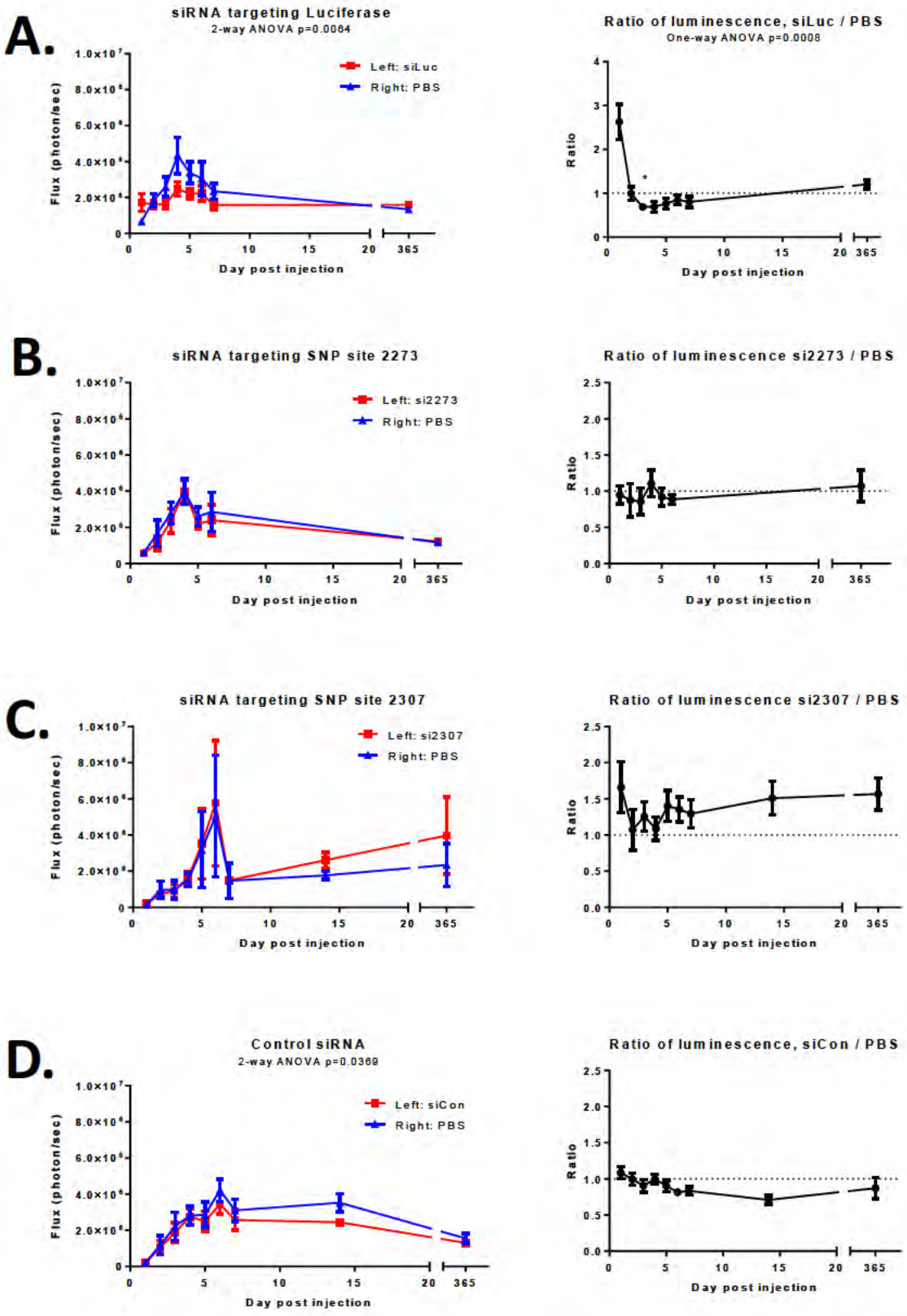

Figure 3-7: siRNA silences luciferase activity in the brain.

Figure 3-8: AAV-shRNA targeting luciferase reduces luminescence in the brain. A.) Mice were co-injected with AAV-shLuc and AAV-Luc-Htt (2:1 ratio of AAV-shLuc to AAV-Luc-Htt) on the left side and PBS and AAV-Luc-Htt on the right. Luminescence was decreased on the AAV-shLuc side compared with the contralateral PBS injection (Mixed model ANOVA, $p=0.0002$, $n=9$). The average difference between the two sides is 23%. B.) Ratio of luminescence from the left side (AAV-shLuc) to the right side (PBS). Average ratio is less than 1.0 for most time points. C.) Representative mouse two days after injection. Data is presented as mean ± SEM.

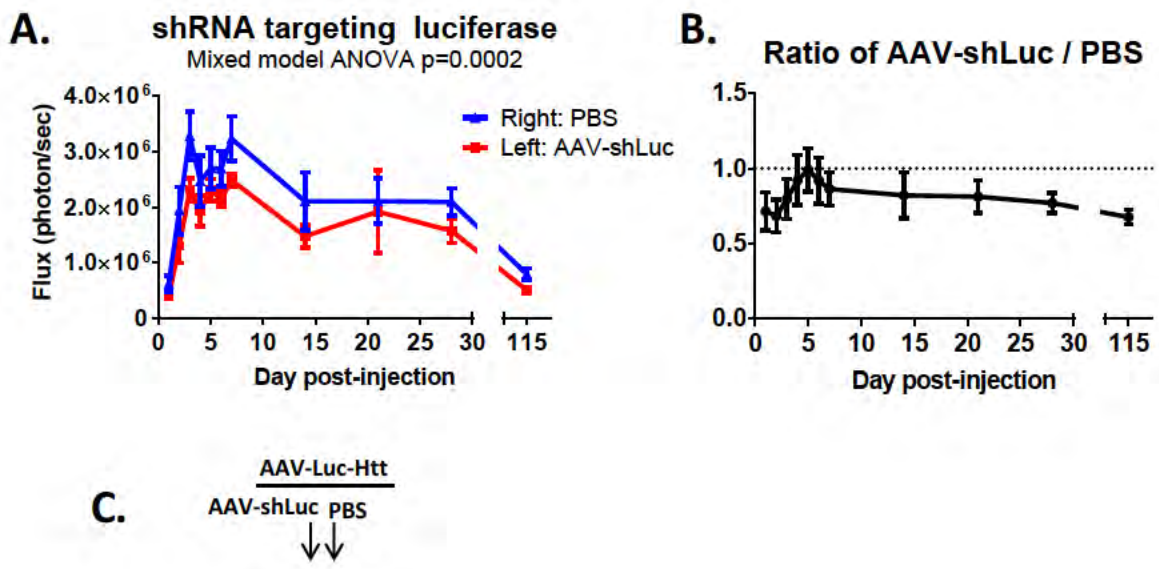

Figure 3-8: AAV-shRNA targeting luciferase reduces luminescence in the brain.

Figure 3-9: AAV-miRNA targeting human huntingtin SNP site 2273 does not decrease luminescence in the brain. (A) We tested a 1:1 ratio of AAV-Luc-Htt to AAV-shRNA targeting human huntingtin SNP site 2273. The left side was injected the AAV-Luc-Htt virus and AAV-miR2273G matching the target sequence. On the right side we injected AAV-Luc-Htt and AAV-sh2273A containing a mismatch at the SNP site. There was no significant difference in the flux between the two sides (2-way ANOVA, n.s. n=8). (B) We then increased the dose of AAV-miR2273 to a 9:1 ratio of AAV-Luc-Htt to AAV-miRNA. One group was co-injected on the left side with AAV-Luc-Htt and AAV-miR2273G matching the target and the right side injected with AAV-Luc-Htt and PBS (n=5). A second group was co-injected with AAV-Luc-Htt and AAV-miR2273A, which has a mismatch to the target sequence (n=5). There was a significant 1.7 fold increase in the AAV-miR2273A injected side (2-way ANOVA $p<0.0496$). The last group was co-injected on the left side with AAV-miRCon that does not match the target at all (n=5). There was a 1.33 fold increase in the AAV-miRCon side (2-way ANOVA $p=0.076$). The right side of all mice was injected with the same amount of AAV-Luc-Htt and PBS. (C) We calculated a ratio of left side to right side for each mouse, and comparing the averages for all groups. There was no difference between the ratios for each group. Data is presented as mean ± SEM. *$p<0.05$, **$p<0.01$, ***$p<0.001$

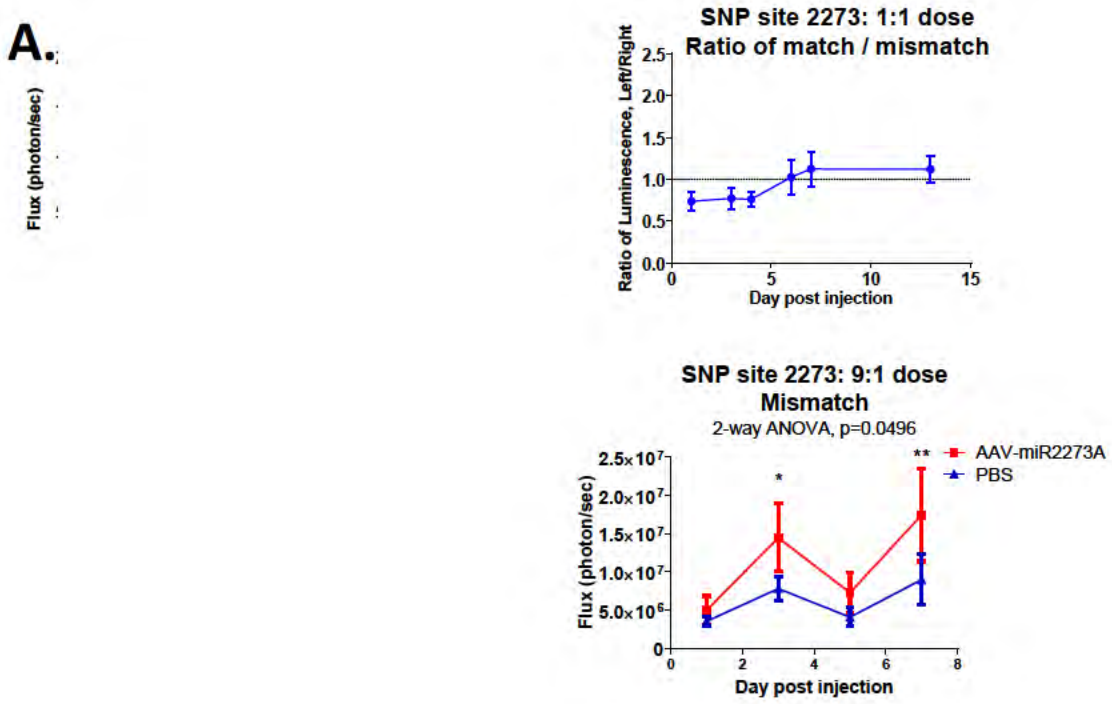

Figure 3-9: AAV-miRNA targeting human huntingtin SNP site 2273 does not change luminescence in the brain.

Figure 3-10: AAV-miRNA targeting huntingtin SNP 2307 results in allele-specific silencing in the brain. (A) We tested a 1:1 ratio of AAV-miRNA targeting the huntingtin 2307 SNP. In a group of mice, the left side was injected with AAV-Luc-Htt with AAV-miR2307 that matches the target. On the right side, AAV-Luc-Htt was injected with PBS in the same volume. There was no significant difference (n=5 for both groups). (B) We tested a 5:1 ratio of AAV-Luc-Htt to AAV-miRNA targeting the human SNP site 2307 (AAV-miR2307). In one set of animals, the left side was injected with AAV-Luc-Htt and AAV-miR2307 matching the target sequence, and the right side was injected with AAV-Luc-Htt and PBS. In another set of animals the left side was injected with AAV-Luc-Htt containing the alternate SNP site with the same AAV-miR2307 resulting in a mismatch of the shRNA and target sequence. There is a significant difference in the luminescence between the two sides of the match injected animals, the AAV-miR2307 side is 42% less than the control side (Mixed methods ANOVA, $p=0.0051$). There is no significant difference between the right and left luminescence of the mismatch injected animals. (C) The ratio of matched vector injected side to control side is 0.8834 ± 0.1287 and the ratio between the mismatch side compared with control side is 1.0665 ± 0.1503. The difference between the means is not statistically significant. (match n =11, mismatch n=8, error bars are SEM). (D) Representative image of mice co-injected with AAV-Luc-Htt and matching AAV-miRNA, mismatching AAV-miRNA, or PBS.

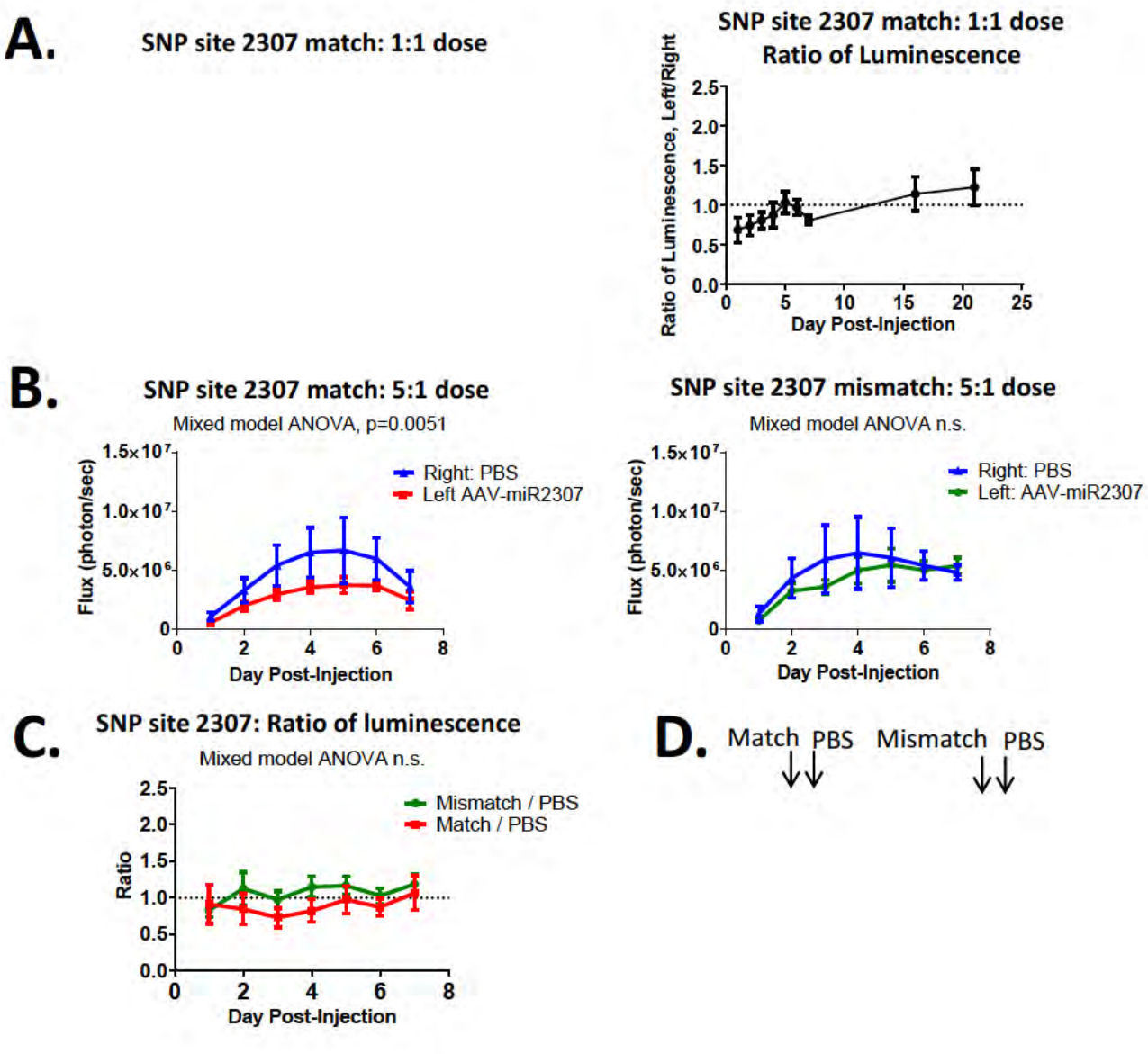

Figure 3-10: AAV-miRNA targeting huntingtin SNP 2307 results in allele-specific silencing in the brain.

Figure 3-11: Re-injection strategy to assess silencing of luciferase in the brain. (A) We tested a re-injection strategy to compare silencing with a baseline measurement of luminescence. One set of mice was bilaterally injected with AAV-Luc-Htt and after 14 days a baseline luminescence was measured. The same mice were then injected on the left side with AAV-miR2307. There was no injection on the right side. In a second group of mice, the left side was re-injected with PBS and the right side was not injected. (B) The left to right ratio for each mouse was calculated. There was no difference in the AAV-miR2307 injected group overall. There was a significant difference in the PBS injected group with an increase one day after PBS injection compared with baseline measurement (One-way ANOVA, $p=0.0157$, Dunnett's multiple comparisons, mean diff. -1.308 (95% CI -2.312 to -0.3029, $p=0.0107$). n=4 per group. Data is presented as mean ± SEM. *$p<0.05$

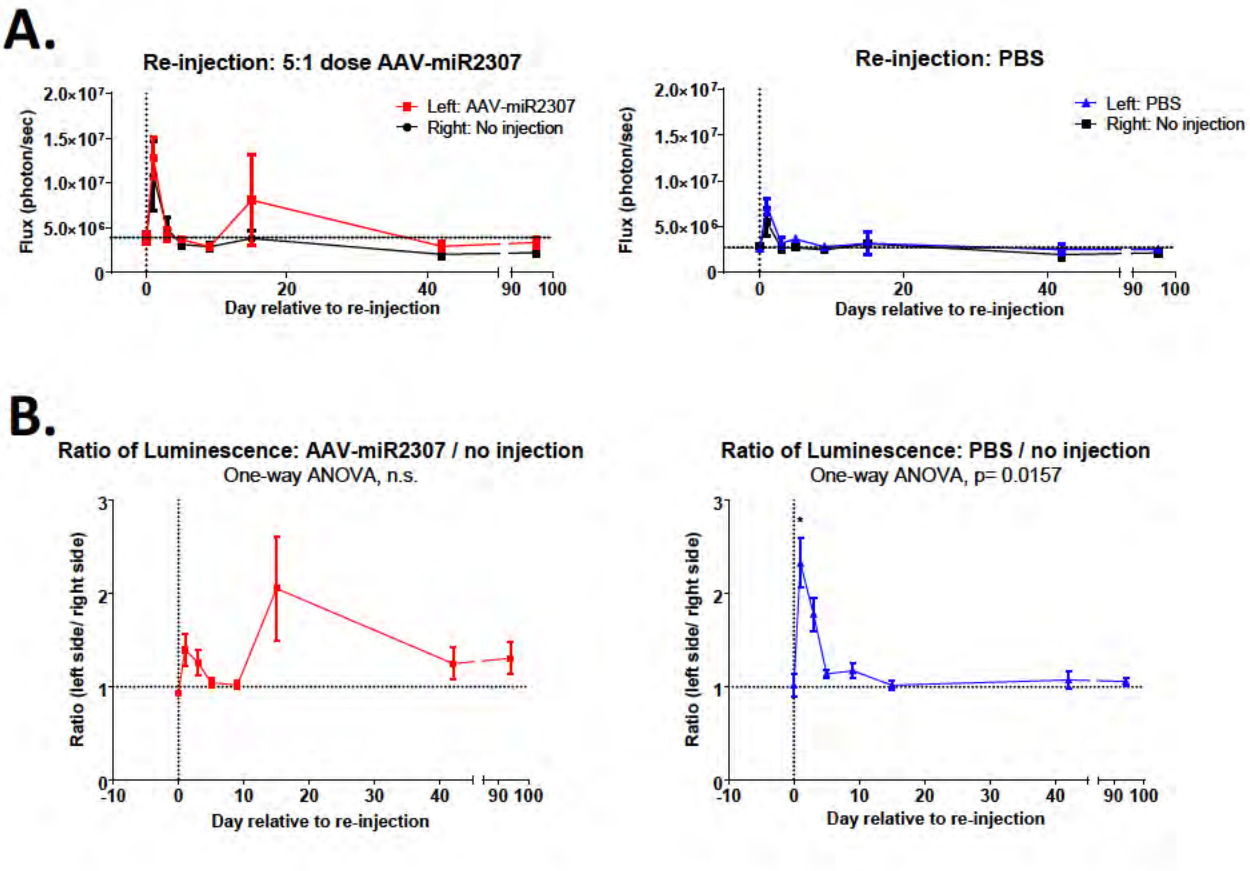

Figure 3-11: Re-injection strategy to detect silencing of luciferase in the brain.

Table 3-1: Sequences, structures and modifications of siRNA and RNA hairpins. Each silencing construct is listed by its full descriptive name, sequence with modifications and/ or hairpin structure, and IC_{50} value if applicable. IC_{50} values were determined as the amount of siRNA needed to decrease luminescence by 50% using a dual luciferase cell culture assay. (* represents phosphorothioate linkage; p represents phosphate group; m represents 2'O-methyl linkage)

	Sequence of siRNA or miRNA	IC_{50} (nmol)
Cholesterol conjugated firefly luciferase siRNA (cc-siLuc)	3′-chol*mU*mU*AAAGCUUCAUGAGUCGCAC-5′ 5′-pUUUCGAAGUACUCAGCGUG*mA*mG-3′	8.27 ± 0.115
Cholesterol conjugated renilla luciferase siRNA (cc-siCon)	3′-chol*mU*mU*GAUCGAUAUUACUUUACGG-5′ 5′pAUAGCUAUAAUGAAAUGCC *mU*mU-3′	8.47 ± 0.149
Firefly luciferase siRNA (siLuc)	3′-mU*mU*AAAGCUUCAUGAGUCGCAC-5′ 5′-pUUUCGAAGUACUCAGCGUG*mA*mG-3′	0.1336 ± 0.082
Renilla luciferase siRNA (siCon)	3′-mU*mU*GAUCGAUAUUACUUUACGG-5′ 5′-pAUAGCUAUAAUGAAAUGCC*mU*mU-3′	0.326 ± 0.09
Huntingtin SNP site 2307T (si2307)	3′-mU*mU*CUGUUACCGUGUCUGAAGG-5′ 5′-pUACAAUGGCACAGACUUCC*mU*mU-3′	0.923 ± 0.046
Huntingtin SNP site 2273G (si2273)	3′-mC*mC*CAACGAGACGUCGUCGUCG-5′ 5′-pUUUGCUCUGCAGCAGCAGC*mU*mU-3′	0.0336 ± 0.014
AAV2-U6-miR2307T-CMV-eGFP (AAV-miR2307)	. . . GGAU A GA C GUAAAGC CC GU GCG AGGAAGUCUGUGCCAUUGUAUCA C GG CA CGC UCCUUCAGACACGGUAACAUAGU A . . . UGGG G UC U GUAGAC	
scAAV8-CB.PI.egfp-U6-shLuc (AAV-shLuc)	CAA . . . GAUCCCGCUUACGCUGAGUACUUCGAUU A . . . UUUUUUGAAUGCGACUCATGAAGCUA A G AC	
scAAV9-CB/CMV-miR2273A-GFP (AAV-miR2273A)	GC UUGGCC . . . UGCUGUUUGCUCUGUA AGTAGCTTGUU A . . . AAACGAGACAU UCAUCGAACAG C UCAGU	
scAAV9-CB/CMV-miR2273G-GFP (AAV-miR2273G)	GC UUGGCC . . . UGCUGUUUGCUCUGCA AGUAGCUUGUU A . . . AAACGAGACGU UCAUCGAACAG C UCAGU	
scAAV9-CB/CMV-miREmpty-GFP (AAV-miRCon)	CU UUGGCC . . . UGCUGUUUCUCGCCCU UCGCUCUUGUU A . . . AAAGAGCGGGA AGCGAGAACAG C UCAGU	

Table 3-1: Sequences, structures and modifications of siRNA and RNA hairpins.

Table 3-2: Summary of AAV constructs and results. Each virus used in this study is listed by the name used to identify it in the text. The table summarizes the serotype, genotype structure, promoter, site of injection, concentration, and effectiveness for each virus with the corresponding figure number. For all experiments, AAV-Luc-Htt was co-injected with one of the silencing constructs. The concentration of the viruses refers to the ratio of silencing vector to AAV-Luc-Htt. For all experiments, the concentration of AAV-Luc-Htt is 5e9GC. N/A, not applicable; CMV, cytomegalovirus (RNA polymerase II); ssDNA, single-strand DNA; scDNA, self-complementary DNA; CBA, chicken beta actin promoter with cytomegalovirus enhancer (RNA polymerase II); U6 an RNA polymerase III promoter for transcribing short hairpin RNA.

Construct	Serotype	Genome structure	Promoter	Injection Site	Ratio	Effective at silencing luciferase *in vivo*?
AAV-Luc-Htt	AAV 9	ssDNA	CMV	Striatum and cortex	N/A	N/A
AAV-shLuc	AAV 8	ssDNA	U6	Striatum	2:1	Yes (Fig. 3-8)
AAV-miR2307T	AAV 1	ssDNA	U6	Striatum	1:1	No (Fig. 3-10A)
					5:1	Yes (Fig. 3-10 B-D)
AAV-miR2237A AAV-miR2237G	AAV 9	scDNA	CBA	Cortex	1:1	No (Fig. 3-9A)
					9:1	Inconclusive (Fig. 3-9 B-C)

Table 3-2: Summary of AAV constructs and results.

CHAPTER IV

THE USE OF NOVEL LUCIFERASE SUBSTRATES TO DETECT LUCIFERASE ACTIVITY IN THE BRAIN

This chapter describes work I performed using novel luminescent substrates to detect low levels of luciferase activity and silencing of luciferase *in vivo*. This work was conducted under the guidance of Neil Aronin. I planned and executed the majority of the experiment presented in this chapter. Wanzhao Liu performed the quantitative real-time PCR. The AAV construct was provided by Guangping Gao. Dr. Stephen Miller designed and synthesized the luminescent substrates. Results from this chapter are included in the published work:

Melanie S. Evans, Joanna P. Chaurette, Spencer T. Adams Jr, Gadarla R. Reddy, Miranda A. Paley, Neil Aronin, Jennifer A. Prescher, and Stephen C. Miller, A synthetic luciferin improves bioluminescence imaging in live mice. *Nature Methods* 11: 393-395, 2014.

A. Abstract

Bioluminescent imaging (BLI) has emerged as a powerful tool for *in vivo* visualization of biological processes. In mice, BLI has been used to study infection spread, tumor growth and metastasis, and gene silencing. The benefits of using BLI are that it is sensitive, low cost, high throughput, and can be used for longitudinal analysis in individual animals. There are limitations: absorbance by hemoglobin and melanin and the depth of tissue affect the detection of luminescence. Ways to improve detection of luciferase reporter activity are to increase luciferase activity or increase light output from the substrate. Our objective in this study is to identify substrates resulting in improved light output from the brain.

To screen luciferase substrates, we used mice expressing AAV-delivered firefly luciferase in the brain. We tested 34 substrate solutions and identified 19 that exhibited increased light output compared with 100mM D-luciferin. From this screen we identified the luciferase substrate, CycLuc1, as the highest light-emitting substrate, finding CycLuc1 to be 120 times more potent than D-luciferin. We next tested CycLuc1 and another potent substrate, iPr-amide, in mice expressing luciferase in dopaminergic neurons (DAT-LUC mice). We were able to detect luminescence from CycLuc1 and iPr-amide but not from D-Luciferin. We also tested iPr-amide, in AAV-luciferase injected mice with or without fatty acid amide hydrolase (FAAH) inhibitor. We found that activation of iPr-amide is dependent upon the activity of FAAH in the brain.

With potent luciferase substrates, *in vivo* bioluminescence can be detected at lower levels with less luminescent substrate. Improved sensitivity of BLI advances the application to the study of fewer cells, deeper structures, and models in which there is a lower level of luciferase expression.

B. Introduction

Reporter molecules are valuable tools for the study of biological processes in living cells and organisms. Following the activity of a reporter molecule *in vivo* requires the expression of a luminescent molecule that can be detected by a cooled charge-coupled device (CCD) camera. Detection of fluorescence requires an excitation light reaching the molecule, which upon activation emits light at a shifted wavelength detected by a CCD camera [294]. Fluorescent reporter molecules can be visualized in living tissue as well as fixed tissue, however autofluorescence impairs the sensitivity of fluorescent imaging [294]. Luminescent reporter molecules are enzymes that react with a chemical substrate to emit light [256]. One benefit of luminescence is that there is little background signal from tissue, so low levels of luminescence can be detected [294]. Drawbacks to both fluorescent and luminescent are that signal detection is limited by the depth of the tissue [294]. For *in vivo* studies using mice and rats, bioluminescent imaging is widely used due to its high sensitivity, efficiency, and relatively low cost [256].

The luciferase gene from the firefly, *Photinus pyralis*, is commonly used in bioluminescence imaging. Firefly luciferase reacts with its substrate, D-luciferin, in the presence of adenosine triphosphate (ATP) and oxygen to create an excited-state oxyluciferin molecule [295]. The coding region of firefly luciferase is 1.633 kb and the gene has been cloned into lentiviral, adenoviral and adeno-associated viral delivery systems as well as delivered in a plasmid form by high pressure tail vein injection [260, 265, 296-298]. Many transgenic mouse

lines expressing firefly luciferase controlled by a variety of promoters also exist. Emission wavelength for firefly luciferase is 560 nm, in the yellow-green spectrum of visible light [273].

D-luciferin analogs have been created by modifying the chemical structure, resulting in brighter light emission, red-shifted light emission, and extended decay kinetics [299-301]. So-called caged analogs of luciferin have also been created. Caged luciferin analogs are inactive until enzymatic cleavage that occurs under specific biological conditions such as caspase-3/7 activation, caspase-8 activation or elevated levels of H_2O_2 [302-304]. Caged luciferin molecules allow luciferin to act as an *in vivo* biosensor for identification and imaging of a specific process. Luciferase mutants have also been characterized that result in prolonged and red-shifted light emission [305, 306]. Each improvement in the luciferase-substrate reaction provides a greater variety of tools for use in bioluminescent imaging.

The light emission properties from luciferase are dependent on the structure of the substrate on which it acts [301]. By modifying the substrate one can engineer reactions with longer duration, greater intensity, and red-shifted emission [301]. Luciferase substrates with enhanced properties could be used to study luciferase as a reporter gene in deeper tissues and fewer cells, expanding the utility of BLI. One objective of this study was to screen a panel of luciferase substrates identifying those with the highest light emission in the brain. To test the utility of these substrates, they were examined in a low-expressing transgenic luciferase mouse, which expresses luciferase in dopaminergic expressing cells in the brain (DAT-LUC mice).

C. Results

1. A screen of modified luciferase substrates identifies molecules with improved light output compared with D-luciferin.

27 luciferase substrates were tested in this study, 14 synthetic cyclic alkaminoluciferins and 13 luciferin derivatives (chemical names and abbreviations listed in Table 4-1). We performed a screen to compare luminescence among the substrates using mice previously injected with AAV-Luciferase (AAV-Luc) in the striatum (Fig. 4-1, Table 4-2). Each mouse was injected with a novel substrate and imaged after 10 minutes, 1 hour, and 2 hours. After 24 hours, a point when previous signal has completely diminished, the same mice were injected with 100mM of D-luciferin and imaged after 10 minutes. For each mouse, the light output relative to 100mM of D-luciferin at the 10 minutes time point was calculated. 18 solutions resulted in greater light output compared with D-luciferin. One substrate was imaged twice, 0.5mM iPr-Amide, which is the same as 0.5mM iPrNH-Amide, both in 1% DMSO. Both substrates demonstrate increased luminescence compared with D-luciferin of 12.7-fold and 6.45-fold, respectively. The difference between two measurements of the same substrate seems relatively substantial, however, we have previously noted a large degree of variation within this *in vivo* imaging system. CycLuc1 was identified to have the greatest light output relative to D-luciferin.

To further investigate the difference between CycLuc1 with D-luciferin, we used groups of AAV-Luc injected FVB mice. We measured the luminescence of 5mM CycLuc1 and 100mM D-luciferin in the same mouse. There was a 6-fold increase in light output from CycLuc1

compared with D-luciferin (Fig. 4-2 B). Equal concentrations of the substrates could not be tested due to CycLuc1 insolubility above 5mM in concentration. This experiment demonstrates that the luciferase substrate CycLuc1 emits more light than D-luciferin and could increase the sensitivity in BLI applications. The 6-fold difference from D-luciferin is substantially less than the 15-fold difference that was initially detected in the screen, possibly reflecting variability of this system.

2. Novel luciferase substrates enable the detection of luminescence in transgenic mice expressing luciferase in dopaminergic neurons.

We wanted to test CycLuc1 and another strong light-emitting substrate, iPr-amide, in a transgenic model of luciferase expression in the brain. We bred transgenic mice to express luciferase in dopaminergic neurons by crossing mice transgenic for Cre-recombinase inserted into the dopamine transporter locus behind an internal ribosome entry site (IRES) ($Dat^{IREScre/wt}$) with mice transgenic a conditional luciferase gene whose activity is dependent upon excision by Cre-recombinase (Rosa26-Fluc) (Fig. 4-3 A) [307, 308]. $Dat^{IREScre/wt}$ mice had black fur and Rosa26-Fluc mice had white fur, therefore the original offspring all displayed black fur (all mice obtained from Jackson Laboratories, Bar Harbor, ME; see methods section for full description). Since luminescence does not cross through black fur, we crossed $Dat^{IREScre}$ offspring with white Rosa26-Fluc to obtain a line of $Dat^{IREScre}$+ Fluc+ progeny with white fur. The resulting offspring express luciferase in all dopaminergic cells of the substantia nigra (SN), ventral tegmental area (VTA), and retrorubal field, and we will refer to them as DAT-LUC mice [307, 308].

We were unable to detect any luminescence in DAT-LUC mice with the standard dose of D-luciferin (100mM). The two top light-emitting substrates, CycLuc1 and iPr-amide, in DAT-LUC mice produced detectable luminescence (Fig. 4-3 B). To increase luciferase expression, we bred DAT-LUC mice to homozygosity for the conditional luciferase gene, Rosa26-Fluc$^{+/+}$. In a preliminary test of two mice, the Rosa26-Fluc$^{+/+}$ mouse emitted twice as much light as the Rosa26-Fluc$^{+/-}$ mouse (Fig. 4-3 C).

3.) FAAH-dependent activation of iPr-amide is required for reaction with luciferase.

Fatty acid amide hydrolase (FAAH) is an enzyme expressed in many tissues that functions to hydrolyze the endocannabinoid, *N*-arachidonoyl ethanolamide, and other amides [309]. The luciferase substrate iPr-amide is inactive until hydrolyzed by an amidase such as FAAH. To test the sensitivity of iPr-amide to FAAH inhibition *in vivo* we injected 10mg/kg of the selective FAAH inhibitor, PF-3845, in AAV-Luciferase injected mice as previously described [310]. Another set of mice were injected with vehicle and for each group, one mouse was not injected with the inhibitor to demonstrate that the iPr-amide was functional. 30 minutes after PF-3845 administration, iPr-amide was injected and the mice were imaged. Results show that FAAH inhibitor blocked luminescence of iPr-amide (Fig. 4-4 A, B) (unpaired t-test, $p=0.0028$, $n=3$ per group). This demonstrates that FAAH inhibition affects the activation of iPr-amide into an active substrate of luciferase.

D. Discussion

In this study we identify CycLuc1 in a screen of 34 test solutions as a luciferase substrate that resulted in greater light emission than D-luciferin in the brain. We tested the two highest light emitters identified in the screen, CycLuc1 and iPr-amide, in DAT-LUC mice. With both CycLuc1 and iPr-amide at 5mM we could detect luminescence in DAT-LUC mice but not with 100mM D-luciferin. These findings demonstrate that luciferase substrates with improved light emission properties result in greater detection of luciferase activity, meaning that lower levels of luciferase expression can be detected with improved substrates. Improved substrates can be used to increase the sensitivity of bioluminescent imaging.

Lastly, we tested whether iPr-amide is being hydrolyzed by FAAH using a selective inhibitor of FAAH. In mice previously injected into the striatum with AAV-Luc, we found that the specific FAAH inhibitor PF-3845 blocked activation of iPr-amide into an active luciferase substrate [310]. This suggests that FAAH is the hydrolase that converts iPr-amide into its active form in the brain. This is significant for several reasons. Using iPr-amide as a luciferase substrate, it might be possible to study the silencing of FAAH. This would be more relevant to the study of gene silencing in the brain than silencing luciferase because it is not an overexpressed transgene. The second use for iPr-amide and luciferase is to study the inhibition of FAAH, a hydrolase that is responsible for cleaving the endogenous cannabinoid, *N*-arachidonoyl ethanolamide, as a strategy for the treatment of chronic pain [311]. One additional control that would be helpful in strengthening the conclusion is to test the FAAH inhibitor with D-luciferin or another luciferase substrate that does not require FAAH cleavage for activation. This would demonstrate that the inhibitor is not interfering with a luminescent or transport process unrelated to blocking the hydrolase activity of FAAH.

In conclusion, we used mice injected with AAV-Luc in the striatum to screen 34 luciferase substrate solutions and identified CycLuc1 as a substrate with improved light-emitting properties compared with D-luciferin, confirming other studies done *in vitro* and in cell culture [301]. Improved light-emitting substrates can be applied to studies involving BLI to improve their sensitivity. BLI has been used in a variety of studies measuring and inhibiting growth of tumor cells, studying spread and replication of infectious diseases, and following gene silencing [257, 260, 263, 264, 312, 313]. BLI is a widespread tool for following biological processes *in vivo* and a promising tool for drug discovery applications [314]. With improved substrate for detection of low levels of luciferase, BLI applications can be expanded to study structures in deeper tissues or when luciferase is expressed in fewer numbers of cells.

E. Materials and Methods

1. Mouse lines and genotyping

14 FVB mice (female, 3-6 months old, FVB/NJ from Jackson Laboratory, Bar Harbor, ME) were injected with 5e9GC AAV-Luc-Htt (described in Chapter III). Experiments in AAV-injected mice were performed one year after injection. Each mouse was used 1 or 2 times to test luciferase substrates.

Mice homozygous for the Rosa26-Fluc transgene (male and female, 3-6 months old, 129S-*Gt(ROSA)26Sor*$^{tm3(CAG\text{-}luc)Tyj}$/J, stock number 009043 from Jackson Laboratory, Bar Harbor, ME) were mated with mice heterozygous for the Dat^{IREScre} allele (male and female, 3-6 months old, B6.SJL-*Slc6a3*$^{tm1.1(cre)Bkmn}$/J, stock number 006660 from Jackson Laboratory, Bar Harbor,

ME) [307, 308]. Genotyping for Rosa26-Fluc and Dat^{IREScre} mice was performed according to protocols found on the Jackson Laboratory website. Primers for presence of Cre-recombinase: oIMR6625 5'-TGGCTGTTGGTGTAAAGTGG-3' "Common", oIMR6626 5'-GGACAGGGACATGGTTGACT-3' "Wild type Reverse", oIMR8292 5'-CCAAAAGACGGCAATATGGT-3' "Mutant Reverse"; mutant band =152 bp, heterozygote=152 bp and 264 bp, and wild type band= 264 bp. Primers for GtRosa-Luciferase: oIMR8038 5'-TAAGCC TGCCCAGAAGACTC-3', oIMR8545 5'-AAAGTCGCTCTGAGTTGTTAT-3', oIMR9493 5'-AAATCAGAGAGATCCTCATAAAGG-3'; mutant band 190 bp, heterozygote bands 235 bp an 190 bp, wild type band 235 bp.

2. Stereotactic injection

Mice were anesthetized with 250 mg/kg tribromoethanol (2.5 g 2, 2, 2, tribromoethanol dissolved in 5mL amylene hydrate into 200mL PBS). Anesthetized mice were placed on a heated pad in a stereotactic frame. Superglue (Loctite) was applied to the surface of the fur between the ears, avoiding eyes and exposed skin. After 10-20 seconds, the glue is gently pulled off to remove fur. The exposed skin is cleaned with betadine and an incision is made posterior to anterior. The skin is pulled aside and the needle is placed over the bregma. Measurements for drilling the hole and placing the needle are: anterior 1mm, lateral 3mm and ventral 2mm from the bregma. Once the needle is lowered, it rests there for 2 minutes before infusion begins. After infusion the mouse rests for 2 minutes before the needle is withdrawn. The incision is closed with clear, undyed suture (monocryl undyed monofilament) and the animals are allowed to recover on a heated pad at 37C.

3. Imaging mice

Mice were anesthetized with 5% isoflurane and placed into the Xenogen (now Caliper) *in vivo* imaging system (IVIS 100). In mice with black fur, the fur was removed with glue as previously described in the stereotactic injection methods.10 minutes prior to imaging, mice are injected with 100mM D-luciferin into the ip space (from a 30mg/mL stock solution dissolved in sterile water). Luminescence measurements were taken by 1 minute exposure. In AAV-injected mice, a region of interest (ROI) is drawn over each injection site to quantify luminescence from the injected area. In transgenic mice, ROI were generated over the entire head for the albino mice or over the exposed skin in the black mice. Data were collected as flux (photons / second) or radiance ($p/s/cm^2/sr$).

4. FAAH inhibition

Eight mice were pre-treated with either 10mg/kg FAAH inhibitor by ip injection (PF-3845, n=3), vehicle by ip injection (n=3), or not injected with inhibitor (no inj. mice) as a negative control. 30 minutes later, all mice received 0.5mM iPr-Amide by ip injection. Mice were imaged 10 minutes after iPr-Amide injection. FAAH inhibition was achieved using PF-3845 dissolved in 18:1:1 v/v/v saline:emulphor:ethanol [310].

Figure 4-1: Screen of luciferase substrates in the brain. Each substrate was tested in a single mouse from a group of fourteen previously injected with AAV-Luc-Htt into the striatum. Each mouse was imaged on a consecutive day with 100mM D-luciferin. The data is displayed as luminescence of the test substrate relative to luminescence from D-luciferin.

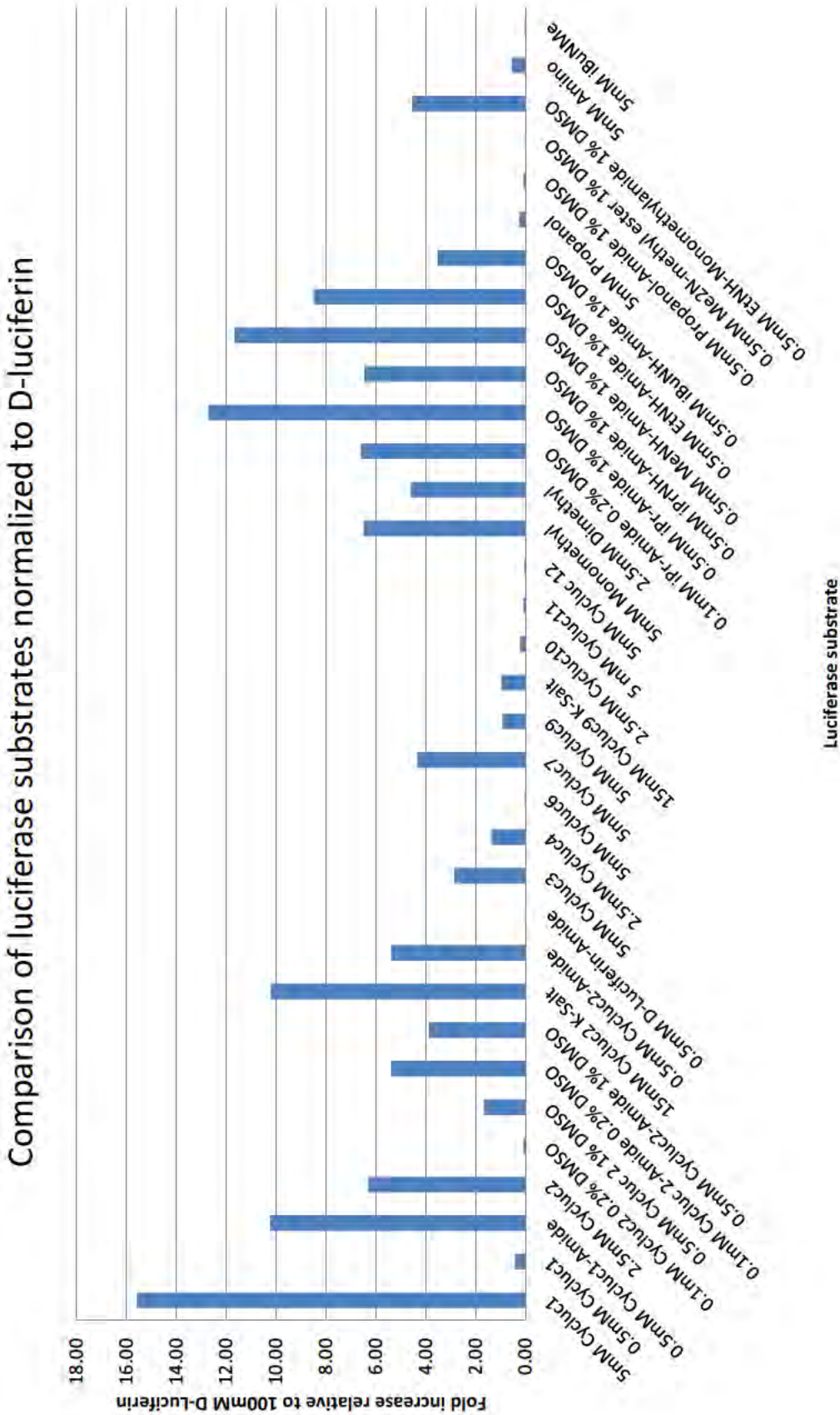

Figure 4-1: Screen of luciferase substrates in the brain.

Figure 4-2: 5mM CycLuc1 results in 6-fold greater luminescence than 100mM D-luciferin. A.) Structures of D-luciferin and CycLuc 1. B.) Mice injected with AAV-Luc-Htt were imaged using 100mM D-luciferin. The same mice were imaged the next day with 5mM CycLuc1. There was a 6-fold increase in luminescence due to the CycLuc1 substrate (paired t-test $p=0.0006$, $n=6$). Data are reported as mean luminescence ± SD.

A.

D-luciferin Cycluc1

B.

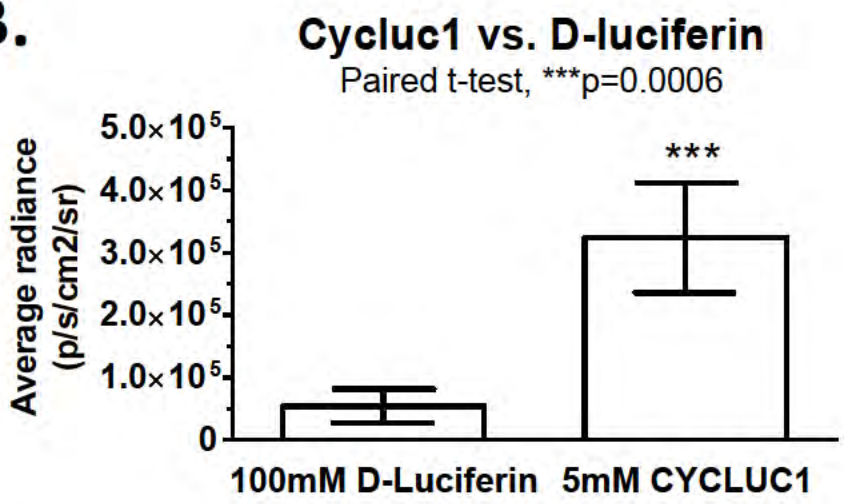

Figure 4-2: 5mM CycLuc1 results in 6-fold greater luminescence than 100mM D-luciferin.

Figure 4-3: Luminescence can be detected with a novel luminescent luciferase substrate but not with D-luciferin. A.) We crossed transgenic mice with the gene for Cre recombinase under control of the dopamine transporter promoter (DAT) with mice expressing the gene for firefly luciferase under control of the GtRosa promoter. Offspring are referred to as DAT-LUC mice and express luciferase in dopaminergic neurons. B.) Luminescence from DAT-LUC mice (black mice with fur removed from the head) is not detectable using D-luciferin as a substrate, but is detectable using two new luciferase substrates. C.) Two DAT-LUC mice were compared for luciferase activity. One mouse was homozygous for luciferase, the other hemizygous for luciferase.

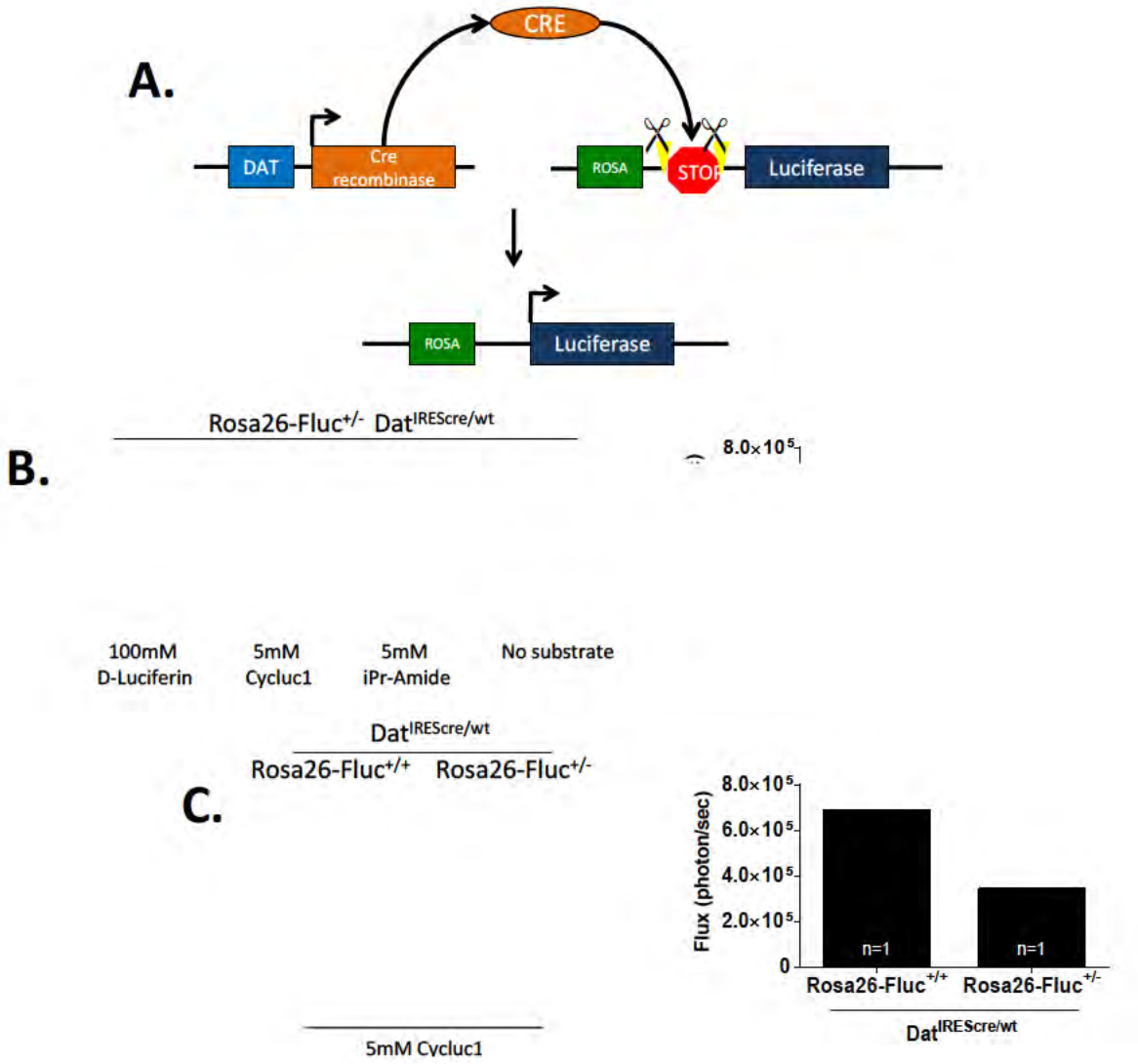

Figure 4-3: Luminescence can be detected with a novel luminescent luciferase substrate but not with D-luciferin.

Figure 4-4: FAAH inhibition prevents activation of iPr-Amide resulting in decreased luminescence in the brain. Eight mice were pre-treated with either injection of FAAH inhibitor, vehicle, or no injection (no inj.) 30 minutes prior to ip administration of 0.5mM iPr-Amide. Mice were imaged 10 minutes after iPr-Amide injection. There was significantly less luminescence with the FAAH inhibitor (unpaired t-test, $p=0.0028$, $n=3$ per group). ** $p<0.01$.

A.

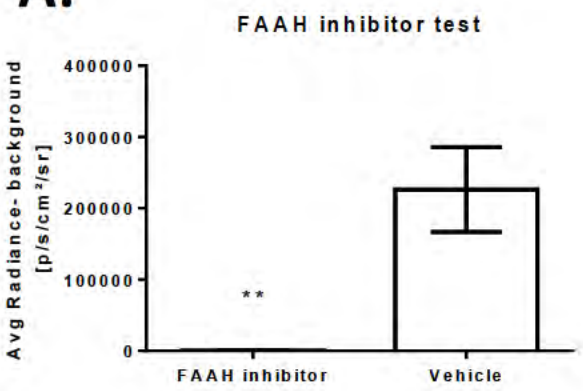

B.

Figure 4-4: FAAH inhibition prevents activation of iPr-Amide resulting in decreased luminescence in the brain.

Table 4-1: Luciferase substrate names and abbreviations. 27 luciferase substrates were used in this study. 14 substrates are synthetic cyclic alkylaminolucferins, and 13 substrates are derivatives of luciferin. The chemical names have been abbreviated for use in figures and text, and are listed in the right column.

Table 4-1: Luciferase substrate names and abbreviations.

Substrate name	Abbreviation
CycLuc1	CycLuc1
CycLuc1 amide	CycLuc1-Amide
CycLuc2	CycLuc2
CycLuc2 amide	CycLuc2-Amide
CycLuc2 potassium salt	CycLuc2 K-Salt
D-Luciferin amide	D-Luciferin-Amide
CycLuc3	CycLuc3
CycLuc4	CycLuc4
CycLuc6	CycLuc6
CycLuc7	CycLuc7
CycLuc9	CycLuc9
CycLuc9 potassium salt	CycLuc9 K-Salt
CycLuc10	CycLuc10
CycLuc11	CycLuc11
CycLuc12	CycLuc12
6'-methylamino luciferin or 6'-$MeNHLH_2$	Monomethyl
6'-dimethylamino luciferin or 6'-Me_2NLH_2	Dimethyl
6'-isopropylamino luciferin amide	iPr-Amide, iPrNH-Amide
6'-methylamino luciferin amide	MeNH-Amide
6'-ethylamino luciferin amide	EtNH-Amide
6'-isobutylamino luciferin amide	iBuNH-Amide
6'-propanolamino luciferin	Propanol
6'-propanolamino luciferin amide	Propanol-Amide
6'-dimethylamino luciferin methyl ester	Me_2N-methyl ester
6'-ethylamino luciferin methyl amide	EtNH-Monomethylamide
6'-aminoluciferin or 6'-NH_2LH_2	Amino
6'-isobutylmethylamino luciferin or 6'-*i*$BuNMeLH_2$	iBuNMe

Table 4-2: Luciferase substrates tested in mice injected with AAV-Luciferase in the brain. Luciferase substrates were ip-injected in mice expressing AAV-delivered Luciferase in the striatum. Mice were imaged 10 minutes, 1 hour, and two hours after injection. On the following day, mice were imaged 10 minutes after ip administration of 100mM D-luciferin. All injections were 100μL. The concentration of luciferase substrate is noted before the name of the substrate, and following the name of the substrate is the concentration of dimethyl sulfoxide (DMSO) if present in the solution. The final column is the ratio between the average radiance-background radiance of substrate injection and D-luciferin for the same mouse. Each value represents one mouse tested.

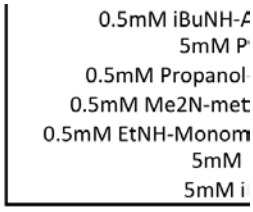

Table 4-2: Luciferase substrates tested in mice injected with AAV-Luciferase in the brain.

CHAPTER V

SUMMARY AND CONCLUSIONS

There is no cure for Huntington's disease, and designing a single therapy is a challenge due to the multiple toxic effects mutant huntingtin has on neuronal function [2]. Several approaches exist for designing treatments for Huntington's disease (HD). One approach attempts to correct the toxic effects of mutant huntingtin, including strategies to increase global transcription, enhance general neuroprotection, and inhibit cleavage of mutant huntingtin into toxic fragments. These strategies often address only a single downstream effect of mutant huntingtin, and a comprehensive treatment based on this approach would require multiple therapies to counteract the toxicities due to mutant huntingtin. A second approach is to decrease the amount of mutant huntingtin either through suppression of transcription or translation or by augmenting its degradation. Through this approach, a single therapeutic agent could prevent all downstream toxicities. This dissertation examines two strategies for reducing mutant huntingtin in the cell: by increasing the degradation of huntingtin protein and silencing mutant huntingtin mRNA.

In Chapter II, I used a transgenic mouse model to explore the effect of a decrease in puromycin sensitive aminopeptidase (PSA) in the progression of HD. To test the effect of decreased PSA on HD-related behavior and pathologies, we bred mice that were heterozygous for the PSA allele and homozygous for the knock-in 140Q huntingtin gene. PSA heterozygosity

in the HD background resulted in mice with a greater number of inclusion bodies and worsened performance on the raised beam test, both of which are markers for the accumulation of mutant protein and the progression of HD. The importance of these results within the field of HD research is in the evaluation of PSA's effect within the brain in a mouse model of Huntington's disease, advancing the work done in studies using cultured cells or transfected muscle tissue. These findings are consistent with what has been seen in other experimental systems and support the hypothesis that normal PSA expression contributes to the defense of neurons against mutant huntingtin.

The mechanism of PSA degradation of huntingtin remains unknown, with reports differing on whether PSA functions directly to degrade huntingtin or indirectly by increase autophagic clearance of aggregated proteins. Alternatively, as studies demonstrate the benefits of PSA-overexpression in other neurodegenerative diseases, it might act by a general neuroprotective mechanism. The ubiquitin-proteasome system represents the primary pathway for degradation of damaged or misfolded proteins where they are digested by endopeptidases into peptides from 3 to 22 residues in length [115, 315]. Peptides exit the proteasome for further degradation by exopeptidases in the cytosol [127]. PSA is one such exopeptidase, able to cleave all amino acid sequences while also possessing the unique ability to cleave polyQ [122]. The mechanism of PSA protection in HD may be in digesting polyglutamine-containing peptides released by the proteasome, especially as mutant huntingtin can lead to ejection of long polyQ peptides, increasing the importance of PSA in clearing the aggregate-prone polyQ peptides [125][121].

The autophagy-lysosomal pathway degrades misfolded and aggregated mutant huntingtin, and differing opinions exist regarding the effect of PSA on autophagy. In cell culture

experiments grossly over-expressing PSA, markers of autophagy were increased [123]. However, in transgenic mice that over-express PSA three-fold in the brain, there was no detected increase in markers for autophagosome formation [200]. It is difficult to compare these findings as they are performed under vastly different conditions, however, it is possible that the observed increase in autophagy in cells may be a response to an acute increase in PSA expression or a response to massive overexpression of PSA (10-100-fold). As PSA is a proteolytic enzyme, increasing expression could result in a toxic insult to the cells, influencing autophagy activation, which would incidentally also increase mutant huntingtin clearance. We observed gliosis and neuron loss in mice expressing the human form of PSA from a viral vector, possibly indicating that the peptidase activity is damaging to neurons at high and unregulated levels. In transgenic animals overexpressing PSA, cells have had the time to adapt and possibly compensate for increased PSA expression, these animals show no toxicity and no increase in autophagy. We looked for a decrease in autophagy in the PSA heterozygous HD mice, however were unable to detect LC3-II under the conditions tested. LC3-II is present at a small amount in wild type animals and slightly increased in HD animals, which we were not able to detect. The debate remains open as to mechanism for PSA in HD and other neurodegenerative diseases.

If PSA is protective against mutant huntingtin, then an increase in PSA activity would ameliorate the disease, representing a therapeutic strategy for the treatment of Huntington's disease. There are several ways to increase PSA activity including gene therapy to increase gene expression and small drug modifiers to enhance its endogenous activity. In this study, we created an AAV expressing the human PSA gene under a CMV promoter. As mentioned previously, it resulted in gliosis and neuronal cell loss, raising many questions about the effect of PSA overexpression in neurons. The majority of published studies overexpressing PSA have shown it

to be tolerated in different cell-types and organisms, however there was mention of toxicity when expressed in *Drosophila* photoreceptors [123, 200]. Our results draw into question the benefit versus risks related to increased PSA activity in the brain, especially if neurons are particularly sensitive to increased expression of PSA. One important question to be answered in future experiments is whether there is a threshold for neurons above which PSA expression becomes toxic.

Future study is needed in the design of AAV-PSA, to test weaker promoters for a low level of constitutive expression, or conditional promoters, such as tetracycline-regulated promoter systems, to control the timing of expression. Aside from viral expression, another approach to study the effect of increased PSA expression on HD *in vivo* is to cross the transgenic PSA overexpressing mouse with an HD mouse to see if ameliorates the disease [200]. These are methods to test in an experimental manner the interaction of PSA and mutant huntingtin. These approaches do not translate easily into therapeutic application, as gene therapy for neurologic diseases is still being tested in large animal studies for viral spread and toxicity.

Another approach is to identify small molecule enhancers of PSA. This would require performing a small molecular screen to identify modifiers of PSA activity in a cell culture or *in vitro* assay. Candidate compounds would be further characterized in cell culture experiments and then ultimately tested HD animal models to look for modification of disease markers such as performance on the raised beam test, rotarod test, or inclusion body formation. A small molecule drug would be therapeutically applicable and less invasive than a gene therapy approach. One drawback to this approach is that a small molecule modifier could be nonspecific, potentially altering other enzymes in the cell or other tissues resulting in adverse effects. Off-target effects

could result in toxicity or create confounding variables in interpreting results, especially in addressing the mechanism of action.

Further research must be done to understand the role of PSA in the brain and other tissues. PSA knockout animals exhibit interesting phenotype as they are smaller than their littermates and behave differently than heterozygous and homozygous littermates during handling and on behavioral tests. These knockout animals are difficult to study because they do not survive at the same rate as their littermates, often dying shortly after birth. It would be fascinating to see the effect of a conditional (brain-specific) knockout of PSA to evaluate the differences in behavior in adult mice.

There were also lessons in experimental design gleaned from performing extensive behavioral tests. Initially, without knowing how severely the PSA deficiency would affect the HD mice, they were tested on the beam at a young age and followed every 2-4 weeks. This presented challenges, as with repeated testing, the mice behaved differently, losing their fear of the open beam, which is thought to be a motivating factor to cross to the platform. Mice would sit in the middle of the raised beam for 15-20 seconds or until prodded gently. From these observations, we chose not to use repeated testing in the later experiments as it interferes with the ability to assess locomotion using the raised beam test. This potentially interfered with the ability to detect differences in the genotypes that were tested repeatedly because when mice walk slowly, inching their way down the beam or refuse to walk altogether, then their locomotor ability is not being accurately evaluated. We found that the raised beam test is most effective when animals are trained once and then tested once before becoming accustomed to the handler and the apparatus.

In addition to investigating ways to reduce mutant huntingtin protein, I examined RNAi as a way to degrade mutant huntingtin mRNA. In chapter III, I described a method for *in vivo* measurement of gene silencing in the brain. Currently, there is no way to screen RNAi constructs in the brain. The general procedure for identifying optimal silencing constructs is to test siRNA and miRNA in cell culture after which the best candidates are chosen for *in vivo* testing. One limitation is that a certain sequence, promoter, or structure may be highly efficient in an immortalized cell line with transfection reagent, but is less effective in neurons of the brain. The goal was to create a model by which gene silencing could be followed in the brain of living mice and to apply the system to test RNAi against therapeutically relevant mutant huntingtin sequences. This model is based on bioluminescent imaging (BLI) using firefly luciferase as a reporter molecule. I created two adeno-associated viruses (AAV) expressing firefly luciferase with six huntingtin RNAi target sites in the 3'-UTR. Furthermore, each huntingtin target site contained a SNP site that can be used to specifically target the mutant huntingtin allele. With a validated system, these two vectors can be used to describe the time course of siRNA, to compare structures, sequences, and delivery strategies, and to study the effectiveness of allele-specific silencing in the brain.

Several challenges arose in the validation of the silencing system. There was significant variation in luminescence between groups of AAV-Luc-Htt injected mice (intermouse variation) as well as between measurements of the same mouse on different days (intramouse variation). We hypothesized that the intramouse variation was due to inconsistent absorption of luciferin from the intraperitoneal space. A comparison of intraperitoneal (ip) and intravenous (iv) injections found that there was less variation in the intravenous injected group, supporting our hypothesis [316]. They also note poor distribution to the brain, compared to other organs, after

both ip and iv injections [316]. To minimize this variation, we injected mice bilaterally and calculated luminescence as a ratio of left side flux divided by right side flux. We compared the variation between just the flux values on one side in that same group. The amount of silencing to achieve silencing when calculating results as a ratio was 35% compared to 40% needed when just looking at the flux. Although both methods resulted in highly variable measurements, the ratio system provided a slightly more sensitive assay to detect silencing. There was significant intermouse variation as well. This has been observed in other experiments within our lab, and described in published studies [270]. Intermouse variation could be due to differences in measurement and placement of the needle during injection, which can affect slightly different anatomical structures within the brain, affecting diffusion and transport of the virus. Meticulous measurement and surgical technique was employed to minimize the variation of luciferase activity between mice. The large variability, even among mice stably expressing luciferase, presents a major limitation of this method and the ability to detect silencing in this study.

To test this BLI silencing system, I targeted silencing of luciferase using three different constructs: cc-siRNA, unconjugated siRNA, and AAV-shRNA. Decreased luminescence was detected with all three RNAi agents. These proof-of-principle experiments show that RNA silencing can be detected in the brain and pave the way for a comparison of huntingtin specific silencing constructs. These luciferase-targeting RNAi molecules demonstrated strong silencing properties in vitro, with >80-90% silencing at maximum concentrations *in vitro*. However, despite the strength in cell culture, silencing *in vivo* was not robust. This draws into question the sensitivity of the assay, especially when evaluating RNAi compounds with weak activity under optimal *in vitro* conditions.

Although cc-siRNA targeting luciferase decreased luminescence compared with control cc-siRNA, an unexpected finding was that both groups of cc-siRNA increased luminescence compared with PBS, and co-transfection in cell culture also increased luminescence independent of serotype, cc-siRNA sequence, and cell type. Two possible mechanisms exist by which this is possible: cc-siRNA could increase the activity of luciferase or improve the transduction of AAV-Luc-Htt in cells and in the brain. The finding that cholesterol conjugated siRNA interacts with AAV raises the possibility that there could be a synergistic effect of co-administering AAV and cc-siRNA. One initial method to test this hypothesis is to label AAV capsid with Cy5 fluorescent dye and mixing it with control (non-silencing) cc-siRNA or non-cholesterol-conjugated siRNA or control solution. The degree of spread and transduction efficiency can be compared between the two groups to evaluate the effect of cc-siRNA on viral uptake. Subsequent to the defense of this dissertation, the experiments with *in vivo* co-injection of AAV-Luciferase and cc-siRNA and the cell culture experiments were repeated by a different member of the lab who could not replicate the findings presented in this dissertation. One possibility is that there was something in the purification of the cc-siRNA from the manufacturer that was subsequently not used in the purification several years later that may have influenced luminescence or viral transduction or expression.

Since siRNA and AAV-shRNA against luciferase demonstrated silencing using this assay, we tested silencing of two huntingtin-specific sequences, containing either SNP site 2273 or 2307. High dose (14nmol) single injections of siRNA targeting these sites did not show silencing *in vivo* with our assay, and neither did AAV-miR2273 co-injected with AAV-Luc-Htt at a high dose. AAV-miR2307 showed some silencing effects when analyzed by luminescence, (but not by the ratio system) compared with the mismatching target. One limitation of this

experiment was that these RNAi sequences were not very effective *in vitro*, reducing their potential effectiveness *in vivo*. The siRNA and AAV-miRNA showed weak activity in cell culture studies, only reaching about 50% silencing at maximal siRNA concentration, whereas the siRNA against luciferase approached 100% silencing at the same concentration. It is likely that the *in vivo* system is not sensitive enough to detect silencing by weak siRNA as it is barely able to detect silencing from siRNA that demonstrate robust silencing cell culture.

Is this system feasible? No, under these conditions, the *in vivo* AAV-Luc-Htt system was not able to adequately detect silencing of a range of RNAi constructs. The goal was for this method to be sensitive enough to compare RNAi compounds and describe their time course of silencing. From my experiments, it appears the system can detect silencing only if it exceeds the variation within the system. While the AAV-Luc-Htt BLI system may have shown positive results with strong silencing RNA constructs, the results do not demonstrate the sensitivity necessary for broad application to a range of RNAi targets as intended. There are several experimental changes that could improve the success of the assay. To overcome the variation in the system, one could increase the potency of the RNAi by increasing dose, frequency of administration, and using silencing sequences demonstrating high efficacy *in vitro*. Published studies using naked siRNA to silence in the brain rely on infusion or pump-delivery system rather than single injection [279, 281, 282]. Using a pump-delivery system could increase the dose and the distribution of siRNA resulting in a higher likelihood of detecting silencing over time. AAV-shLuc at a 2:1 ratio with AAV-Luc-Htt was shown to decrease luminescence, and this dose was increased in subsequent experiments with other silencing vectors. A dose curve of AAV-shLuc would have been useful to identify the range of effective doses. Other methods of increasing potency would be to target multiple binding sites in the 3'-UTR, either repeating the

same sequence or targeting two or more different sequences, and by creating silencing vectors that express multiple hairpin RNAs. To improve siRNA potency, there are numerous conjugations or nanoparticles that may improve diffusion or transport across cell membranes in order to improve delivery of siRNA [274, 280, 317].

It is imperative that future studies with *in vivo* BLI use standardized viral constructs that employ identical serotypes, promoters, and structures, which influence the distribution, transduction efficiency, and potency. The differences in the viruses used in this study are described in Table 3-2. The luciferase virus was the same in all experiments, however the silencing viruses differed in structure (self-complementary or single-stranded), serotype (1, 8, 9), and promoter (CMV, CBA, U6). The results from these experiments cannot be directly compared, however they can provide trends that are useful in guiding future experiments. For example, both successful viral silencing constructs used the U6 promoter, which may provide the strongest miRNA expression able to match the expression from the CMV promoter-driven luciferase.

One limitation in this study is that the serotypes of silencing and reporting vectors were often different, which can affect their relative distribution within the brain. Co-localization of the viruses is vital to the sensitivity of the assay. There are varying reports comparing the spread of different serotypes in the brain, as summarized in Chapter III. In this study, we did not investigate the co-localization of the reporter and silencing vectors. I recommend that this be done in future studies to improve interpretation of results. Several methods exist, including labeling the silencing virus with a fluorescent protein such as GFP and using immunofluorescence against luciferase or FISH for luciferase mRNA to calculate the co-transduction of cells. Fluorescent dyes such can be conjugated to the cc-siRNA to evaluate

spread shortly after injection. These labeling experiments should be done using control AAV silencing vectors because if the hairpin or siRNA degrades the luciferase protein or mRNA, then it will appear as if there is no co-localization. One experimental method that would ensure co-localization of luciferase and hairpin RNA is to use a Cre/ LoxP recombination system. Stop-floxed luciferase gene-containing mice would be injected with a silencing vector expressing both the Cre-recombinase gene and the silencing hairpin RNA. In this case all cells that have the silencing RNA will also express luciferase.

Another limitation of this system is the high level of luciferase expression by the CMV promoter. A lower-expressing promoter would provide more favorable conditions for siRNA-mediated silencing, necessitating lower siRNA concentrations that are more similar to what would be needed to silence an endogenous target. Since it is not practical to use endogenous promoters with the AAV-delivery system due to the size constraints and complexity of regulatory sequences, an alternative approach is to target insertion of the luciferase gene into the genome in a position that it is regulated by a specific promoter. Transgenic mice would express luciferase by the same promoter and at the same level as an endogenous gene, such as huntingtin. One could also target genes specific to the brain, so that luciferase is only expressed in the brain or the striatum using promoters for preproenkephalin, or dopamine 1 receptor [318, 319]. Developments in genome editing make this a possibility using the recently characterized system known as CRISPR for Clustered Regularly Interspaced Short Palindromic Repeats [320, 321]. Somewhat similar to RNAi but targeting double-stranded DNA (dsDNA), CRISPR RNA (crRNA) directs sequence-specific cleavage of dsDNA by Cas (CRISPR-associated) endonucleases [320]. Although it is a system unique to Bacteria and Archaea, the CRISPR-Cas9 complex has been engineered to function in eukaryotic cells, correcting mutant genes in human

and mouse cells, creating targeted knockouts and conditional alleles [322-327]. Two studies have produced targeted knock-in alleles using the CRISPR-Cas9 system, by co-injecting Cas9 mRNA, single guide RNAs, and DNA oligos that incorporate into the nicked or cut dsDNA by homology-directed repair [328, 329]. To target the luciferase gene to a specific promoter, the Cas9 mRNA, CRISPR guide RNA, and luciferase DNA oligos must be injected into a single cell embryo where the Cas9 would introduce a sequence-specific cut to the genome of one or both alleles. Homology-directed repair would insert the luciferase DNA into the genome. Potential drawbacks include that the endogenous gene would likely be disrupted resulting in a total or partial knockout of that gene. Careful gene targeting or use of an internal ribosomal entry site or 2A peptide sequence would be necessary to insert the luciferase gene within a correct reading frame. Off-target effects are also possible, where luciferase would be inserted into other genomic sites, thereby disrupting other genes and possibly expressing more luciferase than intended. Creating a mouse that expresses luciferase at a lower level would be more amenable to silencing but low luminescence could limit detection using D-luciferin. In Chapter IV we test new luciferin substrates *in vivo* that would enable detection of low levels of luminescence.

The experimental design using bilateral injections was intended to decrease variation, however we found that luminescence from one side of the mouse spread across the midline, reducing the ability to detect changes in luminescence. This is likely the result of both virus diffusion to the midline and light-scattering through the tissue. This method was tested with D-luciferin, which emits short wavelength light resulting in high light-scattering. Due to these challenges, I do not recommend that the bilateral injection design to study RNA silencing *in vivo*.

This method could be improved with substrates, such as those tested in Chapter IV, that are red-shifted resulting in less light scattering through tissue. In Chapter IV, we demonstrated that two compounds, CycLuc1 and iPr-amide, have greater activity than D-luciferin and improved sensitivity in luciferase-expressing mice. This capability to detect low luminescence from deep brain structures advances the application of BLI to test more subtle findings in mice or even larger animals. Newer generations of BLI instruments with three dimensional imaging capabilities are now being used with microCT scanning to create three dimensional quantification of luminescence [312, 330]. Renilla luciferase and improved luminescent enzymes are being used for detection of viral expression and for normalization of firefly luciferase expression [313, 331]. A drawback to the viral vectors expressing shRNA in this study is that expression by constitutive promoters cannot be turned off. One advance that could be made is to employ promoters regulated by small molecules enabling control of shRNA expression [332, 333]. This would enable differences in luminescence to be compared with and without shRNA in the same animal, similar to the studies with siRNA.

Taken together these studies employ *in vivo* approaches for testing potential therapeutic agents relevant to Huntington's disease. Neuronal loss following overexpression of PSA raises concerns over the safety and tolerability of this protein in neurons. The implication of this observation is that, although a therapy may be tolerated in cell culture or non-neural tissues, it is imperative to study overexpression in tissue that manifests the disease for safety and toxicity. To a similar extent, this dissertation explores using BLI to follow silencing of luciferase in the brain, proposing a method of tagging luciferase with huntingtin target sequences to test potential therapeutics *in vivo* to identify the most effective design. This system requires further optimization in order to achieve the sensitivity necessary to detect subtle changes in

luminescence for meaningful comparisons. There remain many hurdles to the application of RNAi in the treatment of HD, including delivery and design of structures. Bioluminescent imaging has the potential to provide valuable information, especially with advances in imaging and luminescent substrate design.

Bibliography

[1] MacDonald ME, Ambrose CM, Duyao MP, Myers RH, Lin C, Srinidhi L, et al. A novel gene containing a trinucleotide repeat that is expanded and unstable on Huntington's disease chromosomes. *Cell*. 1993;72:971-83.
[2] Zuccato C, Valenza M, Cattaneo E. Molecular mechanisms and potential therapeutical targets in Huntington's disease. *Physiol Rev*. 2010;90:905-81.
[3] Trottier Y, Biancalana V, Mandel JL. Instability of CAG repeats in Huntington's disease: relation to parental transmission and age of onset. *J Med Genet*. 1994;31:377-82.
[4] van Duijn E, Kingma EM, van der Mast RC. Psychopathology in verified Huntington's disease gene carriers. *J Neuropsychiatry Clin Neurosci*. 2007;19:441-8.
[5] Morton AJ. Circadian and sleep disorder in Huntington's disease. *Exp Neurol*. 2013;243:34-44.
[6] Walker FO. Huntington's disease. *The Lancet*. 2007;369:218-28.
[7] Ross CA, Tabrizi SJ. Huntington's disease: from molecular pathogenesis to clinical treatment. *The Lancet Neurology*. 2011;10:83-98.
[8] Quarrell O, O'Donovan KL, Bandmann O, Strong M. The Prevalence of Juvenile Huntington's Disease: A Review of the Literature and Meta-Analysis. *PLoS currents*. 2012;4:e4f8606b742ef3.
[9] Gonzalez-Alegre P, Afifi AK. Clinical characteristics of childhood-onset (juvenile) Huntington disease: report of 12 patients and review of the literature. *J Child Neurol*. 2006;21:223-9.
[10] Graybiel AM. The basal ganglia: learning new tricks and loving it. *Curr Opin Neurobiol*. 2005;15:638-44.
[11] Stocco A, Lebiere C, Anderson JR. Conditional routing of information to the cortex: a model of the basal ganglia's role in cognitive coordination. *Psychol Rev*. 2010;117:541-74.
[12] Marchand W. Cortico-basal ganglia circuitry: a review of key research and implications for functional connectivity studies of mood and anxiety disorders. *Brain Struct Funct*. 2010;215:73-96.
[13] Hikosaka O, Takikawa Y, Kawagoe R. Role of the Basal Ganglia in the Control of Purposive Saccadic Eye Movements. *Physiol Rev*. 2000;80:953-78.
[14] Vonsattel JPG, DiFiglia M. Huntington disease. *J Neuropathol Exp Neurol*. 1998;57:369-84.
[15] Bolam JP, Hanley JJ, Booth PAC, Bevan MD. Synaptic organisation of the basal ganglia. *J Anat*. 2000;196:527-42.
[16] Haber SN, Nauta WJH. Ramifications of the globus pallidus in the rat as indicated by patterns of immunohistochemistry. *Neuroscience*. 1983;9:245-60.
[17] Gerfen CR, Engber TM, Mahan LC, Susel Z, Chase TN, Monsma FJ, Jr., et al. D1 and D2 dopamine receptor-regulated gene expression of striatonigral and striatopallidal neurons. *Science*. 1990;250:1429-32.
[18] Gerfen CR. The neostriatal mosaic: multiple levels of compartmental organization. *Trends Neurosci*. 1992;15:133-9.

[19] Albin RL, Reiner A, Anderson KD, Dure LSt, Handelin B, Balfour R, et al. Preferential loss of striato-external pallidal projection neurons in presymptomatic Huntington's disease. *Ann Neurol*. 1992;31:425-30.
[20] Reiner A, Albin RL, Anderson KD, D'Amato CJ, Penney JB, Young AB. Differential loss of striatal projection neurons in Huntington disease. *Proc Natl Acad Sci U S A*. 1988;85:5733-7.
[21] Andre VM, Cepeda C, Levine MS. Dopamine and glutamate in Huntington's disease: A balancing act. *CNS Neurosci Ther*. 2010;16:163-78.
[22] Lees AJ, Hardy J, Revesz T. Parkinson's disease. *Lancet*. 2009;373:2055-66.
[23] Jankovic J. Parkinson's disease: clinical features and diagnosis. *J Neurol Neurosurg Psychiatry*. 2008;79:368-76.
[24] Brown P, Williams D. Basal ganglia local field potential activity: Character and functional significance in the human. *Clin Neurophysiol*. 2005;116:2510-9.
[25] Hutchison WD, Dostrovsky JO, Walters JR, Courtemanche R, Boraud T, Goldberg J, et al. Neuronal Oscillations in the Basal Ganglia and Movement Disorders: Evidence from Whole Animal and Human Recordings. *The Journal of Neuroscience*. 2004;24:9240-3.
[26] Cayzac S, Delcasso S, Paz V, Jeantet Y, Cho YH. Changes in striatal procedural memory coding correlate with learning deficits in a mouse model of Huntington disease. *Proceedings of the National Academy of Sciences*. 2011;108:9280-5.
[27] Genworth 2013 Cost of Care Survey. In: Financial G, editor. 2013 ed. https://www.genworth.com/dam/Americas/US/PDFs/Consumer/corporate/130568_032213_Cost%20of%20Care_Final_nonsecure.pdf2013.
[28] Hathorn T, Snyder-Keller A, Messer A. Nicotinamide improves motor deficits and upregulates PGC-1alpha and BDNF gene expression in a mouse model of Huntington's disease. *Neurobiol Dis*. 2011;41:43-50.
[29] Hickey MA, Zhu C, Medvedeva V, Franich NR, Levine MS, Chesselet MF. Evidence for behavioral benefits of early dietary supplementation with CoEnzymeQ10 in a slowly progressing mouse model of Huntington's disease. *Mol Cell Neurosci*. 2012;49:149-57.
[30] Ferrante RJ, Andreassen OA, Jenkins BG, Dedeoglu A, Kuemmerle S, Kubilus JK, et al. Neuroprotective effects of creatine in a transgenic mouse model of Huntington's disease. *J Neurosci*. 2000;20:4389-97.
[31] Andreassen OA, Dedeoglu A, Ferrante RJ, Jenkins BG, Ferrante KL, Thomas M, et al. Creatine increase survival and delays motor symptoms in a transgenic animal model of Huntington's disease. *Neurobiol Dis*. 2001;8:479-91.
[32] Beal MF. Neuroprotective effects of creatine. *Amino Acids*. 2011;40:1305-13.
[33] Tartari M, Gissi C, Lo Sardo V, Zuccato C, Picardi E, Pesole G, et al. Phylogenetic comparison of huntingtin homologues reveals the appearance of a primitive polyQ in sea urchin. *Mol Biol Evol*. 2008;25:330-8.
[34] Duyao MP, Auerbach AB, Ryan A, Persichetti F, Barnes GT, McNeil SM, et al. Inactivation of the mouse Huntington's disease gene homolog Hdh. *Science*. 1995;269:407-10.
[35] Zeitlin S, Liu JP, Chapman DL, Papaioannou VE, Efstratiadis A. Increased apoptosis and early embryonic lethality in mice nullizygous for the Huntington's disease gene homologue. *Nat Genet*. 1995;11:155-63.
[36] Nasir J, Floresco SB, O'Kusky JR, Diewert VM, Richman JM, Zeisler J, et al. Targeted disruption of the Huntington's disease gene results in embryonic lethality and behavioral and morphological changes in heterozygotes. *Cell*. 1995;81:811-23.

[37] Woda JM, Calzonetti T, Hilditch-Maguire P, Duyao MP, Conlon RA, MacDonald ME. Inactivation of the Huntington's disease gene (Hdh) impairs anterior streak formation and early patterning of the mouse embryo. *BMC Dev Biol*. 2005;5:17.
[38] White JK, Auerbach W, Duyao MP, Vonsattel J-P, Gusella JF, Joyner AL, et al. Huntingtin is required for neurogenesis and is not impaired by the Huntington's disease CAG expansion. *Nat Genet*. 1997;17:404-10.
[39] Wexler NS, Young AB, Tanzi RE, Travers H, Starosta-Rubinstein S, Penney JB, et al. Homozygotes for Huntington's disease. *Nature*. 1987;326:194-7.
[40] Myers RH, Leavitt J, Farrer LA, Jagadeesh J, McFarlane H, Mastromauro CA, et al. Homozygote for Huntington disease. *Am J Hum Genet*. 1989;45:615-8.
[41] Lee JK, Mathews K, Schlaggar B, Perlmutter J, Paulsen JS, Epping E, et al. Measures of growth in children at risk for Huntington disease. *Neurology*. 2012;79:668-74.
[42] Fusco FR, Chen Q, Lamoreaux WJ, Figueredo-Cardenas G, Jiao Y, Coffman JA, et al. Cellular localization of huntingtin in striatal and cortical neurons in rats: lack of correlation with neuronal vulnerability in Huntington's disease. *J Neurosci*. 1999;19:1189-202.
[43] Li SH, Li XJ. Huntingtin-protein interactions and the pathogenesis of Huntington's disease. *Trends Genet*. 2004;20:146-54.
[44] Perutz MF, Johnson T, Suzuki M, Finch JT. Glutamine repeats as polar zippers: their possible role in inherited neurodegenerative diseases. *Proc Natl Acad Sci U S A*. 1994;91:5355-8.
[45] Kim MW, Chelliah Y, Kim SW, Otwinowski Z, Bezprozvanny I. Secondary structure of Huntingtin amino-terminal region. *Structure*. 2009;17:1205-12.
[46] Cornett J, Cao F, Wang CE, Ross CA, Bates GP, Li SH, et al. Polyglutamine expansion of huntingtin impairs its nuclear export. *Nat Genet*. 2005;37:198-204.
[47] Atwal RS, Xia J, Pinchev D, Taylor J, Epand RM, Truant R. Huntingtin has a membrane association signal that can modulate huntingtin aggregation, nuclear entry and toxicity. *Hum Mol Genet*. 2007;16:2600-15.
[48] Rockabrand E, Slepko N, Pantalone A, Nukala VN, Kazantsev A, Marsh JL, et al. The first 17 amino acids of Huntingtin modulate its sub-cellular localization, aggregation and effects on calcium homeostasis. *Hum Mol Genet*. 2007;16:61-77.
[49] Rigamonti D, Sipione S, Goffredo D, Zuccato C, Fossale E, Cattaneo E. Huntingtin's neuroprotective activity occurs via inhibition of procaspase-9 processing. *J Biol Chem*. 2001;276:14545-8.
[50] Rigamonti D, Bauer JH, De-Fraja C, Conti L, Sipione S, Sciorati C, et al. Wild-type huntingtin protects from apoptosis upstream of caspase-3. *J Neurosci*. 2000;20:3705-13.
[51] Yamamoto A, Lucas JJ, Hen R. Reversal of neuropathology and motor dysfunction in a conditional model of Huntington's disease. *Cell*. 2000;101:57-66.
[52] Ho LW, Brown R, Maxwell M, Wyttenbach A, Rubinsztein DC. Wild type Huntingtin reduces the cellular toxicity of mutant Huntingtin in mammalian cell models of Huntington's disease. *J Med Genet*. 2001;38:450-2.
[53] Baquet ZC, Gorski JA, Jones KR. Early striatal dendrite deficits followed by neuron loss with advanced age in the absence of anterograde cortical brain-derived neurotrophic factor. *J Neurosci*. 2004;24:4250-8.
[54] Zuccato C, Ciammola A, Rigamonti D, Leavitt BR, Goffredo D, Conti L, et al. Loss of Huntingtin-Mediated BDNF Gene Transcription in Huntington's Disease. *Science*. 2001;293:493-8.

[55] Gauthier LR, Charrin BC, Borrell-Pages M, Dompierre JP, Rangone H, Cordelieres FP, et al. Huntingtin controls neurotrophic support and survival of neurons by enhancing BDNF vesicular transport along microtubules. *Cell*. 2004;118:127-38.
[56] Zuccato C, Tartari M, Crotti A, Goffredo D, Valenza M, Conti L, et al. Huntingtin interacts with REST/NRSF to modulate the transcription of NRSE-controlled neuronal genes. *Nat Genet*. 2003;35:76-83.
[57] Van Raamsdonk JM, Pearson J, Rogers DA, Bissada N, Vogl AW, Hayden MR, et al. Loss of wild-type huntingtin influences motor dysfunction and survival in the YAC128 mouse model of Huntington disease. *Hum Mol Genet*. 2005;14:1379-92.
[58] Zhang S, Feany MB, Saraswati S, Littleton JT, Perrimon N. Inactivation of Drosophila Huntingtin affects long-term adult functioning and the pathogenesis of a Huntington's disease model. *Dis Model Mech*. 2009;2:247-66.
[59] Li X, Standley C, Sapp E, Valencia A, Qin ZH, Kegel KB, et al. Mutant huntingtin impairs vesicle formation from recycling endosomes by interfering with Rab11 activity. *Mol Cell Biol*. 2009;29:6106-16.
[60] Seong IS, Ivanova E, Lee J-M, Choo YS, Fossale E, Anderson M, et al. HD CAG repeat implicates a dominant property of huntingtin in mitochondrial energy metabolism. *Hum Mol Genet*. 2005;14:2871-80.
[61] Zheng S, Clabough EB, Sarkar S, Futter M, Rubinsztein DC, Zeitlin SO. Deletion of the huntingtin polyglutamine stretch enhances neuronal autophagy and longevity in mice. *PLoS Genet*. 2010;6:e1000838.
[62] Atwal RS, Truant R. A stress sensitive ER membrane-association domain in Huntingtin protein defines a potential role for Huntingtin in the regulation of autophagy. *Autophagy*. 2008;4:91-3.
[63] Beal MF, Kowall NW, Ellison DW, Mazurek MF, Swartz KJ, Martin JB. Replication of the neurochemical characteristics of Huntington's disease by quinolinic acid. *Nature*. 1986;321:168-71.
[64] Slow EJ, van Raamsdonk J, Rogers D, Coleman SH, Graham RK, Deng Y, et al. Selective striatal neuronal loss in a YAC128 mouse model of Huntington disease. *Hum Mol Genet*. 2003;12:1555-67.
[65] Fan MM, Raymond LA. N-methyl-D-aspartate (NMDA) receptor function and excitotoxicity in Huntington's disease. *Prog Neurobiol*. 2007;81:272-93.
[66] Laforet GA, Sapp E, Chase K, McIntyre C, Boyce FM, Campbell M, et al. Changes in cortical and striatal neurons predict behavioral and electrophysiological abnormalities in a transgenic murine model of Huntington's disease. *J Neurosci*. 2001;21:9112-23.
[67] Hassel B, Tessler S, Faull RL, Emson PC. Glutamate uptake is reduced in prefrontal cortex in Huntington's disease. *Neurochem Res*. 2008;33:232-7.
[68] Faideau M, Kim J, Cormier K, Gilmore R, Welch M, Auregan G, et al. In vivo expression of polyglutamine-expanded huntingtin by mouse striatal astrocytes impairs glutamate transport: a correlation with Huntington's disease subjects. *Hum Mol Genet*. 2010;19:3053-67.
[69] Dunah AW, Jeong H, Griffin A, Kim YM, Standaert DG, Hersch SM, et al. Sp1 and TAFII130 transcriptional activity disrupted in early Huntington's disease. *Science*. 2002;296:2238-43.

[70] Steffan JS, Bodai L, Pallos J, Poelman M, McCampbell A, Apostol BL, et al. Histone deacetylase inhibitors arrest polyglutamine-dependent neurodegeneration in Drosophila. *Nature*. 2001;413:739-43.
[71] Savas JN, Makusky A, Ottosen S, Baillat D, Then F, Krainc D, et al. Huntington's disease protein contributes to RNA-mediated gene silencing through association with Argonaute and P bodies. *Proc Natl Acad Sci U S A*. 2008;105:10820-5.
[72] Arrasate M, Finkbeiner S. Protein aggregates in Huntington's disease. *Exp Neurol*. 2012;238:1-11.
[73] Steffan JS, Agrawal N, Pallos J, Rockabrand E, Trotman LC, Slepko N, et al. SUMO modification of Huntingtin and Huntington's disease pathology. *Science*. 2004;304:100-4.
[74] Jenkins BG, Koroshetz WJ, Beal MF, Rosen BR. Evidence for impairment of energy metabolism in vivo in Huntington's disease using localized 1H NMR spectroscopy. *Neurology*. 1993;43:2689-95.
[75] Tabrizi SJ, Workman J, Hart PE, Mangiarini L, Mahal A, Bates G, et al. Mitochondrial dysfunction and free radical damage in the Huntington R6/2 transgenic mouse. *Ann Neurol*. 2000;47:80-6.
[76] Panov AV, Gutekunst CA, Leavitt BR, Hayden MR, Burke JR, Strittmatter WJ, et al. Early mitochondrial calcium defects in Huntington's disease are a direct effect of polyglutamines. *Nat Neurosci*. 2002;5:731-6.
[77] Orr AL, Li S, Wang CE, Li H, Wang J, Rong J, et al. N-terminal mutant huntingtin associates with mitochondria and impairs mitochondrial trafficking. *J Neurosci*. 2008;28:2783-92.
[78] Cui L, Jeong H, Borovecki F, Parkhurst CN, Tanese N, Krainc D. Transcriptional repression of PGC-1alpha by mutant huntingtin leads to mitochondrial dysfunction and neurodegeneration. *Cell*. 2006;127:59-69.
[79] Lin J, Wu PH, Tarr PT, Lindenberg KS, St-Pierre J, Zhang CY, et al. Defects in adaptive energy metabolism with CNS-linked hyperactivity in PGC-1alpha null mice. *Cell*. 2004;119:121-35.
[80] DiFiglia M, Sapp E, Chase KO, Davies SW, Bates GP, Vonsattel JP, et al. Aggregation of huntingtin in neuronal intranuclear inclusions and dystrophic neurites in brain. *Science*. 1997;277:1990-3.
[81] Ehrnhoefer DE, Sutton L, Hayden MR. Small changes, big impact: posttranslational modifications and function of huntingtin in Huntington disease. *Neuroscientist*. 2011;17:475-92.
[82] Ratovitski T, Gucek M, Jiang H, Chighladze E, Waldron E, D'Ambola J, et al. Mutant huntingtin N-terminal fragments of specific size mediate aggregation and toxicity in neuronal cells. *J Biol Chem*. 2009;284:10855-67.
[83] Kuemmerle S, Gutekunst C-A, Klein AM, Li X-J, Li S-H, Beal MF, et al. Huntingtin aggregates may not predict neuronal death in Huntington's disease. *Ann Neurol*. 1999;46:842-9.
[84] Gutekunst C-A, Li S-H, Yi H, Mulroy JS, Kuemmerle S, Jones R, et al. Nuclear and neuropil aggregates in Huntington's disease: relationship to neuropathology. *The Journal of neuroscience*. 1999;19:2522-34.
[85] Arrasate M, Mitra S, Schweitzer ES, Segal MR, Finkbeiner S. Inclusion body formation reduces levels of mutant huntingtin and the risk of neuronal death. *Nature*. 2004;431:805-10.

[86] Subramaniam S, Snyder SH. Huntington's disease is a disorder of the corpus striatum: focus on Rhes (Ras homologue enriched in the striatum). *Neuropharmacology*. 2011;60:1187-92.
[87] Steffan JS, Kazantsev A, Spasic-Boskovic O, Greenwald M, Zhu Y-Z, Gohler H, et al. The Huntington's disease protein interacts with p53 and CREB-binding protein and represses transcription. *Proceedings of the National Academy of Sciences*. 2000;97:6763-8.
[88] Nucifora FC, Jr., Sasaki M, Peters MF, Huang H, Cooper JK, Yamada M, et al. Interference by Huntingtin and Atrophin-1 with CBP-Mediated Transcription Leading to Cellular Toxicity. *Science*. 2001;291:2423-8.
[89] Suhr ST, Senut M-C, Whitelegge JP, Faull KF, Cuizon DB, Gage FH. Identities of Sequestered Proteins in Aggregates from Cells with Induced Polyglutamine Expression. *The Journal of Cell Biology*. 2001;153:283-94.
[90] Qin Z-H, Wang Y, Sapp E, Cuiffo B, Wanker E, Hayden MR, et al. Huntingtin Bodies Sequester Vesicle-Associated Proteins by a Polyproline-Dependent Interaction. *The Journal of Neuroscience*. 2004;24:269-81.
[91] Bennett EJ, Bence NF, Jayakumar R, Kopito RR. Global Impairment of the Ubiquitin-Proteasome System by Nuclear or Cytoplasmic Protein Aggregates Precedes Inclusion Body Formation. *Mol Cell*. 2005;17:351-65.
[92] Mitra S, Tsvetkov AS, Finkbeiner S. Single Neuron Ubiquitin-Proteasome Dynamics Accompanying Inclusion Body Formation in Huntington Disease. *J Biol Chem*. 2009;284:4398-403.
[93] Schaffar G, Breuer P, Boteva R, Behrends C, Tzvetkov N, Strippel N, et al. Cellular Toxicity of Polyglutamine Expansion Proteins: Mechanism of Transcription Factor Deactivation. *Mol Cell*. 2004;15:95-105.
[94] Tashiro E, Zako T, Muto H, Itoo Y, Sörgjerd K, Terada N, et al. Prefoldin protects neuronal cells from polyglutamine toxicity by preventing aggregation formation. *J Biol Chem*. 2013.
[95] Kitamura A, Kubota H, Pack C-G, Matsumoto G, Hirayama S, Takahashi Y, et al. Cytosolic chaperonin prevents polyglutamine toxicity with altering the aggregation state. *Nat Cell Biol*. 2006;8:1163-9.
[96] Tam S, Geller R, Spiess C, Frydman J. The chaperonin TRiC controls polyglutamine aggregation and toxicity through subunit-specific interactions. *Nat Cell Biol*. 2006;8:1155-62.
[97] Nekooki-Machida Y, Kurosawa M, Nukina N, Ito K, Oda T, Tanaka M. Distinct conformations of in vitro and in vivo amyloids of huntingtin-exon1 show different cytotoxicity. *Proceedings of the National Academy of Sciences*. 2009;106:9679-84.
[98] Yanai A, Huang K, Kang R, Singaraja RR, Arstikaitis P, Gan L, et al. Palmitoylation of huntingtin by HIP14 is essential for its trafficking and function. *Nat Neurosci*. 2006;9:824-31.
[99] Thompson LM, Aiken CT, Kaltenbach LS, Agrawal N, Illes K, Khoshnan A, et al. IKK phosphorylates Huntingtin and targets it for degradation by the proteasome and lysosome. *J Cell Biol*. 2009;187:1083-99.
[100] Aiken CT, Steffan JS, Guerrero CM, Khashwji H, Lukacsovich T, Simmons D, et al. Phosphorylation of Threonine 3. *J Biol Chem*. 2009;284:29427-36.
[101] Warby SC, Doty CN, Graham RK, Shively J, Singaraja RR, Hayden MR. Phosphorylation of huntingtin reduces the accumulation of its nuclear fragments. *Mol Cell Neurosci*. 2009;40:121-7.

[102] Subramaniam S, Sixt KM, Barrow R, Snyder SH. Rhes, a striatal specific protein, mediates mutant-huntingtin cytotoxicity. *Science*. 2009;324:1327-30.
[103] Subramaniam S, Mealer RG, Sixt KM, Barrow RK, Usiello A, Snyder SH. Rhes, a physiologic regulator of sumoylation, enhances cross-sumoylation between the basic sumoylation enzymes E1 and Ubc9. *J Biol Chem*. 2010;285:20428-32.
[104] Jeong H, Then F, Melia TJ, Jr., Mazzulli JR, Cui L, Savas JN, et al. Acetylation targets mutant huntingtin to autophagosomes for degradation. *Cell*. 2009;137:60-72.
[105] Chan SL, Mattson MP. Caspase and calpain substrates: Roles in synaptic plasticity and cell death. *J Neurosci Res*. 1999;58:167-90.
[106] Li H, Li SH, Johnston H, Shelbourne PF, Li XJ. Amino-terminal fragments of mutant huntingtin show selective accumulation in striatal neurons and synaptic toxicity. *Nat Genet*. 2000;25:385-9.
[107] Martindale D, Hackam A, Wieczorek A, Ellerby L, Wellington C, McCutcheon K, et al. Length of huntingtin and its polyglutamine tract influences localization and frequency of intracellular aggregates. *Nat Genet*. 1998;18:150-4.
[108] Wellington CL, Singaraja R, Ellerby L, Savill J, Roy S, Leavitt B, et al. Inhibiting caspase cleavage of huntingtin reduces toxicity and aggregate formation in neuronal and nonneuronal cells. *J Biol Chem*. 2000;275:19831-8.
[109] Ona VO, Li M, Vonsattel JPG, Andrews LJ, Khan SQ, Chung WM, et al. Inhibition of caspase-1 slows disease progression in a mouse model of Huntington's disease. *Nature*. 1999;399:263-7.
[110] Hermel E, Gafni J, Propp SS, Leavitt BR, Wellington CL, Young JE, et al. Specific caspase interactions and amplification are involved in selective neuronal vulnerability in Huntington's disease. *Cell Death Differ*. 2004;11:424-38.
[111] Graham RK, Deng Y, Slow EJ, Haigh B, Bissada N, Lu G, et al. Cleavage at the caspase-6 site is required for neuronal dysfunction and degeneration due to mutant huntingtin. *Cell*. 2006;125:1179-91.
[112] Landles C, Weiss A, Franklin S, Howland D, Bates G. Caspase-6 does not contribute to the proteolysis of mutant huntingtin in the HdhQ150 knock-in mouse model of Huntington's disease. *PLoS currents*. 2012;4:e4fd085bfc9973.
[113] Gafni J, Ellerby LM. Calpain activation in Huntington's disease. *J Neurosci*. 2002;22:4842-9.
[114] Lunkes A, Lindenberg KS, Ben-Haiem L, Weber C, Devys D, Landwehrmeyer GB, et al. Proteases acting on mutant huntingtin generate cleaved products that differentially build up cytoplasmic and nuclear inclusions. *Mol Cell*. 2002;10:259-69.
[115] Davies JE, Sarkar S, Rubinsztein DC. The ubiquitin proteasome system in Huntington's disease and the spinocerebellar ataxias. *BMC Biochem*. 2007;8 Suppl 1:S2.
[116] Jarome TJ, Helmstetter FJ. The ubiquitin-proteasome system as a critical regulator of synaptic plasticity and long-term memory formation. *Neurobiol Learn Mem*. 2013.
[117] Maheshwari M, Samanta A, Godavarthi SK, Mukherjee R, Jana NR. Dysfunction of the Ubiquitin Ligase Ube3a May Be Associated with Synaptic Pathophysiology in a Mouse Model of Huntington Disease. *J Biol Chem*. 2012;287:29949-57.
[118] Kalchman MA, Graham RK, Xia G, Koide HB, Hodgson JG, Graham KC, et al. Huntingtin is ubiquitinated and interacts with a specific ubiquitin-conjugating enzyme. *J Biol Chem*. 1996;271:19385-94.

[119] Mishra A, Dikshit P, Purkayastha S, Sharma J, Nukina N, Jana NR. E6-AP Promotes Misfolded Polyglutamine Proteins for Proteasomal Degradation and Suppresses Polyglutamine Protein Aggregation and Toxicity. *J Biol Chem*. 2008;283:7648-56.
[120] Yang H, Zhong X, Ballar P, Luo S, Shen Y, Rubinsztein DC, et al. Ubiquitin ligase Hrd1 enhances the degradation and suppresses the toxicity of polyglutamine-expanded huntingtin. *Exp Cell Res*. 2007;313:538-50.
[121] Venkatraman P, Wetzel R, Tanaka M, Nukina N, Goldberg AL. Eukaryotic Proteasomes Cannot Digest Polyglutamine Sequences and Release Them during Degradation of Polyglutamine-Containing Proteins. *Mol Cell*. 2004;14:95-104.
[122] Bhutani N, Venkatraman P, Goldberg AL. Puromycin-sensitive aminopeptidase is the major peptidase responsible for digesting polyglutamine sequences released by proteasomes during protein degradation. *EMBO J*. 2007;26:1385-96.
[123] Menzies FM, Hourez R, Imarisio S, Raspe M, Sadiq O, Chandraratna D, et al. Puromycin-sensitive aminopeptidase protects against aggregation-prone proteins via autophagy. *Hum Mol Genet*. 2010;19:4573-86.
[124] Bennett EJ, Bence NF, Jayakumar R, Kopito RR. Global impairment of the ubiquitin-proteasome system by nuclear or cytoplasmic protein aggregates precedes inclusion body formation. *Mol Cell*. 2005;17:351-65.
[125] Holmberg CI, Staniszewski KE, Mensah KN, Matouschek A, Morimoto RI. Inefficient degradation of truncated polyglutamine proteins by the proteasome. *EMBO J*. 2004;23:4307-18.
[126] Martin-Aparicio E, Yamamoto A, Hernandez F, Hen R, Avila J, Lucas JJ. Proteasomal-dependent aggregate reversal and absence of cell death in a conditional mouse model of Huntington's disease. *J Neurosci*. 2001;21:8772-81.
[127] Rubinsztein DC. The roles of intracellular protein-degradation pathways in neurodegeneration. *Nature*. 2006;443:780-6.
[128] Hara T, Nakamura K, Matsui M, Yamamoto A, Nakahara Y, Suzuki-Migishima R, et al. Suppression of basal autophagy in neural cells causes neurodegenerative disease in mice. *Nature*. 2006;441:885-9.
[129] Ravikumar B, Vacher C, Berger Z, Davies JE, Luo S, Oroz LG, et al. Inhibition of mTOR induces autophagy and reduces toxicity of polyglutamine expansions in fly and mouse models of Huntington disease. *Nat Genet*. 2004;36:585-95.
[130] Schmelzle T, Hall MN. TOR, a Central Controller of Cell Growth. *Cell*. 2000;103:253-62.
[131] Heng MY, Duong DK, Albin RL, Tallaksen-Greene SJ, Hunter JM, Lesort MJ, et al. Early autophagic response in a novel knock-in model of Huntington disease. *Hum Mol Genet*. 2010;19:3702-20.
[132] Arias E, Cuervo AM, de Vries R, Harris S, Kaushik S, Koga H, et al. Cargo recognition failure is responsible for inefficient autophagy in Huntington's disease. *Nat Neurosci*. 2010;13:567+.
[133] Ravikumar B, Duden R, Rubinsztein DC. Aggregate-prone proteins with polyglutamine and polyalanine expansions are degraded by autophagy. *Hum Mol Genet*. 2002;11:1107-17.
[134] Sarkar S, Ravikumar B, Floto RA, Rubinsztein DC. Rapamycin and mTOR-independent autophagy inducers ameliorate toxicity of polyglutamine-expanded huntingtin and related proteinopathies. *Cell Death Differ*. 2009;16:46-56.

[135] Shibata M, Lu T, Furuya T, Degterev A, Mizushima N, Yoshimori T, et al. Regulation of intracellular accumulation of mutant Huntingtin by Beclin 1. *J Biol Chem*. 2006;281:14474-85.
[136] Sarkar S, Davies JE, Huang Z, Tunnacliffe A, Rubinsztein DC. Trehalose, a novel mTOR-independent autophagy enhancer, accelerates the clearance of mutant huntingtin and alpha-synuclein. *J Biol Chem*. 2007;282:5641-52.
[137] Bonsi P, Cuomo D, Martella G, Sciamanna G, Tolu M, Calabresi P, et al. Mitochondrial toxins in Basal Ganglia disorders: from animal models to therapeutic strategies. *Curr Neuropharmacol*. 2006;4:69-75.
[138] Mangiarini L, Sathasivam K, Seller M, Cozens B, Harper A, Hetherington C, et al. Exon 1 of the HD gene with an expanded CAG repeat is sufficient to cause a progressive neurological phenotype in transgenic mice. *Cell*. 1996;87:493-506.
[139] Schilling G, Becher MW, Sharp AH, Jinnah HA, Duan K, Kotzuk JA, et al. Intranuclear inclusions and neuritic aggregates in transgenic mice expressing a mutant N-terminal fragment of huntingtin. *Hum Mol Genet*. 1999;8:397-407.
[140] Hodgson JG, Agopyan N, Gutekunst CA, Leavitt BR, LePiane F, Singaraja R, et al. A YAC mouse model for Huntington's disease with full-length mutant huntingtin, cytoplasmic toxicity, and selective striatal neurodegeneration. *Neuron*. 1999;23:181-92.
[141] Gray M, Shirasaki DI, Cepeda C, Andre VM, Wilburn B, Lu XH, et al. Full-length human mutant huntingtin with a stable polyglutamine repeat can elicit progressive and selective neuropathogenesis in BACHD mice. *J Neurosci*. 2008;28:6182-95.
[142] Wheeler VC, Auerbach W, White JK, Srinidhi J, Auerbach A, Ryan A, et al. Length-dependent gametic CAG repeat instability in the Huntington's disease knock-in mouse. *Hum Mol Genet*. 1999;8:115-22.
[143] Wheeler VC, White JK, Gutekunst CA, Vrbanac V, Weaver M, Li XJ, et al. Long glutamine tracts cause nuclear localization of a novel form of huntingtin in medium spiny striatal neurons in HdhQ92 and HdhQ111 knock-in mice. *Hum Mol Genet*. 2000;9:503-13.
[144] Lin CH, Tallaksen-Greene S, Chien WM, Cearley JA, Jackson WS, Crouse AB, et al. Neurological abnormalities in a knock-in mouse model of Huntington's disease. *Hum Mol Genet*. 2001;10:137-44.
[145] Menalled LB, Sison JD, Dragatsis I, Zeitlin S, Chesselet MF. Time course of early motor and neuropathological anomalies in a knock-in mouse model of Huntington's disease with 140 CAG repeats. *J Comp Neurol*. 2003;465:11-26.
[146] Heng MY, Tallaksen-Greene SJ, Detloff PJ, Albin RL. Longitudinal evaluation of the Hdh(CAG)150 knock-in murine model of Huntington's disease. *J Neurosci*. 2007;27:8989-98.
[147] Hickey MA, Kosmalska A, Enayati J, Cohen R, Zeitlin S, Levine MS, et al. Extensive early motor and non-motor behavioral deficits are followed by striatal neuronal loss in knock-in Huntington's disease mice. *Neuroscience*. 2008;157:280-95.
[148] Andrew SE, Goldberg YP, Kremer B, Telenius H, Theilmann J, Adam S, et al. The relationship between trinucleotide (CAG) repeat length and clinical features of Huntington's disease. *Nat Genet*. 1993;4:398-403.
[149] de Almeida LP, Ross CA, Zala D, Aebischer P, Deglon N. Lentiviral-mediated delivery of mutant huntingtin in the striatum of rats induces a selective neuropathology modulated by polyglutamine repeat size, huntingtin expression levels, and protein length. *J Neurosci*. 2002;22:3473-83.

[150] von Hörsten S, Schmitt I, Nguyen HP, Holzmann C, Schmidt T, Walther T, et al. Transgenic rat model of Huntington's disease. *Hum Mol Genet*. 2003;12:617-24.
[151] Yu-Taeger L, Petrasch-Parwez E, Osmand AP, Redensek A, Metzger S, Clemens LE, et al. A novel BACHD transgenic rat exhibits characteristic neuropathological features of Huntington disease. *J Neurosci*. 2012;32:15426-38.
[152] Yang D, Wang CE, Zhao B, Li W, Ouyang Z, Liu Z, et al. Expression of Huntington's disease protein results in apoptotic neurons in the brains of cloned transgenic pigs. *Hum Mol Genet*. 2010;19:3983-94.
[153] Yang SH, Cheng PH, Banta H, Piotrowska-Nitsche K, Yang JJ, Cheng EC, et al. Towards a transgenic model of Huntington's disease in a non-human primate. *Nature*. 2008;453:921-4.
[154] Jacobsen JC, Bawden CS, Rudiger SR, McLaughlan CJ, Reid SJ, Waldvogel HJ, et al. An ovine transgenic Huntington's disease model. *Hum Mol Genet*. 2010;19:1873-82.
[155] Schiefer J, Landwehrmeyer GB, Lüesse HG, Sprünken A, Puls C, Milkereit A, et al. Riluzole prolongs survival time and alters nuclear inclusion formation in a transgenic mouse model of Huntington's disease. *Mov Disord*. 2002;17:748-57.
[156] Landwehrmeyer GB, Dubois B, de Yebenes JG, Kremer B, Gaus W, Kraus PH, et al. Riluzole in Huntington's disease: a 3-year, randomized controlled study. *Ann Neurol*. 2007;62:262-72.
[157] Kremer B, Clark CM, Almqvist EW, Raymond LA, Graf P, Jacova C, et al. Influence of lamotrigine on progression of early Huntington disease: a randomized clinical trial. *Neurology*. 1999;53:1000-11.
[158] Fekete R, Davidson A, Jankovic J. Clinical assessment of the effect of tetrabenazine on functional scales in huntington disease: a pilot open label study. *Tremor and other hyperkinetic movements (New York, NY)*. 2012;2.
[159] Tang TS, Chen X, Liu J, Bezprozvanny I. Dopaminergic signaling and striatal neurodegeneration in Huntington's disease. *J Neurosci*. 2007;27:7899-910.
[160] Hersch SM, Gevorkian S, Marder K, Moskowitz C, Feigin A, Cox M, et al. Creatine in Huntington disease is safe, tolerable, bioavailable in brain and reduces serum 8OH2'dG. *Neurology*. 2006;66:250-2.
[161] Chaturvedi RK, Beal MF. Mitochondrial approaches for neuroprotection. *Ann N Y Acad Sci*. 2008;1147:395-412.
[162] Menalled LB, Patry M, Ragland N, Lowden PA, Goodman J, Minnich J, et al. Comprehensive behavioral testing in the R6/2 mouse model of Huntington's disease shows no benefit from CoQ10 or minocycline. *PLoS One*. 2010;5:e9793.
[163] Hjorth E, Zhu M, Toro VC, Vedin I, Palmblad J, Cederholm T, et al. Omega-3 Fatty Acids Enhance Phagocytosis of Alzheimer's Disease-Related Amyloid-beta42 by Human Microglia and Decrease Inflammatory Markers. *J Alzheimers Dis*. 2013;35:697-713.
[164] Randomized controlled trial of ethyl-eicosapentaenoic acid in Huntington disease: the TREND-HD study. *Arch Neurol*. 2008;65:1582-9.
[165] Mestre T, Ferreira J, Coelho MM, Rosa M, Sampaio C. Therapeutic interventions for disease progression in Huntington's disease. *Cochrane database of systematic reviews (Online)*. 2009:CD006455.
[166] Ross CA, Biglan K. A Multi-Center, Double-Blind, Randomized, Parallel Group Tolerability Study of Coenzyme Q10 (UbiquinonE) in PRE-manifest Huntington's Disease

ClinicalTrials.gov2010 [cited 2013]. Available from: http://clinicaltrials.gov/show/NCT00920699.
[167] Canals JM, Pineda JR, Torres-Peraza JF, Bosch M, Martín-Ibañez R, Muñoz MT, et al. Brain-Derived Neurotrophic Factor Regulates the Onset and Severity of Motor Dysfunction Associated with Enkephalinergic Neuronal Degeneration in Huntington's Disease. *The Journal of Neuroscience*. 2004;24:7727-39.
[168] Arregui L, Benitez JA, Razgado LF, Vergara P, Segovia J. Adenoviral astrocyte-specific expression of BDNF in the striata of mice transgenic for Huntington's disease delays the onset of the motor phenotype. *Cell Mol Neurobiol*. 2011;31:1229-43.
[169] Olson SD, Pollock K, Kambal A, Cary W, Mitchell GM, Tempkin J, et al. Genetically engineered mesenchymal stem cells as a proposed therapeutic for Huntington's disease. *Mol Neurobiol*. 2012;45:87-98.
[170] Zhu M, Lu C, Li W. Transient exposure to echinacoside is sufficient to activate Trk signaling and protect neuronal cells from rotenone. *J Neurochem*. 2013;124:571-80.
[171] Jiang M, Peng Q, Liu X, Jin J, Hou Z, Zhang J, et al. Small-molecule TrkB receptor agonists improve motor function and extend survival in a mouse model of Huntington's disease. *Hum Mol Genet*. 2013.
[172] Chen M, Ona VO, Li M, Ferrante RJ, Fink KB, Zhu S, et al. Minocycline inhibits caspase-1 and caspase-3 expression and delays mortality in a transgenic mouse model of Huntington disease. *Nat Med*. 2000;6:797-801.
[173] A futility study of minocycline in Huntington's disease. *Mov Disord*. 2010;25:2219-24.
[174] Dunah AW, Jeong H, Griffin A, Kim Y-M, Standaert DG, Hersch SM, et al. Sp1 and TAFII130 Transcriptional Activity Disrupted in Early Huntington's Disease. *Science*. 2002;296:2238-43.
[175] Kazantsev AG, Hersch SM. Drug targeting of dysregulated transcription in Huntington's disease. *Prog Neurobiol*. 2007;83:249-59.
[176] Jia H, Kast RJ, Steffan JS, Thomas EA. Selective histone deacetylase (HDAC) inhibition imparts beneficial effects in Huntington's disease mice: implications for the ubiquitin-proteasomal and autophagy systems. *Hum Mol Genet*. 2012;21:5280-93.
[177] Beconi M, Aziz O, Matthews K, Moumne L, O'Connell C, Yates D, et al. Oral administration of the pimelic diphenylamide HDAC inhibitor HDACi 4b is unsuitable for chronic inhibition of HDAC activity in the CNS in vivo. *PLoS One*. 2012;7:e44498.
[178] Chen JY, Wang E, Galvan L, Huynh M, Joshi P, Cepeda C, et al. Effects of the Pimelic Diphenylamide Histone Deacetylase Inhibitor HDACi 4b on the R6/2 and N171-82Q Mouse Models of Huntington's Disease. *PLoS currents*. 2013;5.
[179] Safety and Tolerability Study of Phenylbutyrate in Huntington's Disease (PHEND-HD) [Internet]. 2005. Available from: clinicaltrials.gov/ct2/show/NCT00212316.
[180] Stack EC, Del Signore SJ, Luthi-Carter R, Soh BY, Goldstein DR, Matson S, et al. Modulation of nucleosome dynamics in Huntington's disease. *Hum Mol Genet*. 2007;16:1164-75.
[181] Sanchez I, Mahlke C, Yuan J. Pivotal role of oligomerization in expanded polyglutamine neurodegenerative disorders. *Nature*. 2003;421:373-9.
[182] Wood NI, Pallier PN, Wanderer J, Morton AJ. Systemic administration of Congo red does not improve motor or cognitive function in R6/2 mice. *Neurobiol Dis*. 2007;25:342-53.

[183] Tanaka M, Machida Y, Niu S, Ikeda T, Jana NR, Doi H, et al. Trehalose alleviates polyglutamine-mediated pathology in a mouse model of Huntington disease. *Nat Med*. 2004;10:148-54.
[184] Abraham RT, Wiederrecht GJ. Immunopharmacology of rapamycin. *Annu Rev Immunol*. 1996;14:483-510.
[185] Rahman SH, Maeder ML, Joung JK, Cathomen T. Zinc-finger nucleases for somatic gene therapy: the next frontier. *Hum Gene Ther*. 2011;22:925-33.
[186] Ramachandran P, Ignacimuthu S. RNA Interference—A Silent but an Efficient Therapeutic Tool. *Appl Biochem Biotechnol*. 2013;169:1774-89.
[187] Bennett CF, Swayze EE. RNA targeting therapeutics: molecular mechanisms of antisense oligonucleotides as a therapeutic platform. *Annu Rev Pharmacol Toxicol*. 2010;50:259-93.
[188] Aronin N, Moore M. Hunting down huntingtin. *N Engl J Med*. 2012;367:1753-4.
[189] Singh S, Narang A, Mahato R. Subcellular Fate and Off-Target Effects of siRNA, shRNA, and miRNA. *Pharm Res*. 2011;28:2996-3015.
[190] DiFiglia M, Sena-Esteves M, Chase K, Sapp E, Pfister E, Sass M, et al. Therapeutic silencing of mutant huntingtin with siRNA attenuates striatal and cortical neuropathology and behavioral deficits. *Proceedings of the National Academy of Sciences*. 2007;104:17204-9.
[191] Kordasiewicz HB, Stanek LM, Wancewicz EV, Mazur C, McAlonis MM, Pytel KA, et al. Sustained therapeutic reversal of Huntington's disease by transient repression of huntingtin synthesis. *Neuron*. 2012;74:1031-44.
[192] Harper SQ, Staber PD, He X, Eliason SL, Martins IH, Mao Q, et al. RNA interference improves motor and neuropathological abnormalities in a Huntington's disease mouse model. *Proc Natl Acad Sci U S A*. 2005;102:5820-5.
[193] Rodriguez-Lebron E, Denovan-Wright EM, Nash K, Lewin AS, Mandel RJ. Intrastriatal rAAV-mediated delivery of anti-huntingtin shRNAs induces partial reversal of disease progression in R6/1 Huntington's disease transgenic mice. *Mol Ther*. 2005;12:618-33.
[194] Dragatsis I, Levine MS, Zeitlin S. Inactivation of Hdh in the brain and testis results in progressive neurodegeneration and sterility in mice. *Nat Genet*. 2000;26:300-6.
[195] O'Kusky JR, Nasir J, Cicchetti F, Parent A, Hayden MR. Neuronal degeneration in the basal ganglia and loss of pallido-subthalamic synapses in mice with targeted disruption of the Huntington's disease gene. *Brain Res*. 1999;818:468-79.
[196] Pfister EL, Kennington L, Straubhaar J, Wagh S, Liu W, DiFiglia M, et al. Five siRNAs targeting three SNPs may provide therapy for three-quarters of Huntington's disease patients. *Curr Biol*. 2009;19:774-8.
[197] Towne CF, York IA, Neijssen J, Karow ML, Murphy AJ, Valenzuela DM, et al. Puromycin-sensitive aminopeptidase limits MHC class I presentation in dendritic cells but does not affect CD8 T cell responses during viral infections. *J Immunol*. 2008;180:1704-12.
[198] Hersh LB. Characterization of membrane-bound aminopeptidases from rat brain: identification of the enkephalin-degrading aminopeptidase. *J Neurochem*. 1985;44:1427-35.
[199] Tobler AR, Constam DB, Schmitt-Graff A, Malipiero U, Schlapbach R, Fontana A. Cloning of the human puromycin-sensitive aminopeptidase and evidence for expression in neurons. *J Neurochem*. 1997;68:889-97.

[200] Kudo LC, Parfenova L, Ren G, Vi N, Hui M, Ma Z, et al. Puromycin-sensitive aminopeptidase (PSA/NPEPPS) impedes development of neuropathology in hPSA/TAU(P301L) double-transgenic mice. *Hum Mol Genet*. 2011;20:1820-33.
[201] Jimenez-Sanchez M, Thomson F, Zavodszky E, Rubinsztein DC. Autophagy and polyglutamine diseases. *Prog Neurobiol*. 2012;97:67-82.
[202] Lee JM, Ramos E, Lee JH, Gillis T, Mysore J, Hayden M, et al. CAG repeat expansion in Huntington disease determines age at onset in a fully dominant fashion. *Neurology*. 2012;78:690-5.
[203] Seo H, Sonntag KC, Isacson O. Generalized brain and skin proteasome inhibition in Huntington's disease. *Ann Neurol*. 2004;56:319-28.
[204] Bence NF, Sampat RM, Kopito RR. Impairment of the ubiquitin-proteasome system by protein aggregation. *Science*. 2001;292:1552-5.
[205] Jana NR, Zemskov EA, Wang G, Nukina N. Altered proteasomal function due to the expression of polyglutamine-expanded truncated N-terminal huntingtin induces apoptosis by caspase activation through mitochondrial cytochrome c release. *Hum Mol Genet*. 2001;10:1049-59.
[206] Ding Q, Lewis JJ, Strum KM, Dimayuga E, Bruce-Keller AJ, Dunn JC, et al. Polyglutamine expansion, protein aggregation, proteasome activity, and neural survival. *J Biol Chem*. 2002;277:13935-42.
[207] Verhoef LG, Lindsten K, Masucci MG, Dantuma NP. Aggregate formation inhibits proteasomal degradation of polyglutamine proteins. *Hum Mol Genet*. 2002;11:2689-700.
[208] Seo H, Sonntag KC, Kim W, Cattaneo E, Isacson O. Proteasome activator enhances survival of Huntington's disease neuronal model cells. *PLoS One*. 2007;2:e238.
[209] Li X, Wang CE, Huang S, Xu X, Li XJ, Li H, et al. Inhibiting the ubiquitin-proteasome system leads to preferential accumulation of toxic N-terminal mutant huntingtin fragments. *Hum Mol Genet*. 2010;19:2445-55.
[210] Petersen A, Larsen KE, Behr GG, Romero N, Przedborski S, Brundin P, et al. Expanded CAG repeats in exon 1 of the Huntington's disease gene stimulate dopamine-mediated striatal neuron autophagy and degeneration. *Hum Mol Genet*. 2001;10:1243-54.
[211] Iwata A, Riley BE, Johnston JA, Kopito RR. HDAC6 and microtubules are required for autophagic degradation of aggregated huntingtin. *J Biol Chem*. 2005;280:40282-92.
[212] Kegel KB, Kim M, Sapp E, McIntyre C, Castaño JG, Aronin N, et al. Huntingtin expression stimulates endosomal–lysosomal activity, endosome tubulation, and autophagy. *The Journal of Neuroscience*. 2000;20:7268-78.
[213] Ravikumar B, Duden R, Rubinsztein DC. Aggregate-prone proteins with polyglutamine and polyalanine expansions are degraded by autophagy. *Hum Mol Genet*. 2002;11:1107-17.
[214] Ravikumar B, Vacher C, Berger Z, Davies JE, Luo S, Oroz LG, et al. Inhibition of mTOR induces autophagy and reduces toxicity of polyglutamine expansions in fly and mouse models of Huntington disease. *Nat Genet*. 2004;36:585-95.
[215] Bauer WO, Nanda I, Beck G, Schmid M, Jakob F. Human puromycin-sensitive aminopeptidase: cloning of 3' UTR, evidence for a polymorphism at a.a. 140 and refined chromosomal localization to 17q21. *Cytogenet Cell Genet*. 2001;92:221-4.
[216] Dyer SH, Slaughter CA, Orth K, Moomaw CR, Hersh LB. Comparison of the soluble and membrane-bound forms of the puromycin-sensitive enkephalin-degrading aminopeptidases from rat. *J Neurochem*. 1990;54:547-54.

[217] Kim E, Kwak H, Ahn K. Cytosolic aminopeptidases influence MHC class I-mediated antigen presentation in an allele-dependent manner. *J Immunol*. 2009;183:7379-87.
[218] Constam DB, Tobler AR, Rensing-Ehl A, Kemler I, Hersh LB, Fontana A. Puromycin-sensitive aminopeptidase. Sequence analysis, expression, and functional characterization. *J Biol Chem*. 1995;270:26931-9.
[219] Lee SH, Kim HG. Cobalt chloride-induced downregulation of puromycin-sensitive aminopeptidase suppresses the migration and invasion of PC-3 cells. *J Microbiol Biotechnol*. 2009;19:530-6.
[220] Osada T, Watanabe G, Sakaki Y, Takeuchi T. Puromycin-sensitive aminopeptidase is essential for the maternal recognition of pregnancy in mice. *Mol Endocrinol*. 2001;15:882-93.
[221] Osada T, Watanabe G, Kondo S, Toyoda M, Sakaki Y, Takeuchi T. Male reproductive defects caused by puromycin-sensitive aminopeptidase deficiency in mice. *Mol Endocrinol*. 2001;15:960-71.
[222] Osada T, Ikegami S, Takiguchi-Hayashi K, Yamazaki Y, Katoh-Fukui Y, Higashinakagawa T, et al. Increased anxiety and impaired pain response in puromycin-sensitive aminopeptidase gene-deficient mice obtained by a mouse gene-trap method. *J Neurosci*. 1999;19:6068-78.
[223] Ren G, Ma Z, Hui M, Kudo LC, Hui KS, Karsten SL. Cu, Zn-superoxide dismutase 1 (SOD1) is a novel target of Puromycin-sensitive aminopeptidase (PSA/NPEPPS): PSA/NPEPPS is a possible modifier of amyotrophic lateral sclerosis. *Mol Neurodegener*. 2011;6:29.
[224] Chow KM, Guan H, Hersh LB. Aminopeptidases do not directly degrade tau protein. *Mol Neurodegener*. 2010;5:48.
[225] Yanagi K, Tanaka T, Kato K, Sadik G, Morihara T, Kudo T, et al. Involvement of puromycin-sensitive aminopeptidase in proteolysis of tau protein in cultured cells, and attenuated proteolysis of frontotemporal dementia and parkinsonism linked to chromosome 17 (FTDP-17) mutant tau. *Psychogeriatrics : the official journal of the Japanese Psychogeriatric Society*. 2009;9:157-66.
[226] Karsten SL, Sang T-K, Gehman LT, Chatterjee S, Liu J, Lawless GM, et al. A Genomic Screen for Modifiers of Tauopathy Identifies Puromycin-Sensitive Aminopeptidase as an Inhibitor of Tau-Induced Neurodegeneration. 2006;51:549-60.
[227] Sengupta S, Horowitz PM, Karsten SL, Jackson GR, Geschwind DH, Fu Y, et al. Degradation of tau protein by puromycin-sensitive aminopeptidase in vitro. *Biochemistry*. 2006;45:15111-9.
[228] Karsten SL, Sang TK, Gehman LT, Chatterjee S, Liu J, Lawless GM, et al. A genomic screen for modifiers of tauopathy identifies puromycin-sensitive aminopeptidase as an inhibitor of tau-induced neurodegeneration. *Neuron*. 2006;51:549-60.
[229] DiFiglia M, Sapp E, Chase K, Schwarz C, Meloni A, Young C, et al. Huntingtin is a cytoplasmic protein associated with vesicles in human and rat brain neurons. *Neuron*. 1995;14:1075-81.
[230] Kim YJ, Yi Y, Sapp E, Wang Y, Cuiffo B, Kegel KB, et al. Caspase 3-cleaved N-terminal fragments of wild-type and mutant huntingtin are present in normal and Huntington's disease brains, associate with membranes, and undergo calpain-dependent proteolysis. *Proceedings of the National Academy of Sciences*. 2001;98:12784-9.

[231] Carty NC, Nash K, Lee D, Mercer M, Gottschall PE, Meyers C, et al. Adeno-associated viral (AAV) serotype 5 vector mediated gene delivery of endothelin-converting enzyme reduces Abeta deposits in APP + PS1 transgenic mice. *Mol Ther*. 2008;16:1580-6.
[232] Tam S, Spiess C, Auyeung W, Joachimiak L, Chen B, Poirier MA, et al. The chaperonin TRiC blocks a huntingtin sequence element that promotes the conformational switch to aggregation. *Nat Struct Mol Biol*. 2009;16:1279-85.
[233] Liebman SW, Meredith SC. Protein folding: Sticky N17 speeds huntingtin pile-up. *Nat Chem Biol*. 2010;6:7-8.
[234] Kita H, Carmichael J, Swartz J, Muro S, Wyttenbach A, Matsubara K, et al. Modulation of polyglutamine-induced cell death by genes identified by expression profiling. *Hum Mol Genet*. 2002;11:2279-87.
[235] Mizushima N, Yoshimori T. How to interpret LC3 immunoblotting. *Autophagy*. 2007;3:542-5.
[236] Lai Y, Hickey RW, Chen Y, Bayir H, Sullivan ML, Chu CT, et al. Autophagy is increased after traumatic brain injury in mice and is partially inhibited by the antioxidant [gamma]-glutamylcysteinyl ethyl ester. *J Cereb Blood Flow Metab*. 2007;28:540-50.
[237] de Mezer M, Wojciechowska M, Napierala M, Sobczak K, Krzyzosiak WJ. Mutant CAG repeats of Huntingtin transcript fold into hairpins, form nuclear foci and are targets for RNA interference. *Nucleic Acids Res*. 2011;39:3852-63.
[238] Fire A, Xu S, Montgomery MK, Kostas SA, Driver SE, Mello CC. Potent and specific genetic interference by double-stranded RNA in Caenorhabditis elegans. *Nature*. 1998;391:806-11.
[239] Valencia-Sanchez MA, Liu J, Hannon GJ, Parker R. Control of translation and mRNA degradation by miRNAs and siRNAs. *Genes Dev*. 2006;20:515-24.
[240] Zhang Y, Engelman J, Friedlander RM. Allele-specific silencing of mutant Huntington's disease gene. *J Neurochem*. 2009;108:82-90.
[241] Aronin N. Target selectivity in mRNA silencing. *Gene Ther*. 2006;13:509-16.
[242] Schwarz DS, Ding H, Kennington L, Moore JT, Schelter J, Burchard J, et al. Designing siRNA That Distinguish between Genes That Differ by a Single Nucleotide. *PLoS Genetics*. 2006;2:e140.
[243] Hu J, Matsui M, Gagnon KT, Schwartz JC, Gabillet S, Arar K, et al. Allele-specific silencing of mutant huntingtin and ataxin-3 genes by targeting expanded CAG repeats in mRNAs. *Nat Biotechnol*. 2009;27:478-84.
[244] Hu J, Liu J, Corey DR. Allele-selective inhibition of huntingtin expression by switching to an miRNA-like RNAi mechanism. *Chem Biol*. 2010;17:1183-8.
[245] Caplen NJ, Taylor JP, Statham VS, Tanaka F, Fire A, Morgan RA. Rescue of polyglutamine-mediated cytotoxicity by double-stranded RNA-mediated RNA interference. *Hum Mol Genet*. 2002;11:175-84.
[246] Zuccato C, Ciammola A, Rigamonti D, Leavitt BR, Goffredo D, Conti L, et al. Loss of huntingtin-mediated BDNF gene transcription in Huntington's disease. *Science*. 2001;293:493-8.
[247] Burgess A, Huang Y, Querbes W, Sah DW, Hynynen K. Focused ultrasound for targeted delivery of siRNA and efficient knockdown of Htt expression. *J Control Release*. 2012;163:125-9.

[248] DiFiglia M, Sena-Esteves M, Chase K, Sapp E, Pfister E, Sass M, et al. Therapeutic silencing of mutant huntingtin with siRNA attenuates striatal and cortical neuropathology and behavioral deficits. *Proc Natl Acad Sci U S A*. 2007;104:17204-9.
[249] Wang YL, Liu W, Wada E, Murata M, Wada K, Kanazawa I. Clinico-pathological rescue of a model mouse of Huntington's disease by siRNA. *Neurosci Res*. 2005;53:241-9.
[250] Harper SQ, Staber PD, He X, Eliason SL, Martins IH, Mao Q, et al. From the Cover: RNA interference improves motor and neuropathological abnormalities in a Huntington's disease mouse model. *Proceedings of the National Academy of Sciences*. 2005;102:5820-5.
[251] Rodriguez-Lebron E, Denovan-Wright EM, Nash K, Lewin AS, Mandel RJ. Intrastriatal rAAV-mediated delivery of anti-huntingtin shRNAs induces partial reversal of disease progression in R6/1 Huntington's disease transgenic mice. *Mol Ther*. 2005;12:618-33.
[252] Machida Y, Okada T, Kurosawa M, Oyama F, Ozawa K, Nukina N. rAAV-mediated shRNA ameliorated neuropathology in Huntington disease model mouse. *Biochem Biophys Res Commun*. 2006;343:190-7.
[253] McBride JL, Pitzer MR, Boudreau RL, Dufour B, Hobbs T, Ojeda SR, et al. Preclinical safety of RNAi-mediated HTT suppression in the rhesus macaque as a potential therapy for Huntington's disease. *Mol Ther*. 2011;19:2152-62.
[254] Grimm D, Streetz KL, Jopling CL, Storm TA, Pandey K, Davis CR, et al. Fatality in mice due to oversaturation of cellular microRNA/short hairpin RNA pathways. *Nature*. 2006;441:537-41.
[255] McBride JL, Boudreau RL, Harper SQ, Staber PD, Monteys AM, Martins I, et al. Artificial miRNAs mitigate shRNA-mediated toxicity in the brain: implications for the therapeutic development of RNAi. *Proc Natl Acad Sci U S A*. 2008;105:5868-73.
[256] Zinn KR, Chaudhuri TR, Szafran AA, O'Quinn D, Weaver C, Dugger K, et al. Noninvasive bioluminescence imaging in small animals. *ILAR journal / National Research Council, Institute of Laboratory Animal Resources*. 2008;49:103-15.
[257] Bartlett DW, Su H, Hildebrandt IJ, Weber WA, Davis ME. Impact of tumor-specific targeting on the biodistribution and efficacy of siRNA nanoparticles measured by multimodality in vivo imaging. *Proc Natl Acad Sci U S A*. 2007;104:15549-54.
[258] Wei J, Jones J, Kang J, Card A, Krimm M, Hancock P, et al. RNA-induced silencing complex-bound small interfering RNA is a determinant of RNA interference-mediated gene silencing in mice. *Mol Pharmacol*. 2011;79:953-63.
[259] Svensson RU, Shey MR, Ballas ZK, Dorkin JR, Goldberg M, Akinc A, et al. Assessing siRNA pharmacodynamics in a luciferase-expressing mouse. *Mol Ther*. 2008;16:1995-2001.
[260] Bartlett DW, Davis ME. Insights into the kinetics of siRNA-mediated gene silencing from live-cell and live-animal bioluminescent imaging. *Nucleic Acids Res*. 2006;34:322-33.
[261] Kobayashi N, Matsui Y, Kawase A, Hirata K, Miyagishi M, Taira K, et al. Vector-based in vivo RNA interference: dose- and time-dependent suppression of transgene expression. *J Pharmacol Exp Ther*. 2004;308:688-93.
[262] Pichler A, Zelcer N, Prior JL, Kuil AJ, Piwnica-Worms D. In vivo RNA interference-mediated ablation of MDR1 P-glycoprotein. *Clin Cancer Res*. 2005;11:4487-94.
[263] Dassie JP, Liu XY, Thomas GS, Whitaker RM, Thiel KW, Stockdale KR, et al. Systemic administration of optimized aptamer-siRNA chimeras promotes regression of PSMA-expressing tumors. *Nat Biotechnol*. 2009;27:839-49.

[264] Gillespie DL, Whang K, Ragel BT, Flynn JR, Kelly DA, Jensen RL. Silencing of hypoxia inducible factor-1alpha by RNA interference attenuates human glioma cell growth in vivo. *Clin Cancer Res*. 2007;13:2441-8.
[265] Deroose CM, Reumers V, Gijsbers R, Bormans G, Debyser Z, Mortelmans L, et al. Noninvasive monitoring of long-term lentiviral vector-mediated gene expression in rodent brain with bioluminescence imaging. *Mol Ther*. 2006;14:423-31.
[266] Badr CE, Tannous BA. Bioluminescence imaging: progress and applications. *Trends Biotechnol*. 2011;29:624-33.
[267] Pendharkar AV, Chua JY, Andres RH, Wang N, Gaeta X, Wang H, et al. Biodistribution of neural stem cells after intravascular therapy for hypoxic-ischemia. *Stroke*. 2010;41:2064-70.
[268] Abraham U, Prior JL, Granados-Fuentes D, Piwnica-Worms DR, Herzog ED. Independent circadian oscillations of Period1 in specific brain areas in vivo and in vitro. *J Neurosci*. 2005;25:8620-6.
[269] Hassani Z, Lemkine GF, Erbacher P, Palmier K, Alfama G, Giovannangeli C, et al. Lipid-mediated siRNA delivery down-regulates exogenous gene expression in the mouse brain at picomolar levels. *J Gene Med*. 2005;7:198-207.
[270] Cearley CN, Wolfe JH. Transduction Characteristics of Adeno-associated Virus Vectors Expressing Cap Serotypes 7, 8, 9, and Rh10 in the Mouse Brain. *Mol Ther*. 2006;13:528-37.
[271] Cearley CN, Wolfe JH. A Single Injection of an Adeno-Associated Virus Vector into Nuclei with Divergent Connections Results in Widespread Vector Distribution in the Brain and Global Correction of a Neurogenetic Disease. *The Journal of Neuroscience*. 2007;27:9928-40.
[272] Steven LJ. Optical properties of biological tissues: a review. *Phys Med Biol*. 2013;58:R37.
[273] Ugarova NN, Brovko LY. Protein structure and bioluminescent spectra for firefly bioluminescence. *Luminescence*. 2002;17:321-30.
[274] Soutschek J, Akinc A, Bramlage B, Charisse K, Constien R, Donoghue M, et al. Therapeutic silencing of an endogenous gene by systemic administration of modified siRNAs. *Nature*. 2004;432:173-8.
[275] Aschauer DF, Kreuz S, Rumpel S. Analysis of Transduction Efficiency, Tropism and Axonal Transport of AAV Serotypes 1, 2, 5, 6, 8 and 9 in the Mouse Brain. *PLoS One*. 2013;8:e76310.
[276] Klein RL, Dayton RD, Tatom JB, Henderson KM, Henning PP. AAV8, 9, Rh10, Rh43 Vector Gene Transfer in the Rat Brain: Effects of Serotype, Promoter and Purification Method. *Mol Ther*. 2007;16:89-96.
[277] McCarty DM. Self-complementary AAV Vectors; Advances and Applications. *Mol Ther*. 2008;16:1648-56.
[278] Wang C, Wang CM, Clark KR, Sferra TJ. Recombinant AAV serotype 1 transduction efficiency and tropism in the murine brain. *Gene Ther*. 2003;10:1528-34.
[279] Stiles DK, Zhang Z, Ge P, Nelson B, Grondin R, Ai Y, et al. Widespread suppression of huntingtin with convection-enhanced delivery of siRNA. *Exp Neurol*. 2012;233:463-71.
[280] Godinho BMDC, Ogier JR, Darcy R, O'Driscoll CM, Cryan JF. Self-assembling Modified β-Cyclodextrin Nanoparticles as Neuronal siRNA Delivery Vectors: Focus on Huntington's Disease. *Mol Pharm*. 2013;10:640-9.

[281] Thakker DR, Natt F, Hüsken D, Maier R, Müller M, van der Putten H, et al. Neurochemical and behavioral consequences of widespread gene knockdown in the adult mouse brain by using nonviral RNA interference. *Proc Natl Acad Sci U S A*. 2004;101:17270-5.
[282] Thakker DR, Natt F, Husken D, van der Putten H, Maier R, Hoyer D, et al. siRNA-mediated knockdown of the serotonin transporter in the adult mouse brain. *Mol Psychiatry*. 2005;10:782-9.
[283] Franich NR, Fitzsimons HL, Fong DM, Klugmann M, During MJ, Young D. AAV vector-mediated RNAi of mutant huntingtin expression is neuroprotective in a novel genetic rat model of Huntington's disease. *Mol Ther*. 2008;16:947-56.
[284] McCaffrey AP, Meuse L, Pham TT, Conklin DS, Hannon GJ, Kay MA. RNA interference in adult mice. *Nature*. 2002;418:38-9.
[285] Bell CL, Gurda BL, Van Vliet K, Agbandje-McKenna M, Wilson JM. Identification of the Galactose Binding Domain of the Adeno-Associated Virus Serotype 9 Capsid. *J Virol*. 2012;86:7326-33.
[286] Wu Z, Miller E, Agbandje-McKenna M, Samulski RJ. α2,3 and α2,6 N-Linked Sialic Acids Facilitate Efficient Binding and Transduction by Adeno-Associated Virus Types 1 and 6. *J Virol*. 2006;80:9093-103.
[287] Akache B, Grimm D, Pandey K, Yant SR, Xu H, Kay MA. The 37/67-Kilodalton Laminin Receptor Is a Receptor for Adeno-Associated Virus Serotypes 8, 2, 3, and 9. *J Virol*. 2006;80:9831-6.
[288] Kashiwakura Y, Tamayose K, Iwabuchi K, Hirai Y, Shimada T, Matsumoto K, et al. Hepatocyte Growth Factor Receptor Is a Coreceptor for Adeno-Associated Virus Type 2 Infection. *J Virol*. 2005;79:609-14.
[289] Taymans J-M, Vandenberghe LH, Haute CVD, Thiry I, Deroose CM, Mortelmans L, et al. Comparative Analysis of Adeno-Associated Viral Vector Serotypes 1, 2, 5, 7, And 8 in Mouse Brain. *Hum Gene Ther*. 2007;18:195-206.
[290] Sondhi D, Hackett NR, Peterson DA, Stratton J, Baad M, Travis KM, et al. Enhanced Survival of the LINCL Mouse Following CLN2 Gene Transfer Using the rh.10 Rhesus Macaque-derived Adeno-associated Virus Vector. *Mol Ther*. 2006;15:481-91.
[291] Burger C, Gorbatyuk OS, Velardo MJ, Peden CS, Williams P, Zolotukhin S, et al. Recombinant AAV Viral Vectors Pseudotyped with Viral Capsids from Serotypes 1, 2, and 5 Display Differential Efficiency and Cell Tropism after Delivery to Different Regions of the Central Nervous System. *Mol Ther*. 2004;10:302-17.
[292] Castle MJ, Gershenson ZT, Giles AR, Holzbaur ELF, Wolfe JH. Adeno-Associated Virus Serotypes 1, 8, and 9 Share Conserved Mechanisms for Anterograde and Retrograde Axonal Transport. *Hum Gene Ther*. 2014;25:705-20.
[293] Weinberg MS, Nicolson S, Bhatt AP, McLendon M, Li C, Samulski RJ. Recombinant Adeno-Associated Virus Utilizes Cell-Specific Infectious Entry Mechanisms. *J Virol*. 2014;88:12472-84.
[294] Massoud TF, Gambhir SS. Molecular imaging in living subjects: seeing fundamental biological processes in a new light. *Genes Dev*. 2003;17:545-80.
[295] Gould SJ, Subramani S. Firefly luciferase as a tool in molecular and cell biology. *Anal Biochem*. 1988;175:5-13.
[296] de Wet JR, Wood KV, DeLuca M, Helinski DR, Subramani S. Firefly luciferase gene: structure and expression in mammalian cells. *Mol Cell Biol*. 1987;7:725-37.

[297] Kim KI, Park JH, Lee YJ, Lee TS, Park JJ, Song I, et al. In vivo bioluminescent imaging of alpha-fetoprotein-producing hepatocellular carcinoma in the diethylnitrosamine-treated mouse using recombinant adenoviral vector. *J Gene Med*. 2012;14:513-20.
[298] Konkalmatt PR, Wang F, Piras BA, Xu Y, O'Connor DM, Beyers RJ, et al. Adeno-associated virus serotype 9 administered systemically after reperfusion preferentially targets cardiomyocytes in the infarct border zone with pharmacodynamics suitable for the attenuation of left ventricular remodeling. *J Gene Med*. 2012;14:609-20.
[299] White EH, Worther H. Analogs of firefly luciferin. 3. *J Org Chem*. 1966;31:1484-8.
[300] Woodroofe CC, Meisenheimer PL, Klaubert DH, Kovic Y, Rosenberg JC, Behney CE, et al. Novel heterocyclic analogues of firefly luciferin. *Biochemistry*. 2012;51:9807-13.
[301] Reddy GR, Thompson WC, Miller SC. Robust light emission from cyclic alkylaminoluciferin substrates for firefly luciferase. *J Am Chem Soc*. 2010;132:13586-7.
[302] Godinat A, Park HM, Miller SC, Cheng K, Hanahan D, Sanman LE, et al. A Biocompatible in Vivo Ligation Reaction and Its Application for Noninvasive Bioluminescent Imaging of Protease Activity in Living Mice. *ACS Chem Biol*. 2013.
[303] Li J, Chen L, Du L, Li M. Cage the firefly luciferin! - a strategy for developing bioluminescent probes. *Chemical Society reviews*. 2013;42:662-76.
[304] Van de Bittner GC, Bertozzi CR, Chang CJ. Strategy for dual-analyte luciferin imaging: in vivo bioluminescence detection of hydrogen peroxide and caspase activity in a murine model of acute inflammation. *J Am Chem Soc*. 2013;135:1783-95.
[305] Harwood KR, Mofford DM, Reddy GR, Miller SC. Identification of mutant firefly luciferases that efficiently utilize aminoluciferins. *Chem Biol*. 2011;18:1649-57.
[306] Branchini BR, Ablamsky DM, Murtiashaw MH, Uzasci L, Fraga H, Southworth TL. Thermostable red and green light-producing firefly luciferase mutants for bioluminescent reporter applications. *Anal Biochem*. 2007;361:253-62.
[307] Backman CM, Malik N, Zhang Y, Shan L, Grinberg A, Hoffer BJ, et al. Characterization of a mouse strain expressing Cre recombinase from the 3' untranslated region of the dopamine transporter locus. *Genesis (New York, NY : 2000)*. 2006;44:383-90.
[308] Soriano P. Generalized lacZ expression with the ROSA26 Cre reporter strain. *Nat Genet*. 1999;21:70-1.
[309] Labar G, Michaux C. Fatty Acid Amide Hydrolase: From Characterization to Therapeutics. *Chem Biodivers*. 2007;4:1882-902.
[310] Ahn K, Johnson DS, Mileni M, Beidler D, Long JZ, McKinney MK, et al. Discovery and characterization of a highly selective FAAH inhibitor that reduces inflammatory pain. *Chem Biol*. 2009;16:411-20.
[311] Roques BP, Fournie-Zaluski MC, Wurm M. Inhibiting the breakdown of endogenous opioids and cannabinoids to alleviate pain. *Nat Rev Drug Discov*. 2012;11:292-310.
[312] Cronin M, Akin AR, Collins SA, Meganck J, Kim JB, Baban CK, et al. High resolution in vivo bioluminescent imaging for the study of bacterial tumour targeting. *PLoS One*. 2012;7:e30940.
[313] Li XF, Deng YQ, Zhao H, Ye Q, Wang HJ, Li SH, et al. Noninvasive bioluminescence imaging of dengue virus infection in the brain of A129 mice. *Appl Microbiol Biotechnol*. 2013.
[314] Kelkar M, De A. Bioluminescence based in vivo screening technologies. *Curr Opin Pharmacol*. 2012;12:592-600.

[315] Kisselev AF, Akopian TN, Woo KM, Goldberg AL. The sizes of peptides generated from protein by mammalian 26 and 20 S proteasomes. Implications for understanding the degradative mechanism and antigen presentation. *J Biol Chem*. 1999;274:3363-71.
[316] Berger F, Paulmurugan R, Bhaumik S, Gambhir S. Uptake kinetics and biodistribution of 14C-d-luciferin—a radiolabeled substrate for the firefly luciferase catalyzed bioluminescence reaction: impact on bioluminescence based reporter gene imaging. *Eur J Nucl Med Mol Imaging*. 2008;35:2275-85.
[317] Whitehead KA, Langer R, Anderson DG. Knocking down barriers: advances in siRNA delivery. *Nat Rev Drug Discov*. 2009;8:129-38.
[318] Drago J, Padungchaichot P, Wong JYF, Lawrence AJ, McManus JF, Sumarsono SH, et al. Targeted Expression of a Toxin Gene to D1 Dopamine Receptor Neurons by Cre-Mediated Site-Specific Recombination. *The Journal of Neuroscience*. 1998;18:9845-57.
[319] Zagon IS, Isayama T, McLaughlin PJ. Preproenkephalin mRNA expression in the developing and adult rat brain. *Molecular Brain Research*. 1994;21:85-98.
[320] Marraffini LA, Sontheimer EJ. CRISPR interference: RNA-directed adaptive immunity in bacteria and archaea. *Nat Rev Genet*. 2010;11:181-90.
[321] Barrangou R, Fremaux C, Deveau H, Richards M, Boyaval P, Moineau S, et al. CRISPR Provides Acquired Resistance Against Viruses in Prokaryotes. *Science*. 2007;315:1709-12.
[322] Mali P, Yang L, Esvelt KM, Aach J, Guell M, DiCarlo JE, et al. RNA-Guided Human Genome Engineering via Cas9. *Science*. 2013;339:823-6.
[323] Schwank G, Koo B-K, Sasselli V, Dekkers Johanna F, Heo I, Demircan T, et al. Functional Repair of CFTR by CRISPR/Cas9 in Intestinal Stem Cell Organoids of Cystic Fibrosis Patients. *Cell Stem Cell*. 2013;13:653-8.
[324] Wu Y, Liang D, Wang Y, Bai M, Tang W, Bao S, et al. Correction of a Genetic Disease in Mouse via Use of CRISPR-Cas9. *Cell Stem Cell*. 2013;13:659-62.
[325] Yang H, Wang H, Shivalila Chikdu S, Cheng Albert W, Shi L, Jaenisch R. One-Step Generation of Mice Carrying Reporter and Conditional Alleles by CRISPR/Cas-Mediated Genome Engineering. *Cell*. 2013;154:1370-9.
[326] Singh P, Schimenti JC, Bolcun-Filas E. A Mouse Geneticist's Practical Guide to CRISPR Applications. *Genetics*. 2015;199:1-15.
[327] Shen B, Zhang J, Wu H, Wang J, Ma K, Li Z, et al. Generation of gene-modified mice via Cas9/RNA-mediated gene targeting. *Cell Res*. 2013;23:720-3.
[328] Ran FA, Hsu Patrick D, Lin C-Y, Gootenberg Jonathan S, Konermann S, Trevino AE, et al. Double Nicking by RNA-Guided CRISPR Cas9 for Enhanced Genome Editing Specificity. *Cell*. 2013;154:1380-9.
[329] Fujii W, Onuma A, Sugiura K, Naito K. Efficient generation of genome-modified mice via offset-nicking by CRISPR/Cas system. *Biochem Biophys Res Commun*. 2014;445:791-4.
[330] Fan W, Sun D, Liu J, Liang D, Wang Y, Narsinh KH, et al. Adipose stromal cells amplify angiogenic signaling via the VEGF/mTOR/Akt pathway in a murine hindlimb ischemia model: a 3D multimodality imaging study. *PLoS One*. 2012;7:e45621.
[331] Bago JR, Aguilar E, Alieva M, Soler-Botija C, Vila OF, Claros S, et al. In vivo bioluminescence imaging of cell differentiation in biomaterials: a platform for scaffold development. *Tissue engineering Part A*. 2013;19:593-603.
[332] Drouet V, Perrin V, Hassig R, Dufour N, Auregan G, Alves S, et al. Sustained effects of nonallele-specific Huntingtin silencing. *Ann Neurol*. 2009;65:276-85.

[333] Manfredsson FP, Bloom DC, Mandel RJ. Regulated protein expression for in vivo gene therapy for neurological disorders: progress, strategies, and issues. *Neurobiol Dis*. 2012;48:212-21.